

**MODELLING CLIMATE CHANGE IMPACT ON SURFACE RUNOFF  
AND SEDIMENT YIELD IN A WATERSHED OF SHIVALIK REGION**

**By**

**ANU D RAJ**

**(2014-20-112)**

**THESIS**

**Submitted in partial fulfilment of the  
requirements for the degree of**

**B. Sc. - M. Sc. (Integrated Climate Change Adaptation)**

**Faculty of Agriculture**

**Kerala Agricultural University**



**ACADEMY OF CLIMATE CHANGE EDUCATION AND RESEARCH**

**VELLANIKKARA, THRISSUR - 680 656**

**KERALA, INDIA**

**2020**

**MODELLING CLIMATE CHANGE IMPACT ON SURFACE RUNOFF  
AND SEDIMENT YIELD IN A WATERSHED OF SHIVALIK REGION**

**By**

**ANU D RAJ**

**(2014-20-112)**

**THESIS**

**Submitted in partial fulfilment of the  
requirements for the degree of**

**B. Sc. - M. Sc. (Integrated Climate Change Adaptation)**

**Faculty of Agriculture**

**Kerala Agricultural University**



**ACADEMY OF CLIMATE CHANGE EDUCATION AND RESEARCH**

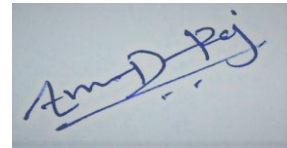
**VELLANIKKARA, THRISSUR - 680 656**

**KERALA, INDIA**

**2020**

## DECLARATION

I, hereby declare that this thesis entitled “**Modelling Climate Change Impact on Surface Runoff and Sediment Yield in a Watershed of Shivalik Region**” is a bonafide record of research work done by me during the course of research and the thesis has not previously formed the basis for the award to me of any degree, diploma, associateship, fellowship or other similar title, of any other University or Society.

A rectangular box containing a handwritten signature in blue ink. The signature appears to be 'Anu D Raj' written in a cursive style.

Vellanikkara,

**Anu D Raj**

Date:


(2014-20-112)

**CERTIFICATE**

Certified that this thesis entitled "**Modelling Climate Change Impact on Surface Runoff and Sediment Yield in a Watershed of Shivalik Region**" is a record of research work done, independently by **Mr ANU D RAJ** under my guidance and supervision and that it has not previously formed the basis for the award of any degree, diploma, fellowship or associateship to him.

Vellanikkara

Date:



**Dr Mary Regina F.**

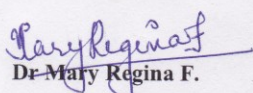
(Major Advisor)

Professor (S&WE), College of  
Horticulture, KAU, Vellanikkara

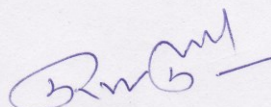


**CERTIFICATE**


We, the undersigned members of the advisory committee of **Mr Anu D Raj**, a candidate for the degree **B.Sc.- M.Sc. (Integrated) Climate Change Adaptation**, agree that the thesis entitled “**Modelling climate change impact on surface runoff and sediment yield in a watershed of Shivalik region**” may be submitted by **Mr Anu D Raj**, in partial fulfilment of the requirement for the degree.

  
**Dr Mary Regina F.**

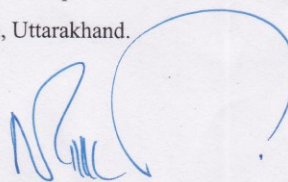
Professor (Soil and Water Engineering)  
College of Horticulture  
Kerala Agricultural University  
Vellanikkara, Thrissur, Kerala.



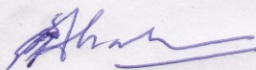
**Dr Suresh Kumar**  
Scientist/ Engineer- SG & Head,  
Agriculture and Soils Department  
Indian Institute of Remote Sensing (IIRS)  
Indian Space Research Organisation (ISRO)  
Department of Space, Government of India  
Dehradun, Uttarakhand.

**Dr Anitha S.** 

Professor (Agronomy) and Head  
Instructional Farm  
Kerala Agricultural University  
Vellanikkara, Thrissur, Kerala.



**Dr P. O. Nameer**  
Special Officer, Academy of Climate  
Change Education and Research (ACCER)  
Kerala Agricultural University  
Vellanikkara, Thrissur, Kerala.



**External Examiner**  
**DR. C. T. ABRAHAM**

## ACKNOWLEDGEMENTS

I owe my deepest gratitude to **Dr Suresh Kumar**, Scientist SG & Head, Agriculture and Soils Department, IIRS, ISRO for giving me the opportunity to carry out my M.Sc. research project under his supreme guidance. He has the attitude and substance of a genius; he repeatedly and convincingly conveyed a spirit of adventure in regard to the research and an excitement in regard to enhancing the knowledge that I am endowed with today. His in-depth knowledge in the field of soil science, agriculture, modelling expertise on remote sensing and research skills has complimented the work done in this thesis. His encouragement, supervision, modesty and support till the final level enabled me to develop an understanding of the subject and without his persistence, this thesis would not have been possible.

I sincerely thank **Dr Prakash Chauhan**, Director, Indian Institute of Remote Sensing, Indian Space Research Organisation and **Dr S. K. Srivastav**, Dean, (Academics), IIRS, ISRO for providing all the necessary facilities required for the research work.

I feel great pleasure to express my cordial gratitude and indebtedness to **Dr Mary Regina F.**, Professor, College of Horticulture, for her constant help and valuable suggestions without which this work would have not been completed.

I remain highly obliged and extremely grateful to **Dr Anitha S.**, Head, Instructional farm for her encouragement and help during my research work.

I owe a great deal of appreciation and gratitude to **Dr P. O. Nameer**, Special officer, ACCER, KAU for giving me the guidance and helping me with all the facilities.

I am also thankful to **Dr E. K. Kurian**, **Dr T. K. Kunhamu**, former Special Officers of ACCER, KAU for the guidance during my academic work.

I am indebted to **Mr Justin George**, Scientist SD, IIRS, ISRO, Dehradun and **Mr Abhishek Kumar Singh**, SRF, IIRS, ISRO for advising and helping me during

research work. A very special thanks goes to **Dr Robert Leonard Wilby** who has been a source of constant support in handling the issues related to the SDSM model and downscaling techniques.

I am quite lucky to have cheering friends. A special thanks to **Miss Sooryamol K. R.** for encouraging and supporting me during the research work. I would like to acknowledge **Mr Sashi Kumar** and **Mr Atin Majumder** for helping me with the modelling and GIS and for sparing their valuable time for me. I sincerely thank **Mr Dinesh Amola**, **Mr Gyan Deep** and **Mr Nitesh** for helping me during soil analysis. It also gives me immense pleasure in acknowledging internship trainees, **Miss Himani Unniyal** and **Mr Ajit Kumar Yadav** for helping me during soil analysis.

I also thank deeply the farmers and peoples of Banh village, Hamirpur, Himachal Pradesh who made me to realize the hardness of field work and without their help the field data collection, would not be done.

I owe my knowledge to all the teachers who taught me and cared for me, they are my true well-wishers, It is their blessing that captured me through the way of success. I owe them all a piece of my heart. I would not be happier than to be known as their student.

I owe my very existence to the love and care that I received from my parents. I am indebted to my family for giving me constant encouragement and support without which I would not have been able to come this far. I thank them generously and dedicate my work to my loving family.

My sincere thanks and gratitude goes to all those unmentioned names who have helped me accomplish this work.

**ANU D RAJ**

## TABLE OF CONTENTS

<b>Chapter Number</b>	<b>TITLES</b>	<b>Page Number</b>
	<b>LIST OF TABLES</b>	<b>xiii - xv</b>
	<b>LIST ILLUSTRATIONS</b>	<b>xvi - xx</b>
	<b>LIST OF PLATES</b>	<b>xxi</b>
	<b>ABBREVIATIONS</b>	<b>xxii-xxiii</b>
<b>1</b>	<b>INTRODUCTION</b>	<b>1- 4</b>
<b>2</b>	<b>REVIEW OF LITERATURE</b>	<b>5- 39</b>
<b>3</b>	<b>MATERIALS AND METHODS</b>	<b>40- 112</b>
<b>4</b>	<b>RESULTS AND DISCUSSION</b>	<b>113- 181</b>
<b>5</b>	<b>SUMMARY AND CONCLUSION</b>	<b>182- 190</b>
	<b>REFERENCES</b>	<b>191- 221</b>
	<b>ABSTRACT</b>	<b>222- 224</b>

## CONTENTS

<b>1. INTRODUCTION</b>	<b>1-4</b>
<b>2. REVIEW OF LITERATURE</b>	<b>5-39</b>
2.1 CLIMATE CHANGE	5
2.1.1 Climate Modelling	8
2.1.2 Emission Scenarios	10
2.2 DOWNSCALING OF GLOBAL CLIMATE DATA	13
2.2.1 Dynamical Downscaling	14
2.2.2 Statistical Downscaling	15
2.2.3 Statistical Downscaling Model (SDSM)	17
2.3 SOIL EROSION	20
2.3.1 Soil Erosion Modelling	24
2.3.1.1 Empirical Models	25
2.3.1.2 Physically Based Models	25
2.3.1.3 Conceptual Models	26
2.3.1.4 Hybrid Models	27
2.3.2 APEX (Process-Based Model)	28
2.4 CLIMATE CHANGE IMPACT ON SOIL EROSION	32
2.5 REMOTE SENSING AND GIS APPLICATIONS	34
2.5.1 Remote Sensing and GIS for Land use-Land Cover Mapping	35
2.5.2 DEM and Terrain Mapping	37
<b>3. MATERIALS AND METHODS</b>	<b>40-112</b>
3.1 STUDY AREA	40
3.1.1 Physiography	40
3.1.2 Geology	42
3.1.3 Land use/ Land cover	43
3.1.4 Drainage	43
3.1.5 Climate	46
3.1.6 Soil	47
3.1.7 Socio-Economic condition	47
3.1.8 Satellite / Remote Sensing and Topographical data	49
3.1.8.1 Cartosat-1 Data	49
3.1.8.2 ResourceSat-2 data	49
3.1.8.3 Toposheet	50
3.1.9 Softwares	50
3.1.9.1 ArcGIS 10.3	50
3.1.9.2 Model Interface- ArcAPEX	51

3.1.9.3	Statistical Package for Social Sciences (SPSS)	51
3.1.9.4	Statistica Version-10	52
3.1.9.5	Soil-Plant-Air-Water (SPAW) Model	52
3.2	THEMATIC MAP PREPARATIONS	53
3.2.1	Slope Map	53
3.2.2	Aspect Map	53
3.2.3	Drainage Map	54
3.2.4	Landform Map	54
3.2.5	Stream Order	54
3.2.6	Drainage Density Map	55
3.2.7	Stream Power Index	55
3.2.8	Topographic Wetness Index	55
3.3	LAND USE/ LAND COVER MAP	56
3.3.1	Normalised Difference in Vegetation Index (NDVI) Map	56
3.4	SOIL LANDSCAPE MAP	57
3.5	FIELD DATA COLLECTION	57
3.5.1	Soil Sampling	57
3.5.2	Soil Analysis	62
3.5.2.1	Soil pH and Electrical Conductivity	62
3.5.2.2	Soil Colour	62
3.5.2.3	Soil Texture	63
3.5.2.4	Bulk Density	64
3.5.2.5	Soil Organic Carbon	64
3.5.2.6	Soil Aggregate Stability	65
3.5.2.7	Carbon and Nitrogen (CHNS Analyser)	66
3.5.2.8	Soil Phosphorus (P)	67
3.5.2.9	Soil Potassium (K)	68
3.5.3	Land use/ Land cover Data Collection	68
3.5.4	Field Erosion Survey	70
3.5.5	Slope Measurements	72
3.5.6	Other Field Observations	73
3.6	SOIL HYDRAULICAL PROPERTIES	73
3.6.1	Infiltration and Hydraulic Conductivity	74
3.6.2	Soil Plant Atmosphere Water (SPAW) Model	76
3.7	METEOROLOGICAL DATA	79
3.7.1	Weather Data (AWS)	79
3.8	DOWNSCALING OF GLOBAL CLIMATE DATA (SDSM)	80
3.8.1	Input Data	81
3.8.1.1	Weather Data	81
3.8.1.2	Global Climate Data	82

3.8.2	Statistical downscaling model (SDSM)	82
3.8.2.1	Quality Control and Data Transformation	84
3.8.2.2	Screening of Downscaling Predictor Variables	84
3.8.2.3	Calibrate Model (Calibration of Model)	85
3.8.2.4	Weather Generator (Validation of Model)	86
3.8.2.5	Scenario Generation	87
3.9	SURFACE RUNOFF AND SEDIMENT DATA	87
3.9.1	Runoff Data	87
3.9.1.1	Surface Runoff Calibration	89
3.9.2	Sediment Data Collection	89
3.9.2.1	Sediment Analysis	91
3.10	MODELLING SURFACE RUNOFF AND SEDIMENT YIELD	91
3.10.1	Model Description- APEX	91
3.10.1.1	Simulating Surface Runoff	93
3.10.1.2	Simulating Peak Runoff Rate	93
3.10.1.3	Simulating Sediment Yield	94
3.10.2	Subarea Delineation	97
3.10.2.1	Dem Setup	98
3.10.2.2	Stream Definition	98
3.10.2.3	Outlet and Inlet Definition	98
3.10.2.4	Main Watershed Outlet Selection and Definition	99
3.10.2.5	Defining Land use/Land cover, Soil and Slope	99
3.10.2.6	Overlay land use, soil and slope layers	101
3.10.3	Subarea Definition	101
3.10.4	Edit APEX Database	101
3.10.4.1	Editing Crop Database	101
3.10.4.2	Editing Fertilizer Database	103
3.10.4.3	Editing Operation Schedules Database	103
3.10.4.4	Editing User Monthly Weather Database	104
3.10.4.5	Editing User Soil Database	104
3.10.5	Defining Weather Database	105
3.10.6	Writing Default Inputs	106
3.10.7	Editing APEX inputs	107
3.10.7.1	Editing APEX Control File	108
3.10.7.2	Editing APEX Site File	108
3.10.7.3	Editing APEX Subarea File	108
3.10.7.4	Editing APEX Herd File	108
3.10.7.5	Editing APEX Soil File	109
3.10.7.6	Editing APEX Print File	109
3.10.8	Write APEX Input Files	109

3.10.9	APEX Run and Output Files	109
3.11	SENSITIVITY ANALYSIS OF THE MODEL	110
3.12	MODEL CALIBRATION AND VALIDATION	111
3.13	SURFACE RUNOFF AND SOIL LOSS ESTIMATION	
3.13.1	Surface Runoff Estimation	111
3.13.2	Soil Loss Estimation	111
3.14	SOIL LOSS RISK ASSESSMENT	112
3.15	GENERATION OF FUTURE SOIL LOSS SCENARIO	112
<b>4.</b>	<b>RESULTS AND DISCUSSION</b>	<b>113-181</b>
4.1	TERRAIN CHARACTERIZATION	113
4.2	DEM ANALYSIS	113
4.3	LAND USE/ LAND COVER MAP (LU/ LC Map)	118
4.4	SOIL LANDSCAPE MAP	119
4.5	PHYSICOCHEMICAL PROPERTIES OF SOIL	120
4.5.1	Soil Physical Properties	121
4.5.2	Soil Chemical Properties	123
4.6	SOIL HYDROLOGICAL PROPERTIES	126
4.7	METEOROLOGICAL DATA	131
4.7.1	Weather Data	131
4.8	DOWNSCALING OF GLOBAL CLIMATE DATA (SDSM)	134
4.8.1	SDSM	134
4.8.1.1	Quality Control and Data Transformation	135
4.8.1.2	Screening of Downscaling Predictor Variables	135
4.8.1.3	Calibrate Model (Calibration of Model)	136
4.8.1.4	Weather Generator (Validation of Model)	138
4.8.1.5	Scenario Generation	140
4.9	IDENTIFICATION OF RUNOFF MECHANISM IN THE WATERSHED	148
4.10	MODELLING SURFACE RUNOFF AND SEDIMENT YIELD	149
4.10.1	Model Description- Apex	149
4.10.2	Subarea Delineation	149
4.10.2.1	Defining Land Use/Land Cover, Soil and Slope	150
4.10.3	Subarea Analysis Report	152
4.11	SENSITIVITY ANALYSIS OF THE MODEL	153
4.12	CALIBRATION AND VALIDATION OF THE MODEL	155
4.12.1	Model Calibration	155
4.12.1.1	Surface runoff	155
4.12.1.2	Sediment yield	158
4.12.2	Model validation and performance assessment	162
4.12.2.1	Surface runoff validation	163



4.12.2.2	Model performance for surface runoff	<b>164</b>
4.12.2.3	Sediment yield validation	<b>165</b>
4.12.2.4	Model performance for sediment yield	<b>167</b>
4.13	<b>SURFACE RUNOFF AND SOIL LOSS ESTIMATION</b>	<b>170</b>
4.14	<b>SOIL LOSS RISK ASSESSMENT</b>	<b>176</b>
4.15	<b>FUTURE SOIL LOSS SCENARIO</b>	<b>178</b>
4.15.1	Soil loss under A2 scenario	<b>178</b>
4.15.2	Soil loss under B2 scenario	<b>180</b>
<b>5.</b>	<b>SUMMARY AND CONCLUSION</b>	<b>182-190</b>
5.1	SUGGESTIONS	<b>189</b>
5.2	FUTURE LINE OF WORK	<b>189</b>
<b>6.</b>	<b>REFERENCES</b>	<b>191-221</b>
<b>7.</b>	<b>ABSTRACT</b>	<b>222-224</b>

## LIST OF TABLES

Table Number	Title	Page Number
1	Average climate of the study area (2000-2018)	46
2	Distribution of various soil samples over land use/land cover	59
3	Instruments and materials used	61
4	Soil erosion proforma	71
5	NCEP predictors used in the screening process	86
6	Major components and capabilities of APEX model	92
7	Various landforms in the watershed	113
8	The aerial extent of slope classes in the watershed	114
9	The area under different aspect class	115
10	The area under different land use classes	119
11	Physiographic soil map units	121
12	Physical properties of soils in the watershed-I	122
13	Physical properties of soils in the watershed -II	123
14	Chemical properties of soils in the watershed-I	124
15	Soil nutrients in the watershed	125
16	Soil hydrological properties in the watershed- I	127
17	Soil hydrological properties in the watershed- II	128
18	Soil hydrological properties in the watershed- III	129
19	Soil erosion survey	130
20	Predictands and their selected NCEP predictors	135
21	Explained variance and standard error during calibration (1985-1999)	136

### LIST OF TABLES (Continued)

<b>22</b>	Coefficient of determination and root mean square error during validation (2000-2014)	138
<b>23</b>	Change in temperature and rainfall (2011-2099) from the base period (1985-2014)	146
<b>24</b>	Percentage change in Average annual rainfall (2011-2099) from the base period (1985-2014) for H3A2 & H3B2	147
<b>25</b>	Various parameters and percentage change with respect to runoff and sediment yield variation	153-154
<b>26</b>	Parameters sensitive to runoff and sediment yield	155
<b>27</b>	Model parameters and values fixed in surface runoff calibration	156
<b>28</b>	Scatter plot statistics for surface runoff calibration	158
<b>29</b>	Box & Whisker plot statistics for surface runoff calibration	158
<b>30</b>	Model parameters and values fixed in sediment yield calibration	159
<b>31</b>	Scatter plot statistics for sediment yield calibration	161
<b>32</b>	Box & Whisker plot statistics for surface runoff calibration	161
<b>33</b>	Scatter plot statistics for surface runoff validation	163
<b>34</b>	Box & Whisker plot statistics for surface runoff validation	164
<b>35</b>	Scatter plot statistics for sediment yield validation	166
<b>36</b>	Box & Whisker plot statistics for sediment yield validation	166
<b>37</b>	Surface runoff and sediment yield in various Subarea	171
<b>38</b>	Surface runoff and sediment yield in various land use	171
<b>39</b>	Average soil loss in various land uses of micro watershed	174
<b>40</b>	Soil loss (ton ha <sup>-1</sup> yr <sup>-1</sup> ) in various Subareas of micro watershed	175

### LIST OF TABLES (Continued)

<b>41</b>	Average soil loss in various slopes of micro watershed	175
<b>42</b>	Soil erosion risk classes in the micro watershed	176
<b>43</b>	Soil loss (t ha <sup>-1</sup> yr <sup>-1</sup> ) under A2 scenario	178
<b>44</b>	Soil loss (t ha <sup>-1</sup> yr <sup>-1</sup> ) under B2 scenario	180

## LIST OF ILLUSTRATIONS

Figure Number	Figure	Page Number
1	Schematic diagram of SRES family storylines.	12
2	Location of the study area (Micro-watershed)	41
3	Location of the study area (Nano watershed)	42
4	Major rivers/ khads in Hamirpur district	45
5	Spatial distribution of rainfall	45
6	Research methodology	48
7	Cartosat DEM imagery of study area	49
8	ResourceSat-2 LISS-IV False Colour Composite of Study Area	49
9	Strahler method of stream ordering	54
10	Soil sampling locations	58
11	Bulk density locations	58
12	Processing of soil samples	60
13	pH measurement	62
14	Conductivity measurement	62
15	Munsell soil colour chart	63
16	Soil mixture in settling cylinder	63
17	Bouyoucos Hydrometer	63
18	Soil textural analysis	64
19	Bulk density analysis (Wax method)	64
20	Soil organic carbon analysis by Walkley and Black method	65
21	Soil aggregate stability analysis	65
22	CHNS Analyzer	67
23	CHNS Data display	67
24	Spectrophotometer	67
25	Flame photometer	67
26	Plant height and density measurement	70
27	Inclinometer and Trimble GPS	72

### LIST OF ILLUSTRATIONS (Continued)

<b>28</b>	Steep slopes observed in the study area	72
<b>29</b>	Farmyard manure application and waterbody observed in a field of the study area	73
<b>30</b>	Soil infiltration rate sampling locations	74
<b>31</b>	Mini disk Infiltrometer	75
<b>32</b>	Mini disk Infiltrometer calculation sheet	76
<b>33</b>	SPAW Model Interface	76
<b>34</b>	Model interface for soil water characteristic solutions	78
<b>35</b>	Applicable textural region (White) for the derived equations	78
<b>36</b>	Automatic weather station	80
<b>37</b>	HadCM3 data downloading window	80
<b>38</b>	A schematic illustrating the standard methodology to downscaling	82
<b>39</b>	Methodology for downscaling of global climate data	83
<b>40</b>	Discharge rating curves and related data for one-and three-foot trapezoidal supercritical flow flumes. (USDA Hand Book)	89
<b>41</b>	Sediment collection pipe	90
<b>42</b>	Sediment tank	90
<b>43</b>	Sediment filtration unit	90
<b>44</b>	ArcAPEX Project Set up Window	97
<b>45</b>	ArcAPEX DEM Setup Window	97
<b>46</b>	ArcAPEX Land Use/ Soil/ Slope Definition Window	100
<b>47</b>	ArcAPEX Subarea Definition Window	100
<b>48</b>	APEX edit database window	102
<b>49</b>	APEX- edit crop database window	102
<b>50</b>	APEX- edit fertilizer database window	103
<b>51</b>	APEX- edit operation schedule window	103
<b>52</b>	APEX- edit weather database window	104
<b>53</b>	APEX- edit soil database window	105

### LIST OF ILLUSTRATIONS (Continued)

<b>54</b>	ArcAPEX- Weather Input Interface	105
<b>55</b>	APEX write file window	106
<b>56</b>	APEX- edit control file window	107
<b>57</b>	APEX- edit subarea file window	108
<b>58</b>	ArcAPEX Model Run Interface	109
<b>59</b>	APEX model execution	110
<b>60</b>	Digital elevation model (DEM)	115
<b>61</b>	Slope map	115
<b>62</b>	Aspect map	116
<b>63</b>	Drainage map	116
<b>64</b>	Stream order	117
<b>65</b>	Drainage density	117
<b>66</b>	Topographic wetness index	118
<b>67</b>	Stream power index	118
<b>68</b>	Land use/ land cover map	119
<b>69</b>	NDVI	119
<b>70</b>	Physiographic soil map of the watershed	120
<b>71</b>	The monthly average temperature of 2017 and 2018	132
<b>72</b>	The monthly average rainfall of 2017 and 2018	132
<b>73</b>	Monsoon rainfall - 2017	133
<b>74</b>	Maximum half-hour rainfall (I30)- 2017	133
<b>75</b>	Monsoon rainfall - 2018	134
<b>76</b>	Maximum half-hour rainfall (I30)- 2018	134
<b>77</b>	Scatter plot of max. and min. temp & near-surface temp	135
<b>78</b>	Scatter plot of rainfall & specific humidity	136
<b>79</b>	Estimated mean monthly maximum temperature (2011-2099) from the base period (1985-2014) for H3A2 scenario	140

### LIST OF ILLUSTRATIONS (Continued)

<b>80</b>	Estimated mean monthly minimum temperature (2011-2099) from the base period (1985-2014) for H3A2 scenario	140
<b>81</b>	Estimated average monthly rainfall (2011-2099) from base period (1985-2014) using H3A2 scenario	141
<b>82</b>	Estimated average annual rainfall (2011-2099) from the base period (1985-2014) using H3A2 scenario	142
<b>83</b>	Estimated mean monthly maximum temperature (2011-2099) from the base period (1985-2014) for H3B2 scenario	143
<b>84</b>	Estimated mean monthly minimum temperature (2011-2099) from the base period (1985-2014) using H3B2 scenario	143
<b>85</b>	Estimated average monthly rainfall (2011-2099) from the base period (1985-2014) using H3B2 scenario	144
<b>86</b>	Estimated average annual rainfall (2011-2099) from the base period (1985-2014) for H3B2 scenario	144
<b>87</b>	Percentage change in average annual rainfall (2011-2099) from the base period (1985-2014) for H3A2 scenario	146
<b>88</b>	Percentage change in average annual rainfall (2011-2099) from the base period (1985-2014) for H3B2 scenario	147
<b>89</b>	Elevation report of the watershed	149
<b>90</b>	ArcAPEX stream definition	150
<b>91</b>	ArcAPEX defined subarea	150
<b>92</b>	ArcAPEX subarea delineation	151
<b>93</b>	Detailed land use, soil, and slope distribution in each subarea	152
<b>94</b>	User-defined land use, soil, and slope in each subarea	152
<b>95</b>	Scatter plot of observed and simulated runoff (Calibration)	157
<b>96</b>	Box & Whisker plot of observed and simulated runoff (Calibration)	157
<b>97</b>	Scatter plot of observed and simulated sediment yield (Calibration)	160



### LIST OF ILLUSTRATIONS (Continued)

<b>98</b>	Box & Whisker plot of observed and simulated sediment yield (Calibration)	160
<b>99</b>	Scatter plot of observed and simulated runoff (Validation)	162
<b>100</b>	Box & Whisker plot of observed and simulated runoff (Validation)	162
<b>101</b>	Nash-Sutcliffe model Efficiency for surface runoff simulation	164
<b>102</b>	Scatter plot of observed and Sediment yield (Validation)	165
<b>103</b>	Box & Whisker plot of observed and sediment yield (Validation)	165
<b>104</b>	Nash-Sutcliffe model Efficiency for sediment yield simulation	167
<b>105</b>	Surface runoff from various subareas of Nano watershed (Gauged)	171
<b>106</b>	Sediment yield from various subareas of Nano watershed (Gauged)	171
<b>107</b>	Rainfall and simulated surface runoff from calibrated APEX model	172
<b>108</b>	Surface runoff from various subareas of Micro watershed	172
<b>109</b>	Sediment yield from various subareas of Micro watershed	172

## LIST OF PLATES

<b>Plate Number</b>	<b>Title</b>	<b>Page Number</b>
<b>1</b>	Aerial view and major streams of study area	44
<b>2</b>	Land cover types in the study area	69-70
<b>3</b>	Gauging station	88
<b>4</b>	Observed and downscaled mean maximum & minimum temperature and rainfall during 1985- 1999	137
<b>5</b>	Observed and downscaled mean maximum & minimum temperature and rainfall during 2000- 2014	139
<b>6</b>	ArcAPEX derived land use/ soil/ slop classification	151
<b>7</b>	Erosion features observed in the study area	168- 169
<b>8</b>	Conservation measures observed in the watershed	169
<b>9</b>	Erosion features observed in the study area	177

## LIST OF ABBREVIATIONS AND EXPANSIONS

<b>Abbreviations</b>	<b>Expansion</b>
AGCM	Atmospheric General Circulation Model
AOGCM	Atmospheric Ocean General Circulation Model
APEX	Agricultural Policy Environmental eXtender
AWC	Available Water Content
AWIFS	Advanced Wide Field Spectrum
AWS	Automatic Weather Station
CHNS	Carbon Hydrogen Nitrogen Sulphur
CN	Curve Number
CNIC	Curve Number Index Coefficient
CNRN	Curve Number Retention
DEM	Digital Elevation Model
DS	Dual Simplex
DTM	Digital Terrain Model
EBM	Energy Balance Model
ENSO	El –Nino in Southern Oscillation
FCC	False Colour Composite
GCM	Global Circulation Model
GHG	Green House Gas Emission
GPS	Global Positioning System
HadCM3	Hadley Centre Model 3
HSG	Hydrologic Soil Group
IMD	India Meteorological Department
IPCC	Intergovernmental Panel on Climate Change
LISS IV	Linear Image Self Scanner IV
MUSLE	Modified Universal Soil Loss Equation
NCEP	National Centers for Environmental Prediction
NDVI	Normalized Difference in Vegetation Index

NSE	Nash- Sutcliffe model Efficiency
OGCM	Ocean General Circulation Model
OLS	Ordinary Least Square
RCM	Regional Climate Model
RCP	Representative Concentration Pathways
RUSLE	Revised Universal Soil Loss Equation
SCM	Single Column Model
SDSM	Statistical Downscaling Model
SPA W	Soil Plant Atmospheric Water Continuum
SPI	Stream Power Index
TPI	Topographic Position Index
TWI	Terrain Wetness Index
USDA	United State Department of Agriculture
USLE	Universal Soil Loss Equation

## 1. INTRODUCTION

In the mountain environment of developing nations, soil erosion frequently hinders rural development and intensifies poverty by disruption of the productive capacity of highland agriculture and livestock raising. According to the United Nations Convention to Combat Desertification (UNCCD) land degradation has been defined as “any diminution or loss within the commercial or biological efficiency of the land due to human activities, accelerated by natural processes and thenceforth increased by the impact of biological diversity losses and climate change” (UNCCD, 1994). Global assessments about land degradation confirm that an increase in the highly degraded land from 15 per cent in 1991 to 25 per cent in 2011, and it is predicted that if land degradation continues to occur at the current rate over the next 25 years, it will reduce the global food production by 12 per cent (IFPRI, 2011). The entire land degradation process has enhanced throughout the last century, with an approximated depletion of twenty-four million tons of fertile topsoil, contributed by agricultural fields across the world (FAO, 2011). Thus, soil erosion is one of the significant causes of land degradation which involves a gradual process of removal of soil particles from land surfaces by runoff, thus, causing deterioration of soil and adversely affect the productivity of all natural ecosystems including agriculture, forest and rangeland (Lal and Stewart, 1990; Pimentel *et al.*, 1995).

As per the ICAR and NASS (2010), approximately 120.7 Mha of land is degraded. The most serious degradation problem in India is due to water erosion, bringing to loss of top soil and landform distortion. Soil erosion has been predominant in India for long, but with the growing population and over exploitation of natural resources, has taken the problem to a more significant extent. 94 Mha of land degradation is mainly due to water (NBSS& LUP, 2004). In India, the average soil erosion rate is 16 tons/ha/yr and leading to reduction of agricultural productivity. Nearly 5333 million tons of soil is removed annually and 29 per cent is diverted by streams into the ocean (Narayan and Babu, 1983). As mentioned above, soil erosion is a significant threat to both plain and high land agriculture.

Soil erosion affects water quality also. Recently, in an extensive study on the effect of soil erosion on crop yield, it was exposed that soil degradation because of water brought about a yield reduction of 13.4 million tons in oilseeds, cereals and pulses and a loss of US\$ 162 billion (Sharda *et al.*, 2010).

Himalayan region is suffering from severe problem of soil erosion and the rivers flowing through this region transport a huge pile of soil. All regions of the Himalayas, especially the Shivalik, which is considered as the lower regions of the Himalayas. The developments are topographically feeble, unsteady and henceforth extremely vulnerable to degradation. In Himachal Pradesh, 4.2 Mha area affected by land degradation, 2.8 Mha is due to soil erosion (NBSS&LUP-ICAR, 2005). As per Garde and Kothyari (1987) the soil erosion rate is 20 to 25 tons/ha/yr in the northern Himalayan districts. In Himachal Pradesh, Jammu and Kashmir and the north-western slopes of Uttar Pradesh, the north-eastern slopes of Bengal and the north-eastern states supply soil loss of 20 Mg/ha/yr. Lower regions of Doon Valley and the Himalayas contribute soil loss of 20 Mg/ha/yr (Singh *et al.*, 1992).

The decrease of forest area coupled with the change in monsoon pattern leads to a friable basin area vulnerable to massive water erosion and sediment yield from agriculture lands in the Himalayan regions (Valdiya, 1985). As per the Intergovernmental Panel on Climate Change (IPCC), it is predicted that the intensity and frequency of extreme rainfall events in the Asian monsoon regions are increasing and leads to flooding. Global warming leads to a more vigorous hydrological cycle, including more rainfall and more frequent high-intensity rainfall events (IPCC, 2007). As per Bharti (2015), Northwest Himalayan region may face dangerous precipitation events.

Soil degradation assessments state that the agrarian fields contribute more soil loss due to of higher rainfall scenarios and erosive power of runoff. The quantity and spatial extent of surface runoff and soil loss in a region depend upon several factors. The influential factors are erosivity, erodibility, slope, management practices and nature of vegetation. The effect of every component is not normally similar however it relies upon local, temporal and spatial features. Soil erosion

comprising removal of soil particles from the surface and transport by erosive agents. At this point when energy is sufficient, deposition occur. Soil erosion may occur due to two forces, either by rainfall energy or by runoff water. Hence rainfall intensity has a significant role in soil erosion. The most critical detaching factor is the rain drop. Because of rain drops striking on an exposed soil surface, soil particles may travel through the air to a few centimeters. Thus higher intensity rainfall can remove the vast amount of soil than lesser intensity rainfall.

Watershed is perceived as a perfect unit for the scheduling and improvement of vegetation land and water properties. Watershed management intends to generate an environment helpful for higher farming efficiency while sustaining natural assets. Information regarding the spatial distribution of soil erosion in a watershed is essential to tackle this problem properly. Henceforth the use of satellite remote sensing and GIS can help to study these problems. GIS plays a vital role in handling spatial data and processing. An environmental model interfaced with geographical information system delivers a tool to analyse the outcomes in a spatial framework. It can be used to solve problems and to provide meaningful answers in formats usable for decision-makers. A rapid and detailed assessment of erosion hazards can be effectively done by employing remote sensing and GIS data along with digital elevation models (DEM) (Jain *et al.*, 2000), by providing necessary inputs to various erosion models like USLE/RUSLE, MMF, WEPP, SWAT, ANSWERS, LISEM and APEX, which are having their specific characteristics and application scopes. Recently created models are interfaced with GIS and have risen as a useful tool in supervision spatial datasets. APEX (Agricultural Policy Environmental eXtender) is a recent model based on a spatial user interface.

Field research can be exorbitantly costly and laborious to perform across all probable landscapes, climate, management practice and cropping system combinations. The agrarian practices on soil and water quality at the watershed level can be studied using simulation models. These models have been widely applied to consider the effect of agricultural management practices. The models fluctuate in unpredictability, adaptability and provide various abilities in simulating

the horticultural system and consequently measuring the impacts of these systems over a variety of landscape, soil and climatic factors.

This research aims to quantify the climate change impact on soil loss of a watershed, which represents the highly erosion-prone Shivalik region. This region is in the relatively low altitude part of Himalayas and has high-intensity rainfall. Anthropogenic invasion and deforestation that occurred in recent years caused the loss of soil cover and nutrient-rich soil is directly exposed to rain. The slope of hills in this region is relatively higher and it enhances soil erosion and presently a few conservation measures are being adopted. In this situation, quantification of soil loss and determination of proper conservation practices are necessary. This study is an attempt to predict soil loss according to diverse future rainfall scenarios. It will facilitate the government and policymakers to plan conservation measures for this region.

This study is accomplished to predict future climatic scenarios and their influence on soil loss of a micro-watershed at the Shivalik region. The major objectives of the study are:

1. To characterize land use/ land cover and soil hydrological parameters in the watershed.
2. To analyze meteorological parameters and stream discharge of the watershed.
3. To simulate surface runoff and sediment yield using the APEX model at Watershed scale.
4. To predict future climatic scenarios and their impact on soil erosion.



## II. REVIEW OF LITERATURE

The current study aims to predict future climatic scenarios and its influence on soil loss of a micro-watershed in the Shivalik region. Prior research performed on this discipline is reviewed in this chapter.

### 2.1 CLIMATE CHANGE

The occurrence of climate change refers to seasonal changes over a long duration concerning the increasing addition of greenhouse gasses in the atmosphere. Tackling this trend is of crucial importance considering the critical role that climate plays in the formation of natural environments and the human economies and societies in which they are centered. According to United Nations Framework Convention on Climate Change, climate change refers to “a change of climate that is attributed directly or indirectly by human activity that alters the composition of the global atmosphere and that is in addition to natural climate variability observed over comparable time periods.”

Intergovernmental Panel on Climate Change (1992) states that the global average temperature will rise in the upcoming eighty years by way of about 2.4-5.1 °C above pre-industrial, with the best figure of 3.5 °C. Expectations of resultant changes in precipitation and wind patterns are significantly much less specific. IPCC (2007) report shows that precipitation intensity increases in IPCC climate models throughout the 21st century. When the severity increases, the number of dry days is often rising and soil moisture in many place decreases, including areas where precipitation rises (Tebaldi *et al.*, 2006; IPCC, 2007). Such patterns originate from decreased precipitation duration, higher intensity rainfall, runoff and increased evapotranspiration. Singh and Kumar (1997) studied rainfall anomalies in various ranges of the Sutlej and Beas basins in the north-western Himalayas, utilizing the station data with limited spatial and temporal resolutions. Authors perceived linear increase in annual rainfall but with an exponential decreasing pattern in the Greater Himalayan range with altitude.

The predicted future increases in Tmax under the emission scenario of A2, during the latter part of the 21st century suggest a surpass of +4 °C in many places of northern India. The most notable characteristic of the estimates is a rise in annual surface temperature during the year 2099, with an ensemble mean of +2 °C by mid-21<sup>st</sup> century and +3.5 °C by the end of the century. All simulations predict that rise in Indian temperatures well above the observed annual values over the last 100 years (Kumar *et al.*, 2011).

El Nino in Sothern Oscillation (ENSO) plays an important role in controlling the worldwide precipitation. Large-scale patterns of precipitation changes are related to ENSO events (Trenberth and Caron, 2000), the distribution and timing of floods and droughts are most profoundly influenced by the progression of El Niño events, especially in the tropics (Diaz and Markgraf, 2000). The effects of reflection rates on average albedo, surface force, wind drag, evaporation, soil moisture and precipitation patterns on the Himalayan grasslands on regional air circulation and hydrology. The changes in the Himalayan region have climatic effects and those changes have effects on global rainfall and temperature trends (Wang *et al.*, 2002). Raymo and Ruddiman (1992) state that, over the previous 40-Million-years uplift of the Tibetan plateau has reflected in stronger directions of the atmospheric Jetstream, greater intense monsoonal circulation and high rainfall on the front slopes of Himalayas.

Mountains are the world's water towers (Viviroli *et al.*, 2007), which also holds for Asia, where rivers are fed from the Tibetan plateau and neighbouring mountain ranges. Hydrologic processes in these areas are important for snow and glacial melting (Cruz *et al.*, 2007) and changes in temperature and precipitation are anticipated to affect the melt characteristics (Barnett *et al.*, 2005). The Indus and Brahmaputra show the greatest quantified changes. That is, Asia's water towers are threatened due to climate change. The impacts on irrigated agriculture and meltwater in the Indus and Brahmaputra basins are likely to be extreme due to the large population and intense water demand (Immerzeel *et al.*, 2010).

Influences of climate change is predominating in the Greater Himalayas (Beniston, 2003; Cruz *et al.*, 2007). The most commonly reported effect is the rapid glacier depletion, which has consequences for potential downstream water supplies (Barnett *et al.*, 2005; IPCC 2007). Continuing climate change would likely have additional negative effects across these mountains, such as enormous cascading effects on river flows, groundwater drainage, natural disasters and variations in biodiversity, morphology, structure and function of the ecosystem and human habitats (Parmesan, 2006; Ma *et al.*, 2009).

The significance of the fragile mountainous environment is described by the United Nations as “Mountains are important sources of water, energy, minerals, forest and agricultural products and areas of recreation. They are storehouses of biological diversity, home to endangered species and a vital part of the global ecosystem. From the Andes to the Himalayas and from Southeast Asia to East and Central Africa, there is serious ecological deterioration. Most mountain areas are experiencing environmental degradation.” (UN, 1992).

Nonetheless, Xu and Rana (2005) and Byg and Salick (2009), indicate that climate change-induced hazards at the rate and scale expected to increase in the Greater Himalayas and cannot be eradicated by a natural gradual adaptation process. People will act now to minimize potential negative effects. For example, floods are threatened by precipitation, but riverbank retaining walls, slope bio stabilization and terracing fields can minimize flood impacts. These interventions can also reduce the damage caused by landslides, rockfalls and mudflows. Mountain people have evolved fine-tuned social systems using conventional ecological skills and practices to cope with the risks involved.

Cayan and Riddle (1993) have highlighted that the impact of climate change on the hydrological response of the lower-elevation watershed is distinct than the high-elevation watershed due to the fact of the difference in their runoff distribution and different climatic regime. Chiew *et al.* (1995) reported that the responses of basins positioned in specific areas are not comparable under changed climatic

scenarios. Rapid and systematic improvements over very short distances in climatic parameters, temperature and precipitation (Becker and Bugmann, 1997) greatly enhance direct runoff and erosion.

Bharati (2015) notes that the frequency of catastrophic severe rainfall events is growing in the North-West Himalayan region. The estimated shift of the monsoon rainfall is significantly less certain according to Kumar *et al.* (2011). The ensemble members represent the yearly cycle of precipitation currently (1961-90) and future period (2070-2098), the present flanking duration of the monsoon is 65 per cent but Hardly Center ensemble members show that rainfall will increase by almost 20 per cent between May and October.

Climate change and variability have increased the function of management and research in agriculture. It is more essential than any other period and also the climatic factor, therefore it should be integrated into any program aimed for preserving and improving the agricultural sustainability of the north-western Himalayan region (Ives *et al.*, 1997).

### **2.1.1 Climate modelling**

A climate model is an attempt to organize the various climatic-driving processes. Such interpretation is carried out by representing the climate system in terms of physical, chemical and biological basics. A computational model may, therefore consisting of a set of equations which describing certain laws (McGuffie and Henderson-Sellers, 2005). Climate models use mathematical techniques to simulate the interactions between key climatic factors, which include atmosphere, ocean, land surface and ice. These are used for several purposes, from the study of climate system dynamics to future climate predictions.

**Energy balance models (EBMs)** are models of zero or one-dimensional nature. These models examine the alterations in the atmosphere framework from an assessment of the energy budget of the Earth. The basis for these EBMs to be carried by Budyko (1969). Their fundamental condition is based on the radiation budget.

That is, the changes in heat-storing are equivalent to the difference in incoming solar radiation and reflected terrestrial radiation.

**One-dimensional model** with a single-section temperature profile, radiative-convective (RC) model, displays radiative methodologies specifically a "convective change," reproducing a pre-determined lapse rate. To achieve a reasonable profile of the thermodynamic equation of temperature needs some more terms. A direct method to compensate this is, by utilizing convective change by Manabe and Strickler (1964).

**Statistical dynamical models** which manage surface processes and dynamics in a zonally averaged system and have a vertically settled atmosphere. These models have been the starting component for the association of reaction chemistry in worldwide models, are also utilized in some Earth Models of Intermediate Complexity. The 2D models have been utilized, among others (Saltzman, 1968; Kurihara, 1970) also defined in this model.

**Global circulation models (GCMs)**- The atmosphere and the ocean are combined in these models by three dimensions. These models are available for testing and evaluation by employing the coupled ocean-atmospheric models or 'coupled atmosphere system models,' as the independent ocean or atmospheric model distribution. These models intend to simulate the same number of approaches as attainable and produce a 3-dimensional image of the time advancement of condition of the ocean and atmosphere. GCM is made out of Atmospheric General Circulation Model (AGCM) and Oceanic General Circulation Model (OGCM). In light of the assessment of AOGCM projections of future climate change, interior fluctuation and the reaction to anthropogenic forcing are basic sources of expected predictability (Hawkins and Sutton, 2009).

The main coupled Ocean-Atmospheric GCM model worked by Manabe and Bryan (1969), a unique methodology for incorporation was utilized to keep away from the assessment of having two collaborating subsystems with various time scales. The coupled models are at the crude phase of advancement in

the last quarter of 20<sup>th</sup> century (Hasselmann, 1988); there are Regional Climate Models (RCMs), which make a consistent display as GCMs, nonetheless for a constrained region of the Earth. Since they spread a lesser area, RCMs can commonly be run more rapidly and at a higher resolution than GCMs. A model with a high resolution has smaller grid cells and subsequently can deliver climate information in more prominent for a remarkable zone.

Model simulation on the effect of climate change on streamflow fluctuate locally and between atmospheric situations, for the most part following anticipated changes in precipitation. In South Asia, HadCM3 demonstrates an expansion in yearly run-off going from 0 to 150 mm/year constantly by 2050, comparative with normal run-off for the period 1961-1990 (Shrestha and Aryl, 2011).

Global atmospheric general circulation models (GCMs) have been progressed to simulate the current atmosphere and have been utilized to predict future climate change. In spite of the fact that GCMs show huge capacity at the continental and hemispheric spatial scales and include an enormous level of the multifaceted nature of the global framework, they are intrinsically incapable to portray nearby sub grid-scale aspects and dynamics (Wigley *et al.*, 1990; Carter *et al.*, 1994).

### **2.1.2 Emission scenarios**

The worldwide climate models simulate the real environment and oceanic phenomena by essential physical conditions to predict future situations, we know that for each process there will be another option. Future climate can have a few options along these lines dependent on monetary development, ozone-depleting substance production and other socioeconomic components. These choices are well-organized by the Intergovernmental Panel on Climate Change (IPCC) and called a Scenario or, the more explicitly, Emission Scenarios.

In 1992, the IPCC provided a standard arrangement of Integrated Science (IS92) emission scenarios, that have been utilized in possibility of going before

evaluations, for example, the U.S. Global Change Research Program for local climate change impact evaluations (US-NAST, 2001 and IPCC, 1992). These situations exemplified a wide cluster of suspicious influences, how future ozone harming substance emissions would be developed without atmosphere strategies farther than those effectively embraced. The various scenarios that the conditions suggest, as far as monetary, social and natural conditions, differ widely and the resulting scope of conceivable ozone harming substance forecasts and navigates right around a significant degree (Leggett *et al.*, 1992; Pepper *et al.*, 1992). The premises for the IS92a and IS92b scenarios most eagerly take after and update those supporting the first SA90 scenario utilized in the First Assessment Report of the IPCC in 1990 (IPCC, 1990).

IS92 scenarios neglected to cover an agreeable scope of potential projections tending to disparage the results of a non-intercession approach towards climate change. In light of these issues, another arrangement of emission scenario had been acknowledged for use, by the IPCC in 2000. These are alluded to as the SRES scenario after the document entitled "Special Report on Emission Scenarios" (IPCC, 2000). The SRES scenario was worked to investigate future inclinations in the worldwide condition with an unmistakable reference to the creation of ozone harming substances and airborne antecedent emissions. The SRES team presented four case narratives illustrated in Fig. 1, such as A1, A2, B1 and B2, which explain the relations between ozone harmful sources and emissions and its production for broad and all-inclusive areas of the world in the 21st century. Every storyline represents social, monetary, mechanical and natural patterns that separate in progressively irreversible manners (Nakicenovic *et al.*, 2000). Besides, the two scenarios produce practically identical examples of climate change over the resulting not many decades and reliable with ongoing discoveries by Knutti *et al.* (2002); Stott and Kettleborough (2002).

By 2100, the entire radiative forcing (the combined calculation for human GHG emissions from all sources expressed in Watts per square metre), direction and degree are favoured and demarcated for four Representative Concentration

Pathways (RCPs). A broad variety of RCP outcomes, primarily based on a literature review, is selected for illustrating and are not forecasted or suggested (Van Vuuren *et al.*, 2011).

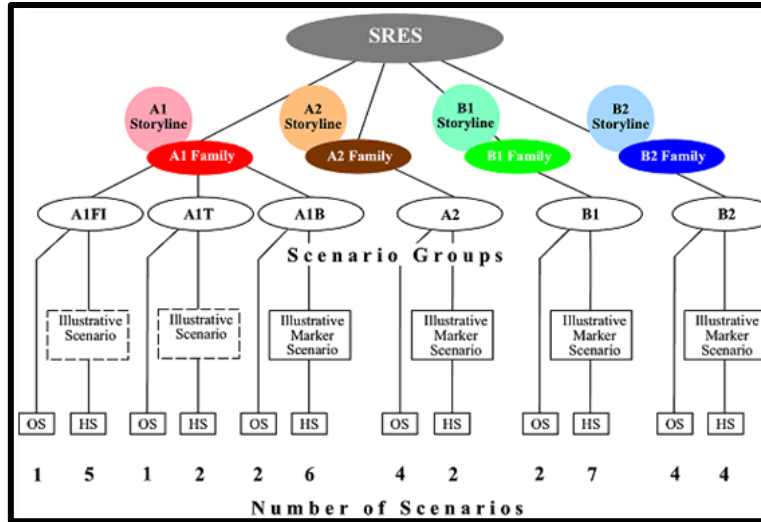


**Figure 1. Schematic diagram of SRES family storylines. Climate projections plotted in the Great Lakes report are these ensuing from the A1FI, A2, B1, and B2 scenarios (IPCC, 2000).**

The expression ‘representative’ means that each RCP offers one of numerous plausible situations that would prompt the exact radiative driving qualities. The term ‘pathway’ underlines that not the drawn-out focus levels are of intrigue, also the direction took extra time to accomplish that result. In outline, the new identical procedure starts with the choice of four RCPs, every one of which compares to a one of a kind radiative driving pathway. There are four RCP Scenarios, for example, RCP 2.6, RCP 4.5, RCP 6.0 and RCP 8.5.

As referenced above, these various scenarios have diverse applicability as indicated by the need. These scenario factors help us to downscale the climate parameters, for example, precipitation and temperature to our locale. Various parameters rely upon climate factors in every region, which will be distinctive for each, because of geology, landscape, nearby disseminations. From these, we find suitable indicator factors and predict our future climatic state for a specific period.



## 2.2 DOWNSCALING OF GLOBAL CLIMATE DATA

Downscaling is the normal name for a process of known data at large scales to predict at local scales. General or global circulation models (GCMs) simulate the Earth's atmosphere by the method of scientific conditions that characterize atmosphere, ocean and biotic processes, associations and contributions. They are the powerful tool that provide sensibly precise worldwide, hemispheric and continental scale atmosphere perceptions and are utilized to perceive present atmosphere and future atmosphere scenario under extended ozone harming substances. A GCM consists of multiple cell frames representing the degrees horizontal and vertical on the surface of the earth. The GCMs include: water vapours and cloud-atmospheric associations, the seasonal radiation, precipitation effect of the aerosols, snow-spreading, sea ice shifts, temperature capability in soils and sea surface, moist surface transitions, large transportation amounts of hot and cold across atmosphere and seas (Wilby *et al.*, 2009). Today, there is an enormous number of global climate models (GCMs) that can be used with distinctive emission circumstances for potential forecasts of climate change (IPCC, 2000).

Global Circulation Models (GCMs) are a chief apparatus utilized for future predictions of climate change, utilizing explicit emission scenarios. These are extensively used to anticipate the impact of climate change on the local precipitation pattern. The resolution of these models, for the most part around  $2^\circ \times 2^\circ$  with a grid dimension of around 100-500 kilometers. Besides, they are commonly compact at the temporal scale of the month to month, it is unsatisfactory for climate change assessments at the basin scale (Buytaert *et al.*, 2010; Mora *et al.*, 2014).

In any case, the GCM cannot be directly used in the regional level, because of the spatial resolution between the GCMs and hydrological models, but can be used to identify the hydrological effects of climate change at the watershed and the local scale. Downscaling is used to customise the performance of a GCM to the hydrological model. (Hashmi *et al.*, 2009). GCMs are also used in a global warming

account on water supplies in the world. GCM yields and hydrological models have largely been used to assess potential hydrological changes in the drainage basin during the latter decade (Roy *et al.*, 2001; Loukas *et al.*, 2002). These heterogeneities are critical for policymakers who need data on probable crop impacts, hydrology, species dissemination and with comparable resolution of 10-50 kilometers.

In synopsis, GCMs give quantitative assessments of upcoming environmental variation that are real at the worldwide continental scale and over extended periods. General Circulation Models (GCMs) provide the most reliable simulation of the worldwide atmosphere system and they give present and future time arrangement of atmosphere variables for the entire globe (IPCC, 1999; Prudhomme *et al.*, 2002). Different analysts have assessed downscaling strategies intended to overcome any issues, particularly as far as their capability to replicate surface temperature and precipitation (IPCC, 2001; Leung *et al.*, 2003).

Dynamic and statistical are the two vital ways for handling of downscaling atmospheric data. Dynamic downscaling calls for high-resolution atmosphere models in territorial subspace, the use of reduced-resolution model performance as a restricted region (Wilby *et al.*, 2004; Chu *et al.*, 2010; Karamouz *et al.*, 2010).

### **2.2.1 Dynamical downscaling**

It relies on the use, in its designs yet with high resolution, of a regional climate model (RCM) like a GCM. RCMs use vast atmospheric information from GCM 's parallel production and incorporate increasingly complex geology, land-ocean differentiation, surface heterogeneity and point-by-point physical methods to deliver realistic atmospheric data at a spatial resolution of approximately 20-50 kilometers.

Much the same as GCMs, RCMs experience problems in accurately replicating convective precipitation, which is the most vital challenge for tropical locales. Most RCMs likewise do not properly simulate extreme precipitation, a

precise inclination that can exacerbate as the resolution is extended. Realistic tendency rectifications regularly accomplished to all the more likely match the model output to the perceptions (Brown *et al.*, 2008). At times, acceptable changes to the convective arrangements can upgrade the authenticity of predicted precipitation, notwithstanding, these modifications require tremendous skill and restricted geographic movability and they make a variant of the model that is properly acclimated to a particular region, however that may also perform ineffectively somewhere else.

Dynamical downscaling needs high computational resources, skill and high volume of information as inputs. It, as a rule, applies to state or regional level evaluations with huge government assistance and possessions (Fowler *et al.*, 2007; Wilby *et al.*, 2009). An investigation led by Hellstrom *et al.* (2001) at Sweden demonstrated that the measurable downscaling model and the RCM are more skilful than driving GCMs in simulating the seasonal precipitation cycle. Both statistical and dynamical downscaling models show around equivalent proficiency in impersonating the seasonal precipitation cycle.

### **2.2.2 Statistical downscaling**

It involves the basis of experimental connections among observed present-day enormous scale atmospheric variables and neighbouring atmosphere factors. Once a relationship is chosen and accepted, future atmospheric factors used to forecast future local atmosphere factors by GCMs. Statistical downscaling can provide site-explicit projections of the atmosphere, which cannot be done by RCMs since they are computerized with a spatial resolution of 20-50 km.

As indicated by the strategies associated with its application, the statistical downscaling strategy can be partitioned into three classifications, be specific, weather generator, climate composing and scenario generator (Wilby *et al.*, 2000). Weather generators are information intensified, require long groupings of every day information and are sensitive to lacking or wrong information in the alignment set (Wilby *et al.*, 2009). Also, some weather generators can represent the coherency

among factors when two or three factors are anticipated, for example, to produce an everyday sequence of insolation that the coordinates created day by day arrangement of wet and dry days. Yet, weather generators have significant use for crop-yield, water and distinctive natural resource modelling and management. (Fowler *et al.*, 2007; Wilby *et al.*, 2009).

The statistical downscaling models have essentially founded on the main theory that, regional climate is for the most part influenced by the method of the global scale circulation models (von Storch, 1992; 1999) and the relationship between the predictor and the predictand factors is invariant under future atmosphere situations. This methodology is based on the fundamental premise that there are precise relation between a present widespread circulation and the local environment under various driving conditions of possible future climates (Zorita and von Storch, 1999). It is unknown if current observable relations between huge and local influences in the environment will be preserved later on.

For statistical downscaling, there is a variety of techniques available- of these methods has specific virtues and limitations in keeping with working standards of technique operation (Xu, 1999). Dynamic downscaling strengthens the local display components and offers better predictors for comparative observable downscaling to a higher resolution (Guyennon *et al.*, 2013).

Statistical downscaling strategies are computationally more affordable as contrasting to RCMs that require complex modelling of physical procedures. In line with these, the foundations do not have the computational capacity and the skills needed for dynamic downscaling, they are successful and often invaluable decision. In any methods observable atmospheric data can provide station-scale data such as RCMs that can generate downscaled estimates of 20-50 kilometers in size.

Statistical downscaling methods are for the most part esteemed to be remarkably helpful for the reproduction of extreme occasions of precipitation (Wilby, 2000). Then again, the recurrence and force of extreme precipitation occasions are entirely plausible to go under the effect of conceived climate change

in many portions of the globe (IPCC, 2007) therefore representing the risk of prolonged floods and dry seasons. In this circumstance, hydrologists need to depend on these measurable downscaling instruments that are similarly proficient for simulating climate.

### **2.2.3 Statistical downscaling model (SDSM)**

General Circulation Models (GCMs) show a rising amount of ozone-depleting substances will have fundamental ramifications for the atmosphere at worldwide and local scales. Lamentably, GCMs are restricted in their value for nearby examination with the aid of their coarse spatial resolution (50,000 km<sup>2</sup>) and lack of ability to determine imperative sub-grid scale resolution, for example, clouds and topography. Statistical downscaling systems have a few handy advantages over dynamical downscaling approaches. In circumstances where ease, quick evaluations of confined climate change impacts are required. It permits the improvement of climate change scenarios for remarkable locales at every-day time scales by the use of grid resolution GCM outcomes.

The SDSM, created by Wilby *et al.* (2002), is a choice to support tool for evaluating the effect of regional climate change. SDSM is a combination of a stochastic weather generator approach and a transfer function model requesting two kinds of the daily information. The principal kind relates to nearby predictands, for example, temperature, precipitation and the subsequent types compares to the data of huge scope predictors, for example, NCEP and GCM of a grid box nearest to the investigation region. Connection and major relationship assessment are done in SDSM, between the predictand of action and predictors to select a lot of indicators generally relevant for the site being referred (Wilby *et al.*, 2002). SDSM works well for downscaling precipitation (Wilby and Dawson, 2013), and can establish observed data behaviours.

SDSM can assess interannual fluctuation better than other statistical downscaling techniques (Wilby and Dawson, 2013). Multilinear equation is utilized to infer a statistical connection among the predictors and the predictand

(Wetterhall *et al.*, 2006). It is a combination of multiple linear regression (MLR) and the stochastic weather generator (SWG), the downscaling procedure techniques Wilby *et al.* (2002) and is a promising and well-performing statistical downscaling model. Two or three similar exploration (Tang *et al.*, 2016; Hassan *et al.*, 2014) have demonstrated that the SDSM is generally simple to run and work, and it has been comprehensively used through the world. Huang *et al.* (2012), led an examination at Yangtze basin inferable from its most phenomenal ability.

These models should be related to long and precise meteorological records and the relationship between broad and regional scales should be acknowledged. Besides, in the long run, decreased results depend on the quality of GCM contributions (Vrac and Vaittinada, 2017). Past research has shown that there are sensitive measurements on the day to day temperature (Liu *et al.*, 2007) total precipitation (Wetterhall *et al.*, 2006; Hashmi *et al.*, 2011) using the Statistical Downscaling Model (SDSM), by Wilby *et al.* (2014).

Noori *et al.* (2014) declared that in a comparable study among SDSM and LARS-WG, both the models display practically identical results for simulating present-day extreme events of precipitation. Future precipitation recurrence examination, because of the downscaled information of both the models, gives two particular pictures. As downscaling tools, the result obtained can be taken with fair confidence to analyse future climate change impact assessments.

An investigation led by Pervez and Henebry (2014), at the Ganges–Brahmaputra basin shows that, aligning and approving SDSM with NCEP re-analysis information and observed information and the observed precipitation can be sensibly replicated at the sub-basin level, which connotes reasonableness of SDSM in these information meagre situations. The downscaled results of CGCM3.1 showed that the precipitation system in the two basins would be essentially influenced by climate change.

A few studies using SDSM in the Indian subcontinent were performed by Meenu *et al.* (2013) and Mahmood and Babel (2013). The daily Tmax, Tmin and

precipitation were reduced by the hydrological effect of climate change in Tungabhadra River Basin, India, and Jhelum Basin, in Pakistan and India, by the Hadley Center Coupled Model indicators, version 3 (HadCM3) under A2 and the B2 scenario.

Singh *et al.* (2015) have studied two global climate models (GCMs) - CGCM3 and HadCM3 which are used for the prediction of the potential maximum temperature (Tmax), the minimum temperature (Tmin) and the precipitation in part of the Sutlej River Basin in the north-western Himalayan region of India, and this study states that the monthly sub-model of SDSM is capable in downscaling of maximum and minimum temperature as high correlation ( $R^2 > 0.80$  for Tmax and  $R^2 > 0.90$  for Tmin for calibration periods and  $R^2 > 0.77$  for Tmax and  $R^2 > 0.89$  for Tmin for validation period, is acquired between downscaled and observed data.

An investigation of soil erosion and classification of soil carbon, carried out by Gupta (2015) in mid-Himalayans for A2, B2 scenarios. The results of the experiment summarised as, the statistical downscaling model (SDSM) were used to downscale the atmospheric factors (Tmax and Tmin. temperatures, precipitation) from coarse target GCM data to fine resolution in the nearby region. The downscaling of the coefficient of temperature ( $R^2 = 0.91 - 0.99$ ) and precipitation ( $R^2 = 0.71- 0.80$ ) was obtained. For temperatures and precipitation, RMSE was evaluated separately in the range 0.89-1.52 °C and 27 mm-50 mm.

In a part of the Narmada basin in Madhya Pradesh, India to have future impacts from climate change for soil degradation, Mondal *et al.* (2015) predicted future precipitation by the downscaling general circulation model (GCM, HADCM3) the LS-SVM and the SD SDSM have been used for downscaling and the Universal Soil Loss Equation (USLE) model has been used for soil loss assessment. The findings have been analysed with various slope, land use, and soil class. The result showed a rise in future precipitation with an increase in soil decay. The rate of progress in SDSM, soil loss in the 2050s and 2080s is 15.52 per cent and 105.80 per cent and decreases by 8.51 per cent in the 2020s.

As a tool to downscale climate information in the upper Godavari stream basin, Saraf and Regulwar (2016) used SDSM downscaling model. To extend future maximum temperatures (Tmax), minimum temperatures (Tmin) and precipitation, two Global Climate Models (GCMs), CGCM3 and HadCM3 were used. The scattered plot and other statistical techniques were used to check the disgusting quality of the forecast. For almost all the situations for both GCMs, the maximum temperatures increase. Furthermore, reduced future precipitation shows increasing trends for all circumstances.

These significant studies proved that statistical downscaling by SDSM software is capable of predicting future climate scenarios of global scale as well as Indian subcontinent. In most of the studies, the R<sup>2</sup> value shows dependable results. The simplicity of SDSM software helps us to synthesize a large amount of climate data.

### 2.3 SOIL EROSION

Soil degradation is a perplexing process that depends upon soil properties, slope, vegetation, precipitation amount and energy. Changes in land use are widely affect soil degradation (Ursic and Dendy, 1965), and it has some time been perceived that degradation over soil formation would in this manner bring about the decreased agricultural potential (Pimentel *et al.*, 1987). The US economy is threatened with soil degradation of 30 billion dollars (Uri and Lewis, 1998) to 44 billion dollars a year (Pimental, 1993). The UK's annual budget is measured at £ 90 million (ECA, 2002). In Indonesia, the expense in Java alone amounts to US\$ 400 million annually (Magrath and Arens, 1989).

The net effect of soil loss is loss of productivity, which brings the expanded use on composts to keep up the yields. When manure is used to compensate for the loss of fertility, arising out of the Zimbabwean soil degradation, this will lead to an annual expense of 1500 million USD (Stocking, 1986), a considerable expense of the financial system for that nation in general. In India, the annual cost of land degradation by use of land is estimated at US\$ 5.35 billion in 2009. Kerala,



Rajasthan, Andhra Pradesh, Orissa and Madhya Pradesh are the most notable of those expenditures (Mythili and Goedacke, 2016).

The essential components liable for soil erosion incorporate precipitation, soil type, vegetation and geographical and morphological qualities of the basin. (Kothyari and Jain, 1997). As indicated by Horton (1945), if precipitation force is significantly less than the invasion limit of the soil, no surface runoff happens, and the infiltration rate rises to the precipitation power. On the off chance that the precipitation amount surpasses the infiltration limit, the overabundance surface runoff occurs (Morgan, 2009). The effect of precipitation power is delineated by utilizing the information for 183 rainfall occasions at Zanesville, Ohio, in the range of 1934 and 1942, which show that normal soil loss per rainstorm events will increase with the energy of the rainfall (Fournier, 1972). Soil degradation has become a lot of consideration as of late, for the most part in developing nations. In India, enormous government programs have dedicated to advance soil protection, yet the results have been disillusioning as appropriation and conservation of accessible preservation revolutions have been constrained (Kerr and Sanghi, 1992).

Roose (1967) surveyed Senegal, has shown that 68 per cent in rainstorms of 15-60 mm occurred somewhere between 1959 and 1963, which occurs about 10 times a year. Mid-Bedfordshire, England (Morgan *et al.*, 1986) found that 80 per cent of disintegration occurred between 1973 and 1979 in the span of 13 rainstorms, which resulted from a 57.2 mm storm, with the most significant soil loss. These rainfalls have a recurrence of somewhere in the range of two and four times each year. It shows that high-energy storms pick more soil degradation.

All things considered, soil degradation causes a decrease in soil productivity (Stone *et al.*, 1985) and significant environmental destruction by draining soil biodiversity and influencing crop formation (Lal, 1991). The seriousness, recurrence and degree of degradation will be modified legitimately by changes in the sum and power of both precipitation and wind and in a roundabout way by changes in vegetation cover and soil organic matter (Valentin, 1998). The most

serious problem in the catchments of these streams is sheet and rill erosion. The horticultural formation of the basin Chambal and Godavari (Verma *et al.*, 1968), therefore, is widely influenced by red soils, which extend an area of 720 000 km<sup>2</sup>. Lately, as a major aspect of land degradation evaluation strategy for tolerable agribusiness and advancement, soil degradation large progressively distinguished as a risk that is increasingly extreme in mountain territories (Millward and Mersey, 1999; Angima *et al.*, 2003).

Soil loss levels are typically expressed in units of mass or volume per unit of the time zone. In normal conditions, 0.0045 t/ha is applied at the annual level for modest assistance regions and 0.45 t/ha for steep region. The agricultural land values are examined for 45-450 t/ha (Young, 1969).

Soil disintegration and the related degradation of land resources are massively noteworthy spatio-temporal phenomena in numerous nations (Fistikoglu and Harmancioglu, 2002; Hoyos, 2005). Soil degradation, for the most part, identified with horticultural practices in tropical and semi-arid nations, prompts a decrease in soil fertility, on an assortment of negative impacts of ecological issues, and has come to be a danger to reasonable agricultural production and water quality in the area. Two billion hectares are measured for the land area that is vulnerable to human degradation. Thus the soil-degraded land zone is measured at 1100 Mha by the disintegration of water and 550 Mha by wind erosion (Saha, 2003).

The cycle of intense soil degradation in sandy areas, gorge and mountain ranges, cultivated waste land, deserts and water logging is affecting about 130 million hectares of soil in India (Kothyari, 1996) i.e. 45 per cent of the total geological surface terrain. Exorbitant soil degradation brings about a high rate of sedimentation in the supplies and diminished fertility of the soil. Soil degradation brings about loss of valuable soil assets for development (Kothyari, 1996; Jain and Dolezal, 2000). In India, about 53 per cent of the entire land is prone to degradation. Every year, 5334 Mt of soil (16.4 t /ha) are separated, of which 29 per cent are

separated into the ocean by waterways and 10 per cent are held in repositories which trigger a gigantic loss in fertility. (Narayan and Babu, 1983).

It is estimated that approximately 167 Mha of the total topographical area of 329 Mha in India was affected by heavy water and wind disintegration. It consists of 127 Mha affected by soil degradation and 40 Mha impaired by gullies, changing cultivation and salinity, shifting river flows, water logging and desertification (Das, 1985).

Singh *et al.* (1992), studied that 64 million ha in Karnataka, Andhra Pradesh, Madhya Pradesh and Maharashtra states, have reported that erosion levels in the black soil region (vertisols) of the country were 20 Mg/ha/yr. Besides, soil losses of 10 to 15 Mg/ha/yr have been reported on red soils in Chhotoanagpur district. In addition to 20 Mg/ha/yr, these are more common on the north-west banks of Jammu and Kashmir, Himachal Pradesh, Uttar Pradesh and the northeast slopes of Bengal and the northeast. 20 Mg/ha/yr of soil loss produced in the lower regions of the Himalayas and the Doon Valley. Alluvial soil erosion rates in the Punjab, Haryana, Uttar Pradesh, Bihar and Western Bengali Alluvial Indo-Gangetic Plains are mild (5-10 Mg/ha/yr); and these plains, in salt and soil, have a 5 Mg/ha/yr reduction.

As per the NBSS&LUP (2004), around 146.8 Mha is degraded. Water erosion is the most extreme degradation problem in India, bringing about soil loss and land distortion. Because of the first assessment of existing soil loss information, the normal soil erosion rate is ~16.4 ton/ha/year, following in a yearly complete soil loss of 5.3 billion tons throughout the nation (Narayan and Babu, 1983). About 29 per cent of absolute disintegrated soil is forever lost to the ocean, while 61 per cent is moved to start with one area then onto the next, and deposited 10 per cent in reservoirs.

The entire Himalayan region has been stressed with a serious problem of erosion of the soil and waterways and transports a tremendous amount of sediments through this area. The Himalayan and Tibetan regions only occupy approximately five percent of the surface of the Earth, and they are versatile in their surroundings

(Raymo and Ruddiman 1992). The delicate catchments have been vulnerable to runoff and the top soil loss found by rivers, as a result of a loss of forest cover, combined with the effect of monsoon precipitation (Valdiya, 1985).

Shivalik districts yield a lot of sediment to Sukhana Lake in Chandigarh (Misra *et al.*, 1975). It is because of high erosion in this locale, even though a few ranges of Shivalik's are vegetated as well. Higher erosion is the after effect of profound vertical rills, which leave islands in the bed of a gully. In this way, an accepted normal soil erosion of 80 Mg/ha is assessed for the Shivalik region. The deterioration and erosion of soil in Shivalik Hills, Hoshiarpur, Punjab State, have caused desertification of the land. In 1852, 2000 km<sup>2</sup> were degraded here and in 1939, the number increased in 1981 to 20,000 km<sup>2</sup> (Patnaik, 1981).

Singh *et al.* (1992) recorded that for the dense forests, cold snow-capped deserts and the arid zone of western Rajasthan, the annual water erosion levels competed from significantly lower than 5 Mg/ha/yr on the Shivalik slopes. Soil loss exceeding 40 mg/ha/yr is also found on the river banks of the Yamuna, Chambal, Mahi, Tapti and Krishna, and in the developing regions of Orissa and the north eastern states. In the Western Ghats, the yearly disintegration rates ranged from 20 to 30 Mg/ha.

### **2.3.1 Soil erosion modelling**

Soil erosion is one of the critical hazards to farming efficiency and ecological quality, explicitly water and soil quality. Arranging and execution of controlling soil protection the erosion control measures are needed. An immense variety of soil erosion models have been created in the past, each contrasting as far as accuracy, complexity, inputs and outputs, processes and their spatial and temporal scales. Commonly, since the physical process are simulated by the model, various kinds of models can be ordered into four.

1. Empirical Models
2. Physically Based Models
3. Conceptual Models, and
4. Hybrid Models

#### *2.3.1.1 Empirical models*

Empirical models simulate the systematic process and largely dependent on statistical properties and regression connections. Besides, it is essential to be referenced that the innate non-direct relations in the catchment framework (Wheater *et al.*, 1993).

The USLE (Universal Soil Loss Equation), established in the mid-1960s, was produced for cropland (Wischmeier and Smith, 1965). Later it was drawn out to various land uses (Wischmeier and Smith, 1978), which is still routinely utilized. The USLE is an index-based, observationally inferred model. The expediency of USLE technology to predict erosion, with revised modifications of this model (Renard *et al.*, 1997), by organizing new data, made available by exploring the last 40 years, to further enhance the including of additional details and consolidating recent research findings (Renard *et al.*, 1994).

#### *2.3.1.2 Physically based models*

Such models are generally based on the principle of mass, momentum and energy conservation, as control conditions that represent stream flow or overland streaming and sediment load management (Bennett, 1974; Kandel *et al.*, 2004). In physically-based models, numerical articulations which are derived from particular processing, have several assumptions that may not be important in much of the natural environment (Beven, 1989). Beven (1991) observed that physically based models are equivalent to any conceptual model.

In the mid-1980s for the Limburg Provincial Government (De Roo *et al.*, 1996), the Limburg Soil Erosion Model was established (LISEM). The effect on the position of common erosion conservation features, such as grass bunds (Jetten and De Roo, 2001), and space-dependent modifications in cultural practices was generated for the most part by LISEM.

Smith *et al.* (1995), developed a model for event-oriented, deterministic and physically dependent, is the KINEROS model for the USDA Agricultural Research Service. Runoff is measured using the Hortonian approach, and Smith and Parlange (1978) method was used to estimate the infiltration.

WEPP (Flanagan and Nearing, 1995) is a reliable process based model created by the USDA-ARS for hillslopes and watersheds. WEPP has the benefit of at least 100 spatially measured soil loss alongside a soil profile and deposition can also be anticipated as a basic Universal Soil Loss Equation (USLE) (Wischmeier & Smith, 1978) over other existing models. The WEPP (GeoWEPP) spatial interface model is also available.

### 2.3.1.3 Conceptual models

Conceptual models are a mixture of empirical and physical models and are increasingly important to address general queries of erosion (Beck, 1987). These models have been created dependent on spatially-lumped types of water and the soil condition (Lal, 1994). The estimation of every parameter in conceptual models are obtained through orientation against observed information, for example, runoff and sediment yield estimations (Abbott, 1986). Along these lines, because of this necessity, conceptual models tend to have recognizability issues of their parameter value (Jakeman and Hornberger, 1993).

This model originally established to investigate the impact of soil erosion on soil productivity, an Erosion-Productivity Impact Calculator (EPIC) model, developed by Williams *et al.* (1984). It has been used as part of the study of the Convention on Soil and Water Supplies in 1977. The model hydrology module

predicts a surface runoff of daily precipitation with an equation Curve Number (CN) Soil Conservation Service (SCS) (USDA, 1972).

Another conceptual model that is frequently under processing and mostly used around the world is the Soil and Water Assessment Tool (SWAT) model. The model is a global, continuous, semi-disseminated river basin centered model on processes. It was developed to assess the impact on water resources and non-point-source pollution in the large riverbed of selected management practices. The design of SWAT is a continuation of the USDA Agricultural Research Service (ARS) which shows the experience of more than 30 years. In anticipation of the landscape sediment yield, uses the Modified Universal Soil Loss (MUSLE) equation (Williams and Berndt, 1977).

#### *2.3.1.4 Hybrid models*

Hybrid models represent a combination of methods to measure soil erosion. The framework of the hybrid model is usually physical or logical in nature, while the model is largely based on empirical assumptions and relies on proven regression relationships in space and time scales. The hybrid models that apply physical and measured soil erosion procedures and models of sedimentation systems. It can be used to predict an environment vulnerable to the erosion of water and find the decline in soil productivity at slope lands, catchments and farms.

SedNet is a mean annual model that produces slope, soil, ravine and bank erosion on an annual basis. A promising method for gauging source and transport of sediment at catchment scales is given by a Sediment River Network Model (SedNet) (Prosser *et al.*, 2001). It is expected that the SedNet model will be implemented at the first-order streams (Shreve, 1966), typically with 25-50 km<sup>2</sup> contributing areas and streams with a length of 10 km.

The Morgan - Morgan - Finney model (Morgan *et al.*, 1984; Morgan, 2001) is a concept that is being used in a wide variety of different circumstances in the fields of land, hillslopes and small-field areas, including Malaysia (Morgan and

Finney, 1982), Indonesia (Besler, 1987), Nepal (Shrestha, 1997) Changes from further refinements to soil deposition methods, which involve the effects of vegetation structure, are as effective as reproducing soil diffusion processes for each soil particle (Lilhare *et al.*, 2014).

### **2.3.2 APEX (Process-based model)**

The Agricultural Policy Environmental eXtender (APEX) model has been developed for use in farm/watershed management. The model was developed to test a variety of land approaches on sustainability, disintegration, financial, availability and quality of water, soil quality, competition from plants, environment and pests. The management facilities include water services, diking of the furrows, buffer strips, harvesting, fertilizing, lagoons, application of pesticides, grassing, and planting. APEX can be used to determine the effect of the changes in the climate/CO<sub>2</sub> of Earth, the structuring of environmental secure local monetary sites, preparation of biomass for energy and various side project applications. The model operates on a daily basis and is capable to replicate for several years (Williams and Izaurralde, 2006).

The progressing advancement of APEX is resulting in user's manuals (Williams *et al.*, 2005; 2006) and complete hypothetical representations (Williams and Izaurralde, 2006; Williams *et al.*, 2008). Gassman *et al.* (2009) provides a total survey of APEX applications as brief portrayals of a few GIS and other interface tools that have been created to help elements of the model. Other elements of APEX enclose an examination of BMPs for a 104 km<sup>2</sup> watershed in north-central Texas (Wang *et al.*, 2011b), the definition for various BMPs and the sediment transport proportions for APEX simulation of Upper Mississippi River Basin (UMRB) local demonstrating tool (Wang *et al.*, 2011a) created for the USDA-NRCS National Conservation Effects Assessment Project (Duriancik *et al.*, 2008), the impacts of agroforestry buffers on diminishing runoff and sediment loss from four small grazing field watersheds in north-central Missouri (Kumar *et al.*, 2011).



A research carried out by (Kumar *et al.*, 2011) the Center for Comprehensive Water Control (CWC) compared runoffs and sediment losses from agro forestry (Agb) watersheds. APEX models were calibrated and validated for runoff and sediment loss during the years 2002 to 2008 with the runoff and sediment data. The simulations had been tested for ten years after the calibration and testing of the software it was run for a long-term analyse. The width of the buffer influenced the runoff considerably. When the buffer width has increased, the Runoff will decrease by 24 per cent.

In the USDA Deep Loess Research Station, near to Treynor, Iowa, the APEX model was utilized to determine the long-term outcomes of the ridge-till and conventional tillage in two watersheds. The software has been carefully calibrated and tested. Scenario studies showed that sediment losses can be decreased by 36-39 per cent and accumulated organic soil carbon loss from sediments by 63-67 per cent, using ridge-till as a replacement for traditional tillering in two watersheds. Even the transition from traditional tillage to ridge tillage was expected to increase the minimum average annual yield of maize grain by 3.8 per cent. The overall output in both watersheds indicates the ability for an erosion-prone site to use conservation tillage to minimize runoff and sediment losses for sustainable agricultural productivity (Wangs *et al.*, 2008).

The research carried out by Yin *et al.* (2009) at Central Huaihe River watershed, China shows that the  $R^2$  range from 0.56 to 0.98 for the calibrated time frame. The adjusted APEX model followed the fluctuation of the day by day runoff and sediment yield well for the validation time frame,  $R^2$  extends between 0.55 and 0.85. The goodness-of-fit tests show that the APEX model has sensibly explained the individual variations within the values observed. APEX is a well fitted method for the evaluation of runoff and soil erosion for different management activities.

An ArcGIS APEX (ArcAPEX) interface which, in addition to the integrated APEX-SWAT scenarios, supports the development of both standalone APEX and SWAT simulations (Tuppad *et al.*, 2009). It provides an analogous overall

modelling provision in SWAT and benefits from the enhanced options included in the ArcGIS platform. ArcAPEX provides its ability to build and replace alternate crop management operation schedules and permissible integration solutions with the Soil and Water Assessment Tool (SWAT) for wide-ranging simulations. The core components for the ArcAPEX interface are implemented including watershed delineation, land use and soil assessment, climate details, input boundary specification, executive model run, and combination of SWAT models.

Tuppad *et al.* (2009) depicted the ArcGIS interface for APEX model and its application in the small scale watershed to consider the water quality effects of a range of agricultural conservation practices in Texas. They likewise observed the possibility to apply APEX inside Arc APEX for simulation of complex agroforestry frameworks in Southeast Asia including tree crops and vegetables. APEX also allows helpful assessment of a scope of frameworks, which incorporates porches, grass conduits, strip cropping, and so forth. (Williams, 2008). Likewise, APEX's capacity to simulate the impact of sediment yield in the soil profile on over land flow and soil losses makes it a perfect tool to distinguish best management practices for specific soil, atmosphere, topography and the management combinations.

Tripathi and Gosain (2013) are conducted studies on APEX in India, which highlight the use of GIS and APEX watershed management systems in the Salasi watershed, Himachal Pradesh, India. Although the model could not be calibrated against the observed stream, the pattern in simulating every day stream followed the pattern in observed precipitation, which brings up that the system can be utilized to show the relative changes in stream segment under particular protection practices as opposed to this basin. This APEX model being an increasingly proper tool for watershed at the field or smaller scale because of the capacity of APEX model to simulate water balance at the higher spatial resolution, for example at field/plot level.

A process-based model was used for estimating watershed surface runoff, soil erosion and nutrient depletion in the lesser Himalayas of Dehradun, Langha, by

Singh (2012). APEX model is well predicted for the surface runoff of pasta micro-watershed ( $r = 0.88$ ), the loss of sediment ( $r = 0.88$ ) and nutrients, TC ( $r = 0.69$ ), TN ( $r = 0.71$ ) and P ( $r = 0.77$ ) for the watershed. Runoff has been predicted very accurately for low and medium rainfall but high rainfall events it was over predicted. Over prediction may be attributed to the unaccountable conservation measures and practices which had been not accounted for by the model. Similarly, sediment loss was estimated daily at the watershed scale and was well predicted for low and medium rainfalls but under estimated for high rainfall events. The area is susceptible to landslips at high rainfalls, which is not accounted for by the model. It may be the cause of under prediction of sediment loss by APEX model. APEX model used to help identify the critical source area for soil erosion. Average annual soil loss was estimated by the model for each HRU representing critical source area. Average annual soil loss was predicted highest in HRU consisting barren/open scrubland with excessive slope ( $>50\%$ ) accompanied by maize cropland in the upper region of the catchment with a soil loss of 39 tons/ha/yr and 30-35 tons/ha/yr, respectively.

These studies regarding APEX proves that APEX is capable of simulating the various hydrologic process at the watershed scale.

#### 2.4 CLIMATE CHANGE IMPACT ON SOIL EROSION

A great part of the increase in precipitation that has been observed worldwide as huge precipitation events (Easterling *et al.*, 2000; IPCC, 2001). For instance, Karl and Knight (1998) states that from 1910 to 1996, total precipitation over the US increased and that 53 per cent of the increase originated from the 10 per cent of precipitation events (the most extreme precipitation). Atmosphere models are anticipating a continued with increase in extreme precipitation events during the 21st century (IPCC, 2001). Soil degradation rates may likewise be relied upon to change in light of the climate for an assortment of reasons, the most immediate of which is the change in the erosive intensity of the precipitation (Favis-Mortlock and Savabi, 1996; Pruski and Nearing, 2002). Soil erosion reacts both to the total

amount of precipitation and to varies in precipitation power. Nonetheless, the predominant variable is by all accounts precipitation power and energy instead of precipitation amount alone. Pruski and Nearing, (2002) anticipated that for each 1 per cent expansion in total precipitation, erosion rate would increase by 0.85 per cent if there had been no increase in precipitation power. Be that as it may, if both precipitation amount and energy were change, anticipated disintegration rate will be expanded by 1.7 per cent for each 1 per cent expansion in absolute precipitation.

A research was carried out by O'Neal *et al.* (2005) to assess possible changes in the Midwestern US erosion rate due to climate change. The modelling of soil erosion showed that in the 2040-2059 era in comparison to the 1990-1999 era, soil loss and runoff may rise dramatically in entire part. Changes in planting dates have a particular impact on erosion, e.g. increased soil loss from later planted maize.

Pruski and Nearing (2002) found that a change in the amount and intensity of precipitation had a far more important impact than the change in the recurrence of storms on the degradation of soil. The changes in the amount and energy of precipitation represented the whole change and resulted in a 2.4 per cent change in soil loss and 2.5 per cent change in runoff. Another research in the USA (Savabi *et al.*, 1993) and the UK (Favis-Mortlock *et al.*, 1991) shows that erosion of the soil increased by 2-4 per cent to 1 per cent when the storm were increased.

In the Changwu district on the Loess Plateau of China, Zhang and Liu (2005), anticipated an increase of 23-37 per cent in annual precipitation, 2.3-4.3 °C in the maximum temperature and a rise in minimum temperature of 3.6-5.3 °C for the area over the century, based on the Hadley Center model, HadCM3. According to the A2a and GGal scenario, the shift in daily precipitation was expected to increase. Due to increased precipitation, surface runoff, loss of soil, ET and yield will usually rise in normal tillage as predicted by the WEPP model.

In the Tehri-Garhwal area, Gupta and Kumar (2017) studied precipitation by 2020, 2050 and 2080. The projected rainfall erosivity for the year 2020s, 2050s, and 2080s was estimated using downscaling precipitation data for future periods.

In the A2 scenario, the erosiveness of rainfall that increases between 546 and 701 m t ha/cm, whereas in the B2 scenario between 546 and 693.8 m t ha/cm. The result also shown that the mean annual soil loss will increase by 28.38, 25.64 and 20.33 percent in the 2020s, the 2050s and the 2080s respectively under the A2 scenario. However, the soil losses have been projected to increase for future times. Similarly, average annual soil loss may also increase, under the B2 scenario from the base period (1985–2013) to 27.06, 25.31 and 23.38 per cent during the 2020s, 2050s and 2080s.

Because of shifts in climate change the energy and precipitation volume, the erosive capacity to absorb and transport soil particles is predicted to increase and future erosion of soil by 9 per cent due to changes in the climate has been anticipated for 2090 (Yang *et al.*, 2003). Disintegration is often known to be a fundamental cause of non-point degradation, influencing the quality of water within a biological system (Cochrane and Flanagan, 1999). According to Bakker *et al.*, (2007), soil degradation is an exceptional natural phenomenon.

Numerous scientists have analysed problems of soil degradation in India. The Dikrong River Basin of Arunachal Pradesh using the Universal Soil loss (USLE) and the Morgan-Finney (MMF) Models were referred to by Dabral *et al.* (2008) and Pandey *et al.* (2009). Soil decomposition is a sensitive factor in the Himalayan region, as the forests are essential factors to prevent the degradation.

Varughese (2016), in a study on Bharathappuzha river basin, found that the tendency in average rainfall is decreasing at a rate of 15 mm/yr throughout 1971-2005, also temperature exhibited an increasing tendency of 0.0069 °C/yr. The future sediment loss was predicted for RCP 4.5 and RCP 8.5 during the 2041- 2070 and it goes up to 7-9 t/ha/yr, from the current condition of 2.5-4 t/ha/yr.

Suhara (2018) conducted a study to identify the erosion prone areas in Kunthippuzha sub-basin using RUSLE and MMF model. The mean soil erosion estimated for the study for the year 2000 was 18.30 and 20.58 t/ha/yr respectively

by MMF as well as RUSLE model. Similarly in the year 2013, it was 32.78 t/ha/yr and 35.10 t/ha/yr respectively.

The above-cited literatures show that soil erosion is affected by climate change. The increase in precipitation intensity negatively affects the topsoil, which leads to loss of nutrient-rich soil and affects our food production. To mitigate this, we have to adopt proper soil and water conservation measures.

## 2.5 REMOTE SENSING AND GIS APPLICATIONS

Satellite remote sensing now provides a significant promise to the ephemeral and convenient assessment of natural resources over vast regions. The term remote sensing includes the acquisition from a distance of data about an object or phenomena without any physical contact with the subject (Colwell, 1983). Remote sensing invention and Geographical Information system (GIS) is a tool for providing points of interest comprising of a concise view, multispectral information, multi-temporal view and cost-adequacy (Stoms and Estes, 1993). Airborne pictures are the most established remote sensing approach (Sabins, 1987). Airborne remote sensing technique gives assortment and investigation of information from ground-based, elevated and Earth-orbiting platforms, with linkages to GPS information, GIS information layers, functions and developing displaying capacities (Franklin, 2001). The quick development of GIS and RS have propelled the field of geomorphology (Vitek *et al.*, 1996).

The principal utilization of remote sensing to forest fire forecasting from the 1960s when various airborne infrared scanners were inspected for fire spot identification. A coordinated assessment of spatial factors is valuable for forest fire study. Remote sensing gives a wellspring of vegetation information, while GIS handling made it attainable to make fire hazard models. The factors picked for the investigation are extensively perceived as fundamental in forest fire anticipation and concealment. (Chuvieco and Congalton, 1989).

In the last 5 years, satellite modules with countless sensors have multiplied (for example Land and ENVISAT) and expanding spatial resolution (for example IKONOS and Quickbird). In reality, the ever-growing constellation of satellites have become a large number of trillions of bytes of information valuable for positioning and land management purposes (Jensen, 2000). It was evaluated that a hundred of new satellites were launched during the ten years somewhere in the range of 1996 and 2006 (Fritz, 1996).

In different domains of geomorphology, GIS advances empower quantitative assessment of transient changes over a generally prolonged period of framework. Spatial varieties in hydrological research are especially manageable to assess with the guide of GIS techniques (McDonnell, 1996). Investigation of airborne photos traversing a very long, while gives a progression of guides and information that delineate spatial inclusion and change. Johnston and Naiman (1990) used the GIS to investigate how the hydrology and vegetation of Voyageurs National Park, Minnesota, United States, was adapted to beaver (*Castor canadensis*). This was completed through the planning of lake dispersion and estimation of lake territory on an assortment of consecutive airborne pictures.

It is very obvious that a worldwide methodology requires for the utilization of new techniques for receiving, preparing and viewing spatial information in an ideal and most real-world manner. This is the essential goal of the Geographic Information System (GIS) approach. A GIS exploits a PC's capacities to store and process huge volumes of information (Burrough, 1987). In this manner, it makes doable to supplant or recover spatial data, as precisely as to infer cartographic models by joining in particular ways and the layers of information canvassed in the database.

### **2.5.1 Remote sensing and gis for land use-land cover mapping**

Geographic Information Systems (GIS) and remote sensing (RS) are helpful and minimal effort tool for surveying the spatial and transient elements of land use/land cover (Hathout, 2002; Serrea *et al.*, 2008). Remote sensing information

provides valuable multi-temporal information on the LULC change, for example; preparing and evaluation (Zhang *et al.*, 2002). Besides, the reliable inclusion of satellites in areas where the transition was rapid (Blodget *et al.*, 1991) is especially important. Besides the geographical changes concerning distinctive natural and human components can be assessed because advanced archives of remotely sensed information offer a possibility of considering significant LULC changes.

Various change detecting strategies have been created to decide varieties in land use/landcover by utilizing satellite information (Coppin *et al.*, 2004). Of these procedures, the pre-and post-characterization correlations have been fundamentally utilized (Singh, 1989; Coppin *et al.*, 2004). The basis of these approaches is that changes in the LULC results in variations between pixel reflection values. While these approaches aid in recognizing improvements, they are also unable to see the essence of progress (Ridd and Liu, 1998). On the other hand, post-arrangement examinations of observed changes between separately organised land cover information. Notwithstanding the difficulties identified with post-characterization examinations (Singh, 1989; Coppin *et al.*, 2004). The LULC change technique is most widely used (Jensen, 1996), specifically under urban conditions (Hardin *et al.*, 2007). One of the demerits found in this approach is that the accuracy of the resulting land distribution maps depends on the precision of each technique, which means these arrangements are contingent on the proliferation of errors (Yuan *et al.*, 2005).

Thenkabail *et al.* (2004) investigated to plan flooded areas in the Ganges and Indus stream basin using a time frame (8-day), 500-m target and 7-band MODIS land information of 2001–2002. The resulting map of 29 land use/land cover (LULC) consisted of 6 exceptional irrigated zone groups within the Ganges and Indus basin of the entire investigation area of 133,021,156 ha. Of the 33.08 Mha, 98.4 per cent of the region was flooded during Kharif, 92.5 per cent was flooded during Rabi and 3.5 per cent continuously as the year progressed.



Sano *et al.* (2009) did an investigation of land cover preparation of the tropical savannah district in Brazil utilizing Landsat pictures. The Brazilian tropical savanna (Cerrado), with more than 204 million hectares in the central part of the nation, is the second most gainful biome in Brazil as far as biodiversity. All things considered, utilizing remote sensing picture they immediately characterized diverse land use and found that shrublands were the predominant regular land cover class, while pasturelands were the prevailing land use class in the Cerrado biome. The latest Cerrado's land cover affirmed that exceptional land-use pressure in this biome. It additionally demonstrated that Landsat-like sensors could give accessible land cover information of Cerrado, though subsidiary information are required to assess image interpretation.

The huge changes in the watershed because of the practice of watershed improvement programs are having reflected in the advancement of vegetation cover because of control of soil degradation. Prasannakumar *et al.* (2012) demonstrated NDVI to be a helpful marker of land-cover conditions and a dependable contribution to models of soil elements by an examination focused at small mountainous sub-watershed in Pamba river basin, Kerala, India for estimation of soil erosion risk by utilizing Revised Universal Soil Loss Equation.

### **2.5.2 DEM and terrain mapping**

A Digital Elevation Model (DEM) is a specific database that expresses the elevation of a surface between the points. The most extensively utilized sources of DEM information are Light Detection and Ranging (LIDAR) and Synthetic Aperture Radar (SAR). Reliant on the sensor flight height, LIDAR permits profoundly precise and indistinctly inspected height points (Woolard and Colby, 2002).

The accessibility of advanced elevation information has been impressively raised with the improvement of valuable spatial information procurement devices, DEM precision properties, and grid size. The affectability of most significant geological subsidiaries utilized in hydrology; the DEM resolution has been

deliberately investigated in a couple of studies. Zhang *et al.* (1999) inspected the effect of framework of cell resolution by on screen delineation and hydrologic simulation utilizing elevation information from two small watersheds. Their outcomes affirmed that expanding the cell size brought about a raised mean geographical profile in light of the expanded contributing zone and diminished slopes.

Wilson and Gallant (2000) conveyed a synopsis of geological properties where direct surface subsidiaries from DEM are considered as essential geographical characteristics. Among the essential traits, most interests to hydrologists as far as DEM resolution are the slope, stream length, upslope contributing region and watershed zone. Digital Elevation Models (DEMs) give an abundance of data with respect to catchment hydrology. During late decades, development in the accessibility, suitability and increase in the flexibility of DEMs inside the fields of hydrology has become progressively clear (Pike, 2000).

Various investigates has demonstrated that the unwavering quality of the determined geographical and hydrologic properties depends upon on the resolution and precision of the information regarding digital elevation model (DEM), a standard arrangement for representing geology carefully (Murphy *et al.*, 2008). For instance, Zhang and Montgomery (1994) revealed that 10 m may be an appropriate resolution and increasing resolution and information volume for representing geomorphic and hydrological forms. DEMs can vary in resolution and precision by the formation method (Chang, 2006). The interval between height points decides the resolution of a DEM.

Ozdemir and Bird (2008) performed a survey to determine the morphometric limits of the drainage systems in Havran River Basin, western Turkey, from geographic maps and the DEM at flood points. Turcotte *et al.* (2000) completed an examination to decide the drainage structure of a watershed utilizing a DEM and computerized stream and lake network at Chaudie's River watershed in southern

Quebec, Canada. In this examination, they used DEM and effectively-recognized the drainage pattern.

Ahmed *et al.* (2010) focused an examination to discover the assessment of morphometric parameters derived from ASTER and SRTM DEM at Bandihole Sub-watershed basin in Karnataka. The outcomes show that the morphometric boundaries obtained from the SRTM and ASTER information give admirable and fulfilling results. The outcomes will be increasingly effective when the DEM cell size is lesser or the resolution of the picture is higher.

### III. MATERIALS AND METHODS

The research work done with the collaboration of Indian Institute of Remote Sensing (IIRS), Indian Space Research Organisation (ISRO), Department of Space, Government of India, Dehradun, Uttarakhand.

This chapter includes various methods used to complete the objectives of the study. Real-time analysis of hydrological, land use and soil characters of the selected watershed were carried out for the calibration and validation of APEX model to simulate climate change impact on surface runoff and soil loss.

#### 3.1 STUDY AREA

The main region surveyed for the study is located (Fig. 2 and 3) within the Hamirpur watershed, which is part of Hamirpur district, Himachal Pradesh and it represents the Shivalik region. It is the smallest district of Himachal Pradesh. It is surrounded on the south and southwest by Bilaspur and Una districts, on the northwest by Kangra district and east by Mandi district. The study area is located between 31°43'26" N to 31°44'45" N latitude and 76°26'49" E to 76°27'4.26" E' longitude with an elevation between 475 to 823 m and covering an area of 500 ha. Hamirpur is situated in a comparatively colder region in western Himachal Pradesh with a high altitude.

##### 3.1.1 Physiography

The terrain of the study area (Plate 1 a) is typically hilly and undulating. The major physiographic units are structural hills, upland (600-900 m) and valley/alluvial plain (400-600 m). The Beas river valley and the lower parts of Kunah Khad the surface height extended from 400 m to 600 m in the northern region. The eastern segment of the district cover a surface height greater than 900 m. A most extreme height of 1145 m of Sola Singhi slope ranges the western limit of the area. The north-eastern segment of the locale deep gulleys and canyons are found. The Sukar and Sir Khad in Bhorang-Jahu-Dhankar of the southern part region the khad/

stream/ river valleys are found to be wide. The drainage basin of river Sutlej and Beas generally slopes in the direction of south and north respectively. Physiographically according to the landform, elevation, slope, geology and soil texture the study region is classified into river valleys, piedmont plains and hilly terrains. The piedmont plains are further classified into upper and lower piedmont.

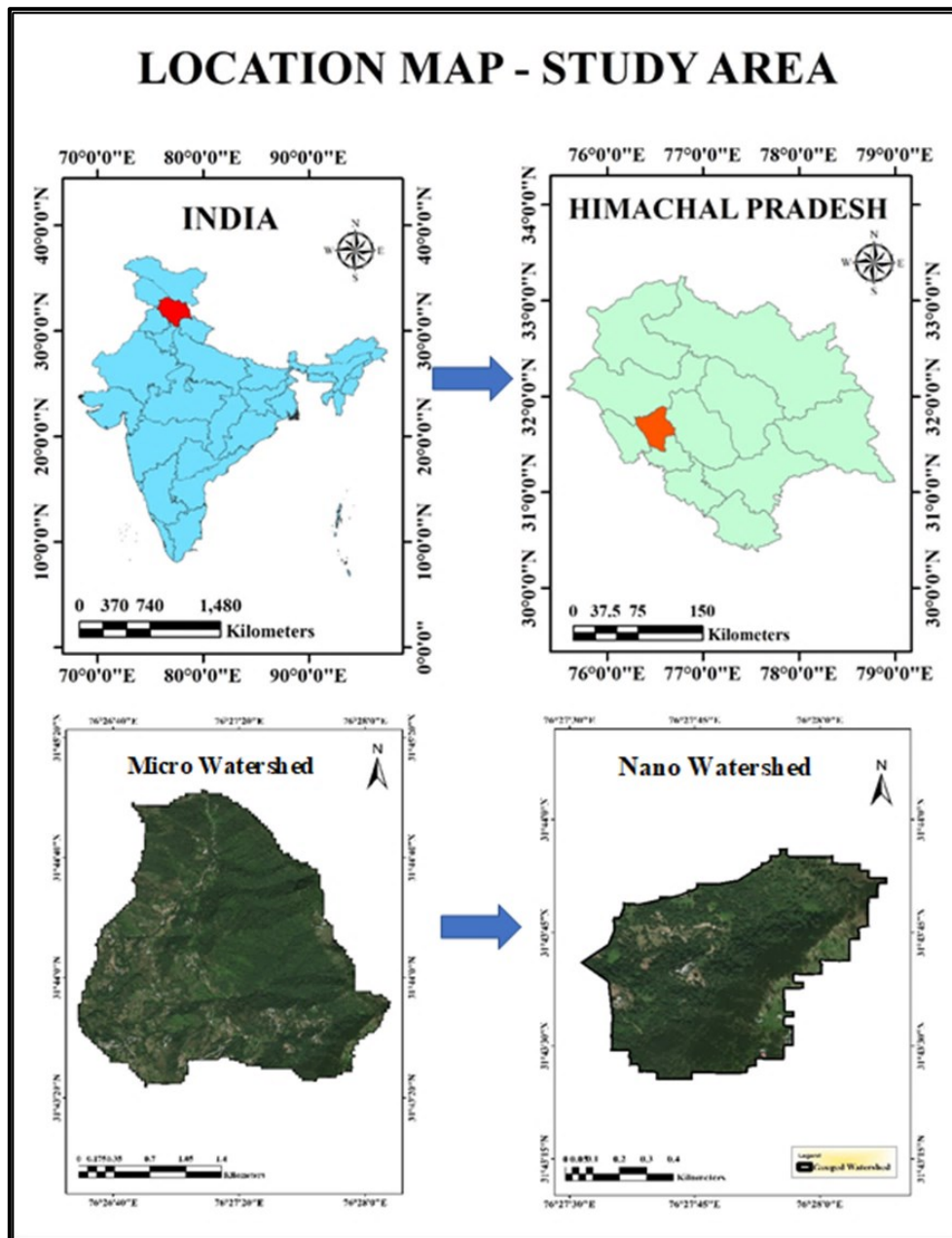
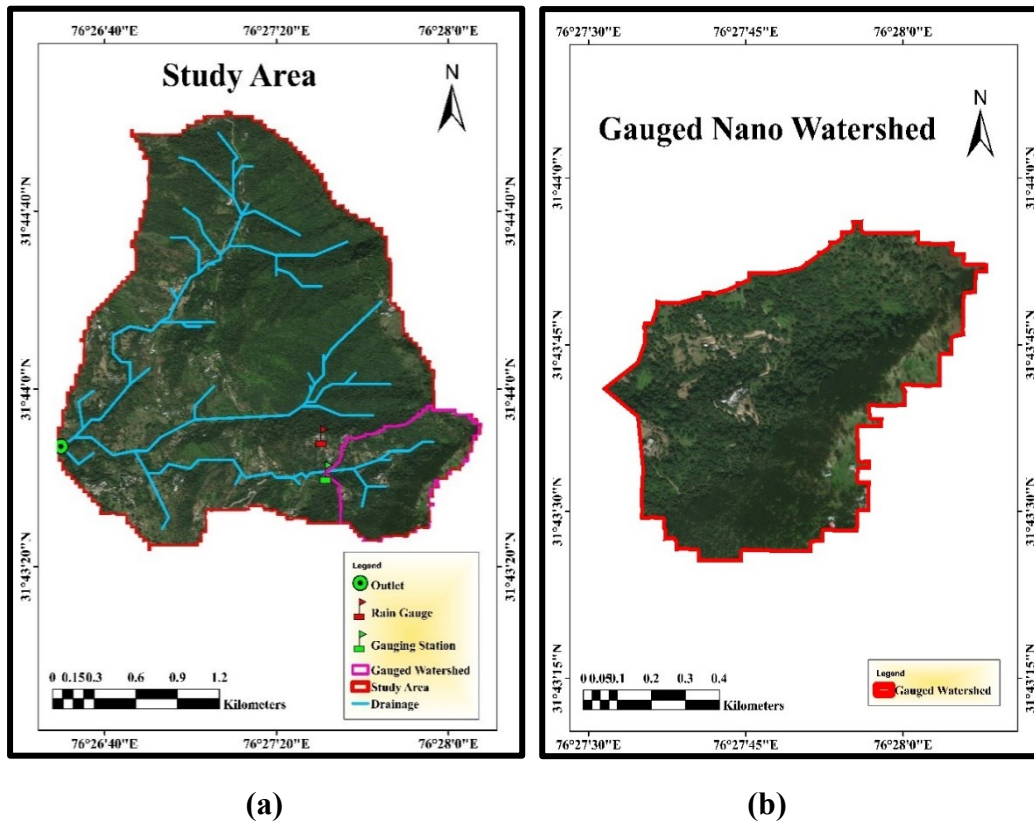


Figure 2. Location of the study area (Micro-watershed and Nano-watershed)



**Figure 3. Location of the study area (Nano watershed), (a) Micro- watershed, (b) Nano- watershed**

### 3.1.2 Geology

In Hamirpur district, two principal geological horizons are found, namely tertiary and post-tertiary formations. The categorization of geological development is described as follows, Post-Tertiary (Quaternary) and Tertiary (Shivalik). Post-tertiary horizons are moulded by alluvial deposition. A depression in front of the growing mountains the Proto-Himalaya was developed at the beginning of the Neogene. The origin of molassic sediments in the Shivalik is formed from this depression. The siltstone, claystone and conglomerates friable micaceous sandstone are the major constituents Shivalik cluster.

Nearly the entire Hamirpur is lying under the tertiary formations. The Shivalik group of upper, middle and lower rocks are formed by these kinds of formations. The purple shales and gigantic dark grey sandstone are the constituents

of Lower Shivalik. The central Shivalik is covered by grey clay and micaceous sandstone. The total thickness is 1600 m and in the western part of the Sarkaghat anticline, it is 1900 m. The Middle Shivalik subgroup encompasses considerable width of coarse micaceous sandstone with interbeds of conglomerate and clay. The coarse-grained sandstone, conglomerates interbedded with grey and pink clays/silts and sandstone or pebbles beds formed by Upper Shivalik.

### **3.1.3 Land use/ land cover**

Forest land, cropland and also grass/scrub land was identified as the main land use/land cover of the study region. Kharif and Rabi are the major cropping seasons. Paddy and maize are major Kharif crops, while wheat is the major Rabi crop. Maize is usually sown either in June or July and harvested in August or September. Wheat is sown in November/ December month and harvested in April/ May. To obtain highest yield from the land the landowners grown-up multiple crops in a year. Besides these, barley, gram, pulses and mustard are also grown.

The forest type of the study area is dry mixed deciduous. The vital assets which originate from the forest are wood, tinder, herbs, resin, fodder and so forth. Khair (*Senegalia catechu*), Chir pine (*Pinus roxburghii*), Neem (*Azadirachta indica*), Shesam (*Dalbergia sissoo*), Kasmal (*Berberis aristata*) and Sirish (*Albizia lebbek*) are the major species of trees found in the Hamirpur. The scrubs found in this region are Bhatindu (*Cissampelos pareira*), Dhai (*Woodfordia fruticosa*), Kamal (*Man philippinensis*) Kural (*Medua helix*) and Tut (*Morus alba*).

### **3.1.4 Drainage**

The general drainage pattern of the streams in the study region is dendritic. The Northern half part of the district form the catchment area of Beas River (Plate 1 b). Fig. 4 gives an idea about the drainage networks flowing through Hamirpur. The study area is inclined towards the South-West direction. At the West side, Kunah Khad (Plate 1 c) is flowing. The mainstream flowing through the study





(a)



(b)



(c)

**Plate 1. (a) Aerial view of watershed, (b) Beas River, (c) Kunah Khad and Pannyala Nala**

area is Pannyala Nala (Seasonal) (Plate 1 c), which joins the Kunah Khad near Rangas. Then Kunah Khad flows towards the northwest direction and joins river



Beas near village Bilkeshwar. The stream is perennial in nature and largest catchment area amongst all the tributaries of river Beas flowing in Hamirpur district.

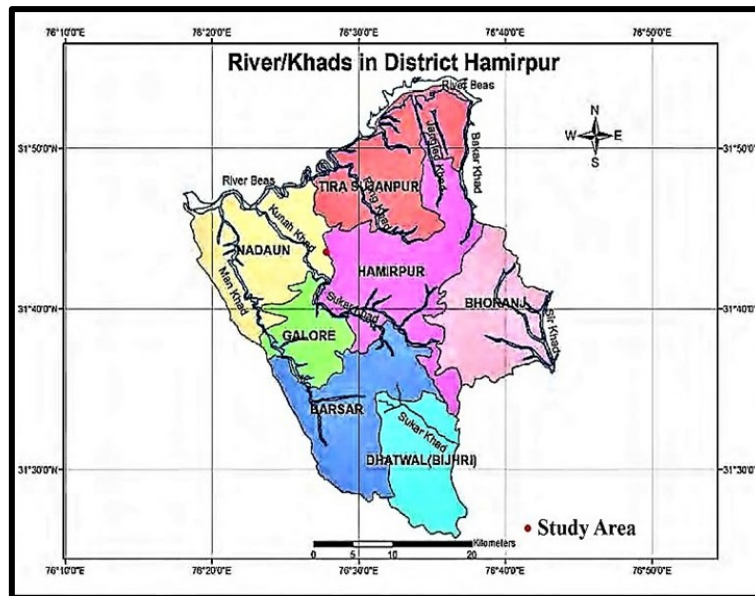


Figure 4. Major rivers/ khads in Hamirpur district

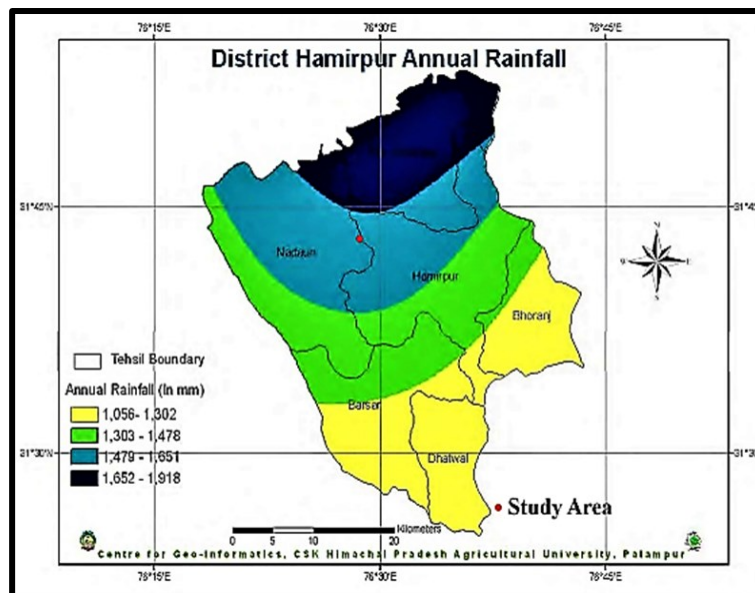


Figure 5. Spatial distribution of annual rainfall (adopted from the Centre for Geo-informatics, CSK Himachal Pradesh Agricultural University, Palampur)

### 3.1.5 Climate

The study area comprises of the humid subtropical zone. The climate in various parts of this area depends predominantly much on the elevation, which ranges from 475 m to 875 m. Fig. 5 illustrates the spatial distribution of annual rainfall of Hamirpur district of Himachal Pradesh. The climate of the study area has

**Table 1. Average climate of the study area (2000-2018)**

Month	Rainfall (mm)	Temperature(°C)		
		Maximum	Minimum	Average
January	61.38	17.10	6.40	11.43
February	59.77	20.00	8.70	13.38
March	59.09	24.80	13.00	20.22
April	34.13	30.60	17.50	25.63
May	42.24	35.30	22.40	29.00
June	131.03	36.00	24.60	31.07
July	328.75	30.70	23.20	29.21
August	432.79	29.40	22.50	27.54
September	143.97	29.90	21.20	26.84
October	18.09	28.10	16.50	23.81
November	6.69	24.00	10.80	18.25
December	23.93	19.50	7.70	13.39
<b>Annual Average</b>	1341.86	27.12	16.21	22.48

four full seasons. The summer period is from March to June. The rainy season, for the most part, stretches out from July to September. Winter is commonly from December to February. October and November exhibit autumn. The average annual rainfall in the district is 1341 mm, out of which 82 per cent occurs from June to September and about 60 per cent is received in July and August. The coldest month is January, with an average temperature of 11.43 °C and June is the hottest month with an average temperature of 31.07 °C. Table 1. shows the average climate of the study area.

### **3.1.6 Soils**

The soils in Hamirpur is mainly non-calcic brown soils and soil in the most region, neutral to acidic. The texture differs from clay loam to loamy sand. The main soil texture is identified as sandy loam. Organic matter content varies from low to medium. These soils are analogous to hapludalfs and Eutrochrepts corresponding to USDA Soil Taxonomy. Most of the land in this area is under shallow to moderately deep soils. Bulk density of soil varies from 1.1-1.65 g/cm<sup>3</sup>.

### **3.1.7 Socio- economic condition**

Agriculture is the major livelihood of people in this area with about 75 per cent of people involved in agriculture, horticulture, forestry as well as animal husbandry. Wheat, maize, paddy and vegetables are major crops whilst cow, buffalo and goat are the major livestock. Agriculture is mainly based on rain-fed cultivation and very less area is under irrigated. The farmers have adopted mixed farming for efficient utilisation of agricultural land. The majority of agricultural land is in highland and results in limited agricultural productivity. Literacy is quite high as compared to the state and is 85 per cent.

The different kinds of data collection methods adopted, data collected for the study and research frame work illustrated in Fig. 6.

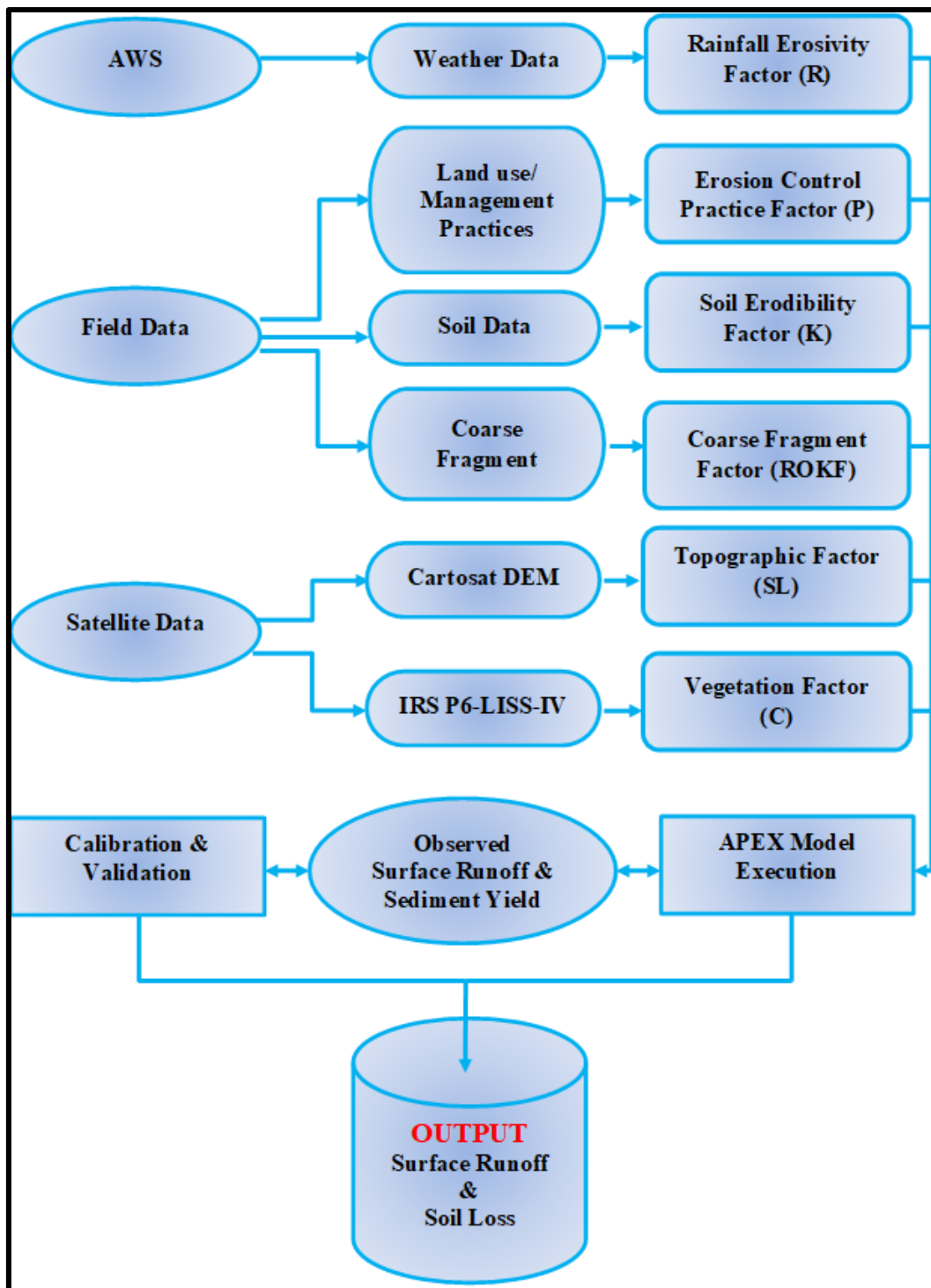
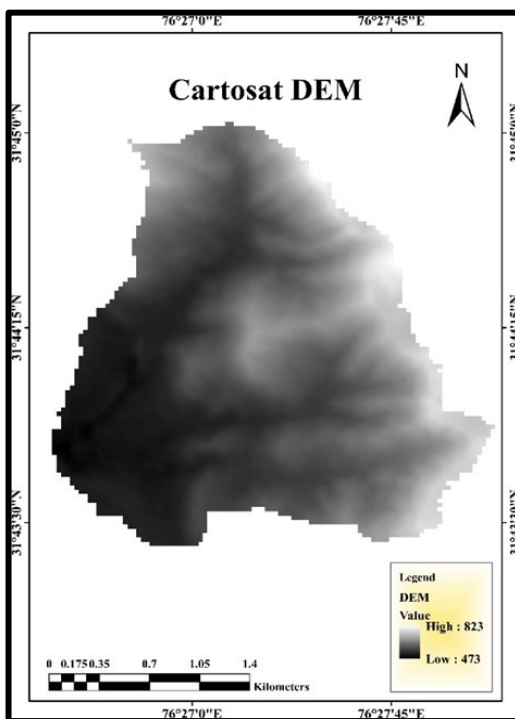


Figure 6. Research Methodology

### 3.1.8 Satellite / remote sensing and topographical data

#### 3.1.8.1 Cartosat-1 data

The primary Indian Remote Sensing Satellite equipped for capturing stereo pictures is Cartosat-1. These pictures have been utilized for different cartographic applications in worldwide. The Cartosat DEM extracted for the area of interest watershed is shown in Fig. 7. It has a spatial resolution of 30 m. This information is utilized in the preparation of DEM (Digital Elevation Model) and DTM (Digital Terrain Model), land use updating, cadastral mapping, different GIS applications and so forth. Cartosat DEM was used for terrain analysis, drainage, slope and aspect extraction.



**Figure 7. Cartosat DEM**

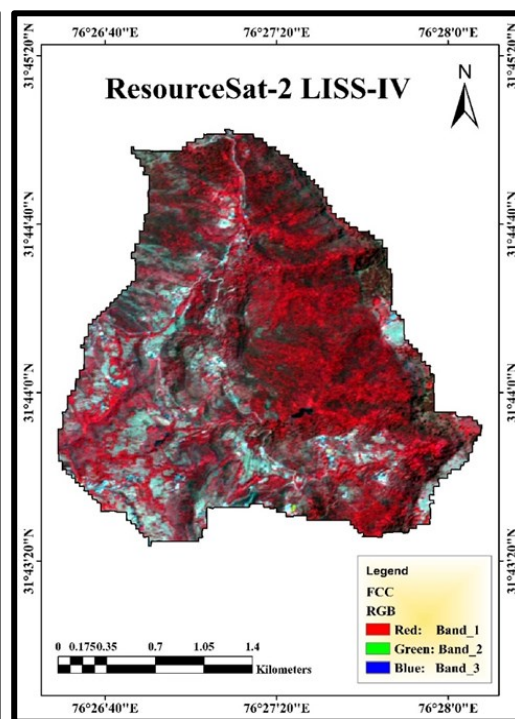


**Figure 8. ResourceSat-2 LISS-IV**

#### 3.1.8.2 ResourceSat-2 data

Indian Remote Sensing Satellite- ResourceSat-2 is an earth monitoring satellite of India. The management of integrated water and land resources the IRS mission (ResourceSat-1/ResourceSat-2) deliver continuous remote sensing data for

an operational basis. The three sensors on-board in the satellites are, viz. A LISS-IV sensor which can function in two modes: multi-spectral and mono mode, Advanced Wide Field Sensor (AWiFS) sensor and LISS- III.

In this study, a LISS-IV sensor data was used to characterise land use/land cover of the study area. The LISS-IV multispectral high-resolution camera is the major instrument of this sensor complement. LISS-IV is a three-band push-broom camera has a spatial resolution of 5.8 m and a swath width of 70 km. LISS-IV can be functioned in any of the two approaches. It has three spectral bands, viz. B2- 0.52-0.59 (green), B3- 0.62-0.68 (red), and B4-0.77-0.86 (NIR). Fig. 8 shows the LISS IV FCC of the study area which was adopted to characterise land use and land cover data.

#### *3.1.8.3 Toposheet*

Topographic Sheet number 53A/5 of 1: 50,000 scale was adopted in the study for location, land use, field surveys and basic information. It is also used to find micro details of elevation, vegetation, land use, settlements, drainage patterns, transport network, communication lines, latitude and longitude.

### **3.1.9 Softwares**

#### *3.1.9.1 ArcGIS 10.3*

ArcGIS is a software to build, manage, share and examine spatial information. It comprises of server segments, desktop applications and developer tools. The designer of ArcGIS is Environmental System Research Institute (ESRI) and was at first released in 1999 at New York. ArcGIS 10.3, which was released in 2014 was utilized for this study. It was used for building maps, sharing and finding geographic area, combining geographic data, exploring the area of interest and managing geographic information in a database. ArcGIS has a preeminent standard geographic information model for analysing spatial data, for example features, raster and other spatial data types. ArcGIS reinforces the execution of the

information model for both document frameworks and database frameworks. ArcMap, Arc Catalogue, Arc Globe and Arc Toolbox are some incorporated applications of ArcGIS software. ArcMap is the application used to visualise, alter, query geospatial information and also to create new maps. Arc Catalogue is the information application adopted to examine datasets and documents on the database, PC or different folder. ArcToolbox encompasses geoprocessing, information transformation and analysis tools with numerous dimensions in Arc info.

In this study, ArcGIS 10.3 installed in the desktop of computer lab (Agriculture and Soils Department) of the Indian Institute of Remote Sensing (IIRS) was used for the study. The setting interface for all the APEX inputs viz., DEM, soil map and land use data prepared by ArcGIS. Digitization and preparation of thematic maps, for example, land use, soil, aspect, slope, soil for the study area has also been done with this software.

#### *3.1.9.2 Model interface- ArcAPEX*

The model was created and maintained by Texas A&M AgriLife Research. Agricultural Policy Environmental eXtender (APEX) is a hydrologic model interfaced with a spatial dataset of ArcAPEX. This interface coordinate geological, spatial, land use, soil and an inherent database that contains spatial dataset important to simulate a wide scope of plant development, manuring, culturing and pesticide applications over a farm/field to the basin-scale drainage area. The significant constituents for the ArcAPEX are the examination of land use and soils, watershed delineation, input boundary definition, climate information, model run management and SWAT model coordination. The product downloaded from the site <https://epicapex.tamu.edu/>.

#### *3.1.9.3 Statistical package for social sciences (SPSS)*

SPSS Statistics is employed for statistical and realistic investigation. Delivered by SPSS Inc., it was gained by IBM in 2009. The recent version (2015)

is named IBM SPSS Statistics. SPSS is a broadly employed software for statistical examination in sociology. The original SPSS manual (Nie *et al.*, 1970) has been described as one of "sociology's most fascinating books" for permitting normal analysts to perform their accurate examination. Notwithstanding accurate investigation, information and information documentation are the major highlights of this software. SPSS was used for statistical analysis such as correlation, regression and so forth.

#### *3.1.9.4 Statistica version-10*

Statistica is a dynamic examination programming package at first settled by Stat Soft which was then changed to Dell in March 2014. Statistica offers data examination, data management, measurements, information mining, visualisation techniques, text investigation and information of machine learning. Statistica contains explanatory and exploratory charts notwithstanding standard 2 and 3-dimensional diagrams. It contains intelligent naming, stamping and data rejection and considers the investigation of exceptions and exploratory information examination. It gives comprehensive charts which help the client to decipher the information without any confusion. Statistica was likewise utilized for statistical examination, for example, correlation, box-plot and relationship chart generation.

#### *3.1.9.5 Soil-Plant-Air-Water (SPAW) hydrological model*

The SPAW model was created by the United States Department of Agriculture. There is two method to replicate day to day water budget for fields in SPAW model, one is for pond and another one is for farm fields. Soil, atmosphere, and vegetation information documents for lakes and fields are chosen from the system. Different combinations of the information records promptly express to changing landscapes and ponding variabilities.

The main soil hydrological properties available are water content, infiltration, saturated and unsaturated hydraulic conductivity, wilting point, field capacity, saturation and so forth. Among this infiltration rate and unsaturated hydraulic



conductivity directly estimated from the field utilizing mini-disk Infiltrometer and remaining properties required were obtained from Soil Plant Atmosphere Water (SPAW) model dependent on soil texture, gravel content, salinity and organic matter.

## 3.2 THEMATIC MAP PREPARATIONS

Four types of thematic maps are needed for this study, such as land use/ land cover, soil, slope and aspect. ArcGIS 10.3 software was used to prepare these maps. The Information necessary for preparing thematic maps were obtained through field data collection, soil analysis and satellite data. The detailed description of procedures for preparing maps is described below.

### 3.2.1 Slope map

The slope is usually expressed in degrees/percentage. Cartosat -1 derived DEM was used for the study. These are prepared using a stereo pair image. DEM gives an idea of the height of every point. The slope map was created using the spatial analyst tool in ArcGIS, and the slope was classified as eight classes in percentage.

### 3.2.2 Aspect map

The aspect distinguishes the downslope path of the greatest step of variation in value from every cell to its neighbours. It is also represented as slope direction. The estimates of every cell in the raster demonstrate that the surface facing in which direction. It is represented in degrees from 0 to 360 degree and ending up at ground zero with clockwise direction. Plain regions are given an estimation of -1. It characterizes primarily nine classes such as Flat, North, Northeast, East, Southeast, South, Southwest, West, and Northwest. The aspect map was prepared with the spatial analyst tool in ArcGIS.

### 3.2.3 Drainage map

Drainage systems are the patterns formed by the streams and rivers in a particular drainage basin. The drainage line flows through the relatively lower region. ArcGIS can delineate the entire area flowing into a specified outlet, based on DEM. The flow direction, flow accumulation and fill sinks options in ArcGIS were used to determine the area draining to any specified point on the DEM.

### 3.2.4 Landform map

A landform incorporates a geomorphological unit. They are essentially characterized by their surface structure and part in the landscape. Landforms are classified by features, for example, height, inclination, positioning, direction and soil type. Major landform elements, such as hill-top, shoulder, back slope, toe slope and valley can be detected on numerous geomorphological landforms. Using Topographic wetness index (TPI) (Jennes, 2006), these landform elements were identified. The TPI is the premise of the grouping framework and is the contrast between a pixel height and the normal elevation of the area around that pixel. A positive value indicates that the pixel is higher than its neighbour, whereas a negative value indicates it is lower than the neighbour.

### 3.2.5 Stream order

The stream order is a positive whole number used in hydrology to designate the level of branching in a river system (Strahler, 1953). There are various types of

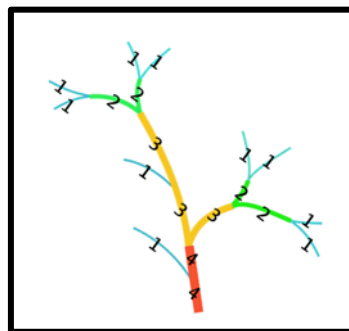


**Figure 9. Strahler method**

stream ordering methods; among this Strahler stream ordering method is simple and familiar. Strahler method (Fig. 9) is a “top-down” ordering method. ArcGIS was used to determine stream ordering of the study area.

### **3.2.6 Drainage density map**

Drainage density is defined as the length of the whole number of streams and waterways in a drainage basin divided by the entire area of the drainage basin. It is a level of how well a watershed is drained by streams. It depends on both the climatic and physical features of a drainage basin. Soil infiltration, profile of the drainage basin, rainfall and land cover affects drainage density. ArcGIS was used to determine the drainage density of the study area.

### **3.2.7 Stream power index**

The stream power index (SPI) was adopted to evaluate the erosive power of the landscape. The areas with high potential for erosion certainly have a high stream power index. Stream power index (Moore *et al.*, 1991) was generated from the DEM of the study area in ArcGIS using the raster calculator and the equation given below.

$$\text{SPI} = \text{Catchment area} \times \tan \omega$$

Where,  $\omega$  = Degree slope

### **3.2.8 Topographic wetness index**

The topographic wetness index was used to detect accumulation potential. It is also represented as topographic moisture index/compound topographic index. The topographic position index at a specific point is the fraction of the catchment area, contributing to that point and slope at that point (Wilson and Gallant, 2000). Wetter region indicates higher positive values and lower negative values with the drier region. Topographic wetness index was generated from the DEM of the study area in ArcGIS using the raster calculator and the equation given below.

$$\text{Topographic wetness index} = \ln [\text{Catchment area} / \tan \omega]$$

Where,  $\omega$  = Degree slope

### 3.3 LAND USE/ LAND COVER MAP

ResourceSat - 2 LISS IV sensor data of standard false colour composite was used for preparing land use maps. Vegetation appears in shades of red because vegetation reflects much near-infrared light. Supervised classification was implemented by the maximum likelihood classifier, wherein a pixel is relegated to the class which has the higher possibility. For supervised classification, the sampling (training areas) sites were marked using the geocoded ground observation of diverse land use/land cover. A sample of a definite class, encompassing several training pixels, develop a cluster in the feature space. The clusters selected were representative of the feature class and avoided overlapping with multiple clusters. These training samples were saved in signature file format. The maximum likelihood classifier considers cluster centre, size, orientation and shape. The maximum likelihood also allows defining a threshold distance by defining a maximum probability value. Using the signature mentioned above, the maximum likelihood classification was executed.

The standard False Colour Composite (FCC) of Resourcesat-2 data was visually interpreted on-screen using ArcGIS software to prepare land use/ land cover type map of the watershed.

#### 3.3.1 Normalised difference in vegetation index (NDVI) map

It is a simple arithmetical indicator that adopted the visible and infra-red bands of the electromagnetic spectrum to measure whether the target being observed contains live green vegetation or not. The value of NDVI ranges from -1 to +1. Water bodies indicated by negative values, bare earth or barren lands indicated by values close to zero, and +1 indicated for high vegetation.

$$\text{NDVI} = (\text{NIR} - \text{RED}) / (\text{NIR} + \text{RED})$$

LISS IV satellite data was used to create NDVI image. NDVI was described as

$$\text{NDVI} = (\text{Band 3} - \text{Band 2}) / (\text{Band 3} + \text{Band 2})$$

### 3.4 SOIL LANDSCAPE MAP

The standard FCC was visually interpreted to prepare physiographic- soil map by on-screen interpretation using GIS software. Soil samples were collected from various soil map units in the watershed.

### 3.5 FIELD DATA COLLECTION

The data collection was carried out in two stages, during monsoon season in September and then in the post-monsoon period, of January. Soil erosion survey was done in this period to identify the erosion class of the study area. Additionally, land use and land cover of the study area was observed and geocoded for ground-truthing. In January soil sample collection was carried out to find soil physical and chemical properties. Transect sampling was done to cover all different land use/land cover. Each sampling point was identified using Trimble GPS receiver with an accuracy of  $\pm 5\text{m.}$ , also various other features such as slope steepness (using inclinometer) and slope length, coarse fragment percentage, soil colour (Munsell colour chart), conservation practices implemented and various past erosion features were recorded. Furthermore, the data such as crop density, the maximum and minimum height of the plant were collected for model input. Data of the time of sowing, time of harvest, fertilizers used, and manuring were recorded.

#### **3.5.1 Soil sampling**

Soil samples were collected in January because there is no rain in the study area in these months. A detailed sampling plan was prepared before sampling to obtain more precise and representative samples, by the aid of both the Survey of India 53A /5 of 1: 50,000 scale topographic sheet and Google satellite imagery. The study area primarily comprises of forest land, agricultural land and scrubland.

Correspondingly different kinds of landforms such as a hilltop, upper slope, middle slope, lower slope and valley and also north and south aspects were taken.

Grid sampling was challenging because most of the part is dense forest. So mainly transect sampling was carried out according to different streams and this helped to cover almost all land use and area. The soil sample collection points were georeferenced using a Trimble GPS receiver. To obtain more precise soil map of study area soils samples were collected from both surface (0-15 cm) and subsurface (16-30 cm). A total of 144 soil samples were collected from 72 sites. Fig. 10 and 11 shows the schematic representation of soil and bulk density sampling points.

In fields having standing crops in a row, samples among rows were taken and mixed with the samples drawn from all spots within one field. In the forest and undisturbed area, a slight layer of topsoil was peeled off and then the sample was taken.

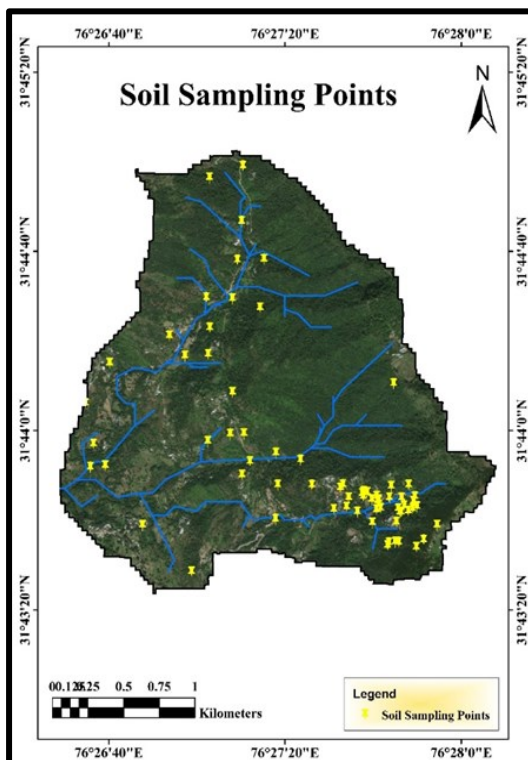


Figure 10. Soil sampling locations

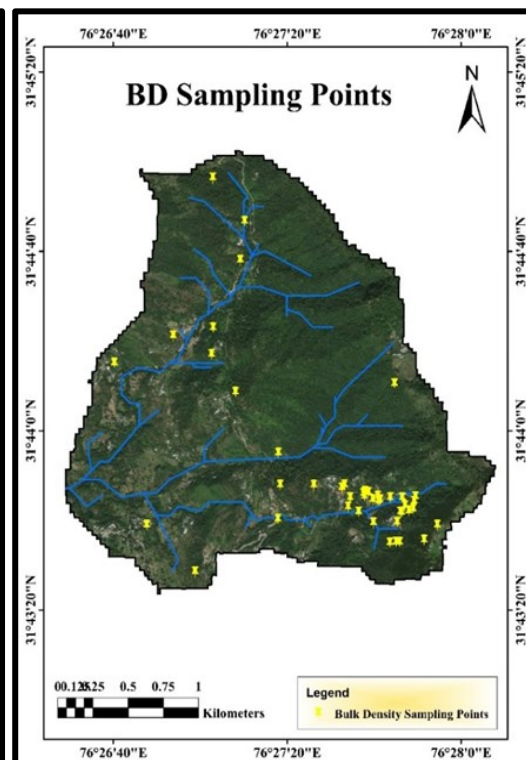


Figure 11. Bulk density locations

Recently fertilized fields, marshy tracts, bunds, channels, composite piles, the area near trees, wells and other non-representative sites were evaded during sampling. The soil samples taken were collected in a polythene cover and labelled appropriately. Labels having all information about the samples such as sample number, sampling depth, sampling location name, coordinates (latitude and longitude), date, land use and other remarks. The sampling density is more on the south-east corner of the study area, and this is because of the water level gauging station and sediment collecting tank were located in this region. The APEX model needs more detailed data on soil properties in the gauged region. A tabular (Table 2) representation of samples collected from each land use are mentioned below.

**Table 2. Distribution of soil sampling over various land use/land cover**

Sl. No.	Land use/ Land cover	No. of Samples (72)
1	Dense Forest	14
2	Open Forest	5
3	Agriculture	36
4	Scrub Land	7
5	Current Fallow	10

All soil samples were air-dried (Fig. 12) in the Central Analytical Laboratory (CAL), IIRS to make sure the removal of soil moisture and the dried soil samples were crushed with the help of wooden pestle and mortars, the plant residues, gravels and other unnecessary materials were removed. The entire crushed soil samples were passed through 2 mm stainless steel sieve, remixed and stored in airtight labelled containers. The entire soil samples collected from the field were analysed in Central Analytical Laboratory (CAL), Indian Institute of Remote Sensing(IIRS). For determining the bulk density, 50 soil clods were collected along with the soil sampling. These clods were kept in aluminium cans and for avoiding collision with sidewalls of containers, clods are placed with cotton wool.

Tests to determining physical properties such as bulk density, texture, soil colour, aggregate stability and chemical properties like pH, Electrical conductivity, organic carbon, nitrogen, phosphorus, and potassium of soil were carried out in Central Analytical Laboratory, IIRS.



(a)



(b)



(c)



(d)

**Figure 12. Processing of soil samples: (a) soil sample collection, (b) air drying, (c) sieving, (d) packed soil samples**



**Table 3. Instruments and materials used**

<b>Sl. No.</b>	<b>Instruments</b>	<b>Usage</b>
<b>1</b>	GPS (Trimble)	Identifying geolocation of sampling point.
<b>2</b>	Soil Auger, Spade, Pickaxe, Khurpi, Field Knife, Polythene bag	Soil sample collection and storing.
<b>3</b>	pH and EC Meter	Measuring soil pH and EC.
<b>4</b>	Hydrometer	Determining soil texture.
<b>5</b>	Millipore	For filter, the runoff water collected samples to determine sediment concentration.
<b>6</b>	Inclinometer	For measurement of the slope.
<b>7</b>	Infiltrometer	For the measurement infiltration rate and soil hydraulic conductivity.
<b>8</b>	Pressure based water level recorder	For measuring runoff.
<b>9</b>	CHNS Analyser	To determine Carbon(C&N) content.
<b>10</b>	Flame Photometer	For the analysis of Potassium (K).
<b>11</b>	Spectro Photometer	For the analysis of Phosphorus (P).
<b>12</b>	Wet Sieving Apparatus	For determining soil aggregate stability.
<b>13</b>	Digital Camera	For taking field photographs

### 3.5.2 Soil analysis

#### 3.5.2.1 Soil pH and Electrical Conductivity

Soil pH refers to the acidity or alkalinity of a soil. SYSTRONICS  $\mu$  pH System 362 (Fig. 13) was used to measure the pH of the soil sample. The pH meter was calibrated using buffer solutions of pH 4, 7 and 9.2. After calibration, soil pH was measured for the 142 soil samples.



**Figure 13. pH measurement**



**Figure 14. EC measurement**

Electrical conductivity was measured using SYSTRONICS Conductivity TDS Meter 308 (Fig. 14). It is the reciprocal of resistance. Wheatstone meter bridge principle is used. The conductivity meter was calibrated using a standard KCl solution (0.01M KCL) of electrical conductivity 1.412 mS/ cm. Soil electrical conductivity (EC) is the extent of the number of salts in the soil also represented as the salinity of the soil. It is a vital factor in soil health. The soil electrical conductivity was measured EC in mS/ cm.

#### 3.5.2.2 Soil colour

Soil colour is formed by the minerals and by the organic matter content. Soil colour was determined in the laboratory by observing soil colour in sunlight and its comparison with the Munsell colour chart (Fig. 15)



**Figure 15. Munsell soil colour chart**

### 3.5.2.3 Soil texture

The hydrometer (Fig. 16-18) method (Bouyoucos, 1962) depends on the law that the density of the suspension (Fig. 16) at a certain temperature reduces as at first homogenous distributed suspension settle.



**Figure 16. Settling cylinder**



**Figure 17. Bouyoucos Hydrometer**

The rate of reduction in density of certain temperature is identified with the speeds of settling particles, which, thus, is identified with their sizes. The time needed by the particles of a certain size to settle can be determined by applying Stokes law (Stokes, 1851). Texture analysis of soil samples were done by this method.



**Figure 18. Soil textural analysis**



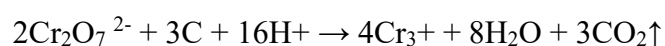
**Figure 19. Bulk density analysis**

#### *3.5.2.4 Bulk density*

The modified wax method (Blake and Hartge, 1986) was used to measure bulk density (Fig. 19). It is based on the Archimedes principle. A total of 48 bulk density samples were analysed.

#### *3.5.2.5 Soil organic carbon*

Walkley-Black chromic acid wet oxidation method (Walkley and Black, 1934) was adopted to assess the soil organic carbon (Fig. 20). An oxidizable substance in the soil is oxidised by 1 N  $K_2Cr_2O_7$  solution. The reaction is aided by the heat produced when 2 volumes of  $H_2SO_4$  are mixed with 1 volume of the dichromate. The residual dichromate is titrated with ferrous sulphate.



In some soils, there was abundant carbon. In such soils, titre value less than 6 ml were obtained. So instead of 0.5g soil, 0.2 g of soil was taken and titrated again. The titre value is inversely associated with the quantity of carbon existing in the soil sample.

Per cent of oxidizable organic carbon =  $(10 (B-S)/ B) \times 0.003 \times (100/ \text{wt. in gm})$

Where B and S stand for titre values (ml) of blank and sample respectively.  
Per cent total organic carbon in soil = Per cent of oxidizable organic carbon x 1.3  
Per cent of organic matter = total organic carbon in soil (%) x 1.72



**Figure 20. Soil organic carbon analysis**

### 3.5.2.6 Soil aggregate stability

Aggregate stability of soil was estimated using the Eijkelkamp wet sieving apparatus.

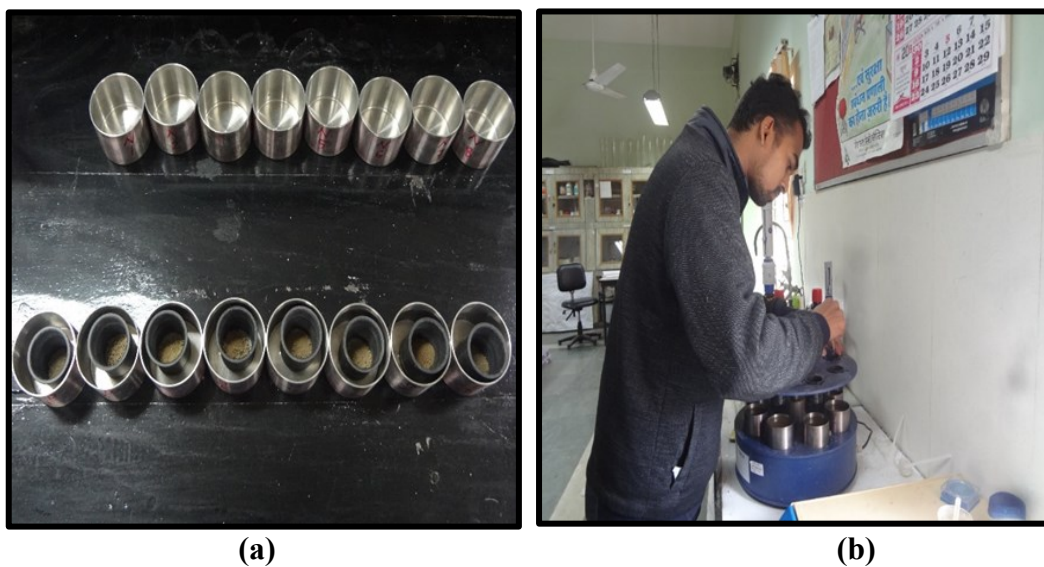


**Figure 21. (a) Aluminium cans and sieves, (b) Wet sieving apparatus**

It is the resistance of soil structure against physicochemical or mechanical destructive forces. This method of aggregate stability was mainly beneficial for soil erosion studies. It is based on the principle that unstable aggregates will break down more quickly than stable aggregates when immersed in water.

At first, 4 gm of 0.25 and 0.50 mm air-dried aggregates were taken in the sieves. To prevent slaking of the aggregates, these were moistened using a fine sprayer. The soil samples were put in sieves of 0.25 mm as Fig. 21 (a) and cans are placed below the sieves. The cans were filled with sufficient distilled water to cover soil aggregates. The sieve holder was placed in working position as Fig. 21 (b). Then the motor was started by putting the main switch into '3 min' position and allowed it to raise and lower the sieve holder for 3 min. After that, the sieve holder was raised and allowed to leak out. These cans were removed, and new cans were placed. Instead of distilled water, filled the can with sodium hydroxide solution because the pH of the soil is found almost less than 7. Again sieving was continued till the sand and roots remain in the sieve. Both sets of samples were placed in a hot air oven until all the moisture content disappeared. After drying, weight of soil samples were taken. Dividing the weight of stable aggregates over total aggregate weight gives an index for the aggregate stability. The same procedure was repeated for 0.50 mm sieve also. Only surface soil was used for aggregate stability measurement.

#### *3.5.2.7 Carbon and nitrogen (CHNS Analyser)*

CHNS Analyser was used to measure total carbon, hydrogen, nitrogen and sulphur in the soil. It is based on the principle of the Dumas method, which comprises the complete and immediate oxidation of the sample by flash combustion. Catalytic combustion is carried out at a temperature of up to 1200 °C in the combustion tube. It is followed by a reduction of the combustion gases when hot in the reduction tube. The combustion products are parted by a chromatographic column and sensed by the thermal conductivity detector, which gives an output signal proportional to the concentration of the individual components of a mixture.



Weighed 40 to 60 mg of dried 0.2 mm sieved soil taken in the tin boat and added 8 to 10 mg of tungsten oxide powder. It increases the temperature during combustion and helps for better combustion of soil. Noted the weight and kept it in the boat holder box (Fig. 22-23). This tin-coated soil sample was used for determining carbon, hydrogen, nitrogen and sulphur. High purity Sulphanilamide ( $C_6H_8N_2O_2S$ ) was used as a standard for calibrating the instrument.



**Figure 22. CHNS Analyser**



**Figure 23. CHNS Data display**

### 3.5.2.8 Soil phosphorus (P)

The extraction of available phosphorus from soils with 0.03 N Ammonium

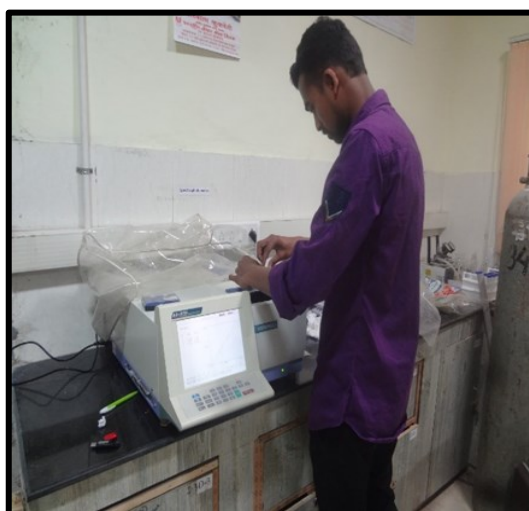


**Figure 24. Spectrophotometer**



**Figure 25. Flame photometer**

Fluoride in 0.025 N Hydrochloric acid (Bray and Kurtz, 1945) extractant method was used because is slightly acidic in nature. The extractant was used to estimate soil phosphorus with the help of spectrophotometer (Fig. 24).

#### *3.5.2.9 Soil Potassium (K)*

Potassium in the soil found as water-soluble, exchangeable, non-exchangeable and lattice-K. For removal and assessment of exchangeable K along with water-soluble k is adequate. The solution prepared using the Ammonium Acetate method (Hanway and Heidel, 1952) was used to estimate Potassium with the help of flame photometer (Fig. 25). The Ammonium ions are very close in size to  $K^+$  and replace the latter efficiently.

### **3.5.3 Land use/ Land cover data collection**

A detailed survey of agricultural fields, forest land, scrubland and current fallow was performed from September to January. It was mainly during monsoon and post-monsoon season for classifying crop parameters (Plate 2) and modelling surface runoff and sediment yield. An interview accompanied by a farmer (Banh Village) to determine cropping practices in the study area. During October crop data such as plant density and plant height from three different areas of the same field were collected (Fig. 26) and an average of these parameters were taken. In some areas instead of maize, farmers are cultivating paddy also. It was observed that paddy fields are relatively less in the study area. Ginger, turmeric, chilli etc. were also cultivated in the study area. It was observed that in Rabi season during November and December wheat is the major crop and it was harvested during April/ May. In barren/scrub land during the June and July months, plants were absent but after the rainy season the growth of scrub is seen and in open and dense forest increased growth of scrubs were observed.





(a)



(b)



(c)



(d)



(e)



(f)





(g)



(h)

**Plate 2. Land cover types in the study area (a) Paddy, (b) Maize, (c) Banana, (d) Mustard, (e) Scrub land, (f) Agroforestry system, (g) & (h) Settlements.**



(a)



(b)

**Figure 26. Plant height and density measurement: (a) Maize and (b) Paddy**

### **3.5.4 Field erosion survey**

An intensive field survey was done during the monsoon season, which facilitated to identify areas susceptible to erosion and various erosion structures. It was observed that rain during monsoon is highly intensive. In erosion prone area check dams and gabions were observed. The erosion classes vary from moderate to

very severe. Almost all the fields have adopted terracing, but it was not sufficient to overcome soil erosion. Few grass bunds and stone bunds were seen. Soil erosion is proforma used for the survey is given in Table 4.

**Table 4. The soil erosion proforma used for the field erosion survey**

<b>Obs.No. 7</b>	<b>Village: Banh</b>	<b>District: Hamirpur</b>		<b>Date: 10/10/2018</b>				
<b>GPS</b>	<b>Lat. 31 43 50.038</b>	<b>Long. 76 27 37.092</b>		<b>Altitude 630.16m</b>				
<b>Land form/ physiography</b>	Middle Hillslope							
<b>Site characteristics</b>	Surface coarse fragment factors 0-10%							
<b>Terrain slope (%)</b>	0-3	3-5 ✓	5-8	8-15	15-25	25-33	33-50	>50
<b>Soil depth (cm)</b>	<10	10-25	25-50	50-75	75-100	100-150	>150	
<b>Stoniness (%)</b>	<15 (Slight)	15-40 (Moderate) ✓	40-75 (Severe)	>75 Very severe)				
<b>Field size (Length/ width)</b>								
<b>Land use/ cover</b>	Cropland : Current fallow/ permanent fallow/- Harvested Maize field Forest: Open (<10%)/ moderate (10-40%)/ Forest type :							
<b>Conservation practices</b>	Terracing/ Bunding/ Grassed bunding/ Stone bunding ✓							
<b>Erosion features (rills/ gully others)</b>	Sheet							
<b>Past erosion class</b>	Slight (e1),/ moderate (e2)/ severe (e3)/ very severe (e4) ✓						Field photo no. 25	
<b>Soil Layer</b>	Coarse Fragments (%)		Soil Colour (moist)				Sample no.	
0-15cm.	15						21	
15-30 cm.								
30- 50 cm.								
>50 cm.								
<b>Soil classification</b>								
<b>Soil drainage class</b>	Excessive/ well/ moderate well/ poor/ very poor ✓							
<b>Land capability class</b>	Class I/ Class II/ Class III/ Class IV				Class V/ Class VI/ Class VII/ Class VIII			
<b>Remarks</b>	Near settlements							



### 3.5.5 Slope measurements

The slope is the most important parameter in erosion modelling. An inclinometer (Fig. 27 a) was used to measure the slope of different locations which delivers on-site slope (Fig. 28 a and b) of an area. Field observations are necessary for validating the computer/mathematically generated slope map generated using

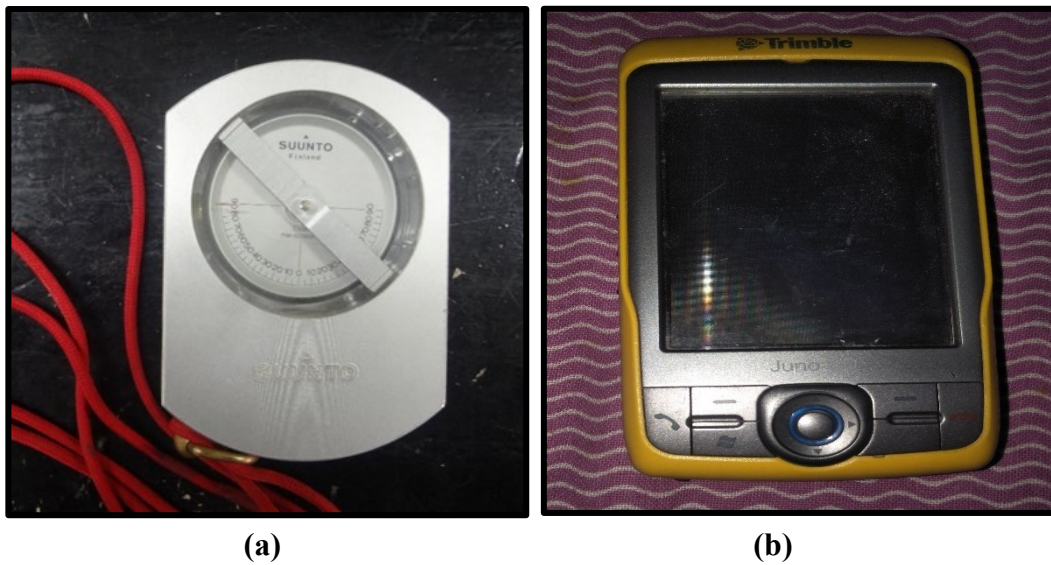


**Figure 27. (a) Inclinometer, (b) Trimble GPS**

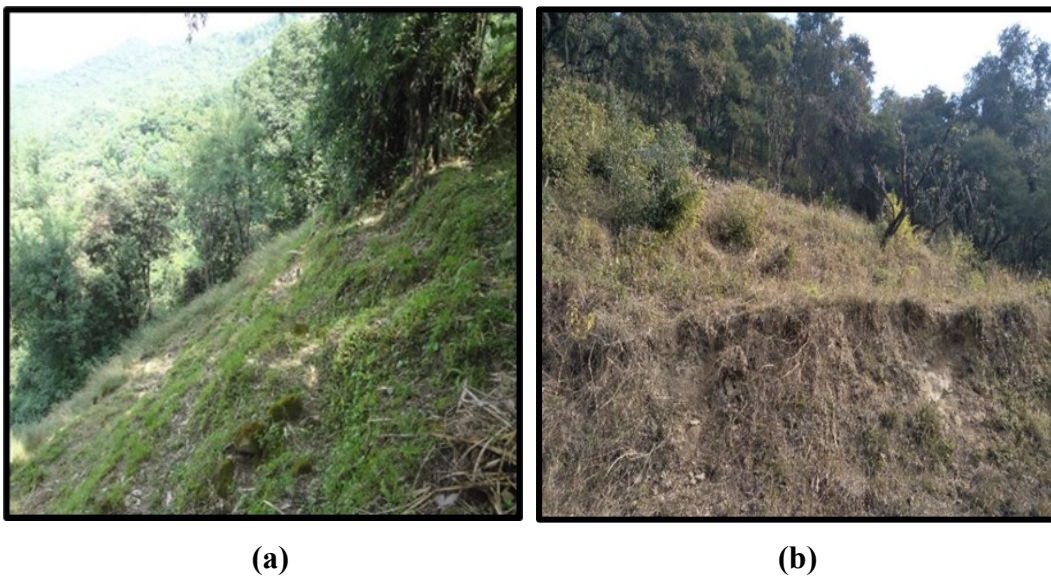


**Figure 28. Steep slopes observed in the study area (a and b)**

(ArcGIS). Several numbers of observations at different physiographic units such as steep side slopes, moderately steep side slopes and in valley fields were taken and georeferenced using Trimble GPS receiver (Fig. 27 b) (accuracy  $\pm 5\text{m}$ ).

### 3.5.6 Other Field Observations

Fertilizer and pesticides application rate, timing and type was observed and enquired. It was observed that cow dung (Fig. 29 a) is the major fertilizer used in the field. Usually, the first application was approximately  $2 \text{ Kg/m}^2$ . Urea was used at the rate of  $50 \text{ grams/m}^2$  in the second application pesticides and weedicides were used against pest and weeds respectively. There are some water bodies (Fig. 29 b) were also observed in the field.

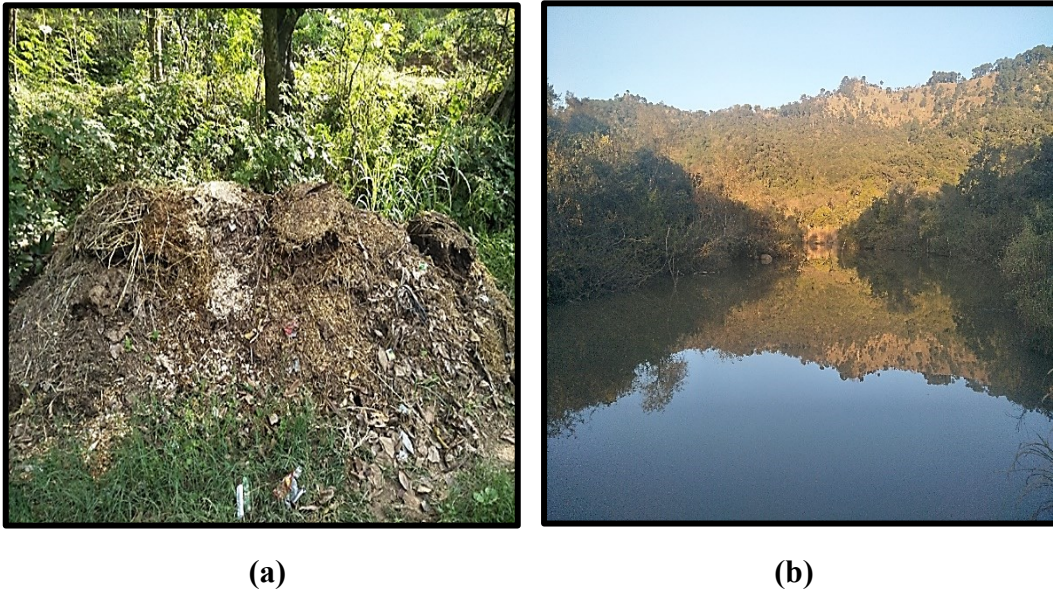


**Figure 29. (a) Farmyard manure application observed in a field of the study area, (b) Waterbody**

### 3.6 SOIL HYDRAULICAL PROPERTIES

Mini Disk Infiltrometer was used to measure unsaturated hydraulic conductivity and infiltration rate. A total of 32 sites selected for hydraulic conductivity and infiltration rate measurement, at different land use/land cover. Each measuring site was georeferenced with a Trimble GPS receiver. Infiltrometer was set to a smooth spot on the soil surface. At times the surface remained not level,



a slight layer of fine silica sand was placed to the area straightforwardly underneath the Infiltrometer stainless steel plate. It ensures proper interaction among the soil and the Infiltrometer. A schematic representation of hydraulic conductivity sampling locations is given in Fig. 30.

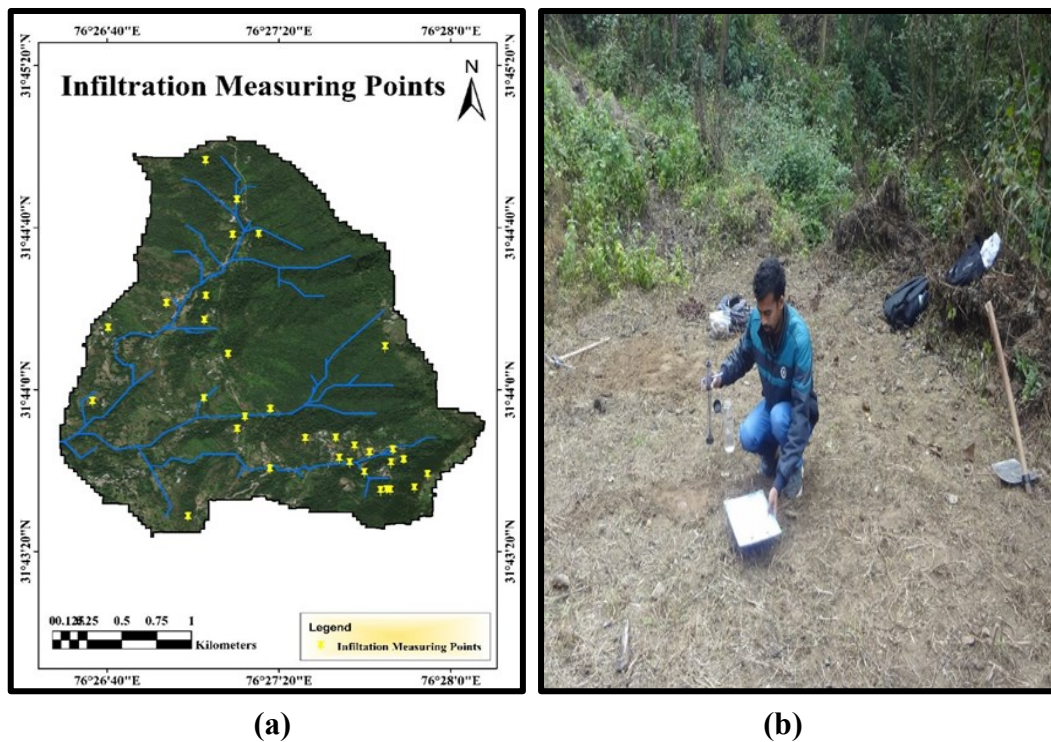


**Figure 30. (a) Soil infiltration rate sampling locations, (b) Infiltration and hydraulic conductivity measurement**

### 3.6.1 Infiltration and Hydraulic Conductivity

Infiltration is the process by which water on the ground surface enters the soil. The hydraulic conductivity of the soil is the rate at which water can travel through the soil under specific conditions and hydraulic gradients. Naturally, water movement through soil occurs in saturated and unsaturated circumstances. Mini Disk Infiltrometer (Fig. 31) was used to measure infiltration and hydraulic conductivity of the soil. It is a tension infiltrometer and it measures the unsaturated hydraulic conductivity of the medium while it is placed on at different applied tensions. It has suction heads of 0.5 to 7 cm.



**Figure 31. Mini disk Infiltrometer**

At first, the bubble chamber was filled three-quarters full. Then the suction control tube was slide down, detached the lowermost elastomer with the porous disk and filled the water reservoir. Set the position of the end of the Mariotte tube 6 mm from the end of the plastic water reservoir tube. Infiltrometer was held vertically and ensured that no water leaking out. Then selected the suction rate as 2 cm. After that, infiltrometer was placed on a smooth spot on the soil surface and ensured that there is good contact between the soil and the Infiltrometer.

At first, noted the initial volume and placed the instrument in levelled surface and taken the reading at 2-minute interval until a constant rate was obtained or allowed 15 to 20 ml of water to enter the soil (Fig. 30 b). The data was noted in a specific format mentioned below. The Microsoft Excel spreadsheet (Fig. 32) of METER was used to calculate the slope of the curve of the cumulative infiltration versus the square root of time-based on the data gathered.

$$k = C1/A$$

Where, k = hydraulic conductivity; C1 = slope of the curve of the cumulative infiltration versus the square root of time; A = Van Genuchten parameters for a specified soil type.

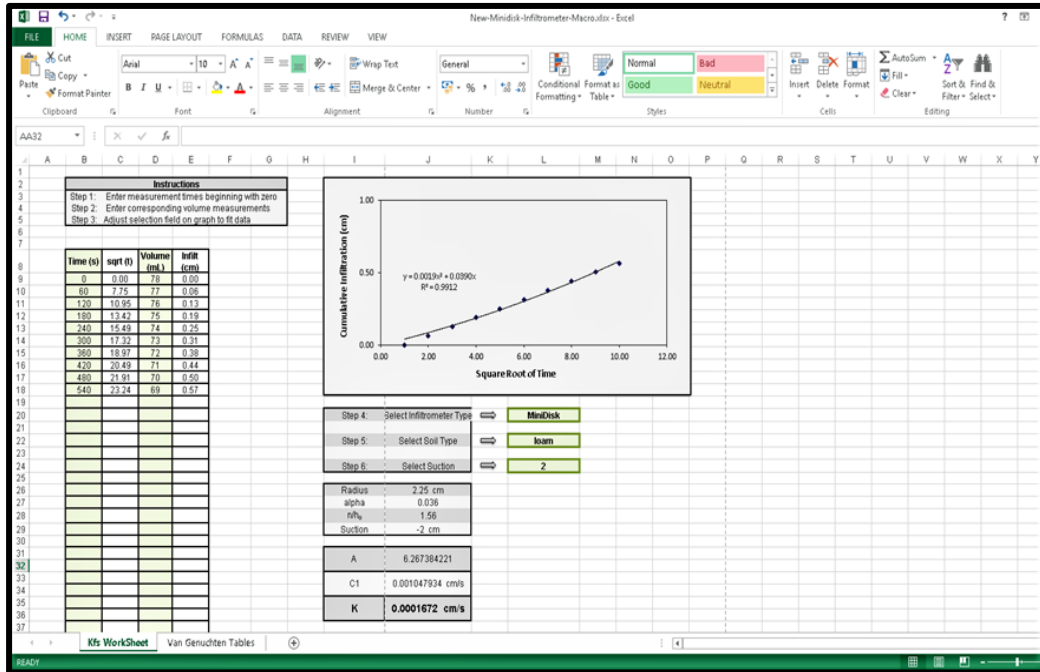


Figure 32. Mini disk Infiltrometer calculation sheet

### 3.6.2 Soil Plant Atmosphere Water (SPAW) Model

The SPAW model is a daily hydrologic budget model for agrarian fields, with

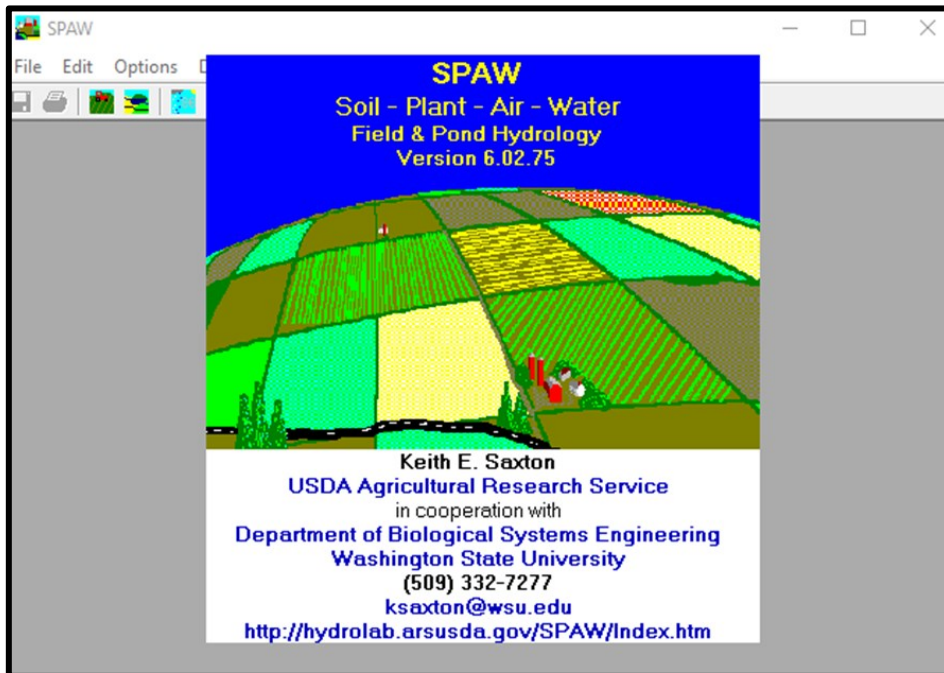


Figure 33. SPAW Model Interface



a sensible degree of multifaceted nature, to represent the fundamental hydrologic forms. The model (Fig. 33) inputs the atmosphere, soils and crops of a specific farm in the one-dimensional vertical plane. The climatic factors, hydrologic input, daily precipitation, air temperature, climate hydrology are included. The soil and crop inputs are given in a daily basis and the water into and out of the field calculated by soil plant-air-water (SPAW) model.

Hydrologic examinations frequently and contain the evaluation of soil water storage, soil water infiltration, conductivity and plant-water interactions. To depict the hydrologic soil water impacts, attributed by utilizing soil factors, for example, texture, structure and organic matter. Field and lab investigation is complex, costly and inadequate for various hydrologic examinations. Realistic relationships between soil water potential, soil texture and hydraulic conductivity can convey evaluations agreeably precise for some investigations.

The texture evaluations are improved by the four useful factors and can be chose on the neighbouring slide bars: salinity, organic matter, gravel and density (compaction). Every factor varies the whole arrangement unequivocally. The factors have cut off points to continue computation legitimacy. The organic matter was estimated with the texture condition correlations. Different modifiers were determined from literature and information sources. Aggregate with the texture conditions, they convey a more real soil water description than any single assessing technique.

Soil depth is another significant factor concerning soil. It is the depth of soil profile from top to the parent material or bedrock or layer of obstructions for roots. Soil profile has an important role in identifying the hydrological properties. The soil in the investigation zone is shallow, that is under 50 cm, higher elevation has lower soil depth, and in valley agricultural fields generally higher depth were observed. The shallow and sandy soil in the study area is suitable to find the hydrological properties using SPAW model. Fig. 35 shows the diagram for all textures aside from those with clay content surpassing 60 per cent.

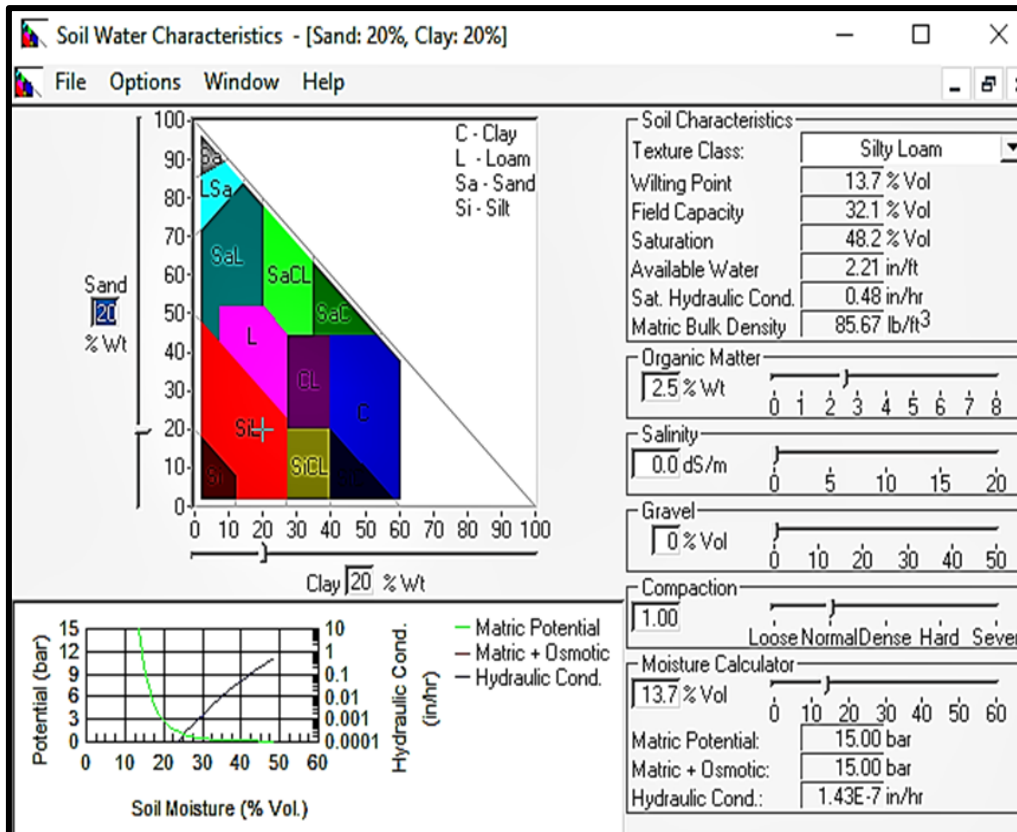


Figure 34. Model interface of soil water characteristics

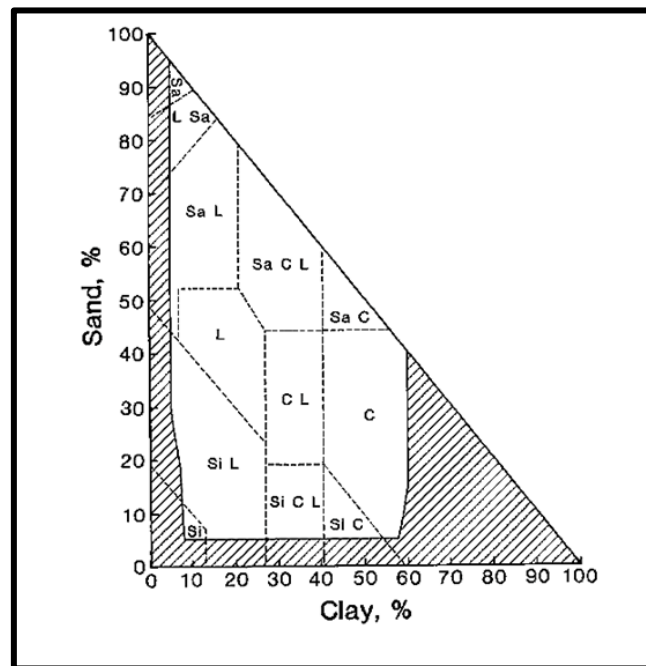


Figure 35. Applicable textural region (white) for the derived equations

A dynamic arrangement of the subsequent conditions will evaluate soil water qualities appropriate to numerous hydrologic and water management with least input estimations of texture and organic matter. Equations and parameters are evaluated for the full range moisture-tension and moisture-conductivity connections which likewise provide a few standard moisture values, for example, SAT, WP, FC, PAW,  $\rho_n$  and KS. Average texture and organic matter values, such as (Rawls *et al.*, 1998) local references, will regularly provide valuable hydrologic solutions.

The equations were likewise customized as the water characteristic evaluations in the SPAW hydrologic model (Saxton and Willey, 2005) as a switch for the recently characterized conditions detailed by Saxton *et al.* (1986). For assessment, the two arrangements of equations are available as an alternative option in the SPAW model and the graphical interface program (Fig. 34).

### 3.7 METEOROLOGICAL DATA

#### 3.7.1 Weather data (AWS)

The study area has an Automatic Weather Station (AWS) (Fig. 36) maintained by the Space Application Centre (SAC), ISRO. It provides rainfall, maximum and minimum temperature, solar radiation, relative humidity, wind speed and direction and dew point temperature. Only rainfall and temperature (maximum and minimum) are required for the study. AWS works with the help of a solar panel, and it has satellite telemetric antenna to upload weather data to the satellite. The data can be retrieved either from the SAC website or using a passcode with the flash drive directly from AWS. In addition to this, a tipping bucket rain gauge was installed near the watershed observatory. It has a data logger to store and retrieve the data. It measures instantaneous rain. Rainfall data from this rain gauge was used for the study. The maximum and minimum temperature from AWS was used for analysis. Rainfall intensity (mm/hr) was calculated from rainfall data, which was used as model input.



**Figure 36. Automatic weather station**

### 3.8 DOWNSCALING OF GLOBAL CLIMATE DATA (SDSM)

The spatial data sets needed for future climate projection was downloaded from (Fig. 37) Data portal of the Canadian Government which provide HadCM3 A1, B1, A2, & B2 scenario. A1 and B1 scenario represents global scenario and A2a

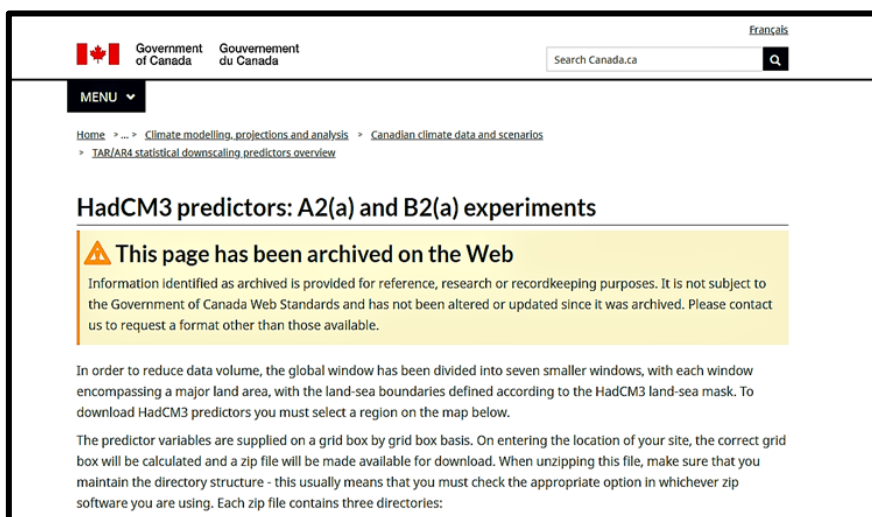


**Figure 37. HadCM3 data downloading window**

and B2a provide regional scenarios. 'A' scenario represents greater economic development and 'B' represents an environment-friendly developmental approach. For this study, A2a & B2a scenario was used.

The latitude and longitude of the study area were used to download the data. Each latitude and longitude have specific grid numbers. After selection of the desired site, the precise grid box was generated, and a zip file was made available for download. It contains three types of files. Viz,

**NCEP\_1961-2001:** This registry incorporates 41 years of daily observed predictor information, from the NCEP reanalyses, standardized over the entire (1961-1990) period. This information was merged to the indistinguishable network as HadCM3 of 2.5 °N x 3.75 °E resolution before standardization was executed.

**H3A2a\_1961-2099:** This catalogue includes 139 years of daily GCM predictor information, derived from the HadCM3 A2 (a) experiment, standardized during 1961-1990 period.

**H3B2a\_1961-2099:** This registry incorporates 139 years of daily GCM predictor data, derived from the HadCM3 B2 (a) experiment, standardized over the 1961-1990 period.

### **3.8.1 Input data**

#### *3.8.1.1 Weather data*

Daily rainfall, maximum and minimum temperature data were collected from the India Meteorological Department (IMD), Pune. The data from 1985 to 2014 of Una station was used for the study. The daily data from 1985 to 1999 were selected for calibration and the other half of 2000 to 2015 were selected for validation.

### 3.8.1.2 Global climate data

HadCM3 (short name for Hadley Center Coupled Model, version 3) is a coupled atmosphere-ocean general circulation model (AOGCM) created by the Hadley Center in the United Kingdom. It was one of the significant models utilized in the IPCC Third Assessment Report in 2001. HadCM3 is made out of two parts: the atmospheric model HadAM3 and the sea model (which incorporates a sea ice model). Simulations regularly utilize a 360-day schedule, where every month is 30 days. The HadCM3 atmospheric model (HadAM3) is a grid point model and has a horizontal resolution of  $3.75 \times 2.5$  degrees in longitude  $\times$  latitude. The resolution of the ocean model (HadOM3) is  $1.25 \times 1.25$  degrees. Contrasted with later models, HadCM3 has generally low resolution however keeps on performing sensibly well, at any rate concerning its mean climate (Reichler and Kim, 2008; Flato *et al.*, 2013).

### 3.8.2 Statistical downscaling model (SDSM)

SDSM (Fig. 38-39) is a decision support tool for the evaluation of local climate change impacts. It was created by Wilby *et al.* (2002). It is a combination

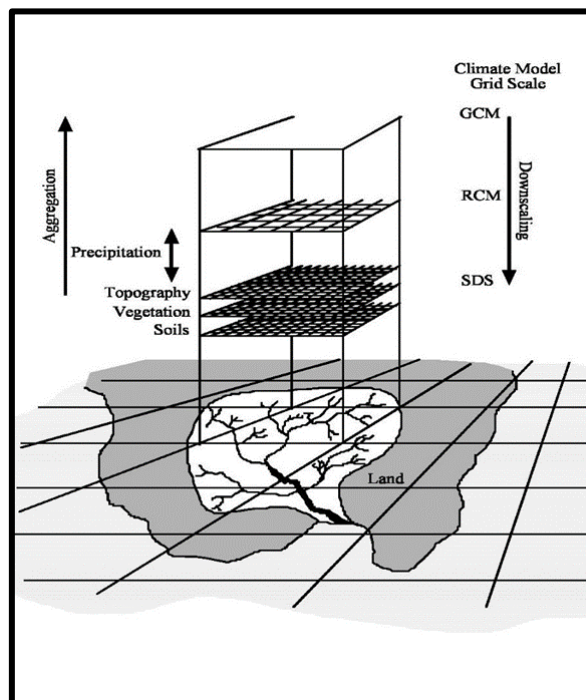
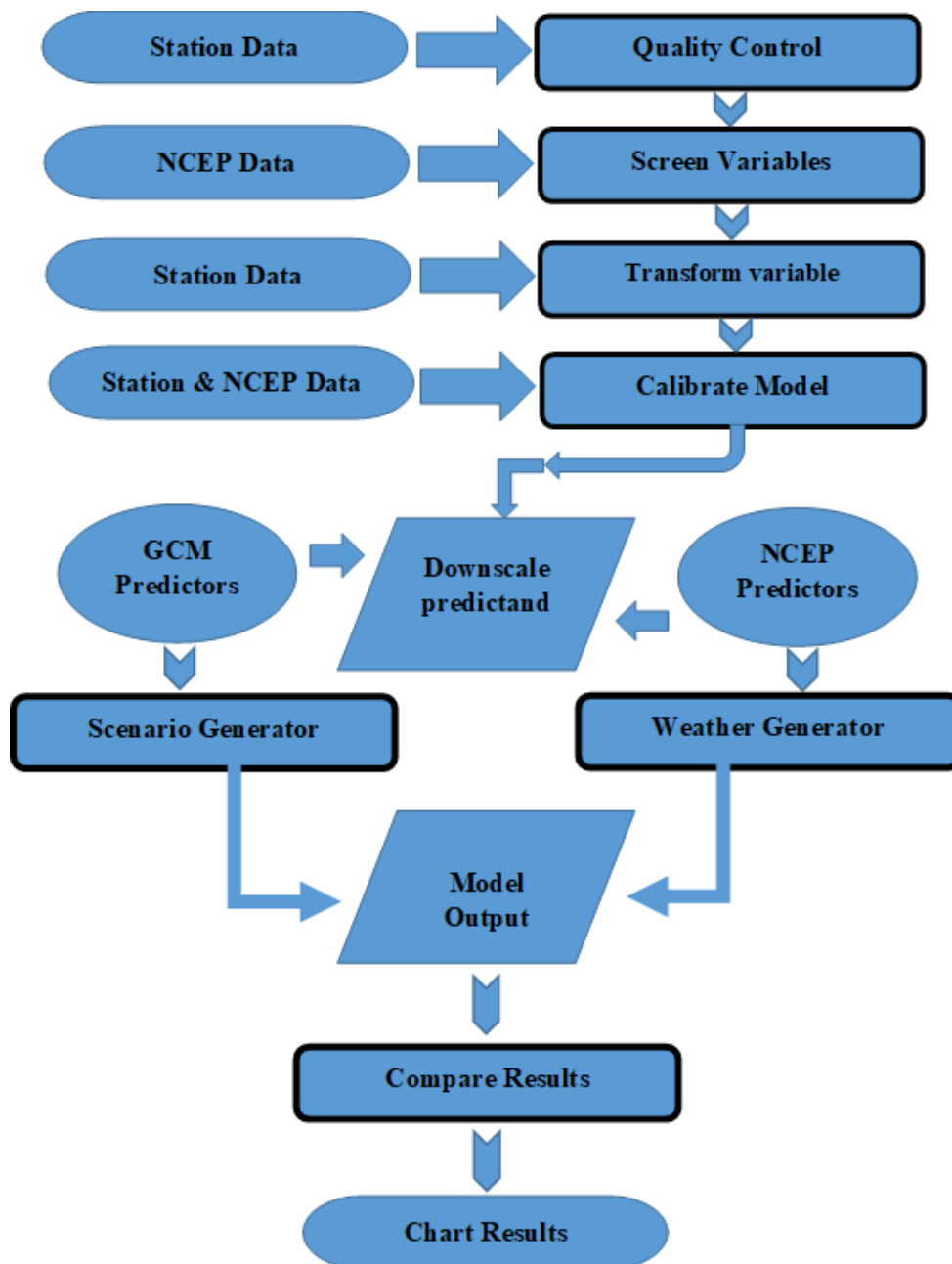


Figure 38. Common methodology to downscaling



**Figure 39. Methodology for downscaling of global climate data**

of multiple linear regression model and a stochastic weather generator. It builds up the empirical relation between GCM large scale predictors and locally observed climate data. It encourages the fast advancement of numerous minimal efforts, single-site scenarios of daily surface weather parameters under present and future climate forcing.

Furthermore, the tool performs auxiliary steps such as data quality control and transformation, predictor variable pre-screening, automatic model adjustment, vital diagnostic testing, statistical examinations and plotting of climate data. Statistical downscaling is the more promising alternative for local climate prediction. It empowers the development of climate change scenarios for single locales at the daily time-interval, utilizing grid resolution GCM output (Wilby and Dawson, 2007).

#### *3.8.2.1 Quality control and data transformation*

Few meteorological stations of India Meteorological Department (IMD) have complete and precise data sets. In practical situations quality checking of missing data is essential. Quality Control in SDSM allows the user to find out data errors, specification of missing data codes, maximum and minimum range before model calibration.

Before the calibration of the model, it is necessary to change predictors and the predictand. The Transform option allows the user to select desired data records and applies selected changes such as logarithm, power, inverse, lag, binomial and so forth. The biased precipitation data to change over a normal distribution, for application in regression analysis the fourth root change was applied. (Khan *et al.* 2006; Huang *et al.* 2012).

#### *3.8.2.2 Screening of downscaling predictor variables*

Screen Variables is to support the user in the choice of fitting downscaling predictor factors listed in Table 5. This is one of the most difficult stages in any statistical downscaling model since the selection of predictors generally decides the character of the downscaled climate condition. The decision technique is likewise entangled by the way that the explanatory power of individual predictor factors changes both spatially and temporally. Screen Variables encourages the assessment of seasonal variabilities in predictor ability. In this way, the predictors were chosen cautiously for the study. At first, the percentage of variance elucidated



unambiguously by predictand-predictor sets were found. An aggregate of 26 NCEP predictor was accessible for the study. The power of individual predictors frequently changes, especially monthly. The Correlation button is utilized to examine the relationships for determined sub-periods of yearly, seasonal or monthly. SDSM additionally reports a partial correlation between the chosen predictors and predictand. These statistics aid to recognize the extent of explanatory power that is one of a kind to every predictor. The Scatter button is utilized for visual investigations between indicated sub-periods (yearly, seasonal or month to month). The resultant scatterplot(s) demonstrate the idea of the association (direct, non-direct, and so forth.), regardless of whether data transformation(s) might be required, and the significance of outliers.

### *3.8.2.3 Calibrate model (Calibration of model)*

The Calibrate Model option allows user to choose predictand joined with a lot of predictor factors and ascertain the parameters of multiple linear regression through an optimisation calculation (either dual simplex (DS) or ordinary least squares (OLS)). Huang *et al.* (2011) observed that the OLS inferred proportionate results as DS and was also quicker than DS. The user can decide the model structure: whether or not month to month, seasonal or yearly sub-models whatever required. The SDSM model was set to run on a yearly basis for ease in the calibration of the model since it gave a satisfying result over a month to month period (Mahmood and Babel, 2013).

In this manner, the model produced one equation for all the months utilizing the OLS technique. The procedure can be unconditional or conditional. In unconditional models, an instant connection is expected between the predictors and predictand. In conditional models, there is a transitional technique between regional forcing and local climate.

The available data set (predictand) from 1985 to 1999 of 15 years was selected to calibrate the model. The summary report generated the percentage of explained variance, standard error, and Durbin- Watson statistic for each month.

After these parameters were obtained satisfactory, the regression model was finalised.

**Table 5. NCEP predictors used in the screening process**

Sl. No.	Predictor	Description	Sl. No.	Predictor	Description
1	mslp	Mean sea level pressure	14	p8_f	850hPa geostrophic airflow velocity
2	p_f	Surface geostrophic airflow velocity	15	p8_u	850hPa zonal velocity
3	p_u	Surface zonal velocity	16	p8_v	850hPa meridional velocity
4	p_v	Surface meridional velocity	17	p8_z	850hPa vorticity
5	p_z	Surface vorticity	18	p8th	850hPa wind direction
6	p_th	Surface wind direction	19	p8zh	850hPa divergence
7	p_zh	Surface divergence	20	p500	500hPa geopotential height
8	p5_f	500hPa geostrophic airflow velocity	21	p850	850hPa geopotential height
9	p5_u	500hPa zonal velocity	22	r500	500hPa relative humidity
10	p5_v	500hPa meridional velocity	23	r850	850hPa relative humidity
11	p5_z	500hPa vorticity	24	rhum	Surface relative humidity
12	p5th	500hPa wind direction	25	shum	Surface specific humidity
13	p5zh	500hPa divergence	26	temp	Mean temperature at 2m height

#### 3.8.2.4 Weather generator (Validation of model)

The Weather Generator process produces groups of ensembles synthetic day by day weather data from observed (or NCEP reanalysis) atmospheric predictor factors. The methodology facilitates the authentication of calibrated models and the

synthesis of artificial time series for present climate conditions. The daily data from 2000 to 2014 of 15 years was used for the validation. The 20 ensemble members out of 100 were used to simulate the data using a weather generator. The summary statistics such as mean, standard error and coefficient of determination ( $r^2$ ) were used to determine the accuracy of the model.

#### *3.8.2.5 Scenario generation*

The Scenario Generator process produces ensembles of synthetic daily weather data from atmospheric predictor factors provided by a climate model, as opposed to from observed predictors. When the model precision was seen as good, at that point it was utilized to downscale the HadCM3 GCM data for the baseline period/ current period (1985 to 2014) and the three future periods; the 2020s from 2011 to 2040, 2050s from 2041 to 2070 and 2080s from 2071 to 2099 respectively using scenario generator. The HadCM3 had year length of 360 days so the model setting was altered from the calendar to 360 days. The data was then transformed into 365 days.

### 3.9 SURFACE RUNOFF AND SEDIMENT DATA

#### **3.9.1 Runoff data**

The pressure-based water level recorder was installed in the watershed observatory (Plate 3). The Levellogger Junior Edge includes a pressure sensor and a temperature detector. Vented pressure sensors use a vented link, a tiny vent tube that runs towards the length of the wire from the surface and ends behind the pressure transducer. This vent tube goes about as a channel to make up for barometric pressure changes at the surface, along these lines, permitting the barometric pressure on the water segment to be counteracted by the weight transmitted in the cylinder. It records water level and temperature with 15 min. interval. Trapezoidal flume structure was constructed at the outlet of the watershed by IIRS, to measure surface runoff water. Rating table was used to estimate surface runoff of each event daily. Runoff data was collected for the rainy



(a)



(b)



(c)



(d)

**Plate 3. Gauging station: (a) and (b) Trapezoidal flume, (c) Stilling well, (d) pressure-based water level recorder**

season (July-September) and was analysed and used to calibrate and validate the model. A total of 22 rainy day readings for the year 2017 and 2018 were collected. Nevertheless, some essential rainfall event readings were missed due to blockage of the connected pipeline due to high silt content choking in the pipe.

### 3.9.1.1 Surface runoff calculation

The Solinst Pressure based water level recorder measure water level at every 15 minutes interval. It helps to get instantaneous water level of the stream. According to the duration of rainfall and water level, either the average water level or peak water level was used to calculate runoff. The USDA trapezoidal flume rating table (Fig. 40) was used to measure the flow rate. The water level is first converted into feet for easiness of calculation, and the rating table gives cubic feet/second flow rate according to the height of water level in feet. This flow rate is then converted into cubic meter/second after which, the flow rate is converted into per day and then divided by total catchment area (square meter) to get total surface runoff of a day. Further, this data was used for APEX model calibration.

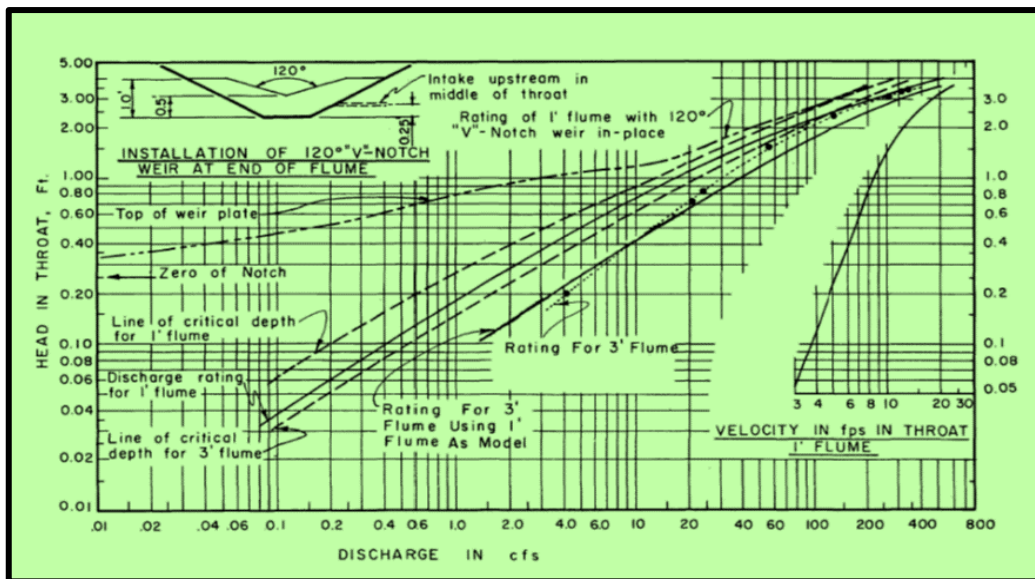


**Figure 40. Discharge rating curves and related data for one-and three-foot trapezoidal supercritical flow flumes. (USDA Hand Book)**

### 3.9.2 Sediment data collection

A 500-litre tank (Fig. 42) was also built by IIRS at the outlet which collects sediments continuously during the rainfall. A perforated steel pipe (Fig. 41) fitted at the middle of the flume structure collects the runoff water entering and stored in the sediment tank.

After rain every day at 08:00hrs (IST), runoff water samples were collected in a one-litre bottle. It denotes the runoff sample on the cumulative basis of the day. Sediment data of 20 rainy days were collected. The readings for sediment yield of the year 2017 and 2018 was available and used in calibration and validation the model.



**Figure 41. Sediment collection pipe**



**Figure 42. Sediment tank**



**(a)**



**(b)**

**Figure 43. Sediment filtration unit (a and b)**



### 3.9.2.1 Sediment analysis

Sediment filtration process was used to analyse the sediment samples collected from the gauging station (Fig. 43). Initially measured the dry filter weight. The filter containing sediments were oven-dried and the weight of the filter and sediment were recorded. By subtracting the weight of filter, the sediment weight was estimated. The sediment weight was then equated with the volume of water to obtain the sediment concentration in mg/litre. The sediment (mg/litre) is multiplied with total water (L) flow through the flume, gives total sediment at a given period.

## 3.10 MODELLING SURFACE RUNOFF AND SEDIMENT YIELD

### 3.10.1 Model description- APEX

The Agricultural Policy/Environmental eXtender (APEX) model (Williams *et al.*, 2008a;b) was created to expand the EPIC's abilities to reproduce land management practices for small to medium watersheds and various farms. The Agricultural Policy Environmental eXtender (APEX) model is a hydrologic/water quality model and is equipped for performing long term simulations. The watershed might be separated into numerous identical (based on soils, land use, topography and so on.) subareas. The routing segment simulate stream starting with one subarea to the next over channels and flood fields to the watershed outlet and transports sediment, pesticides and supplements. The management practices incorporate irrigation system, drainage, buffer strips, furrow diking, waterways, terraces and pesticide application. Other than these farms the management practices; APEX is utilized in assessing the impacts of climate and carbon dioxide changes; planning naturally protected and monetary landfill sites. The model works on a daily time step and is equipped for simulating several years if needed.

ArcAPEX is an ArcGIS-UI, intended to systematize the input characterization of the APEX hydrologic/water quality model. The interface coordinates geographical, land use and soil spatial datasets and an implicit APEX variables database that contains model variables mandatory to simulate a wide

possibility of plant development, culturing, manure and pesticide applications over a field to the basin-scale drainage area. ArcAPEX interface is introduced with watershed delineation, characterization of land use and soils, climate information, input boundary definition, model executions and run and SWAT model incorporation. (Tuppad *et al.*, 2009).



**Table 6. Major components and capabilities of APEX model**

Major Components	Major capabilities
<ul style="list-style-type: none"> <li>• Climate Inputs</li> <li>• Hydrologic Balance</li> <li>• Water and Wind Erosion</li> <li>• Routing Component</li> <li>• Reservoir Component</li> </ul>	<ul style="list-style-type: none"> <li>• Soil Erosion</li> <li>• Soil</li> <li>• Crop/Plant</li> <li>• Tillage</li> <li>• Water Routing</li> <li>• Climate Change</li> <li>• Peak Runoff Rate</li> <li>• Runoff Volume Estimate</li> </ul>

APEX can simulate long term simulations for modelling the effects of various nutrient management, tillage, conservation, cropping system and other management practices on surface runoff and losses of sediment.



## *Basic Concepts and Principle of the APEX model*

### *3.10.1.1 Simulating surface runoff*

The daily precipitation is used to simulate surface runoff and peak runoff rate. Two approaches are accommodated for assessing runoff. First one is the modification curve number method developed by Soil Conservation Service (SCS) (U.S. Branch of Agriculture and Soil Conservation Service, 1972) and another one is Green and Ampt infiltration method (Green and Ampt, 1911). The curve number method was chosen for use since it is dependable, inputs are promptly accessible, computationally effective and it depends on soil type, management practices and the land use.

Runoff Volume- The SCS Curve Number Method

$$Q_{dr} = (RF - 0.2*rt) / (RF + 0.8*rt); RF > 0.2*rt$$

$$RF < 0.2*rt$$

$Q_{dr}$  is the daily runoff, RF is the daily rainfall, and  $rt$  is a retention parameter. The ' $rt$ ' differs between regions due to soils, management, land use, slope and variation in soil water content. The parameter  $rt$  is associated with curve number (CN).

$$rt = 254 * (100 / CN - 1)$$

The CN is the curve number and can be obtained for an entire region by the APEX model user manual (William *et al.*, 2008).

### *3.10.1.2 Peak runoff rate*

Primarily two choices for evaluating the peak runoff rate, the first one is the modified rational formula and the second one is SCS TR-55 approach (USDA-SCS, 1986). A stochastic component is added to permit sensible reproduction of peak runoff rate, given the daily precipitation and monthly precipitation intensity.

$$Q_{pr} = q_c * i * WA / 360$$

$Q_{pr}$  ( $m^3 s^{-1}$ ) denoted by the peak runoff rate,  $q_c$  is runoff coefficient based on the infiltration features,  $i$  ( $mm h^{-1}$ ) is the rainfall intensity for the watershed's time of concentration and watershed area in ha denoted by WA.

$$q_c = Q_{dr} / RF$$

### 3.10.1.3 Simulating sediment yield

The APEX model can simulate erosion due to both precipitation and runoff. To simulate erosion due to precipitation and runoff, APEX comprises 7 erosion simulation equations such as the USLE (Wischmeier and Smith, 1978), the Onstad-Foster modification of the USLE (Onstad and Foster, 1975), RUSLE (Renard *et al.*, 1997), the MUSLE (Williams, 1975).

The six settings are indistinguishable except for their energy segments. The USLE relies sensibly on precipitation as a marker of erosive energy. The MUSLE and its varieties utilize just runoff factors to simulate erosion and sediment yield. Runoff factors expanded the forecast precision, dispensed with the requirement for a transport proportion, and empowered the equation to obtain single storm assessments of sediment yields. The USLE gives just annual measures.

Thus, the water erosion model uses an equation of the form

$$Y_s = X_r * E_{Ks} * C_{Mv} * P_{Ec} * S_{Lt} * C_{Fs}$$

Where, sediment yield is denoted by  $Y_s$  ( $t ha^{-1}$ ), soil erodibility denoted by  $E_{Ks}$ , crop management factor represented by  $C_{Mv}$ , erosion control practice factor denoted by  $P_{Ec}$ , the slope length and steepness factor represented by  $S_{Lt}$  and coarse fragment factor represented by  $C_{Fs}$ .

The Erosivity factor,  $X_r$  calculated by Onstad-Foster equation, comprises a hybrid of the USLE and MUSLE energy factors (Onstad and Foster, 1975).

$$Xr = 0.646*EI+0.45*(Qdr*Qpr)^{0.33}$$

The soil erodibility factor, EKs, is assessed for the topsoil layer at the beginning of each year of simulation.

$$EKs = Z1*Z2*Z3*Z4$$

$$Z1 = 0.2+0.3*\exp(-0.0256*SND*(1-01*SLT))$$

$$Z2 = (SLT / (CAY+SLT))^{0.3}$$

$$Z3 = 1.0-0.25*OC / (OC+\exp(3.718-2.947*OC))$$

$$Z4 = 1.0-0.7*SA1 / (ZZ+\exp(-5.509+22.899*SA1))$$

$$SA1 = 1.0-0.01*SND$$

Where SND, SLT, CAY and OC are expressed in percentage and represented as the sand, silt, clay and organic carbon content. It permits EKs to change from about 0.1 to 0.5. The primary term allows low EKs values for soils with high coarse-sand content and high values for soils with less sand. The fine sand content is assessed as the product of sand and silt divided by 100. The representation for coarse sand in the primary term is the difference between sand and the measured fine sand. The second term decreases EKs for soils that have high clay to silt proportions. The third term diminishes EKs for soils with high organic carbon matter. The fourth term decreases EKs additionally for soils with remarkably high sand substance (SND>70%).

The crop management factor is assessed for all days when runoff occurs by using the modified RUSLE equation,

$$CMv = FRS*FBI*FRU$$

$$FRS = \exp(-0.75*CVR)$$

$$FBI = 1.-FG*\exp(-0.1*CPH)$$

$$FRU = \exp (-0.026*(RRU-6.1))$$

$$FG=SLt/ (SLt+\exp (1.175-1.748*SLt))$$

Where FRD is the crop residue factor, FBI is the growing biomass factor, FRU is the soil random roughness factor, CVR is the above ground crop residue in t ha<sup>-1</sup>, CPH is the crop height in m, RRU is the soil surface random roughness in mm, SLt is the standing live biomass of the crop in t ha<sup>-1</sup>, and FG is the fraction ground cover by the growing crop.

The PEc value is calculated primarily by taken care of the conservation practices to be applied. The value of SL is calculated for RUSLE with the equation (Renard *et al.*, 1997).

$$SLt=RS*RL$$

$$RS=10.8*ST+0.03; SPG>4.57; ST<0.09$$

$$RS=16.8*ST-0.5; SPG>4.57; ST>0.09$$

$$RS=W1; SPG<4.57$$

$$W1=3.*STP0.8+ 0.56$$

$$RL= (SPLG/22.127) RX$$

$$RX=B/ (1+B)$$

$$B=ST/ (.0896*W1)$$

Where ST (m m<sup>-1</sup>) is denoted as the land surface slope in and SPG (m) is the slope length. The coarse fragment factor is assessed with the equation (Simanton *et al.*, 1984).

$$CFs=\exp (-0.03*RK)$$

Where RK is the percentage of coarse fragments in the surface soil layer.

## APEX model implementation

The model was implemented on both gauged nano-watershed and micro-watershed for detailed study. The process is described below.

### 3.10.2 Subarea delineation

After setting up (Fig. 44), the new APEX project, the Automatic Subarea

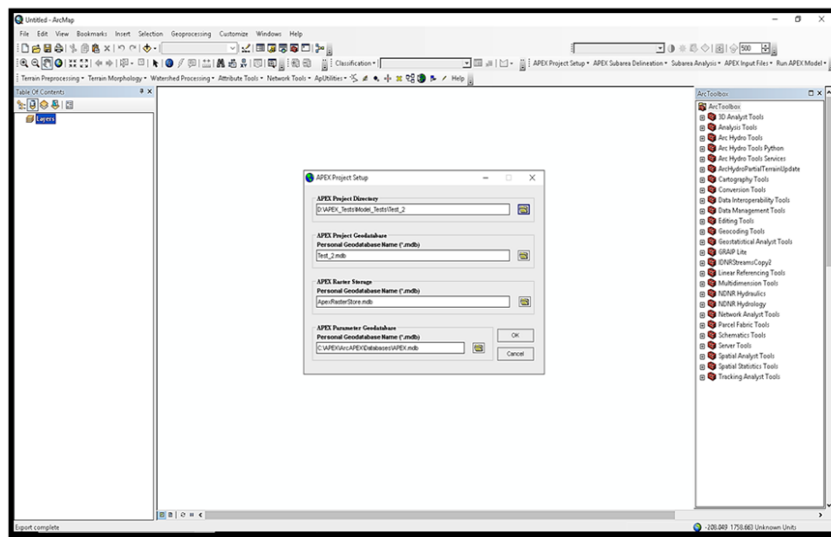


Figure 44. ArcAPEX Project Set up Window

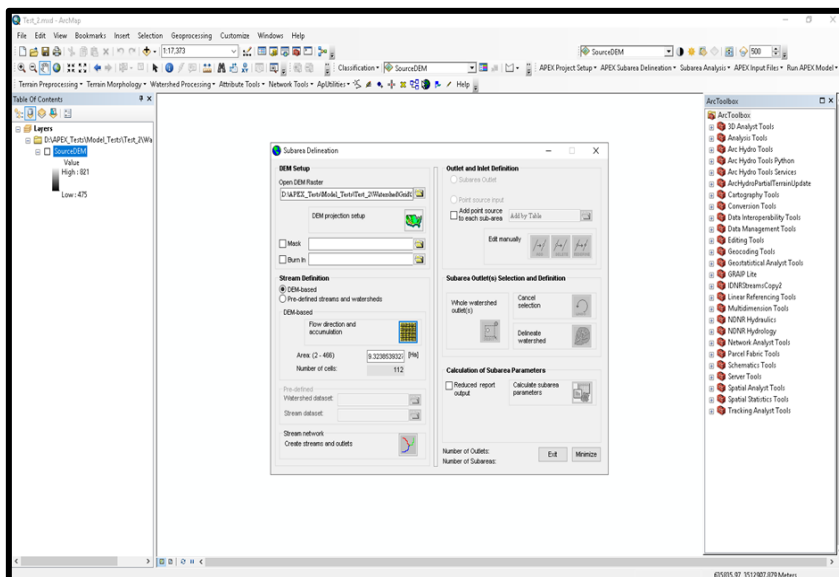


Figure 45. ArcAPEX DEM Setup Window

Delineation option under the APEX Subarea Delineation menu was activated and then APEX Standalone Delineation selected. The Subarea Delineation tool is divided into five sections, such as DEM setup, Stream Definition, Outlet and Inlet Definition, Subarea Outlet(s) Selection and Definition and Calculation of Subarea Parameters. This tool was used to create subarea delineations using a combination of DEM, digitized network (User-defined), and other user inputs.

#### *3.10.2.1 Dem setup*

The first phase in modelling was characterising the DEM (Fig. 45). DTM generated from stereo Cartosat-1 data was chosen as DEM for the model, because of its high resolution and the vertical accuracy. 30 m resolution DEM was used for the study. The DEM was masked for the study area for reducing the time of processing.

#### *3.10.2.2 Stream definition*

Stream definition states both the subarea outlets and stream network. Further Flow accumulation and direction was generated. The interface listed has optimum sub-basin area. After DEM processing, a minimum, maximum, and proposed subarea area (in hectares) icon were enabled in the drainage area box. This function has a vital role in determining the details of the stream network and the size and number of subareas created. The threshold area defines the drainage area required to form a stream. A small area will produce a very detailed stream network; whereas, a larger drainage area will produce fewer streams. After setting the threshold value of subarea, the stream network and outlets were delineated using the stream network option. The drainage network and stream junction points, used to describe subarea outlets, are shown on the DEM map grid.

#### *3.10.2.3 Outlet and inlet definition*

Outlet represents the points where one stream empties into another or is a point which is being monitored and validation data is available for. Inlets represent

any point source loading into the study area or the inlets of drainage into the watershed from an upstream area. Outlets were added using coordinate points acquired from the field by GPS.

#### *3.10.2.4 Main Watershed Outlet(s) Selection and Definition*

In this step, one or more outlet locations were selected to characterise the boundary of the main watershed. Watershed delineation needs outlet location, and the spatial location was defined manually for more refined delineation of the watershed. A total of 24 subareas were delineated based on flow and stream network. Also selected the adjacent watershed outlet which included in the study area for simulating runoff and sediment yield.

#### *3.10.2.5 Defining land use/land cover, soil and slope data*

The Land Use, Soil and Slope Definition option as Fig. 46 in the Subarea Analysis menu was adopted to specify the soil, land use and slope. APEX entails land-use data to find the area of each land category to be simulated within each subarea. In addition to land use information, APEX depends on soil data to find the range of hydrologic characteristics found within each subarea.

Land Use/ Land Cover- The land use/cover map was prepared for the area of interest. The lookup table containing various land use/cover class codes was used for linking the APEX's land use database to the land use layer.

Soil Database- Soil physical and chemical attributes were initially stored to the APEX soil database. Appropriate data mandatory for hydrological and soil erosion modelling was provided to the model. The database was linked to soil map through a lookup table and used as input for subarea analysis.

Slope Map- Slope is an essential factor that determines the water, sediment and nutrients movement. Slope map was generated for a micro watershed from DEM and divided into five classes.

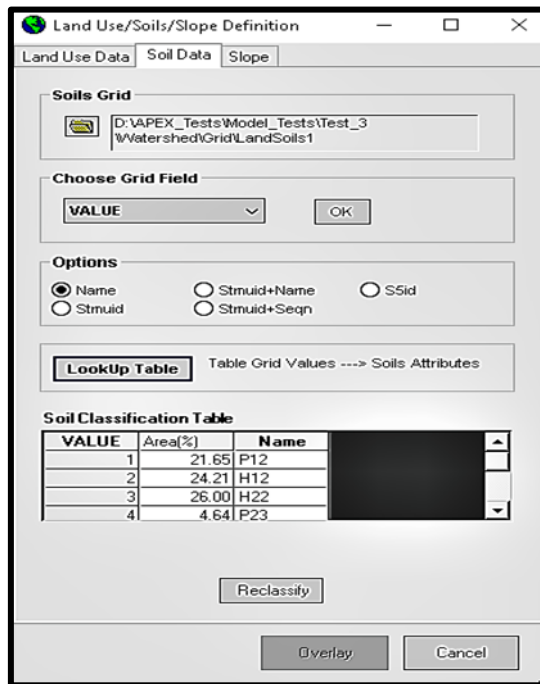


Figure 46. ArcAPEX Land Use/ Soil/ Slope Definition Window

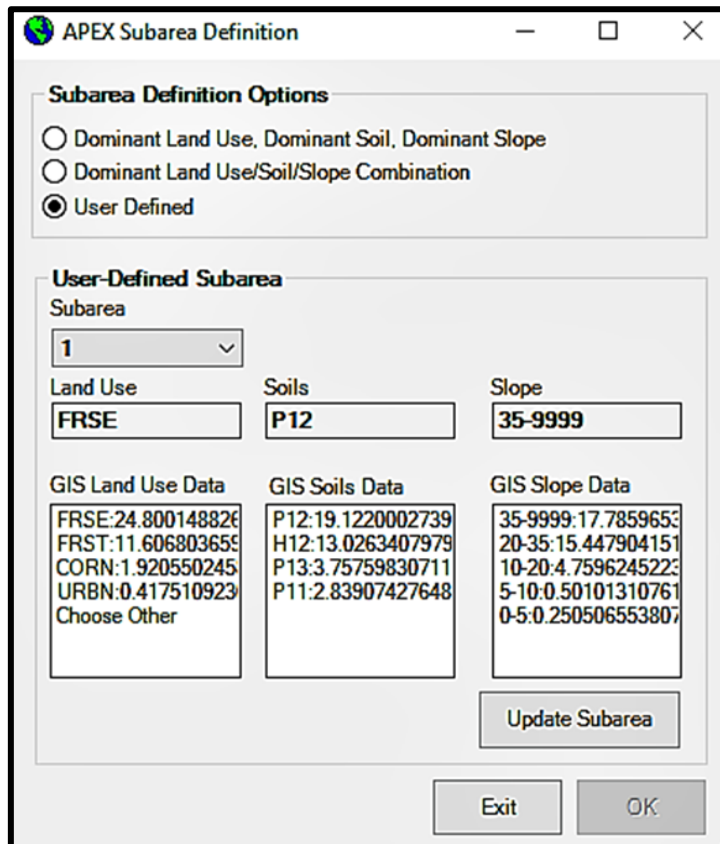


Figure 47. ArcAPEX Subarea Definition Window



#### *3.10.2.6 Overlay land use, soil and slope layers*

The land use, soil and slope layers were overlaid together using the OVERLAY option in the model.

#### **3.10.3 Subarea definition**

Subdividing the watershed into zones having different land use, soil and slope combinations enable the model to replicate differences in evapotranspiration for various crops and soils. Runoff, sediment, nutrient and pesticide loss is predicted distinctly for each subarea and routed to acquire the total runoff for the watershed. It increases precision and gives a much better physical description of the water balance. The criteria for subarea definition was chosen as Fig. 47 and ArcAPEX analysed the land use, soil and slope independently of each and assigned the dominant land use, dominant soil and dominant slope for each subarea. It can be verified using the subarea analysis report.

#### **3.10.4 Edit APEX database**

The ‘Edit APEX Databases’ (Fig. 48) option in the ‘APEX Input Files’ menu can be used to create input adjustments during the model calibration process, to the databases containing specific data used for running the model.

In this section, crop, fertilizer, pesticide, tillage, operation schedules, user monthly weather, user monthly wind and user soil were edited. Thus crop, fertilizer, operation schedules, user monthly weather and user soil database files were created.

##### *3.10.4.1 Editing crop database*

Crop database (Fig. 49) is most significant for soil erosion study. There are 137 different land uses (crop, forest, water bodies, urban etc.) are given in the crop database. This database contains different physiological properties of crops such as leaf area index at each stage, tolerance capacity, plant density and plant height. The study area has different land use/land cover such as maize, rice, forest, water bodies

and settlements, and these files were edited accordingly. As the study area dominated by maize and very few rice fields are there only maize fields were considered. The database of maize (CORN) was edited with seeding rate, plant density and plant height and other properties were kept the same as the default. There were no changes made for the forest, water bodies, and settlement database which keeps default.

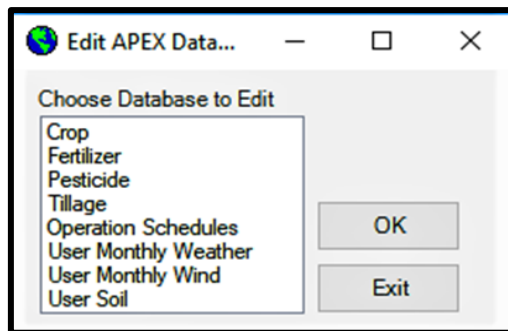


Figure 48. APEX edit database window

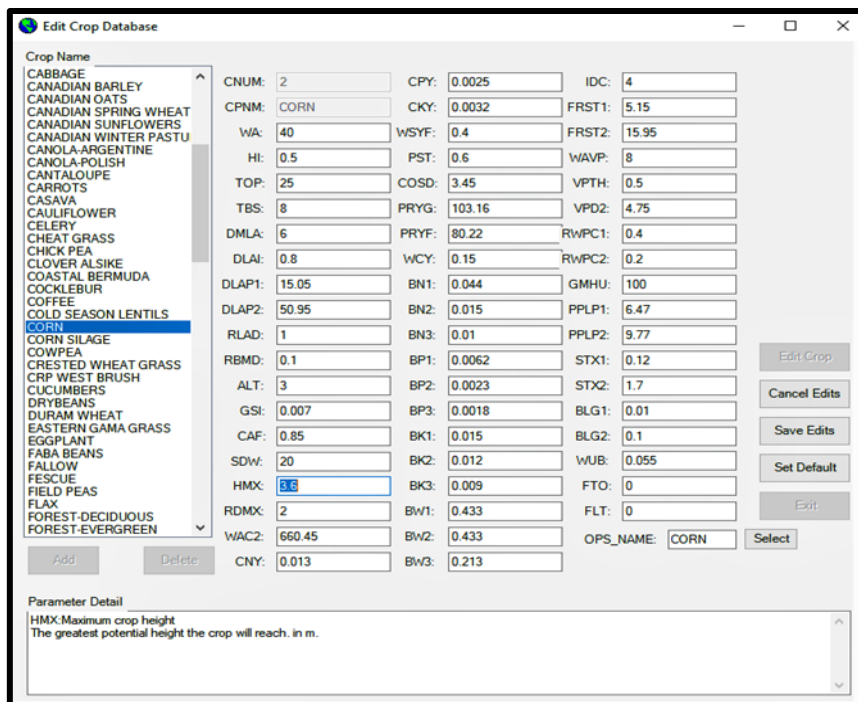


Figure 49. APEX edit crop database window

### 3.10.4.2 Editing fertilizer database

The fertilizer database (Fig. 50) allows different properties of fertilizer like N, P, K and carbon etc. It was observed that in the study area only manures were using, so manure file was changed accordingly.

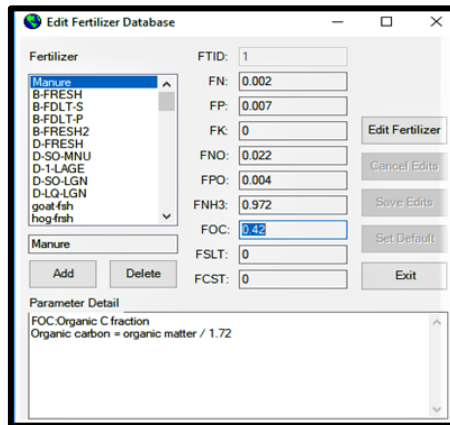


Figure 50. APEX edit fertilizer database window

### 3.10.4.3 Editing operation schedules database

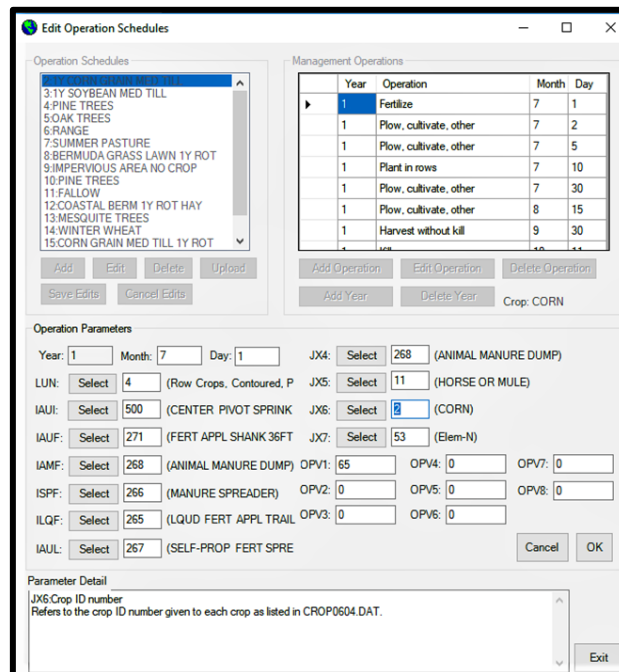


Figure 51. APEX edit operation schedule window

In this section (Fig. 51), fertilizer application, ploughing, planting and harvesting date for each crop were defined. The ploughing and other field operations were done with the help of animals, so ‘ANIMALS’ option was selected instead of a tractor. Operation schedule for the forest was set as matured.

#### 3.10.4.4 Editing user monthly weather database

User monthly weather (Fig. 52) option allows defining weather station name, coordinates and elevation. In this section, the monthly average of maximum, minimum temperature, rainfall, number of rainy days per month, the standard deviation of maximum, minimum temperature and maximum half-hour rainfall intensity (mm/hr) were added. Majority of the rainfall occurred in July, August and September. Therefore rainfall intensities of these months were provided to the model.

Jan	Feb	Mar	Apr	May	Jun
19.96	25.07	30.11	36.26	42.85	41.38
Jul	Aug	Sep	Oct	Nov	Dec
35.42	34.73	34.45	34.5	27.37	26

**Figure 52. APEX edit weather database window**

#### 3.10.4.5 Editing user soil database

The soil data (Fig. 53) needed for the study was added manually using ‘add new’ menu. In this section, soil physico-chemical properties for each type of soil was defined. Soil name, soil layers, soil hydrologic group, soil depth, soil textural

class, percentage of sand, silt and clay, bulk density, hydraulic conductivity, available water content, soil carbon, rock percentage, erodibility factor, soil albedo, and electrical conductivity were added for each soil layer separately. Anion exchange capacity and soil crack volume were kept the same as the default.

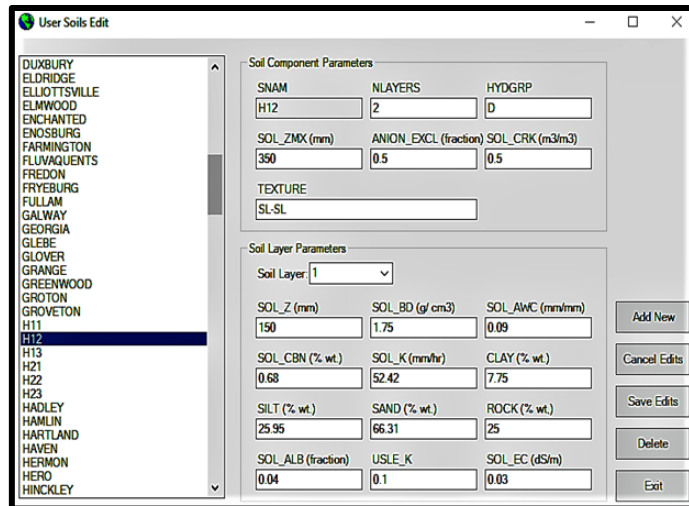


Figure 53. APEX edit soil database window

### 3.10.5 Defining weather database

The APEX model entails daily time series of solar radiation rainfall,

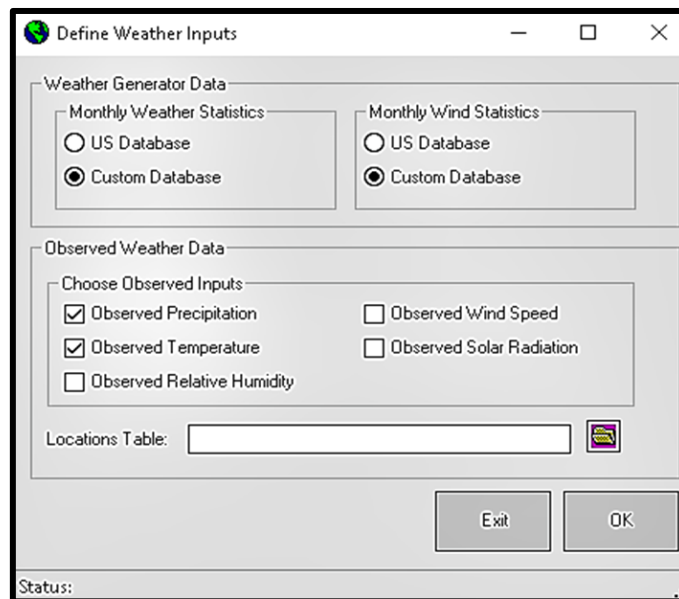


Figure 54. ArcAPEX Weather Input Interface

maximum and minimum temperature, relative humidity and wind speed for modelling of the various physical process. Relative humidity, solar radiation and wind speed are not much important in this study, so only rainfall, maximum and minimum temperature and rainfall intensity was provided in the weather database (Fig. 54).

Rainfall data were collected from automatic rain gauge station installed in the watershed. The spatial location was defined in the model and the data file was linked with the gauge site. The latitude and longitude of automatic weather station (AWS) were provided with the data file prepared for the year 2017-2018 and was used for modelling erosion processes. A location table contains weather station ID, coordinates, elevation, start date, month , year and end date, month and year also selected as location table of daily weather data.

### 3.10.6 Writing default inputs

This option was used to write default input files (Fig. 55) (database) to the model. The user can choose, write specific input files or write all the input files by this option. It includes APEX control, site, subarea, operation schedule, herd and print files.

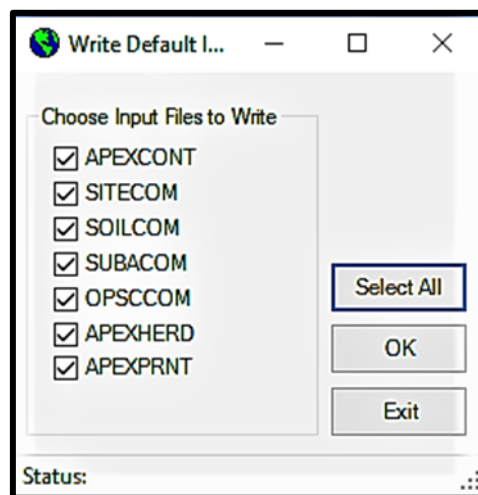


**Figure 55. APEX write file window**

### 3.10.7 Editing APEX inputs

This menu is used to edit default inputs loaded to the model according to the study area. APEX control, site, soil, subarea, operation schedule, herd and print files options were edited based on the data collected. These are the same files loaded to the model in the previous step.

#### 3.10.7.1 Editing APEX control file

The APEX control file (Fig. 56) comprises data that controls the run. The run length, print type, weather daily, monthly, seasonal and annual, for calibration daily and erosion prediction, annual simulation were selected. APEX aids the user to use

Parameter	Value
NBYR	2
YR	2017
IMO	1
IDA	1
IPD	1
NGN	2
IGN	0
IGSD	0
LPYR	0
IET	0
ISCN	1
ITYP	0
IPRK	0
ISTA	0
IHUS	0
NVCN	4
INFL	0
MASP	0
IERT	0
LBP	0
NUPC	1
MNUL	0
LPD	0
MSCP	0
ISLF	0
NTV	0
NAQ	0
IHY	0
ICO2	0
ISW	0
IGMX	1
IDIR	0
IMW	0
IOX	0
IDNT	0
IAZM	0
IPAT	0
IHRD	0
ICP	0

Parameter Detail  
ISCN: Stochastic CN Estimator Code (cols. 41-44)  
The final step in APEX's estimation of runoff volume is an attempt to account for uncertainty. The runoff retention parameter or curve number is based on land use, management, hydrologic soil group, land slope, soil water content and distribution. It is also adjusted for frozen soil. However, many natural processes and management factors that can affect runoff are not accounted for in the model. APEX enables the user to use either a deterministic or a stochastic method of estimating CN. If the deterministic method is chosen, the curve number is adjusted daily for soil water content (and frozen soil). If the stochastic method is chosen, the deterministic value is varied stochastically on a daily basis using a triangular

Figure 56. APEX edit control file window

either a deterministic or a stochastic method of estimating CN. The deterministic method was chosen and the curve number was adjusted daily for soil water content, hence daily variable soil moisture index option was selected. The modified rational method was selected to estimate the peak runoff rate. For soil erosion simulation

the Onsted- Foster modification of USLE was selected. All other parameters were kept constant.

### 3.10.7.2 Editing APEX site file

The study involves several sites (fields, farms, or watersheds). In site file latitude, longitude and elevation of site outlet were described, also the weather station file was selected. All the remaining options kept the same as the default.

### 3.10.7.3 Editing APEX subarea file

Fig. 57 contains management, upland, channel, reservoir/ groundwater, irrigation, fertilization, manure, grazing files for all the subareas. Each subarea has different land use and soil and is shown in the common window. Curve number type, practice factor, land use number, operation schedule file, weather station, channel erodibility factor, channel cover factor and channel Manning's N were defined for each subarea, and others kept the default.

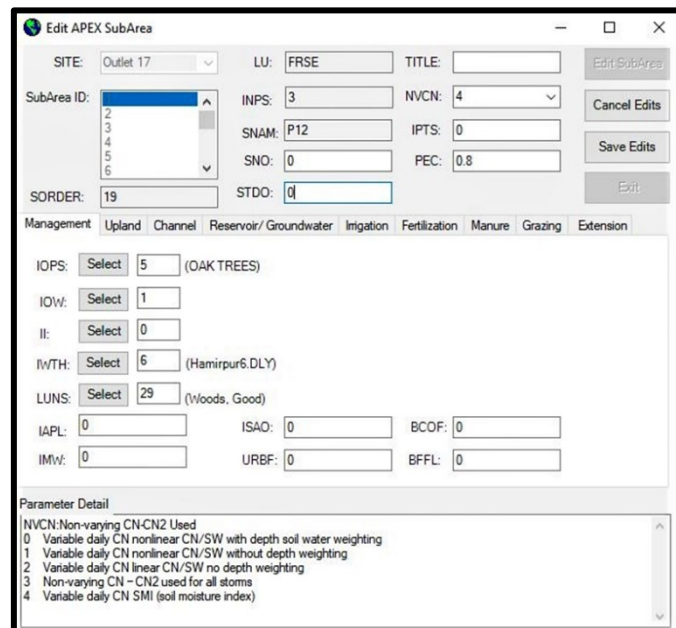


**Figure 57. APEX edit subarea file window**

### 3.10.7.4 Editing APEX herd file

In this study, herding was not considered, so all the options kept as default.



### 3.10.7.5 Editing APEX soil file

Data needed for soil file was defined in the soil database. So all the options kept default.

### 3.10.7.6 Editing APEX print file

The standard output (OUT) file, special reach (RCH) file for ArcGIS, and special subarea (SUB) file were selected as the output.

## 3.10.8 Write APEX input files

After changes have been made to the APEX database files, the files were rewritten for the changes to take effect.

## 3.10.9 APEX model run and output files

The model (Fig. 58-59) was run daily for given inputs. The model output was equated with observed runoff and sediment yield and calibrated accordingly following sensitivity analysis of the model.

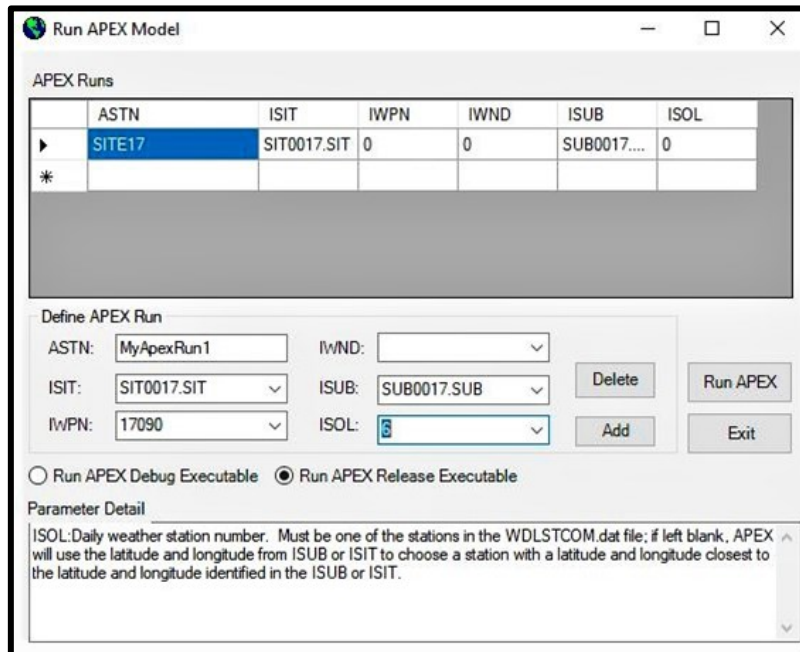


**Figure 58. ArcAPEX Model Run Interface**

```

C:\Windows\system32\cmd.exe
FSITE SITECOM.DAT
FSUBA SUBACOM.DAT
FWPM WPM10604.DAT
FWIND WIND0604.DAT
FCROP CROPCOM.DAT
FTILL TILLCOM.DAT
FPEST PESTCOM.DAT
FFERT FERTCOM.DAT
FSOIL SOILCOM.DAT
FOPSC OPSCCOM.DAT
FTR55 TR55COM.DAT
FPARAM PARM1501.DAT
FMLRN MLRN1501.DAT
FPRINT PRINT1501.DAT
FHERD HERD1501.DAT
FWLST WDLSTCOM.DAT
FPSOD PSOCOM.DAT
FRFDT RFDTLST.DAT
RUN # = 0 SUBAREA FILE = SUB0017.SUB

YEAR 1 OF 40

YEAR 2 OF 40

YEAR 3 OF 40

```

**Figure 59. APEX model execution**

### 3.11 SENSITIVITY ANALYSIS OF THE MODEL

Sensitivity analysis was conducted on the effects of watershed parameters on runoff rate and sediment loss, considering realistic ranges of values under field conditions. The parameter values were uniformly altered by –15 per cent to + 15 per cent. It was assumed that the variations in the estimation of these parameters are uniform.

Sensitivity analysis was done by changing the specified parameter, for example, CN value was increased by 5 per cent keeping other parameters constant. The output was observed in terms of average daily runoff and sediment loss. The ‘X’ is average daily runoff/sediment yield without altering the value of the specified parameter and ‘Y’ is average daily runoff/sediment yield by altering the value of the specified parameter.

$$\text{Percentage change in Runoff/ Sediment yield} = (X-Y/X)*100$$

### 3.12 MODEL CALIBRATION AND VALIDATION

The daily runoff and sediment yield at the watershed outlet was used to calibrate and validate the model. Low to medium rainfall events were selected for calibration. Runoff and sediment data collected for 28 and 20 rainy days were used for calibration and validation, out of which 17 and 12 was used for calibration and remaining 11 and 8 used for validation respectively. The observed data were compared with the predicted data using the linear regression function. The correlation coefficient ( $r$ ), coefficient of determination ( $r^2$ ) the root mean square error (RMSE) and Nash- Sutcliffe model efficiency (NSE) (Nash and Sutcliffe, 1970) were computed.

### 3.13 SURFACE RUNOFF AND SOIL LOSS ESTIMATION

#### 3.13.1 Surface runoff estimation

APEX model was run daily to simulate surface runoff. SCS Curve Number (CN) method was used to simulate runoff. The curve number was defined by the model according to land use and soil hydrological group (HSG). The model calculates CN by daily soil moisture index. APEX model was run based on these parameters. The model predicted the surface runoff and this indicates that the model needs calibration.

#### 3.13.2 Soil loss estimation

In the study area, high-intensity rainfall occurs which results in a large amount of sheet and inter-rill erosion. Also, a large number of rills and gullies were observed. It indicates that in the study area soil erosion occur due to both rainfall and runoff energy factor. APEX has seven various erosion simulation equations. Due to the above mentioned two energy factors, the equation developed by Onstad and Foster (modification of USLE and RUSLE) was used by APEX to calculate sediment loss in the study area.

### 3.14 SOIL LOSS RISK ASSESSMENT

Soil loss rates are classified into five major groups based on the severity of soil loss such as very low ( $<5 \text{ ton ha}^{-1} \text{ yr}^{-1}$ ), low ( $5 \text{ to } 10 \text{ ton ha}^{-1} \text{ yr}^{-1}$ ), moderate ( $10 \text{ to } 20 \text{ ton ha}^{-1} \text{ yr}^{-1}$ ), severe ( $20 \text{ to } 40 \text{ ton ha}^{-1} \text{ yr}^{-1}$ ), very severe ( $>40 \text{ ton ha}^{-1} \text{ yr}^{-1}$ ), which helps to identify erosion-prone areas in the study area.

### 3.15 GENERATION OF FUTURE SOIL LOSS SCENARIO

The APEX model was run for future climate scenarios of H3A2 and H3B2 for three periods; 2011-2040, 2041- 2070, and 2071-2099 after the calibration and validation. For predicting future soil loss scenario, only climate data was altered and other parameters were kept constant. According to this downscaled the rainfall and temperature and future soil loss scenarios were developed.

## IV. RESULTS AND DISCUSSION

The current study was carried out to analyse the impact of climate change on surface runoff and sediment yield in a watershed of the Shivalik region. The future climate projected with the aid of statistical downscaling method. The process-based APEX model was used to analyse the impact of climate change on surface runoff and soil loss. The results of the study are illustrated and discussed in this chapter.

### 4.1 TERRAIN CHARACTERIZATION

Terrain analysis was carried out using Cartosat DEM and LISS IV satellite data. The analysis was done using ArcGIS 10.3. Drainage extraction, watershed delineation, slope, aspect and land use/land cover analysis were done.

### 4.2 DEM ANALYSIS

The terrain analysis using DEM (Fig. 60) revealed that the height of the watershed ranges from 473- 821m. The physiography map was analysed for identifying physiographic elements. Various physiographic features such as upper hill slope, middle hill slope, lower hill slope, upper piedmont, middle piedmont and valley were identified. The slope analysis reveals that there are steep slope, medium slope, and gentle slope area. The aspect map was classified into nine classes. Also, using DEM, drainage map was created for the study area. The streams were numbered in ArcGIS, according to Strahler method.

**Table 7. Various landforms in the watershed**

Sl. No.	Landform Elements	Area (ha)	Area (%)
1	Upper Hill Slope	132.71	26.02
2	Middle Hill Slope	142.57	27.95
3	Upper Piedmont	142.32	27.90
4	Lower Piedmont	92.47	18.13

Middle hill slope is identified as the major landform (Table 7) element followed by upper piedmont, upper hill slope and lower piedmont. A total of 27.95 per cent of land contribute to middle hill slope, most of the area is prone to soil erosion. Slope analysis (Table 8) reveals that the study area is divided into six slope classes (Fig. 61), from gentle slope (0-5 %) to very steep slope (> 35 %). A total of 33.06 per cent of the study area has moderately steep slope (16-25 %) followed by 20.20 per cent of moderate slope, 18.88 per cent of gentle slope, 13.27 per cent of very gentle slope, 12.34 per cent of steep slope and 2.26 per cent of very steep slope. These steep slopes are also a major reason for soil erosion.

**Table 8. The aerial extent of slope classes in the watershed**

Sl. No.	Percentage Slope	Description	Area(ha)	Area (%)
1	0-5	Very Gentle	67.56	13.27
2	6-10	Gentle	96.14	18.88
3	11-15	Moderate	102.86	20.20
4	16-25	Moderately Steep	168.35	33.06
5	25-35	Steep	62.86	12.34
6	35-50	Very Steep	11.49	2.26

Aspect map (Fig. 62) was prepared using Cartosat DEM. Aspect map gives the idea about the direction to a slope face. From the aspect map, it is clear that most of the slopes are in west and southwest direction, which indicates that water flow is in the slope direction. The mainstream in the study area flows in this direction. Also, a ground-truthing was carried out to validate this. Table 9 gives different aspects and percentage of area covered under each aspect.

DEM derived landform, slope and aspect maps provide a clear idea of the physical appearance of the study area. It helped to determine representative sampling locations for collecting soil samples. Also, it is correlated to the soil loss

from the study area; According to the aspect, since the water flows in the same direction of aspect, the deposition of sediments also occurs in the same direction.

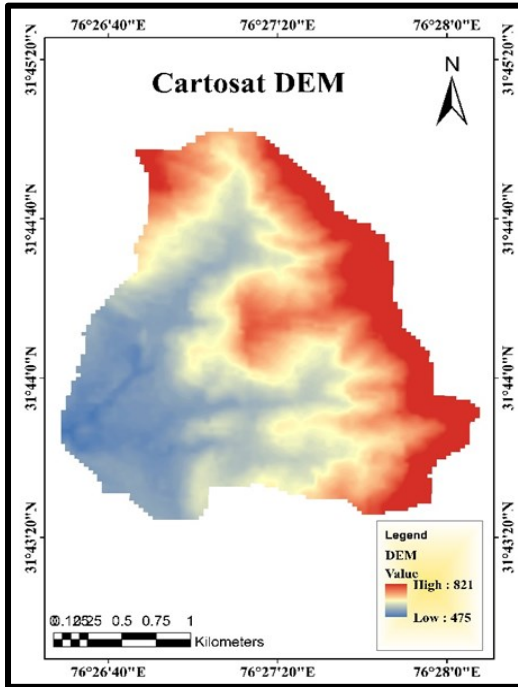


**Figure 60. Digital elevation model**

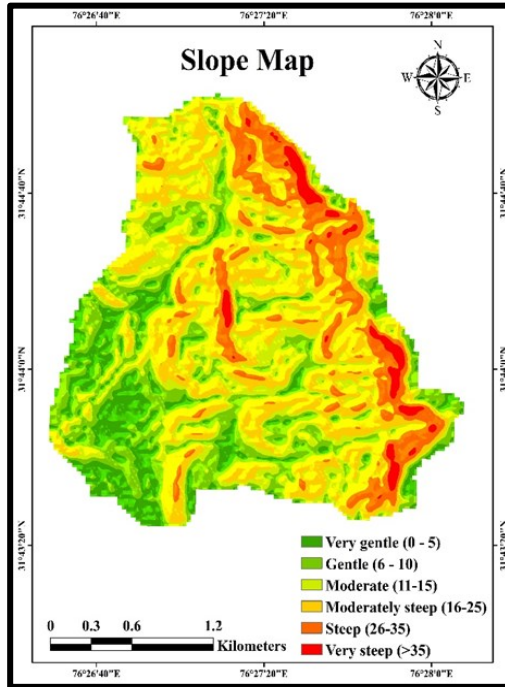


**Figure 61. Slope map**

**Table 9. Area under different aspect class**

Sl. No.	Aspect Angle(°)	Aspect Class	Area (ha)	Area (%)
1	-1	Flat	0.17	0.03
2	0-22.5	North	16.04	3.15
3	22.5-67.5	Northeast	25.52	5.01
4	67.5-112.5	East	35.82	7.03
5	112.5-157.5	Southeast	72.84	14.30
6	157.5-202.5	South	67.55	13.27
7	202.5-247.5	Southwest	90.45	17.76
8	247.5-292.5	West	97.76	19.20
9	292.5-337.5	Northwest	80.40	15.79
10	337.5-360	North	22.67	4.45

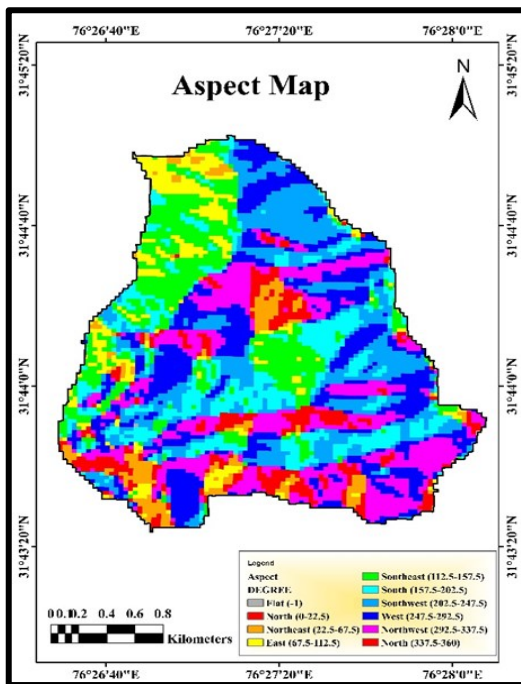


**Figure 62. Aspect map**

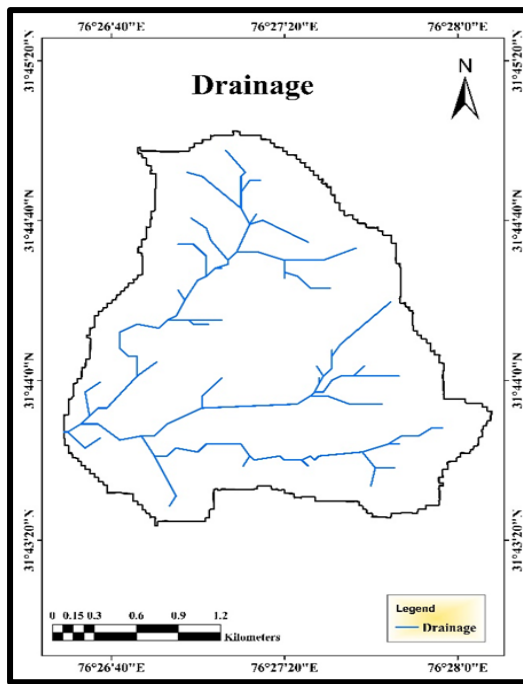


**Figure 63. Drainage map**

The study area is ranked as a fourth-order stream based on Strahler (1953) stream ordering method (Fig. 63-64). According to this method, there are 23 first-order streams, seven second-order streams, three third-order streams and one fourth-order stream. Apart from stream ordering, another important watershed morphometric parameter is drainage density. It is based on length of drainage per unit area which is calculated by dividing the total length of streams within a unit area inside a watershed. A minimum drainage density of 0.20 to a maximum of 2.40 was observed per unit area. A maximum drainage density indicates a relatively high hydrologic response to rainfall storms, while low drainage density indicates a low hydrologic response to the storms (Meltan, 1957). The average drainage density of the study area is 2.0 unit hectare, which is considered moderate and could consequently be damaging rapid hydrologic response of rainfall (Yildiz, 2002). A spatial map of drainage density is shown in Fig. 65.



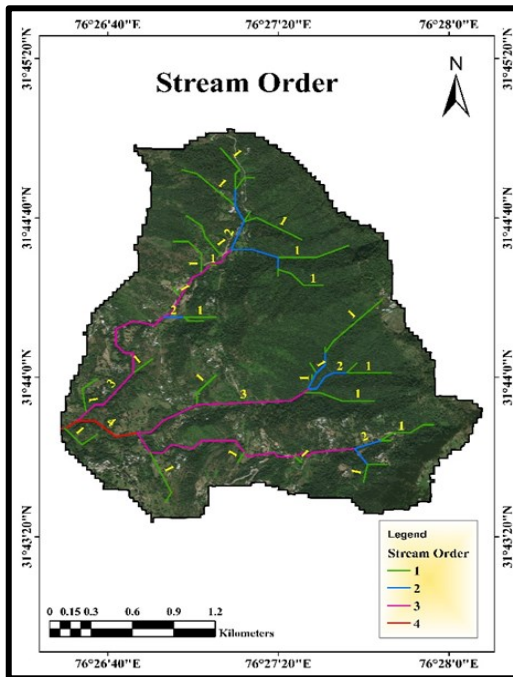


**Figure 64. Stream order**

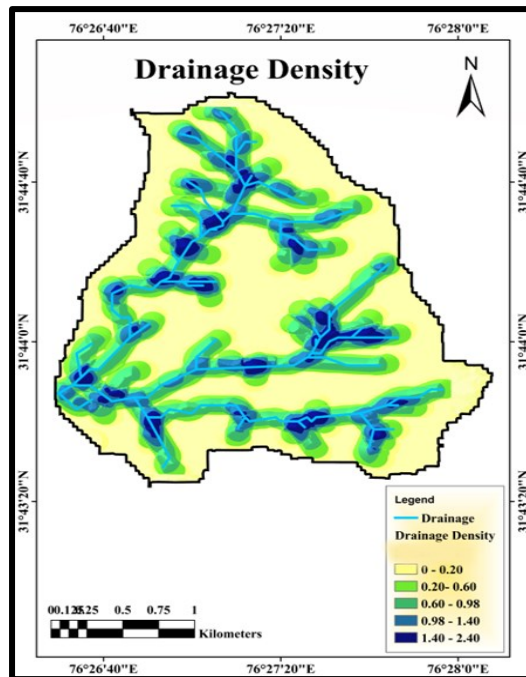


**Figure 65. Drainage density**

The stream power index gives erosive power of terrain. Negative values indicate less stream power, which is observed in hilltop, upper hill slopes and positive values observed in upper piedmont and valleys. Spatial distribution (Fig. 66) clearly shows that index value more in streams. A higher positive index of six was observed in valleys of the study area, and a lower negative index of thirteen was observed on hilltops. It was identified that the valleys and lower piedmonts have higher erosion risks based on ground observation. The terrain wetness index (Fig. 67) gives water accumulation potential of a particular area. A higher positive index thirteen was observed in the valley, which means soil moisture is more in valleys and lower negative index of six observed on hilltops. The positive index indicates wetter area and negative index indicate a drier area. Based on the ground observation, it was identified that the valley area has more water content than hilltop. These two indices quantify flow intensity and flow accumulation potential of the study area.

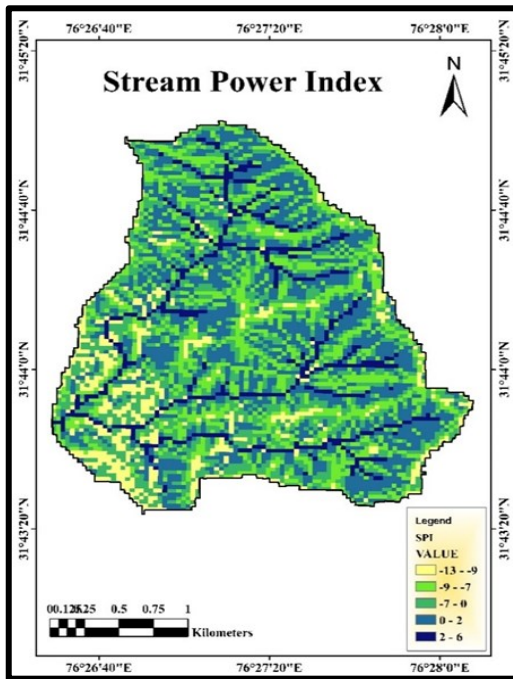


**Figure 66. Stream power index**

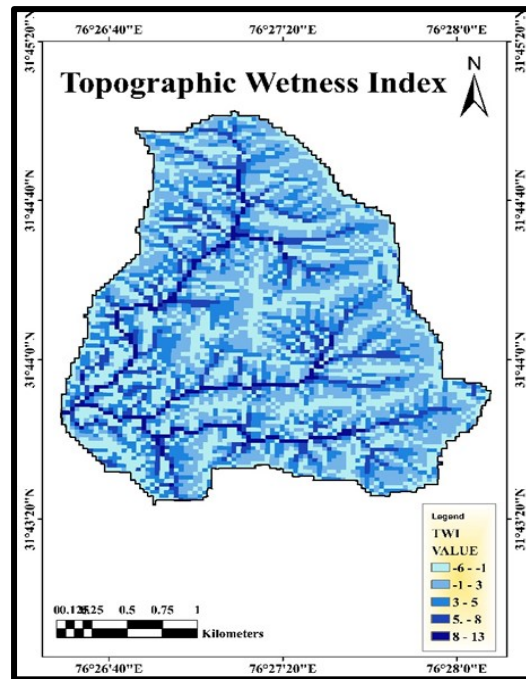


**Figure 67. Topographic wetness index**

#### 4.3 LAND USE/ LAND COVER MAP (LU/LC Map)

The land use/land cover classification results are provided in (Table 10). From the composite map, LU/LC map was prepared by the superimposition of the visually interpreted map, attained from supervised classification. It was estimated that (Fig. 68 - 69) dense forest (45.24 %) is the prominent land use in the watershed, open forest cover comes (26.75 %) second most dominating land cover followed by agriculture (18.90 %) among this maize is cultivated in most of the area. Very few rice fields are observed in the field. It is mainly owing to the absence of adequate water in the mountain area. It is costly to cultivate rice in the mountain region, as it requires irrigation, but in the study area, there was no irrigation facility. 5.87 per cent of the study area is scrub land and is located in the lower-lying area of the watershed. 3.10 per cent area is covered by settlements, and 0.14 per cent contribute to water bodies such as ponds, check dams and dykes.

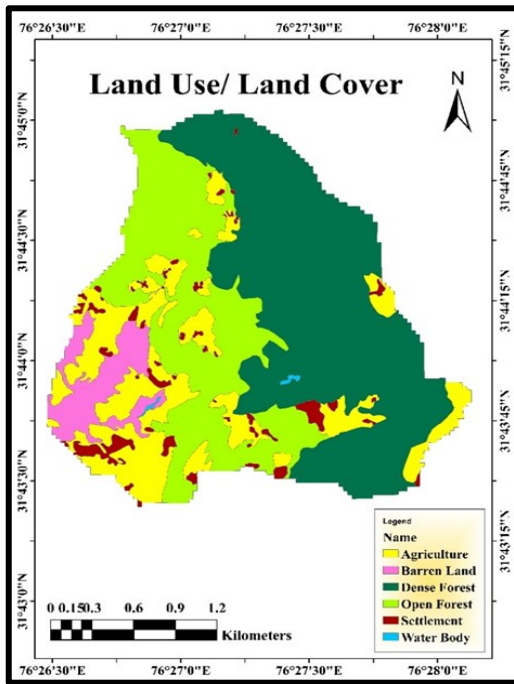


Figure 68. Land use/ land cover map

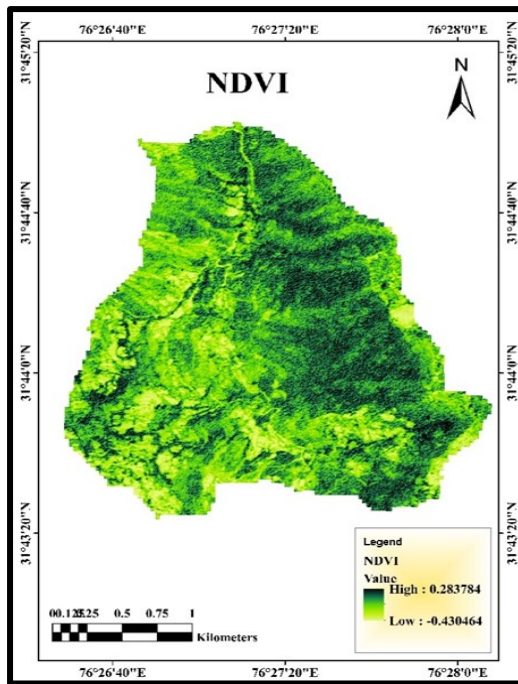


Figure 69. NDVI

Table 10. Watershed Area – Land Use Classes

Sl. No.	Land Use	Area(ha)	Area (%)
1	Open Forest	136.45	26.75
2	Dense Forest	230.74	45.24
3	Barren Land	29.96	5.87
4	Agriculture( Maize, Rice)	96.40	18.90
5	Water Body	0.73	0.14
6	Settlements	15.80	3.10

#### 4.4 SOIL LANDSCAPE MAP

The soil landscape map of the watershed was generated by intersecting the topography map, slope map, aspect map and land use map. According to this, the watershed has 11 major landscape classes (Fig. 70). Each class has unique soil physicochemical properties. The significant physical and chemical properties are

grouped into tables (11-19). Sandy loam is the dominant soil textural class and in most of the soil types, sand content is dominated, followed by silt and clay. Among this, upper hill slope has low clay and silt content and high sand content. This indicates the severity of erosion. Forest has a good land cover, so it was observed that compared with the same landscape, forest soil constitutes more clay content than less covered agricultural fields. Dominant soil colour of the study area was identified as yellowish-brown. Dark coloured forest soil indicates relatively high organic matter content than others. Among the different land uses agriculture and forest has more organic matter content and it is very low in scrubland.

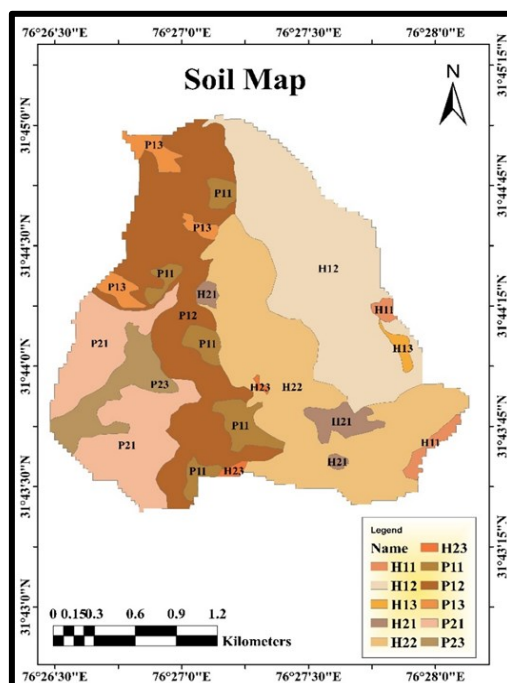


**Figure 70. Physiographic soil map of the watershed**

#### 4.5 PHYSICOCHEMICAL PROPERTIES OF SOIL

The significant physical properties are soil colour, texture (sand, silt and clay), structure, bulk density and surface coarse fragment percentage. Significant chemical properties are pH, electrical conductivity, organic carbon content, and soil nutrients (macro and micro). Soil aggregate stability is based on physical, chemical and biological properties (Doran *et al.*, 1996).

**Table 11. Physiographic soil map units**

Sl. No.	Landscape Unit	Class	Area (ha)	Area (%)	Soil Texture	Soil Colour
1	Upper Hill Slope Agriculture	H11	106.53	20.88	Loamy Sand	Light Yellowish Brown
2	Upper Hill Slope Forest	H12	124.04	24.32	Sandy Loam	Light Yellowish Brown
3	Upper Hill Slope Scrub	H13	129.04	25.30	Sandy Loam	Light Brown
4	Middle Hill Slope Agriculture	H21	23.05	4.52	Sandy Loam	Light Yellowish Brown
5	Middle Hill Slope Forest	H22	69.42	13.61	Sandy Loam	Dark Greyish Brown
6	Middle Hill Slope Scrub	H23	2.59	0.51	Sandy Loam	Light Brown
7	Upper Piedmont Agriculture	P11	6.08	1.19	Sandy Loam	Light Yellowish Brown
8	Upper Piedmont Forest	P12	11.66	2.29	Sandy Loam	Pale Brown
9	Upper Piedmont Scrub	P13	1.88	0.37	Sandy Loam	Yellowish Brown
10	Middle Piedmont Agriculture	P21	23.89	4.68	Sandy Loam	Brown
11	Middle Piedmont Scrub	P23	11.90	2.33	Sandy Loam	Brown

#### 4.5.1 Soil physical properties

The analysis results of soil physical properties are shown in Table 11-13. Due to erosion, fine clay particles were eroded and left coarser sand and loam particles. So the dominant textural class is sandy loam and the dominant soil colour is

yellowish-brown. Since scrub land is the least disturbed land use higher bulk density was observed in map unit H13, P13 and P23. Lower bulk density was observed in the agricultural field due to ploughed loose soil. Higher bulk density indicates compaction of soil and low organic matter content.

**Table 12. Physical properties of soils in the watershed-I**

Sl. No.	Soil Landscape Unit	Soil Colour (colour code)	Sand (%)	Silt (%)	Clay (%)	Textural Class
1	H11	Light Yellowish Brown (10 YR 6/4)	66.31	25.95	7.75	Sandy Loam
			54.31	35.28	10.41	Sandy Loam
2	H12	Light Yellowish Brown (10 YR 6/4)	76.72	17.28	6.00	Loamy Sand
			76.72	19.28	4.00	Loamy Sand
3	H13	Light Brown (7.5 YR 6/4)	55.84	35.64	8.52	Sandy Loam
			55.84	35.64	8.52	Sandy Loam
4	H21	Dark Greyish Brown (10 YR 4/2)	53.51	31.15	15.35	Sandy Loam
			55.87	30.24	13.89	Sandy Loam
5	H22	Light Yellowish Brown (10 YR 6/4)	55.43	29.74	14.83	Sandy Loam
			55.97	28.76	15.27	Sandy Loam
6	H23	Light Brown (7.5 YR 6/4)	57.84	33.64	8.52	Sandy Loam
			57.84	33.64	8.52	Sandy Loam
7	P11	Pale Brown (10 YR 6/3)	61.80	26.52	11.68	Sandy Loam
			56.80	31.52	11.68	Sandy Loam
8	P12	Light Yellowish Brown (10 YR 6/4)	58.84	30.08	11.08	Sandy Loam
			61.64	27.28	11.08	Sandy Loam
9	P13	Yellowish Brown (10 YR 5/4)	57.64	30.61	11.75	Sandy Loam
			64.97	25.95	9.08	Sandy Loam
10	P21	Brown (10 YR 5/3)	54.66	34.15	11.18	Sandy Loam
			57.06	32.15	10.78	Sandy Loam
11	P23	Brown (10 YR 5/3)	57.84	29.64	12.52	Sandy Loam
			60.84	28.64	10.52	Sandy Loam

**Table 13. Physical properties of soils in the watershed –II**

Sl. No.	Soil Landscape Unit	Bulk Density (g/cm <sup>3</sup> )	Soil Aggregate Stability Index		Coarse Fragment (%)
			0.25mm	0.50mm	
1	H11	1.50	0.68	0.57	25
2	H12	1.54	0.77	0.74	20
3	H13	1.65	0.60	0.52	30
4	H21	1.51	0.76	0.65	20
5	H22	1.57	0.64	0.43	20
6	H23	1.55	0.54	0.54	25
7	P11	1.25	0.76	0.64	15
8	P12	1.62	0.71	0.55	15
9	P13	1.67	0.71	0.61	22
10	P21	1.49	0.71	0.60	12
11	P23	1.62	0.78	0.67	15

The aggregate stability index values of two different sieves show that particle size less than 0.25 mm has a higher index than of size less than 0.50 mm. It indicates that finer soil particles are more stable than coarser particles. The soils in higher elevation (H11, H13, H22 and H23) show a decreased aggregate stability index value than lower elevation (P11, P12, P13, P21 and P23). It is because of higher erosion and lower organic matter content; the clay particles were eroded from higher elevation soils. Due to higher erosion rate in the upper part of the watershed, the coarse fragment percentage shows a decrease in trend from higher to the lower elevation.

#### 4.5.2 Soil chemical properties

The analysis of soil chemical properties in the watershed shown in Table 14 and 15. Soil pH is an indication of soil reaction. Soils with excessive clay and

organic matter content material are more capable to resist rise or fall in pH than sandy soils. The sandy soils typically have low organic matter content, ensuing in

**Table 14. Chemical properties of soils in the watershed-I**

Sl. No.	Soil Landscape Unit	pH	EC ( $\mu\text{S/cm}$ )	Organic Carbon (%)	Organic Matter (%)
1	H11	5.59	26.76	1.24	2.13
		5.66	24.31	0.95	1.63
2	H12	6.54	63.98	1.30	2.23
		6.67	58.38	1.01	1.74
3	H13	5.40	24.23	0.17	0.30
		5.20	21.59	0.16	0.28
4	H21	5.60	37.5	2.09	3.60
		5.54	33.61	1.42	2.44
5	H22	6.27	80.90	0.80	1.37
		6.31	64.67	0.54	0.93
6	H23	5.51	20.64	0.24	0.41
		5.40	25.03	0.12	0.21
7	P11	5.47	39.54	1.26	2.16
		5.50	24.96	1.02	1.75
8	P12	5.78	62.00	0.83	1.42
		5.97	40.26	0.59	1.02
9	P13	6.22	41.63	0.42	0.73
		6.18	35.00	0.33	0.57
10	P21	6.12	103.42	0.94	1.62
		6.03	77.78	0.78	1.35
11	P23	6.63	29.99	0.38	0.65
		6.61	21.42	0.28	0.48



a low buffering capacity, high rates of water percolation and infiltration making them susceptible to acidification. The pH of the study area is acidic and ranges from 5.2-6.7. High pH value is found in agricultural land followed by forest and less in scrub land.

It is mainly due to the application of lime in the agricultural field. Higher acidic soils were found in scrubland at the upper part of the watershed, this may be due to higher erosion rate, which lowers the buffering capacity of the soil. It was observed that the acidity in scrub land is also changing with the elevation. The results show that the study area has a non- saline soil.

**Table 15. Soil nutrients in the watershed**

Sl. No.	Soil Landscape Unit	Nitrogen (%)	Phosphorus (Kg/ha)	Potassium (Kg/ha)
1	H11	0.080	203.00	88.65
		0.071	193.46	84.43
2	H12	0.140	244.26	125.14
		0.100	196.82	91.89
3	H13	0.050	110.23	78.59
		0.048	68.32	48.26
4	H21	0.118	201.79	105.59
		0.089	189.52	95.86
5	H22	0.090	278.67	121.69
		0.075	239.11	104.42
6	H23	0.030	153.46	86.23
		0.040	33.60	14.67
7	P11	0.097	181.13	79.09
		0.077	126.50	55.24
8	P12	0.084	217.80	95.11
		0.074	196.16	85.66
9	P13	0.072	160.72	81.54
		0.072	110.32	67.37
10	P21	0.104	257.44	112.42
		0.091	216.47	94.53
11	P23	0.076	128.75	56.22
		0.059	100.21	40.22

High salinity observed in the agricultural field (P21) may be due to nutrient application and is followed in forest and scrubland. Higher acidity also lowers the salt contents in the soil. More organic matter was found in agriculture and forest soil. It was estimated that, forest soil contain average of 1.67 per cent of organic matter in surface soil and 1.23 per cent in subsurface soil. In the Agriculture field, organic matter in surface soil contains 2.33 per cent and 1.86 per cent in subsurface soil. Scrubland contains a very less organic matter of 0.52 per cent in the surface layer, and the sub-surface layer has 0.39 per cent.

Also, it was observed that higher elevation has lower and lower elevation has a relatively higher amount of organic matter content. This is mainly due to the erosion process. Scrub land contains a lesser quantity of soil nutrients due to higher erosion rates, and higher soil nutrients were observed in agricultural land and forest land. In agricultural land, fertilizer applications increase the nutrient content and soil conservation structures reduce the loss of soil nutrients, which results in higher nutrients in agricultural land. The higher nutrient content in forest land is due to leaf litter, organic matter content, good cover and reduced runoff and erosion.

#### 4.6 SOIL HYDROLOGICAL PROPERTIES

More infiltration rates were observed in the agricultural field and less in scrubland. In the agricultural field, there was more infiltration rate because of ploughed loose soils. It helps rapid entry of water into the soil. Fewer infiltration rates were observed in scrubland and this is the reason for higher erosion potential. Unsaturated hydraulic conductivity refers to the measure of soil's water- retaining ability when soil pore space is devoid of water and also it is subjected to a hydraulic gradient. Scrubland has low unsaturated hydraulic conductivity followed by forest and more in agricultural land. Loose soil in the agricultural field is the reason for higher unsaturated conductivity value. A high saturated hydraulic conductivity is observed in agricultural land and it was low in scrubland. Available water content (AWC) is the volume of water that is available to plants if the soil is at field capacity. High AWC was observed in agricultural land and less in scrubland.

Similarly, field capacity, wilting point and saturation were derived using SPAW (Table 16). Percentage wilting point is observed to be high in agricultural land and less in scrubland. High field capacity was observed in both forest and agricultural land. A higher saturation volume was observed in both agricultural land and forest and low volume in scrubland. Among these hydrological properties, it was identified that agricultural land has a high value of hydrological properties followed by forest and scrubland. While the ploughed loose soils help the rapid entry of water, in the forest canopy, interception and organic matter increases water holding capacity. Less the land cover and undisturbed compact soil reduce the hydrological properties in the scrubland.

**Table 16. Soil hydrological properties in the watershed- I**

Sl. No.	Soil Landscape Unit	Available Water Content (cm/cm)*	Wilting Point (%Volume)*	Field Capacity (%Volume)*	Saturation (%Volume)*
1	H11	0.09	5.70	14.80	41.80
2	H12	0.08	5.40	13.00	44.90
3	H13	0.07	6.90	18.40	43.10
4	H21	0.12	9.50	22.30	43.90
5	H22	0.11	10.10	21.10	42.00
6	H23	0.08	5.70	16.60	39.30
7	P11	0.11	8.40	18.20	42.20
8	P12	0.10	7.70	18.20	42.00
9	P23	0.09	6.30	18.60	41.20
10	P21	0.11	8.00	19.40	42.70
11	P23	0.10	6.90	16.60	40.10

\* SPAW model-derived variables

Soil hydrologic groups were defined according to U.S Natural Resource Conservation Service (NRCS), which categorizes soils into four hydrologic groups based on infiltration characteristics of the soils. NRCS Soil Survey Staff (1996) defines a hydrologic group (Table 17) as a group of soils having similar runoff potential under analogous storm and cover conditions. Cumulative infiltration rate, mean permeability, depth to bedrock, depth of water table and shrink-swell potential properties were used to determine the hydrological soil group. Scrubland has D hydrologic group, and forest and agriculture have both B and C. This indicates the poor condition of the soils in the study area.

**Table 17. Soil hydrological properties in the watershed- II**

<b>Sl. No.</b>	<b>Soil Landscape Unit</b>	<b>Soil Depth (mm)</b>	<b>Infiltration Rate (mm/hr)</b>	<b>Unsaturated Hydraulic Conductivity (mm/hr)</b>	<b>Saturated Hydraulic Conductivity (mm/hr)*</b>
<b>1</b>	<b>H11</b>	250	45.90	10.40	52.42
<b>2</b>	<b>H12</b>	300	37.80	9.91	81.81
<b>3</b>	<b>H13</b>	200	30.25	6.24	37.31
<b>4</b>	<b>H21</b>	300	37.80	6.80	26.21
<b>5</b>	<b>H22</b>	350	62.50	10.47	30.69
<b>6</b>	<b>H23</b>	200	31.73	9.65	34.13
<b>7</b>	<b>P11</b>	350	37.70	7.07	35.38
<b>8</b>	<b>P12</b>	400	52.60	12.60	36.00
<b>9</b>	<b>P23</b>	250	33.70	6.26	23.95
<b>10</b>	<b>P21</b>	500	78.00	19.30	34.22
<b>11</b>	<b>P23</b>	300	32.00	7.80	26.69

\* SPAW model-derived variables

Soil permeability class was defined according to FAO, by using textural class. Each texture has a different permeability rate. The study area includes a moderately slow to moderate permeability class. The soil drainage class was defined through field observation by observing erosion features, slope and land cover. Higher altitude comes under ‘excessive’ drainage class, and relatively lower altitude has a ‘well’ drainage class.

**Table 18. Soil hydrological properties in the watershed- III**

Sl. No.	Soil Landscape Unit	Hydrological Soil Group	Permeability Class	Drainage Class	USLE K
1	H11	D	Moderate	Excessive	0.09
2	H12	C	Moderate	Well	0.10
3	H13	D	Moderately Slow	Excessive	0.11
4	H21	C	Moderately Slow	Excessive	0.08
5	H22	B	Moderate	Well	0.08
6	H23	D	Moderate	Excessive	0.11
7	P11	C	Moderately Slow	Excessive	0.09
8	P12	B	Moderate	Well	0.09
9	P23	D	Moderately Slow	Excessive	0.10
10	P21	B	Moderate	Well	0.08
11	P23	C	Moderate	Excessive	0.10

USLE K factor or soil erodibility factor determines the vulnerability of soil to erosion. USLE soil erodibility factor is a function of the percentage of sand, silt and clay, organic matter content, permeability class and soil drainage class. Higher

erodibility values are observed in scrubland due to lower hydrological properties and low organic matter content. A lower erodibility observed in forest land is due to higher organic matter content and increased soil aggregate stability. The Table-18 shows different erodibility values for different soil-landscape units.

**Table 19. Soil erosion survey**

SL No.	Physiography	Land use	Slope (degree)	Elevation (m)	Conservation practices	Erosion Class
1	Upper hill slope	Forest	>35	> 750m	Natural	e2/e3
		Agriculture	>35	> 750m	Terracing	e3
		Scrubland	>35	> 750m	Natural	e4
2	Middle hill slope	Forest	25-35	650-750m	Natural	e2
		Agriculture	25-35	650-750m	Terracing	e3
		Scrubland	25-35	650-750m	Natural	e3/e4
3	Upper piedmont	Forest	15-25	550-650m	Natural	e2
		Agriculture	15-25	550-650m	Terracing	e2/e3
		Scrubland	15-25	550-650m	Natural	e3
4	Middle piedmont	Agriculture	<15	<550m	Terracing	e2
		Scrubland	<15	<550m	Natural	e3

Soil erosion survey conducted during monsoon season and post-monsoon season are shown in Table 19. During the survey, many erosion structures were identified such as rills, gullies and landslips. Higher elevation and less covered areas were identified as more prone to erosion. Erosion class are defined as e1- slight, e2- moderate, 3e- severe, e4- very severe. Both agricultural fields and scrub

lands have relatively less cover, but the practice of conservation measures reduce further soil loss from agricultural fields.

According to erosion survey, scrub land comes under higher erosion class (e4) followed by agricultural field and very less as dense forest. In the majority of agricultural fields, farmers adopt terracing practices which reduces erosion rate to moderate class. The higher slopes are in severe erosion class whereas lower slopes are in moderate erosion class. Although the dense forest has no conservation measures, the cover factor helps it to be included in moderate erosion class.

## 4.7 METEOROLOGICAL DATA

### 4.7.1 Weather data

During the year 2017 and 2018, the mean maximum temperature was observed during May and the mean minimum temperature during January (Fig. 71). But the long term average of mean maximum temperature during June. During the study period, August received the highest rainfall of about 588.4 mm and negligible range of rainfall is recorded in May, October, and November.

In the study area, the maximum rainfall (Fig. 72) occurs from July to September. During the year 2017, peak rainfall occurred on July 7<sup>th</sup> with an amount of 122.17 mm, while in 2018 July 13<sup>th</sup> recorded peak rainfall of 151.64 mm. There were 74 rainy days in 2017, while in 2018 it increased to 103 days. August had the greatest number of rainy days in both years, followed by July, and September. During 2017 August had 25 rainy days, while it was 21 rainy days in 2018. 2018 shows an increase in monsoon and winter rainfall than in 2017. The total rainfall obtained in 2017 is 1106.67 mm, while during 2018, a total of 1482.63 mm rainfall was obtained.

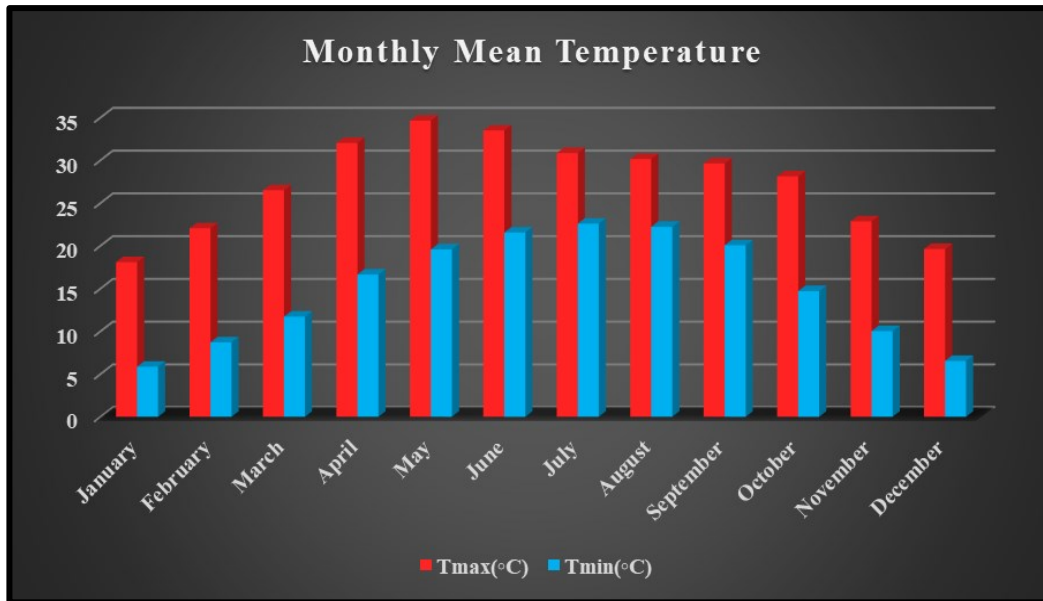


**Figure 71. The monthly average temperature of 2017 and 2018**

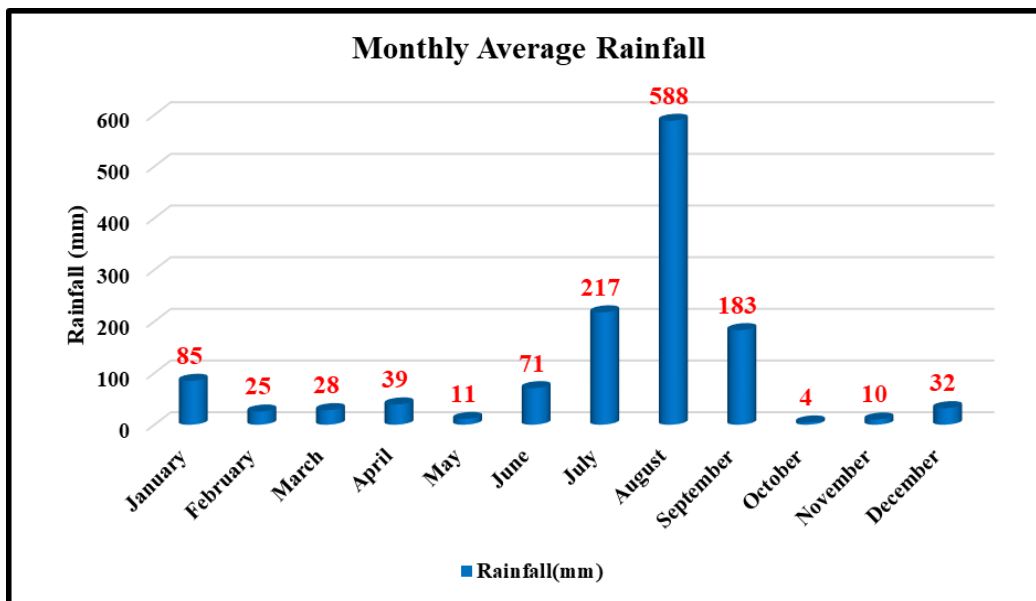


**Figure 72. The monthly average rainfall of 2017 and 2018**

The intensity of rainfall is defined as rainfall occurred per unit time. The maximum half-hour (I30) intensity (Fig. 74 and 76) of the rainfall was calculated according to Wischimer and Smith method. During the year 2017 maximum half-hour rainfall observed is 67.06 mm/hr and in 2018 the maximum half-hour rainfall observed is 73.66 mm/hr. It was observed that from Fig. 73 and 75, if the amount



of rainfall is more, then the intensity will be more in most of the case. In both years August received the highest half-hour intensity rainfall.

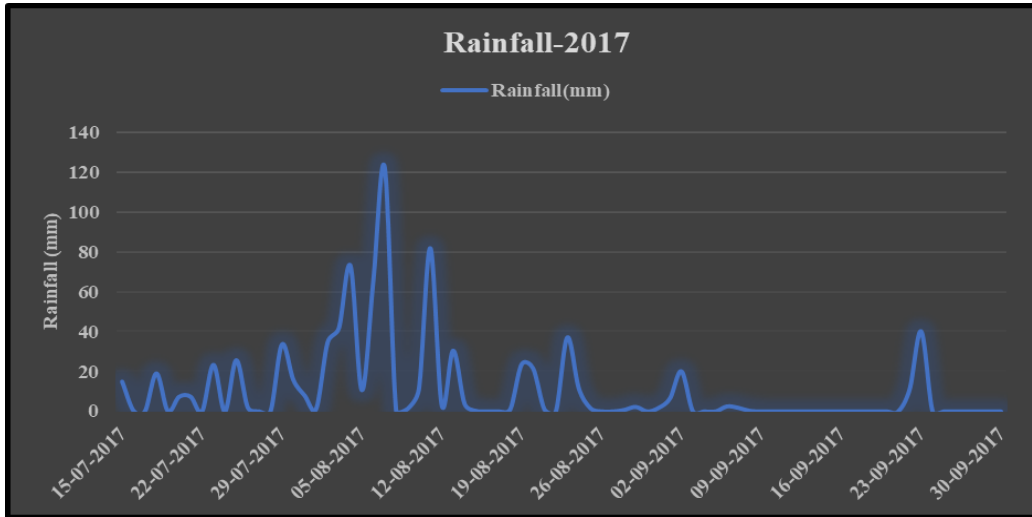


**Figure 73. Monsoon rainfall -2017**

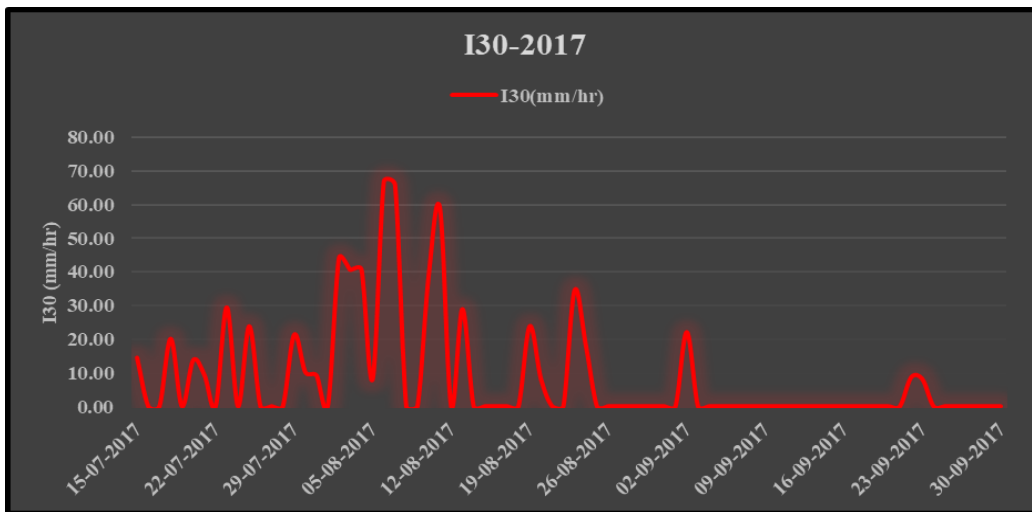


**Figure 74. Maximum half-hour rainfall (I30)**

The rainfall obtained in 2017 was below the long term average of the annual rainfall of 1341.90 mm (Fig. 73), while during 2018 rainfall was above the long term total annual average rainfall (Fig. 75). From the graph, it is evident that 2018 (Fig. 76) has relatively higher rainfall intensity when compared to 2017 (Fig. 74).

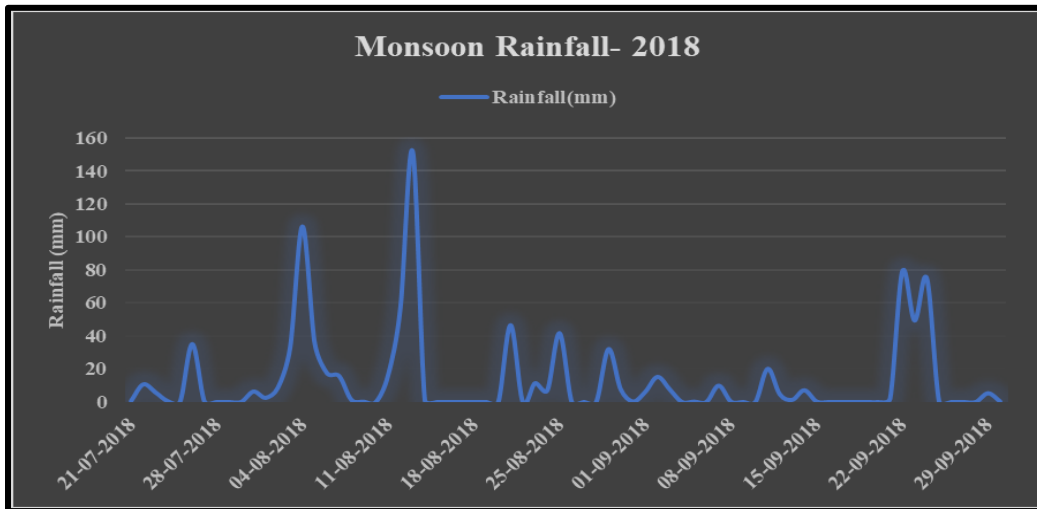


**Figure75. Monsoon rainfall -2018**

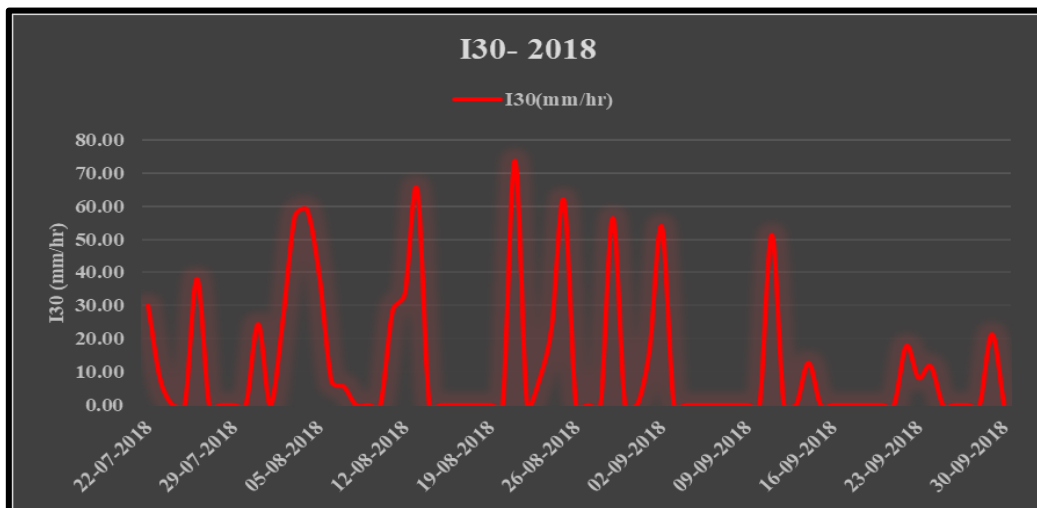


**Figure 76. Maximum half-hour rainfall (I30)**

#### 4.8 DOWNSCALING OF GLOBAL CLIMATE DATA (SDSM)

The global climate data was downscaled into fine resolution (local scale) using statistical downscaling model. The period from 1985 to 2014 of the weather station data (Una) was used to calibrate and validate the SDSM model. The results found discourse below.

##### 4.8.1 Statistical downscaling model (SDSM)

The major results obtained from each step is described below.

4.8.1.1 *Quality control and data transformation*

As all parameters in the model needed complete data, missing data were filled using the weather generator option. There was no transformation applied for temperature, while for rainfall fourth root transformation was applied.

4.8.1.2 *Screening of downscaling predictor variables*

It is an essential step for selecting appropriate predictor variables. These parameters were designated based on variance, correlation, p values and scatter plots. The results showed that temp (near-surface air temperature), was the major predictor for both maximum and minimum temperatures and shum (near-surface specific humidity) for rainfall (Table 20 and Fig. 77 and 78).

**Table 20. Predictands and their selected NCEP predictors**

Maximum temperature	Minimum temperature	Rainfall
ncep_temp	ncep_temp	ncep_shum
ncep_p500	ncep_p500	ncep_r500
ncep_r850	ncep_shum	ncep_p5zh
ncep_shum	-	ncep_pt
-	-	ncep_pzh

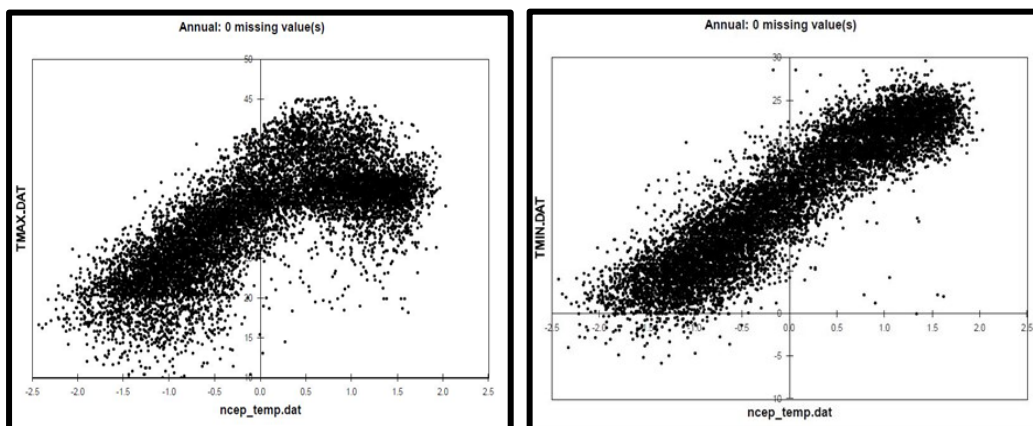


**Figure 77. Scatter plot of max. and min. temp & near-surface temp**

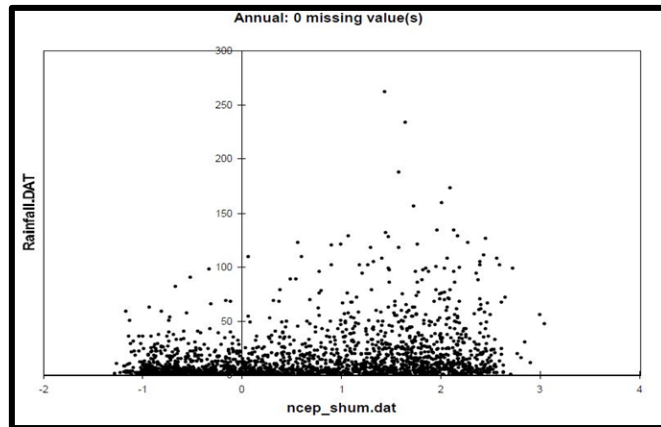


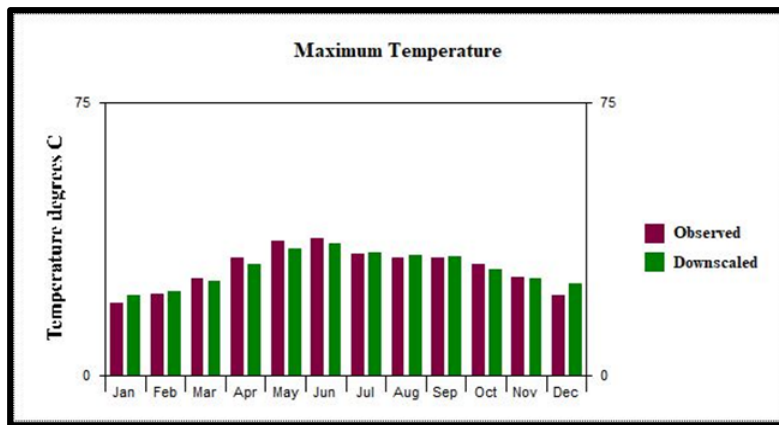
**Figure 78. Scatter plot of rainfall & specific humidity**

*4.8.1.3 Model calibration*

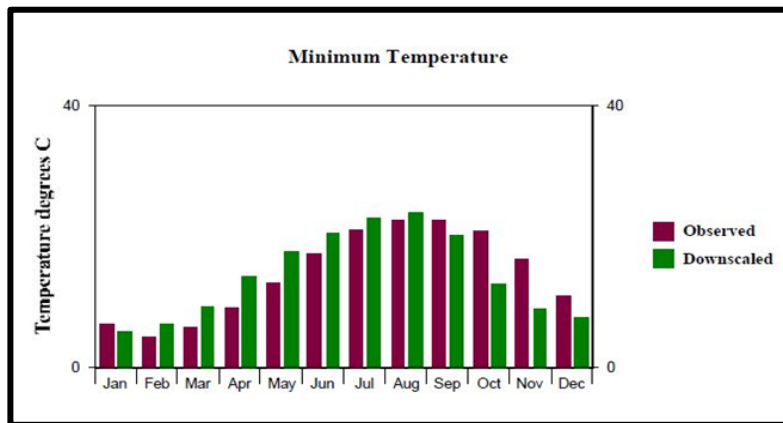
The model was calibrated using weather station data from 1985 to 1999 for 15 years. According to the explained variance ( $r^2$ ) and standard error (Table 21) the regression model was selected. The calibrated rainfall shows under-estimation of rainfall. It was adjusted using the bias correction button, for increasing the under-predicted values, increased the bias correction value from 1 to 1.3. Results exposed that the variance and standard error for maximum and minimum temperatures were 68.1 per cent, 2.64 °C, and 83.8 per cent, 2.01 °C correspondingly whereas, for rainfall it was 23.9 and 35.00 mm/month. The observed and downscaled parameters are given in Plate 4.

**Table 21. Explained variance and standard error during calibration (1985-1999)**

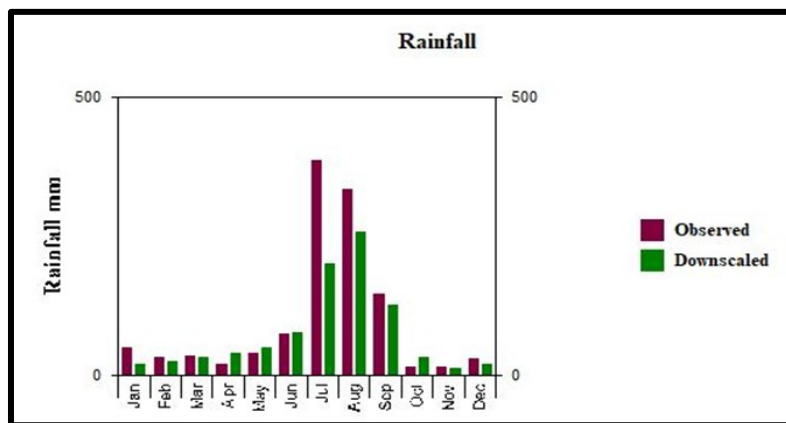
<b>Variable</b>	<b>Explained variance (%)</b>	<b>Standard error (°C or mm/month)</b>
<b>Maximum temperature</b>	68.1	2.64
<b>Minimum temperature</b>	83.8	2.01
<b>Rainfall</b>	23.9	35.00



(a)



(b)



(c)

Plate 4. (a, b and c) Observed and downscaled mean maximum & minimum temperature and rainfall from 1985 to 1999

Explained variance in case of rainfall is 23.9 per cent, similarly very less explained variance was observed in a comprehensive study conducted by Gupta, 2015; Singh *et al.*, 2015. The results obtained from calibration indicate small values of E (%) and high SE which expose the complexity of downscaling station scale precipitation from predictor variables.

#### 4.8.1.4 Weather generator (Validation of model)

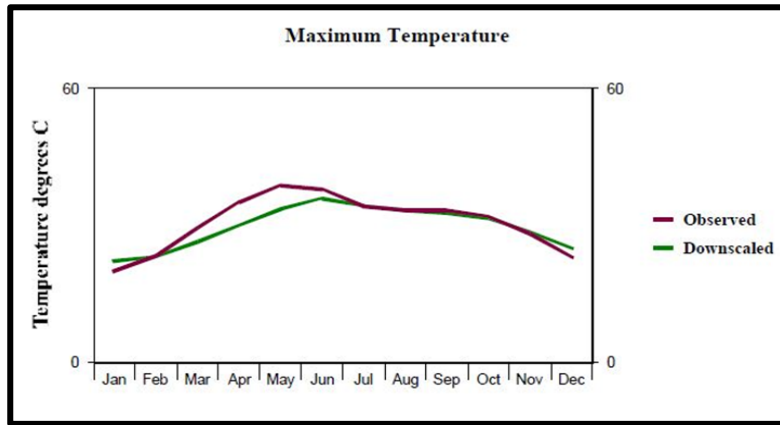
The model was validated using weather station data from 2000 to 2014 for 15 years. The model performance was analysed based on the coefficient of determination ( $r^2$ ), root means square error (RMSE), and line charts.

It indicated that (Table 22) (Plate 5) that the coefficient of determination and root mean square error for maximum and minimum temperature was 0.86, 2.51 °C and 0.72, 2.48 °C respectively whereas, for rainfall it was 0.94, 32.02 mm/month.

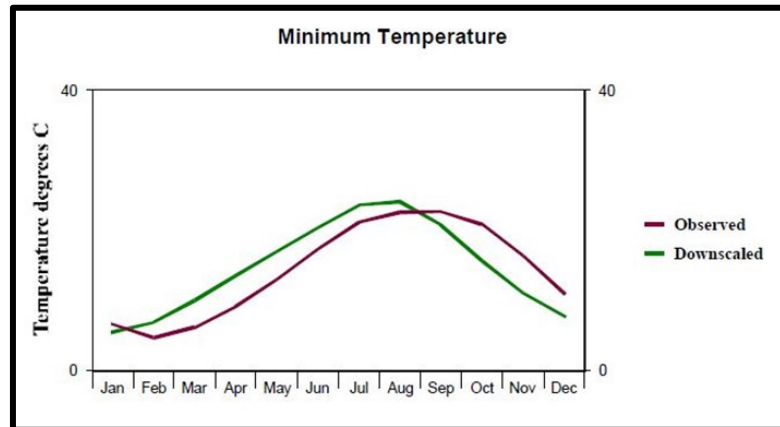
**Table 22. Coefficient of determination and root mean square error during validation**

<b>Variable</b>	<b>Coefficient of determination (<math>r^2</math>)</b>	<b>RMSE (°C or mm/month)</b>
<b>Maximum temperature</b>	0.86	2.51
<b>Minimum temperature</b>	0.72	2.48
<b>Rainfall</b>	0.94	32.02

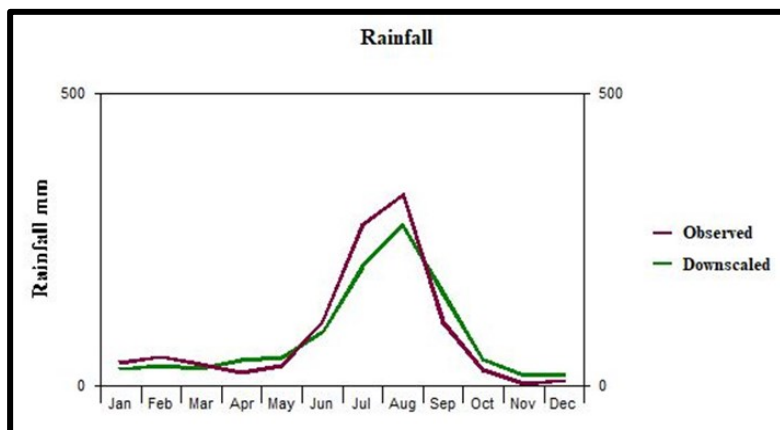
A higher  $r^2$  was obtained for precipitation than maximum and minimum temperature whereas in case of standard error it is quite higher for precipitation than maximum and minimum temperature. The results obtained from validation indicates high values of RMSE which expose the complexity of downscaling station scale precipitation and temperature from predictor variables.



(a)



(b)



(c)

**Plate 5. (a, b and c) Observed and downscaled mean maximum & minimum temperature and rainfall from 2000 to 2014**

#### 4.8.1.5 Scenario generation

After the calibration and validation model was run for the future periods of the 2020s (2011-2040), the 2050s (2041-2070), and the 2080s (2071-2099) for H3A2 and H3B2 scenarios.

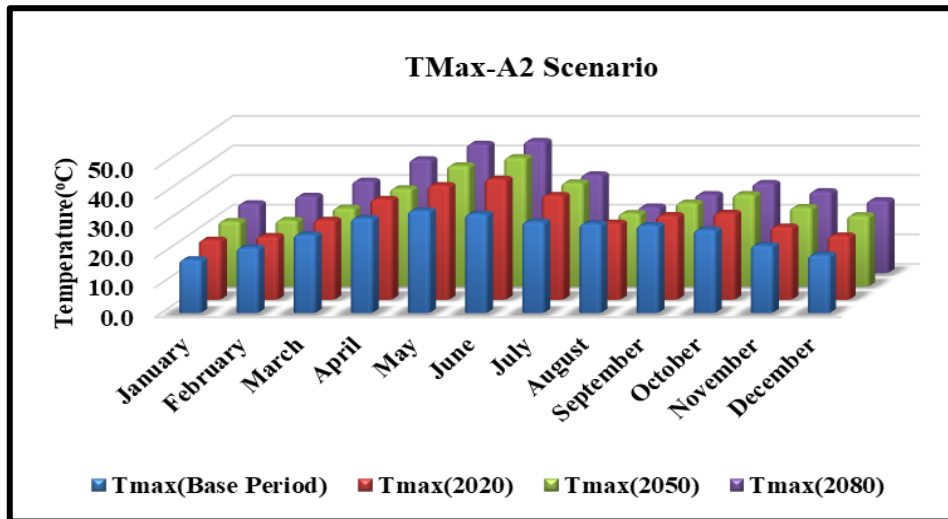


Figure 79. Estimated mean monthly maximum temperature (2011-2099) from the base period (1985-2014) for H3A2 scenario

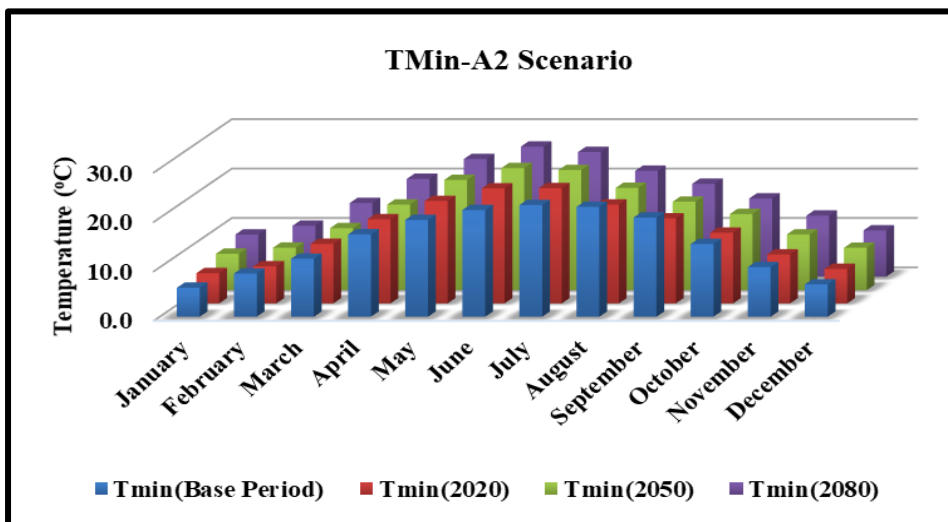
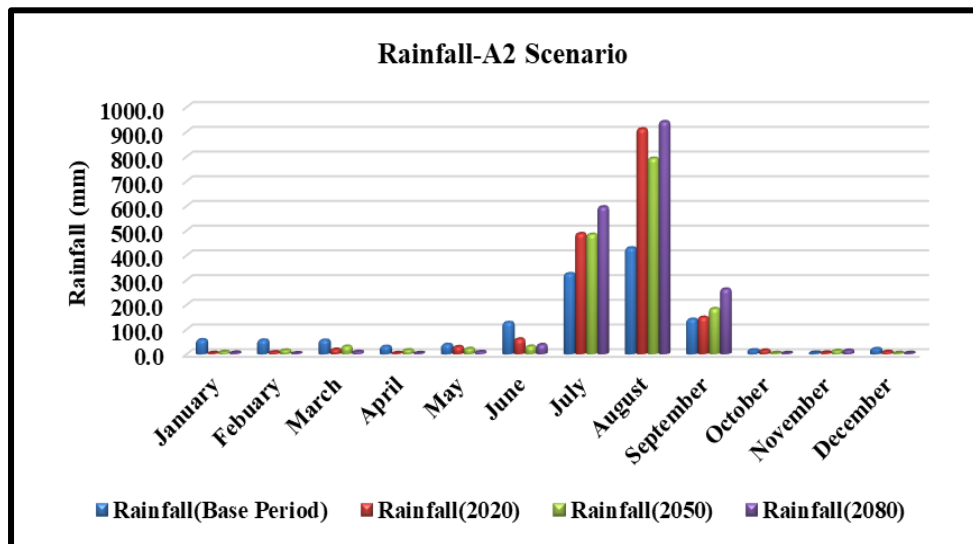


Figure 80. Estimated mean monthly minimum temperature (2011-2099) from the base period (1985-2014) for H3A2 scenario



The downscaled data of maximum temperature, minimum temperature and rainfall were analysed with the baseline period (1985-2014) to find future changes in temperature and rainfall for the years 2020s, 2050s, and 2080s. It was observed that the average annual maximum temperature is likely to increase by 1.6 °C, 2.5 °C and 3.7 °C for H3A2 emission scenario in the 2020s, 2050s, and the 2080s, respectively (Fig. 79).

The average annual minimum temperature (Fig. 80) is likely to increase by 1.2 °C, 2.3 °C and 3.6 °C for H3A2 emission scenario in the 2020s, 2050s, and the 2080s respectively. Almost similar pattern was observed in the case of both maximum and minimum temperatures. It also showed that the hottest month (June) becomes hotter than the previous tri decades.



**Figure 81. Estimated average monthly rainfall (2011-2099) from base period (1985-2014) for H3A2 scenario**

The average annual total rainfall (Fig. 81 - 82) of the study area showed an increasing trend under the H3A2 scenario. The average annual rainfall of the base period (1985 to 2014) is 1341.90mm, while the estimated rainfall was 1707.80 mm, 1612.20 mm and 1896.80 mm in 2020s, 2050s and 2080 respectively. The graph represents an overall increase in rainfall in July, August and September (monsoon months). The remaining months show a decrease in rainfall.

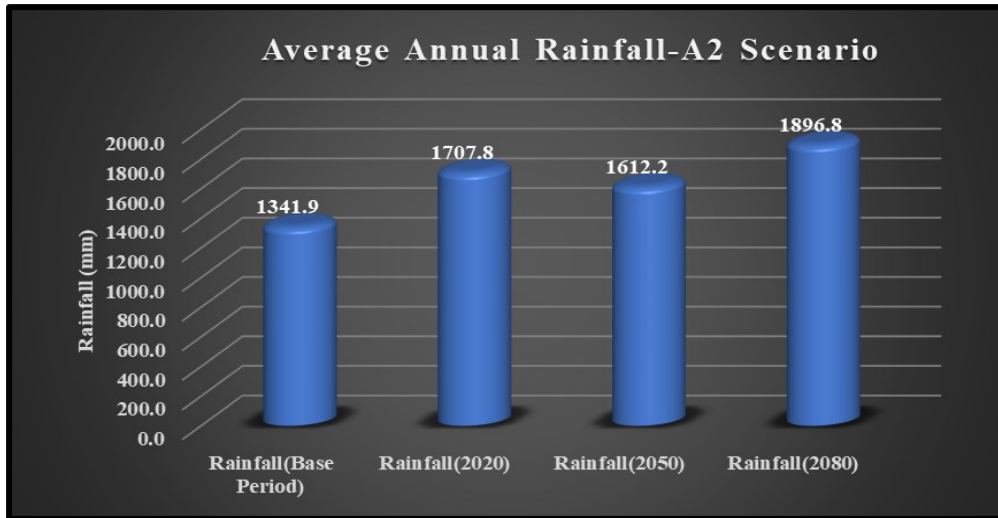


**Figure 82. Estimated average annual rainfall (2011-2099) from base period (1985-2014) for H3A2 scenario**

It was observed that the annual mean maximum temperature is projected to increase by 1.9 °C, 2.2 °C and 2.6 °C for H3B2 emission scenario in the 2020s, 2050s and the 2080s respectively (Fig. 83). It was also observed that the annual mean minimum temperature is projected to increase by 1.3 °C, 2.0 °C and 2.7 °C for H3B2 emission scenario in 2020s, 2050s and the 2080s respectively. The results clearly showed that maximum temperature is projected to increase by 0.3 °C to 1.1 °C under H3A2 scenario than H3B2 scenario.

It was observed that minimum temperature will increase by 0.3 °C to 0.9 °C under the H3A2 scenario than H3B2 scenario (Fig. 84). According to IPCC, surface air temperature shows similar increasing trends in A2 as well as B2 scenarios. The temperatures are anticipated to increase by as much as 3-4 °C in the century. Almost similar results were observed in the current study under H3A2 and H3B2 scenarios. Akarsh (2013) as well expresses that mean temperature shows an intensifying pattern in the two scenarios over Doon valley. The change is extreme under A2a (+4.1°C) contrasted with B2a (+2.97°C). Gupta and Kumar (2017) led an investigation at mid-Himalayas likewise detailed that “the average annual temperature may increase by 0.83 °C, 1.85 °C and 3.00 °C for H3A2 and 0.91 °C, 1.51 °C and 2.2 °C for H3B2 emission scenario in 2020s, 2050s and 2080s

respectively. While the output demonstrated that the maximum temperature would be expanding from 0.29 °C to 0.8 °C under H3A2 scenario than H3B2 scenario. It indicated increase in annual mean temperature by 0.95 °C, 2.26 °C and 3.79 °C for H3A2 and 1.02 °C, 1.83 °C and 2.75 °C for H3B2 emission scenario in 2020s, 2050s, and 2080s respectively”.

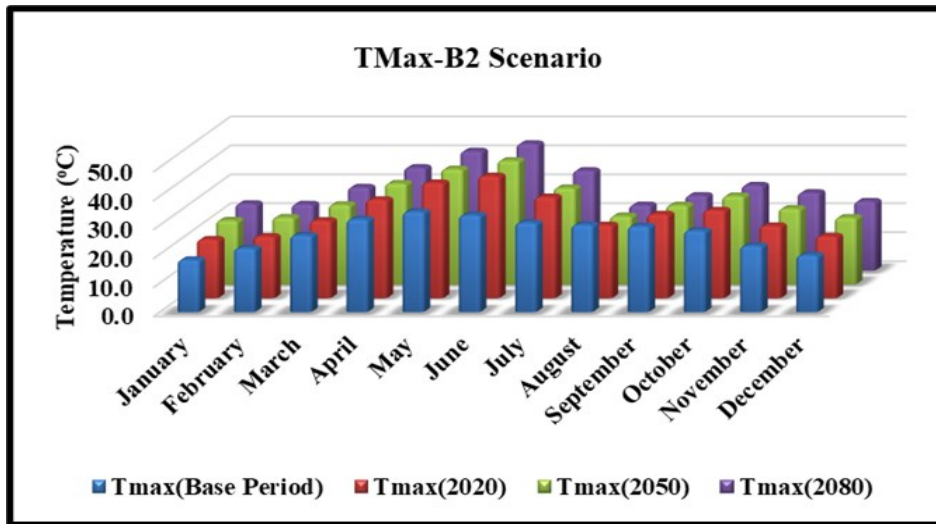


Figure 83. Estimated mean monthly maximum temperature (2011-2099) from base period (1985-2014) using H3B2 scenario

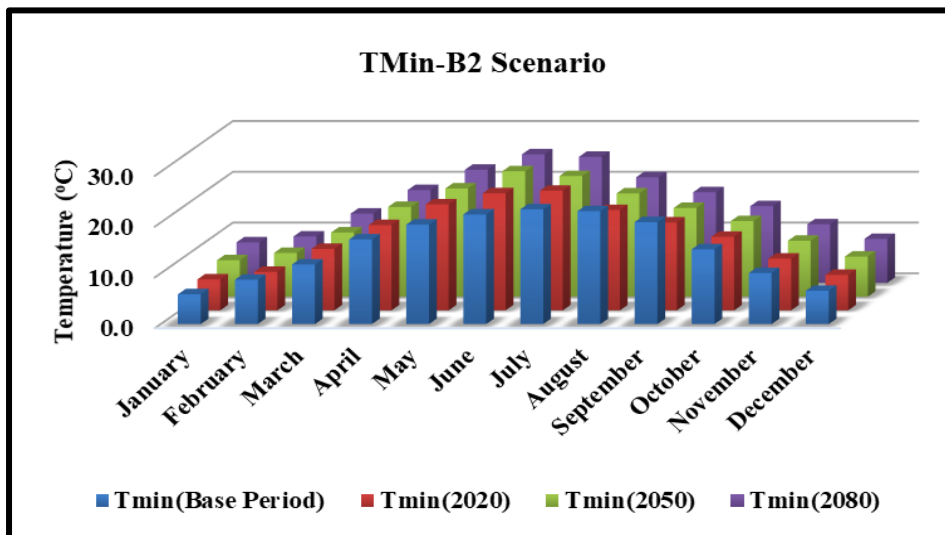
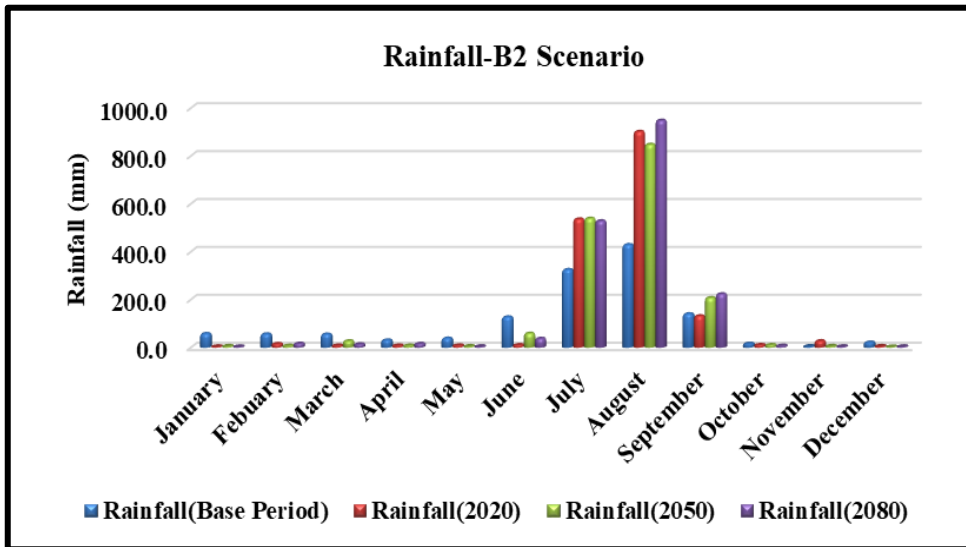
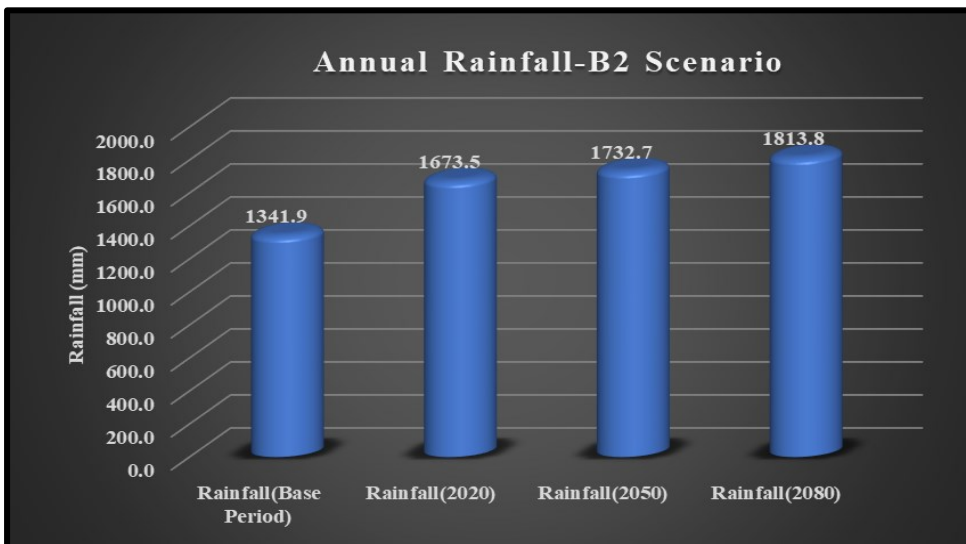


Figure 84. Estimated mean monthly minimum temperature (2011-2099) from base period (1985-2014) using H3B2 scenario



**Figure 85. Estimated average monthly rainfall (2011-2099) from the base period (1985-2014) for H3B2 scenario**



**Figure 86. Estimated average annual rainfall (2011-2099) from the base period (1985-2014) for H3B2 scenario**

The average annual rainfall (Fig. 85 - 86) of the study area show an increasing trend under the H3B2 scenario. The estimated rainfall under the B2 scenario is relatively lesser than that under the A2 scenario (IPCC, 2014). The average annual rainfall during the base period is 1341.90mm, while the estimated figures are 1673.50 mm, 1732.70 mm and 1813.80 mm in the 2020s, 2050s and 2080s respectively. Similarly, under H3A2 and H3B2 scenario the overall increase in rainfall is during July, August and September (monsoon months) and remaining

months showed a decreasing trend in rainfall. The study revealed that the intensity of rainfall is increased during the monsoon period.

The rainfall from the base period under the H3A2 scenario is likely to increase by 27.27 per cent, 20.14 per cent and 41.35 per cent in the years (Fig. 87 - 88) 2020s, 2050s and 2080s respectively (Table 23). At 2050s the rate of rainfall is decreasing slightly and then increasing up to 41.35 per cent. Akarsh (2013) also reports that “in Doon valley under A2a scenario there will be an increase in rainfall of about 25 per cent, 35 per cent and 70 per cent during 2020s, 2050s and 2080s and 21 per cent, 41 per cent and 54 per cent and during 2020s, 2050s and 2080s respectively. In the current study rainfall under the H3B2 scenario is projected to increase by 24.71 per cent, 29.13 per cent and 35.16 per cent during 2020s, 2050s and 2080s, respectively”. The rainfall amount increasing up to 35.16 per cent under H3B2 scenario. It is evident that the projected rainfall increase up to 27.27 per cent in 2020. It is also projected that it will reduce 7 per cent in 2050 and 14 per cent under H3A2 scenario as of 2080. Similarly, under H3B2 scenario, rainfall increased up to 24.71 per cent, and it may get decreases from 4 per cent in 2050s to increases 10 per cent after 2080s. Gupta and Kumar (2017) conducted an investigation at mid-Himalayas exposed that “average yearly precipitation may increase by 33.3 per cent, 30.02 per cent and 23.79 per cent for H3A2 and 31.67 per cent, 29.60 per cent and 27.87 per cent for H3B2 scenario in 2020s, 2050s and 2080s respectively. It was similarly revealed that precipitation will increase by 33.3 per cent from the base period to 2020s (2011-2040). But, it might get diminished 3 per cent -10 per cent after 2020”.

The contribution of average annual rainfall during monsoon periods (June-September) was 77.25 per cent of the total rainfall of the base period (Table 24). It is likely to increase by 94.18 per cent, 92.56 per cent and 96.85 per cent for H3A2 and 94.46 per cent, 95.40 per cent and 95.83 per cent under H3B2 emission scenario in 2020s, 2050s and 2080s respectively. The IPCC, 2014 also states that there are substantial spatial differences in the projected rainfall changes. The maximum

expected increase in rainfall in India is 10- 30 per cent, and some places it may go up to 50 per cent. The current study also confirms results on par with IPCC.

**Table 23. Change in temperature and rainfall (2011-2099) from the base period (1985-2014)**

Parameter	Scenario	2011-2039 (2020)	2040-2069 (2050)	2070-2099 (2080)
Rainfall	A2	27.27%	20.14%	41.35%
	B2	24.71%	29.13%	35.16%
Tmax	A2	1.6°C	2.5°C	3.7°C
	B2	1.9°C	2.2°C	2.6°C
Tmin	A2	1.2°C	2.3°C	3.6°C
	B2	1.3°C	2.0°C	2.7°C

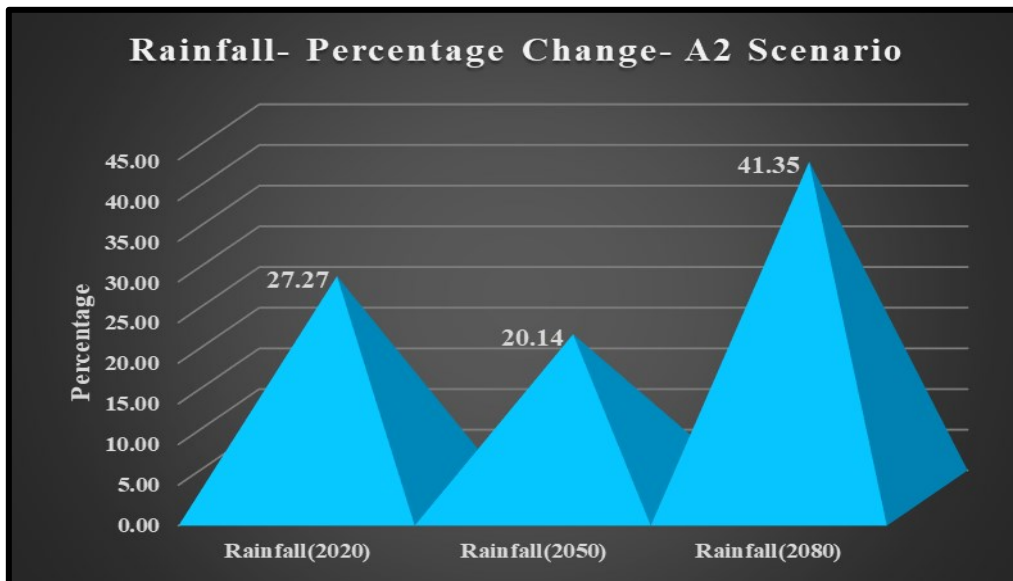


**Figure 87. Percentage change in average annual rainfall (2011-2099) from base period (1985-2014) for H3A2 scenario**

Bhutyani *et al.* (2009) carried out an investigation over north-western Himalayan (NWH) region utilizing long term precipitation information for 140

years (1866–2006) and temperature data. Temperature shows a rising trend however measurably inconsequential pattern (at 95% certainty level).

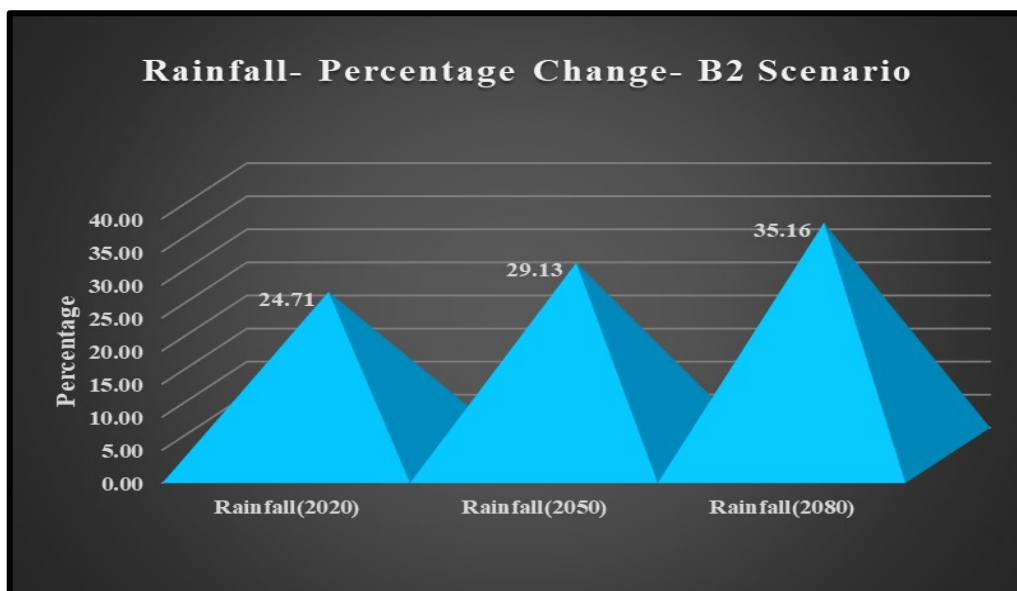


**Figure 88. Percentage change in average annual rainfall (2011-2099) from base period (1985-2014) for H3B2 scenario**

**Table 24. Percentage change in monsoon rainfall (2011-2099) from base period (1985-2014) for H3A2 & H3B2**

Scenarios	Base Period (%)	2020s (%)	2050s (%)	2080s (%)
<b>H3A2</b>	77.25	94.18	92.56	96.85
<b>H3B2</b>	77.25	94.46	95.40	95.83

The comparable outcomes were received for a few resulting studies (Goswami *et al.*, 2006; Kumar *et al.*, 2011; Bharati, 2015;) There is an extensive increase in water vapour over the monsoon region, likely because of increases in

temperature and rainfall (IPCC, 2007). The combination of this extra moisture over India within the horizontal divisions of the monsoon circulation may alone prompt increased precipitation and it is the principal drive behind the general Indian monsoon precipitation increase. Sensitivity tests utilizing singular climate models of monsoon precipitation changes and under prolonged GHG forcing additionally recommend elevated thermodynamical changes that intend to cause a plenty of monsoon precipitation (Meehl and Arblaster 2003; Sugi and Yoshimura 2004; Dairaku and Emori 2006). Kumar *et al.* (2006) observed an anticipated increase of 20 to 30 per cent in precipitation for the western Himalayan region before the 21st century's end.

#### 4.9 IDENTIFICATION OF RUNOFF MECHANISM IN THE WATERSHED

In the study area, the watershed runoff is generated mostly by saturation excess due to rainfall. The dominant soil observed in the study area is sandy loam, which contains 60 per cent of sand and only 10.58 per cent of clay content and saturation occurs very fast. The watershed has a humid subtropical climate. Thus stated bits of evidence prove the dominance of saturation excess runoff in the study area.

In addition to this, the infiltration rate of the study area is higher at a range of 33- 78 mm/hr, which is higher than the average rainfall intensity of 18 mm/hr in most regions of the study area and the chances of infiltration excess runoff are less. Consequently, omitting the roads, settlements, water bodies, hilltop and barren land (less cover), which together comprise less than 9.11 per cent of the area, so most of the watershed area is dominated by saturation excess runoff mechanism. In APEX surface runoff is simulated according to the curve number (CN) method. Also, CN changes daily based on soil moisture retention in the soil. Soil moisture index variable is used in APEX, based on the wet-dry day probabilities, and calculates the CN for each day.



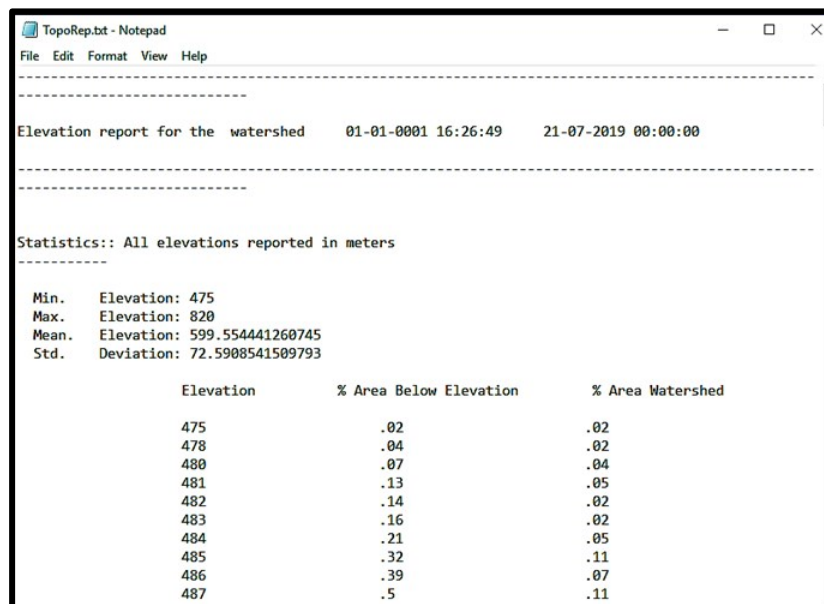
## 4.10 MODELLING SURFACE RUNOFF AND SEDIMENT YIELD

### 4.10.1 Model Description- APEX

APEX is a complex process-based model. It requires a vast amount of data to simulate each natural processes. APEX model was implemented in the study area. The model simulates each process based on given inputs and equations. This simulated data tested using the observed value to calibrate the model for the study area. The APEX model implementation described as follows.

### 4.10.2 Subarea delineation

APEX subarea is based on Cartosat 30m resolution DEM. After completion of the subarea, delineation model, gives a ‘topo report’ as Fig. 89-92 and subarea delineation map. Analysing the topo report, it is seen that minimum elevation of the watershed is 475 m, maximum elevation is 820 m, mean elevation 599.55 m and standard deviation 72.59 m. It also gives percentage area below specific elevation and area covered by particular elevation.



```
TopoRep.txt - Notepad
File Edit Format View Help
-----
Elevation report for the watershed    01-01-0001 16:26:49    21-07-2019 00:00:00
-----
Statistics:: All elevations reported in meters
-----
Min.   Elevation: 475
Max.   Elevation: 820
Mean.  Elevation: 599.554441260745
Std.   Deviation: 72.5908541509793

      Elevation      % Area Below Elevation      % Area Watershed
      475             .02                          .02
      478             .04                          .02
      480             .07                          .04
      481             .13                          .05
      482             .14                          .02
      483             .16                          .02
      484             .21                          .05
      485             .32                          .11
      486             .39                          .07
      487             .5                           .11
```

**Figure 89. Elevation report of the watershed**

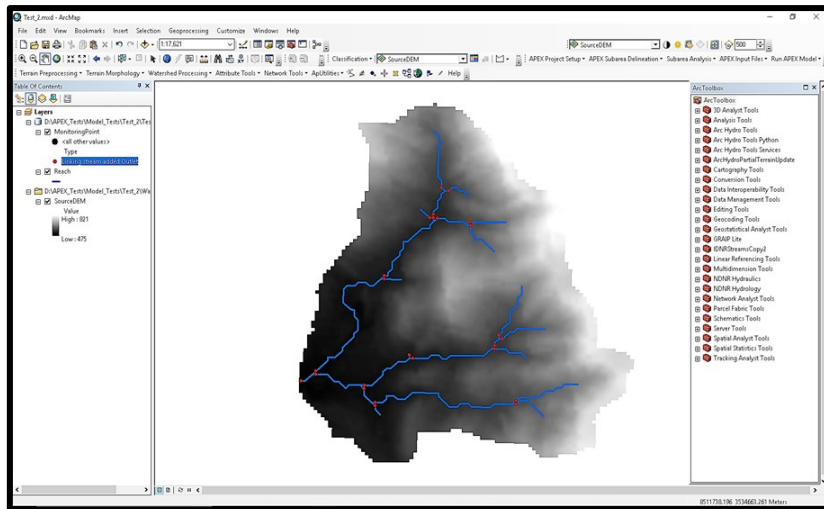


**Figure 90. ArcAPEX stream definition**

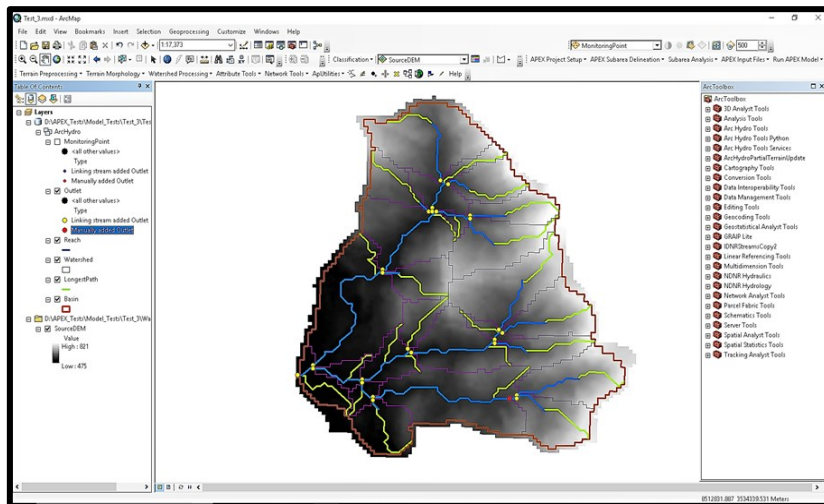


**Figure 91. ArcAPEX defined subarea**

#### 4.10.2.1 Defining land use/land cover, soil and slope data

APEX defines (Plate 6) land use by linking it with APEX land use/ land cover database. FRSE, FRST, CORN, RNGE, URBN, WATR stands for the evergreen forest, mixed forest, barren land, settlements and water bodies respectively. The model also gives the area of each land use. User-defined soil properties were used for soil definition, a total of 11 user-defined soil class is included in the APEX model. It also gives the percentage of the area enclosed by each soil type. The model also allows the user to classify slope and provide maximum, minimum and

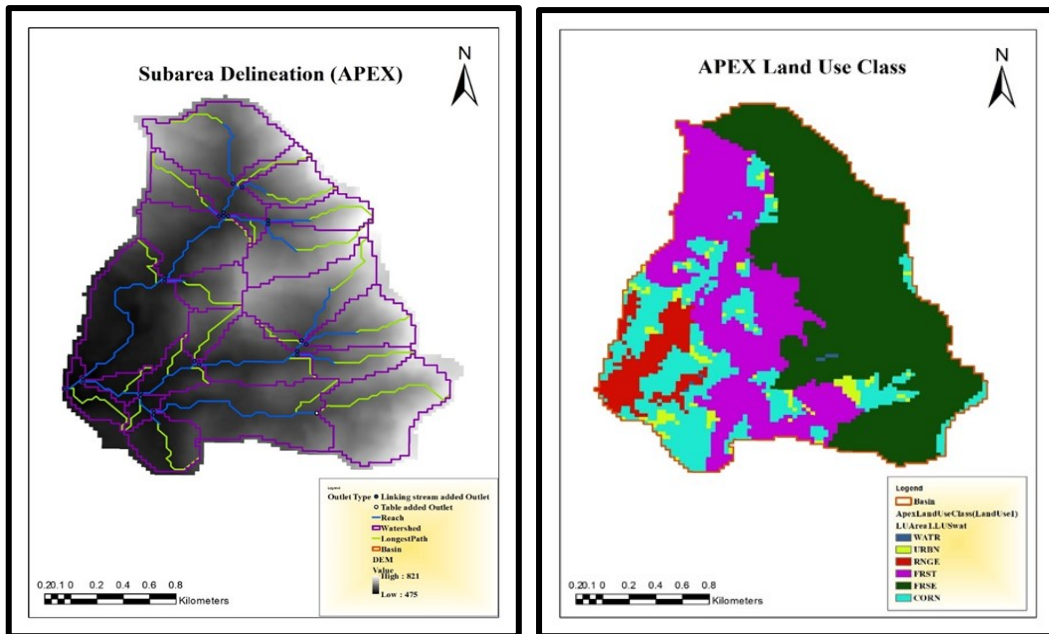
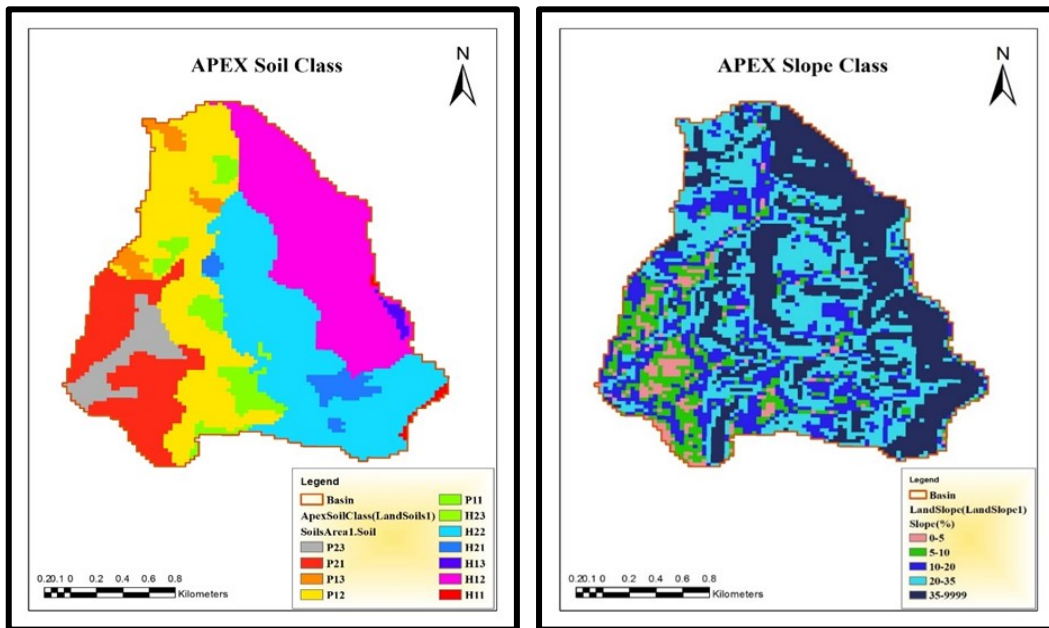


Figure 92. ArcAPEX subarea delineation

(a)



(b)

(c)

Plate 6. ArcAPEX derived land use/ soil/ slope classification (a) Land use, (b) soil class, (c) slope class

average slope. The user-defined slope class is added into the model and based on this model slope map is created.

### 4.10.3 Subarea analysis report

After defining sub-area by dominant land use, soil and slope by user-defined method, model defines each subarea according to this, and provides two reports, one provides land use, soil, slope covered by each sub-area (Fig. 93) and another provides dominant land use, soil and slope defined to each subarea (Fig. 94).

Detailed LANDUSE/SOIL/SLOPE distribution APEX model class Date: 21-07-2019 00:00:00 Time: 16:29:55.5210460

Watershed		Area [ha]	Area[acres]	
Number of Subareas: 24		466.2762	1152.1918	
LANDUSE:		Area [ha]	Area[acres]	%Mat. Area
	FOREST-MIXED --> FRST	128.2594	316.9353	27.51
	FOREST-EVERGREEN --> FRSE	214.9346	531.1142	46.10
	RANGE --> RNGE	26.6372	65.8218	5.71
	CORN --> CORN	83.3352	205.9254	17.87
	WATER --> MATR	0.6680	1.6507	0.14
	PAVEMENT --> URBN	12.4418	30.7444	2.67
SOILS:				
	H11	2.0041	4.9521	0.43
	H12	112.8950	278.9691	24.21
	H13	2.5051	6.1901	0.54
	H21	11.3563	28.0620	2.44
	H22	121.2452	299.6029	26.00
	H23	1.2525	3.0951	0.27
	P11	22.5456	55.7113	4.84
	P12	100.9541	249.4627	21.65
	P13	9.6028	23.7289	2.06

Figure 93. Detailed land use, soil, and slope distribution in each subarea

APEX model simulation Date: 21-07-2019 00:00:00 Time: 00:00:00  
USER DEFINED OPTION  
Number of Subareas: 24

Watershed		Area [ha]	Area[acres]	
Number of Subareas: 24		466.2762	1152.1918	
LANDUSE:		Area [ha]	Area[acres]	%Mat. Area
	FOREST-EVERGREEN --> FRSE	254.0971	627.8868	54.49
	FOREST-MIXED --> FRST	112.0599	276.9057	24.03
	RANGE --> RNGE	68.3048	168.7845	14.65
	CORN --> CORN	31.8143	78.6148	6.82
SOILS:				
	P12	91.0174	224.9085	19.52
	H12	138.4466	342.1085	29.69
	H22	136.6931	337.7754	29.32
	P23	58.2845	144.0240	12.50
	P21	41.8346	103.3754	8.97
SLOPE:				
	35-9999	175.4381	433.5163	37.63
	20-35	190.6355	471.0698	40.88

Figure 94. User-defined land use, soil, and slope in each subarea

#### 4.11 SENSITIVITY ANALYSIS OF THE MODEL

The fundamental objective of sensitivity analysis is to define the degree of changes in the model outputs due to changes in the value of the specified parameter. A total of 8 parameters were selected according to the APEX user manual for sensitivity analysis (Table 25). Total four parameters for surface runoff and another four for sediment yield were tested by changing the specific parameters by  $\pm 5$  per cent,  $\pm 10$  per cent and  $\pm 15$  per cent. It was detected that altering most of the parameters by  $\pm 5$  per cent does not show ample change in the output results, which specifies the model is sensitive to error due to any inexplicable reason in the inputs up to 5 per cent. The sensitive analysis of surface runoff reveals (Table 25) that Curve number (CN) is most sensitive to it, followed by curve number retention

**Table 25. Various parameters and percentage change with respect to runoff and sediment yield variation**

Sl. No.	Parameters	Percentage Change	Runoff	Sediment
1	Curve Number(CN)	+4	+57.12	+31.24
		-4	-32.28	-24.67
2	Curve Number Retention Parameter	+5(%)	-5.03	-0.78
		+10(%)	-7.20	-3.30
		+15(%)	-14.08	-6.63
		-5(%)	+4.55	+1.11
		-10(%)	+6.25	+3.20
		-15(%)	+8.00	+4.23
3	Curve Number Index Coefficient	+5(%)	+1.10	+0.66
		+10(%)	+1.72	+1.24
		+15(%)	+5.12	+1.83
		-5(%)	-0.76	-0.68
		-10(%)	-3.36	-1.44
		-15(%)	-4.68	-2.11

**Table 25 Contd.**

Sl. No.	Parameters	Percentage Change	Runoff	Sediment
4	Available water content	+0.05	-1.70	0.00
		-0.05	-7.58	0.00
5	Erosion control practice factor	+5(%)	+0.18	+4.96
		+10(%)	+1.02	+9.92
		+15(%)	+1.40	+14.87
		-5(%)	-0.24	-5.05
		-10(%)	-0.31	-10.07
		-15(%)	-0.36	-15.08
6	Channel Cover Factor	+5(%)	0.00	+0.03
		+10(%)	+1.11	+3.24
		+15(%)	+1.98	+8.42
		-5(%)	0.00	-2.80
		-10(%)	-0.11	-2.79
		-15(%)	-0.60	-8.01
7	Erodibility Factor	+5(%)	+0.07	+0.28
		+10(%)	+0.06	+3.28
		+15(%)	+0.96	+7.25
		-5(%)	0.00	-0.01
		-10(%)	-0.02	-0.50
		-15(%)	-0.60	-1.46
8	Average Upland Slope	+5(%)	+0.05	+0.03
		+10(%)	+2.00	+1.07
		+15(%)	+11.39	+8.38
		-5(%)	-0.01	-0.02
		-10(%)	-4.98	-4.88
		-15(%)	-3.30	-9.13

parameter (CNRN), average upland slope (S), available water content (AWC) and curve number index coefficient (CNIC). As for sediment yield, erosion control practice factor (P) is found to be most sensitive followed by the cover factor (C), average upland slope (S) and erodibility factor (K).

**Table 26. Parameters sensitive to runoff and sediment yield**

<b>Sl. No.</b>	<b>Runoff</b>	<b>Sediment</b>
<b>1</b>	Curve Number(CN)	Erosion Control Practice Factor (P)
<b>2</b>	Curve Number Retention Parameter (CNRN)	Channel Cover Factor (C)
<b>3</b>	Available Water Content (AWC)	Average Upland Slope (S)
<b>4</b>	Curve Number Index Coefficient (CNIC)	Erodibility Factor (K)

(Most sensitive parameters in decreasing order)

#### 4.12 CALIBRATION AND VALIDATION OF THE MODEL

##### 4.12.1 Model calibration

The model calibration was carried out to reduce the difference between observed and simulated runoff and sediment yield values. The model calibration was done by improving the inputs given to the model (Table 26) and found the most suitable values for better simulation. The gauged nano watershed from the micro watershed was used to calibrate the model. The calibration was done according to sensitivity analysis performed by changing the sensitive parameters.

##### 4.12.1.1 Surface runoff

The first change was made by decreasing the curve number by 4. Then model-simulated and observed runoff were obtained as almost similar. Further decrease in the curve number resulted in very less runoff than observed, so eliminated the curve number decrease. It means that the model needed some fine-tuning. Then the curve

number retention parameter increased by 5 per cent. To obtain closer value, decrease the curve number index coefficient by 10 per cent, and finally to make the simulated runoff more or less equal to observed values the subsequent changes were made, and the absolute values of each parameter are given in the Table 27.

**Table 27. Model parameters and values fixed in surface runoff calibration**

Sl. No.	Calibrated Parameter	Prescribed range	Value used
1	SCS Curve Number	0-98	Forest-70, Range Land-81, Agriculture-74
2	Curve Number Retention Parameter(16)	1-1.5	1.2
3	Curve Number Index Coefficient(42)	0.3-2.5	0.70
4	Available Water Content	0-1	0.09-0.12

After calibration (Fig. 95), the model performed reasonably well for surface runoff with a correlation coefficient ( $r$ ) of 0.963 and coefficient of determination ( $r^2$ ) of 0.928 (Table 28). While analysing other statistical parameters such as mean, standard deviation and maximum, it was clear that model slightly over predicted the surface runoff. Similarly, the box and whisker (Fig. 96) plot also give a clear picture of over prediction of surface runoff (Table 29). It was observed during the calibration model predict quit well for low to medium rainfall and for higher rainfall model over predicts. Singh and Kumar (2012) carried out a research in lesser Himalayas, states that over-prediction may be attributed to the coarse fragments and stony surfaces in the area contributed high runoff while for low and medium rainfall events its effect was minimal due to time lag and not accounted by model.



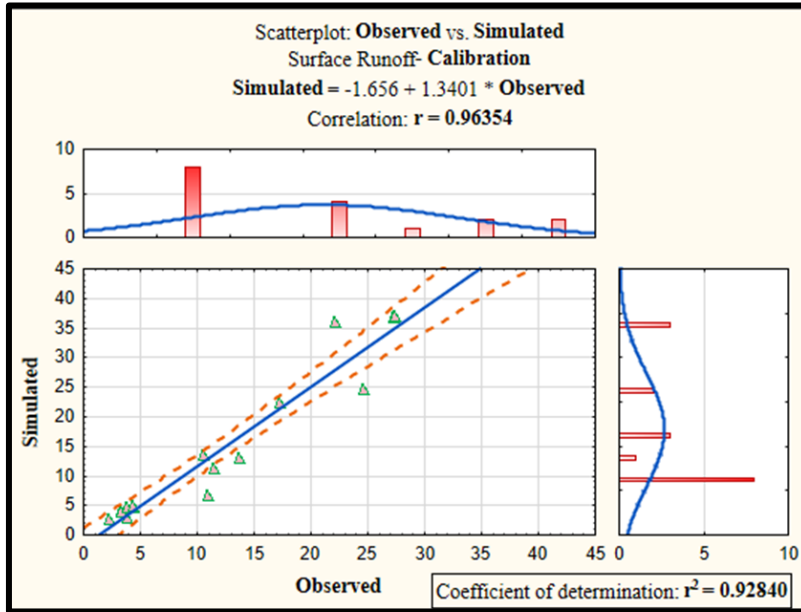


Figure 95. Scatter plot of observed and simulated runoff (Calibration)

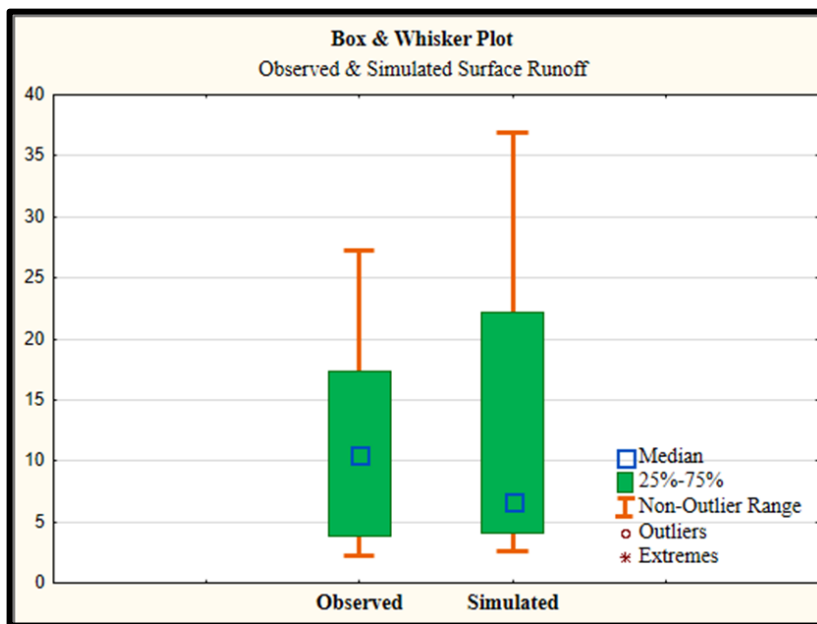


Figure 96. Box & Whisker plot of observed and simulated runoff (Calibration)

Similarly, the study area contains relatively higher surface coarse fragments and stoniness. Also, rainfall data managements and runoff calculations are more efficient for data taken daily than at smaller intervals. One of the significant criticisms of the curve number technique is its inability to represent precipitation

intensity (Wang *et al.*, 2015). So it legitimizes over prediction is because of the explanation referenced previously.

**Table 28. Scatter plot statistics for surface runoff calibration**

Statistical Parameter	Surface Runoff (mm)	
	Observed	Simulated
Total Number (N)	17	17
Mean	11.39	13.60
Standard Deviation	9.12	12.69
Maximum	27.31	36.93
Minimum	2.18	2.58
Root Mean Square Error (RMSE)	4.982	
Correlation Coefficient (r)	0.963	
Coefficient of Determination (r <sup>2</sup> )	0.928	
Nash- Sutcliffe model Efficiency (NSE)	0.710	

**Table 29. Box & Whisker plot statistics for surface runoff calibration**

Box & Whisker parameters	Surface runoff (mm) -Validation	
	Observed	Simulated
Median	10.56	6.65
25 percentiles	3.82	4.13
75 percentiles	17.29	22.17
Non-Outlier minimum	2.18	0.12
Non- Outlier maximum	27.31	36.93
Interquartile range	13.47	18.04

#### 4.12.1.2 Sediment yield

The model was calibrated using 12 rainy days data obtained from 2017 and 2018. Before, the calibration model was over predicted. For high rainfall event model over predicted with a higher range. It was mainly due to high erosion control

practice factor (P) and low cover factor (C). Adjustment in the value of erosion control practice was made first, as, among the sensitive parameters, erosion control practice factor (P) is seen as most sensitive. Again adjustments were made using the cover factor (C). Then for fine-tuning the erodibility factor (K) and average upland slope (S) was adjusted and finally to make the simulated sediment yield more or less equal to observed values and the absolute values of each parameter are given in the Table 30. After proper calibration, model under predicted the sediment yield. Over predicted calibration values were far from observed, but under-predicted values were quiet near as observed. Other than rainfall and runoff the sediment loss is related to numerous other parameters as identified by sensitivity analysis. The various sensitive parameters used in calibration with their respective values are given in Table 30.

**Table 30. Model parameters and values fixed in sediment yield calibration**

Sl. No.	Calibrated Parameter	Prescribed range	Value used
c	Erosion Control Practice Factor (P)	0-1	0.15-0.8
2	Channel Cover Factor (C)	0.0001-0.6	0.1-0.4
3	Average Upland Slope (S)	0.001-0.7	0.3
4	Erodibility Factor (K)	0.0001-0.5	0.1-0.4

After the calibration process, the model simulated reasonably well for sediment yield with a correlation coefficient (r) of 0.938 and a coefficient of determination ( $r^2$ ) of 0.881(Fig. 97). After analysing other statistical parameters (Table 31) such as mean, standard deviation and maximum it was identified that the model slightly under-predicted the sediment yield.

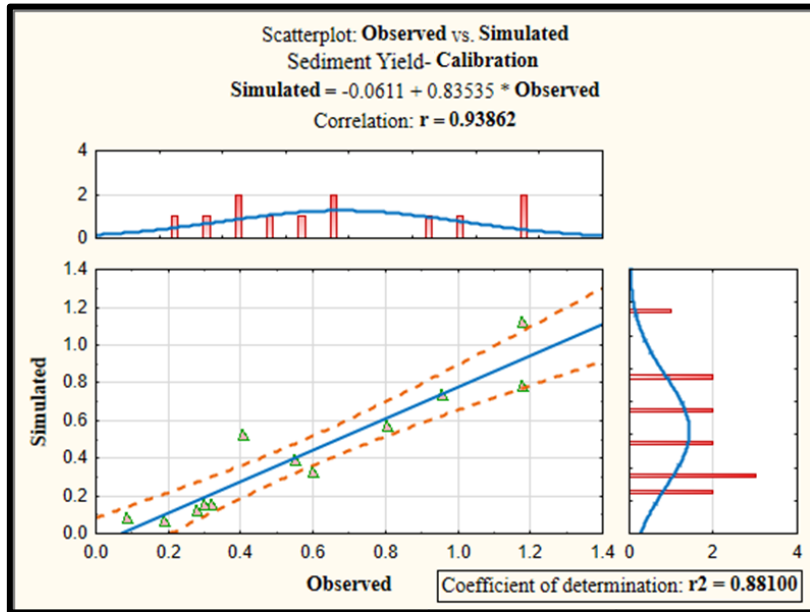


Figure 97. Scatter plot of observed and simulated sediment yield (Calibration)

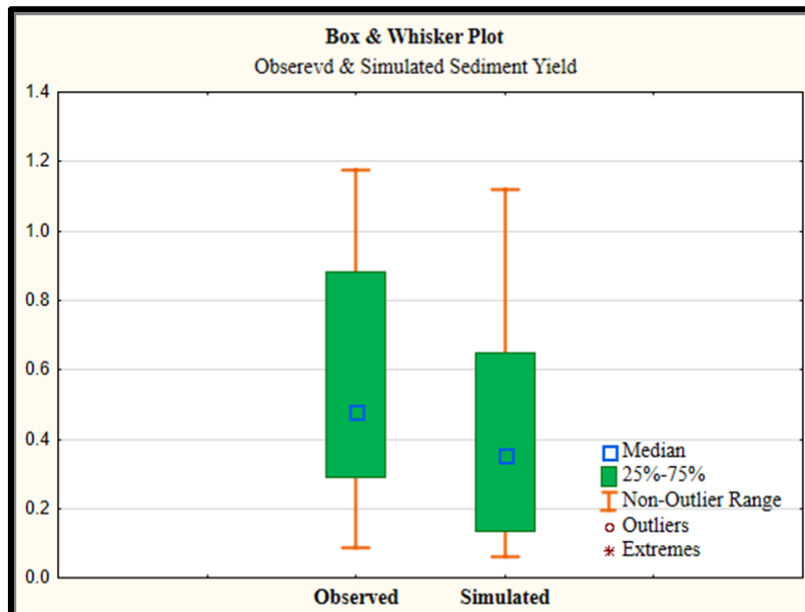


Figure 98. Box & Whisker plot of observed and simulated sediment yield (Calibration)

Similarly, the box and whisker plot (Fig. 98) also gives a clear picture of under prediction of sediment yield (Table 32). It was observed that during the calibration, model predict quiet well for low to medium rainfall event and for higher

rainfall event model over predicts. The under prediction of low to medium rainfall is explained by the study conducted by Singh and Kumar (2012) is mainly due to landslips. In the watershed area, landslips due to excess saturation contribute to sediments at the outlet. The model did not predict sediment due to the landslip.

**Table 31. Scatter plot statistics for sediment yield calibration**

Statistical Parameter	Sediment Yield (t/ha)	
	Observed	Simulated
<b>Total Number (N)</b>	12	12
<b>Mean</b>	0.57	0.42
<b>Standard Deviation</b>	0.38	0.34
<b>Maximum</b>	1.18	1.12
<b>Minimum</b>	0.088	0.060
<b>Root Mean Square Error (RMSE)</b>	0.201	
<b>Correlation Coefficient (r)</b>	0.938	
<b>Coefficient of Determination (r<sup>2</sup>)</b>	0.881	
<b>Nash- Sutcliffe model Efficiency (NSE)</b>	0.700	

**Table 32. Box & Whisker plot statistics for sediment yield calibration**

Box & Whisker parameters	Sediment yield (t/ha) -Validation	
	Observed	Simulated
<b>Median</b>	0.48	0.35
<b>25 percentiles</b>	0.29	0.13
<b>75 percentiles</b>	0.88	0.65
<b>Non-Outlier minimum</b>	0.088	0.06
<b>Non- Outlier maximum</b>	1.17	1.12
<b>Interquartile range</b>	0.59	0.52

#### 4.12.2 Model validation and performance assessment

The APEX model was simulated and simulated surface runoff and sediment yield compared with field observations and measurements obtained from the study area watershed during 2017- 2018. The validation and performance

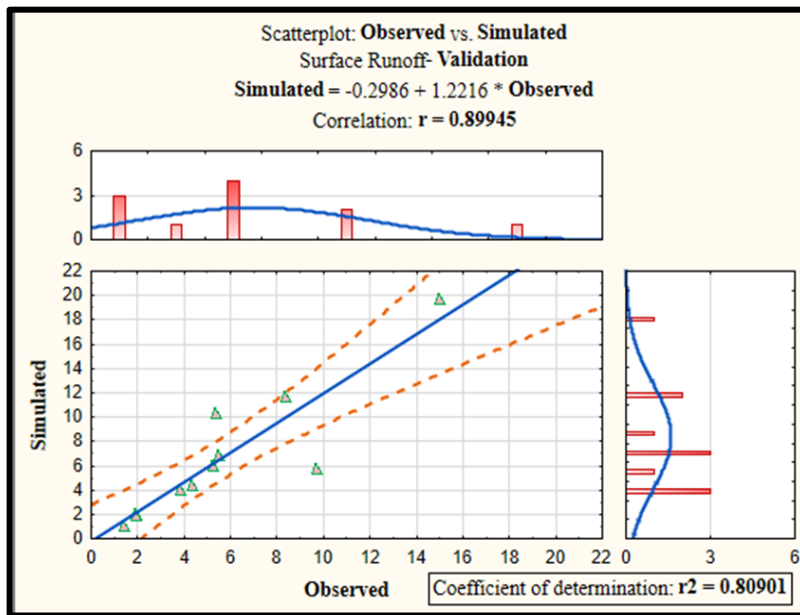


Figure 99. Scatter plot of observed and simulated runoff (Validation)

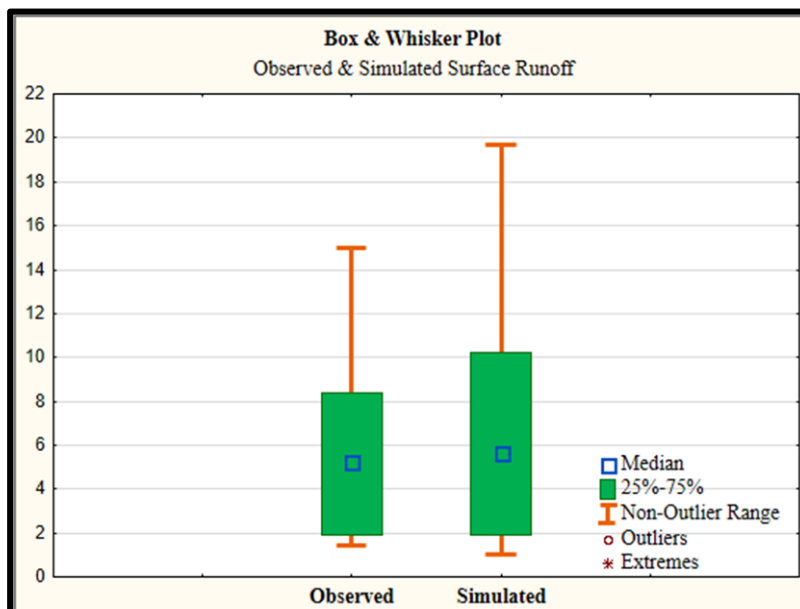


Figure 100. Box & Whisker plot of observed and simulated runoff (Validation)

obtained from the study area watershed during 2017- 2018. The validation and performance of the model were assessed based on correlation coefficient ( $r$ ), coefficient of determination ( $r^2$ ), root mean square error (RMSE), and Nash Sutcliffe model efficiency (NSE). The selected rainfall events of the year 2017 and 2018 were used in the study; a total of 28 rainfall days for surface runoff and 20 rainfall days for sediment yield. Among this for 11 and 8 used for validation of surface runoff and sediment yield, respectively.

#### 4.12.2.1 Surface runoff validation

After the validation process, model performance reasonably well for surface runoff with a correlation coefficient ( $r$ ) of 0.899 and coefficient of determination ( $r^2$ ) of 0.809 (Fig. 99). After analysing other statistical parameters (Table 33) such as mean, standard deviation and maximum, it was identified that similarly in the calibration, model slightly over predicted the surface runoff. Further analysis by box and whisker plot (Fig. 100) also gives a clear picture of the over prediction of surface runoff. There are no outliers for the runoff validation process (Table 34).

**Table 33. Scatter plot statistics for surface runoff validation**

Statistical Parameter	Surface Runoff (mm)	
	Observed	Simulated
<b>Total Number (N)</b>	11	11
<b>Mean</b>	5.68	6.64
<b>Standard Deviation</b>	4.03	5.47
<b>Maximum</b>	15.00	19.70
<b>Minimum</b>	1.42	1.02
<b>Root Mean Square Error (RMSE)</b>	2.616	
<b>Correlation Coefficient (r)</b>	0.899	
<b>Coefficient of Determination (<math>r^2</math>)</b>	0.809	
<b>Nash- Sutcliffe model Efficiency (NSE)</b>	0.710	

**Table 34. Box & Whisker plot statistics for surface runoff validation**

Box & Whisker parameters	Surface runoff (mm) -Validation	
	Observed	Simulated
Median	5.24	5.68
25 <sup>th</sup> percentile	1.91	1.93
75 <sup>th</sup> percentile	8.38	10.25
Non-Outlier minimum	1.42	1.02
Non- Outlier maximum	15.00	19..70
Interquartile range	6.47	8.32

*4.12.2.2 Model performance for surface runoff*

Model performance of surface runoff was evaluated by the Nash-Sutcliffe model efficiency (Fig. 101), which gives satisfactory NSE value of 0.71.

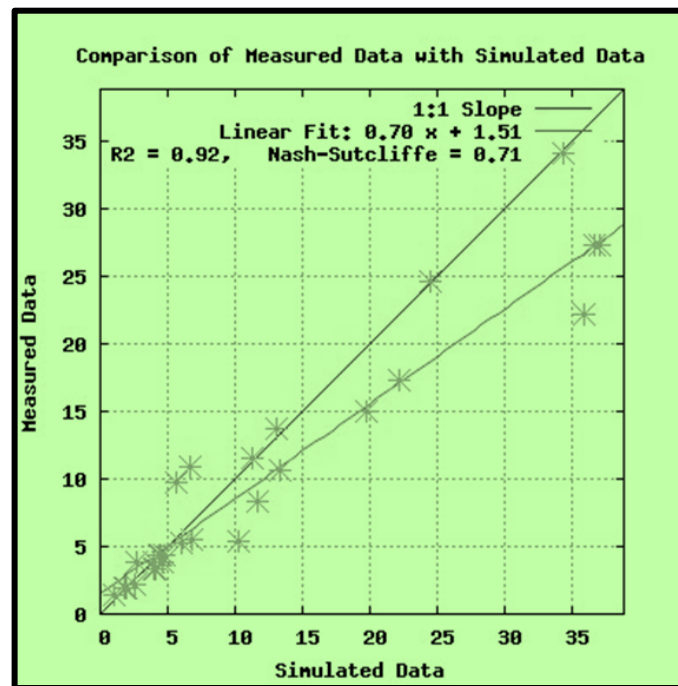


**Figure 101. Nash-Sutcliffe model Efficiency for surface runoff simulation**



#### 4.12.2.3 Sediment yield validation

After the validation process, the model performed reasonably well for sediment yield with a correlation coefficient ( $r$ ) of 0.899 and coefficient of determination ( $r^2$ ) of 0.809 (Fig. 102). On analysing other statistical parameters

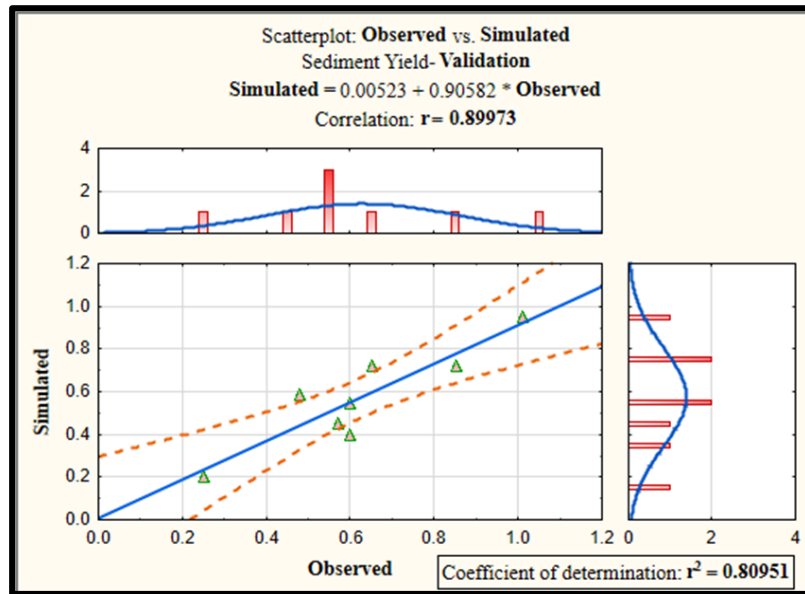


Figure 102. Scatter plot of observed and Sediment yield (Validation)

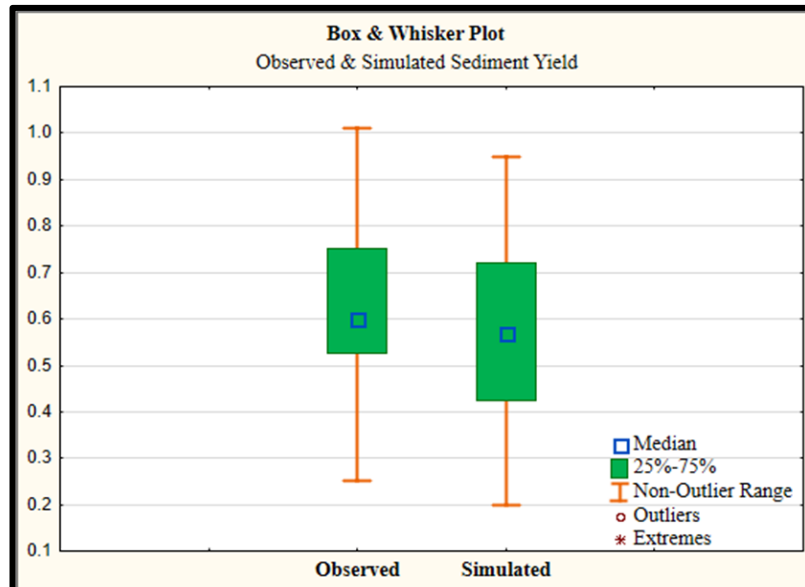


Figure 103. Box & Whisker plot of observed and sediment yield (Validation)

such as mean, standard deviation and maximum (Table 35), it is seen that in the calibration, model slightly under-predicted the sediment yield. Further analysis by box and whisker plot (Fig. 103) also gives a clear picture of under prediction of sediment yield (Table 36).

**Table 35. Scatter plot statistics for sediment yield validation**

Statistical Parameter	Sediment Yield (t/ha)	
	Observed	Simulated
Total Number (N)	8	8
Mean	0.63	0.57
Standard Deviation	0.23	0.23
Maximum	1.01	0.95
Minimum	0.25	0.20
Root Mean Square Error (RMSE)	0.11	
Correlation Coefficient (r)	0.899	
Coefficient of Determination (r <sup>2</sup> )	0.809	
Nash- Sutcliffe model Efficiency (NSE)	0.700	

**Table 36. Box & Whisker plot statistics for sediment yield validation**

Box & Whisker parameters	Sediment yield (t/ha) -Validation	
	Observed	Simulated
Median	0.60	0.57
25 percentiles	0.525	0.425
75 percentiles	0.75	0.72
Non-Outlier minimum	0.25	0.20
Non- Outlier maximum	1.01	0.95
Interquartile range	0.225	0.295

#### 4.12.2.4 Model performance for sediment yield

Model performance of sediment yield was evaluated by the Nash-Sutcliffe model efficiency (Fig. 104), which gives satisfactory NSE value of 0.70.

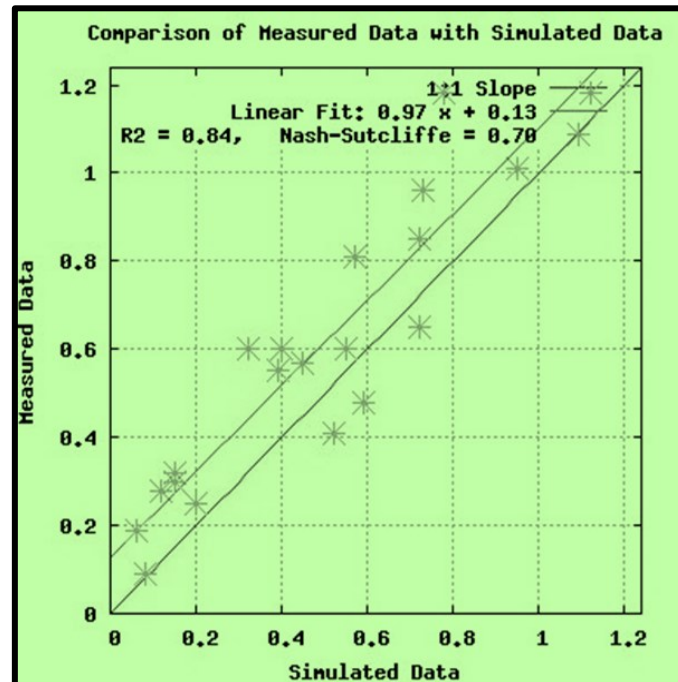


**Figure 104. Nash-Sutcliffe model Efficiency for sediment yield simulation**

The validation statistics and model performance results show that model simulated quite well for low to medium rainfall events for both surface runoff and sediment yield, while the model over predicted for the surface runoff at high rainfall events and under predicting for sediment yield. In the study area, the challenging problem of landslips (Plate 7- (c), (d), and (e)) increases the sediment loss. These events were not considered by the model and this may have led to the under prediction of sediment loss.

To prevent erosion there are several conservation measures adopted in the study area. Some of the agricultural fields are contoured and terraced, some of them have stone bunds and grass-covered bunds (Plate 8- (a), (b), (c), (d)). To prevent bank erosion, gabions are constructed and also to reduce the water flow check dams were constructed in the study area.



(a)



(b)



(c)



(d)



(e)



(f)





(g)



(h)

**Plate 7. Erosion features observed in the study area: (a) Scrub land-moderate erosion, (b) Crop land- moderate erosion, (c,d,e) Land slips, (f) sheet erosion, (g,h) Rill erosion**



(a) Surface dykes



(b) Check dams



(c) Stone bunds



(d) Gabion sidewall

**Plate 8. Conservation measures observed in the watershed**

#### 4.13 SURFACE RUNOFF AND SOIL LOSS ESTIMATION

After calibration validation, and model performance testing, APEX was run based on a yearly scale to identify surface runoff and soil loss from each subarea. APEX model divided the nano watershed based on land use, soil and slope into 5 subareas. In APEX model, surface runoff simulation is using curve number, based on land use and soil hydrological properties. Generally, surface runoff is 40-60 per cent of the total rainfall received in the catchment area. Fig. 107 shows daily observed runoff and simulated runoff.

The total average rainfall for the study area is 1295 mm. Agriculture land has more surface runoff (Fig. 105) of 486.61 mm, which is about 37.57 per cent of rainfall followed by the dense forest with 443.51 mm, and the open forest contributes very less surface runoff of 429.66 mm, which is about 33.17 per cent of rainfall. In this nano watershed area, the open forest is only 0.37 per cent of the total. This smaller catchment size reduced the surface runoff. Forest has a good land cover, which reduced the surface runoff, and less land cover in the agricultural field cause an increased surface runoff.

APEX model uses the Onsted- Foster equation for simulating sediment yield. This equation considers both rainfall and runoff energy for calculating sediment yield. The subarea (Fig. 106) with agriculture has more soil loss. Along with the land cover, slope also plays a significant role in soil loss. Open forest with 10-20 per cent slope observed very low soil loss. Slope, greater than 35 per cent observed more soil loss in the different subarea. In subareas where the slope is less and has less cover, high soil loss occurred. Among different land uses dense forests has very less average soil loss of 15.68 ton ha<sup>-1</sup> yr<sup>-1</sup> followed by the open forest of 22.22 ton ha<sup>-1</sup> yr<sup>-1</sup>, and higher rates observed in maize field of 27.50 ton ha<sup>-1</sup> yr<sup>-1</sup>. Table 37 and 38 gives detailed results of soil loss from different subareas on the slope, and land use based criteria.

**Table 37. Surface runoff and sediment yield in various Subarea**

Subarea No.	Land use	Slope (%)	Area (%)	Surface runoff (mm/ year)	Soil Loss (ton ha <sup>-1</sup> yr <sup>-1</sup> )
1	Dense Forest	>35	32.16	443.51	15.58
2	Dense Forest	>35	9.85	446.85	16.29
3	Open Forest	10-20	0.37	429.66	22.22
4	Agriculture (Maize)	20-35	15.80	486.61	27.50
5	Dense Forest	>35	41.82	440.34	16.49

**Table 38. Surface runoff and sediment yield in various land use**

Sl. No.	Land use	Subarea (%)	Average surface runoff (mm/ year)	Average Soil Loss (ton ha <sup>-1</sup> yr <sup>-1</sup> )
1	Dense Forest	49.05	443.56	15.68
2	Open Forest	29.65	429.66	22.22
3	Agriculture (Maize)	6.82	486.61	27.50

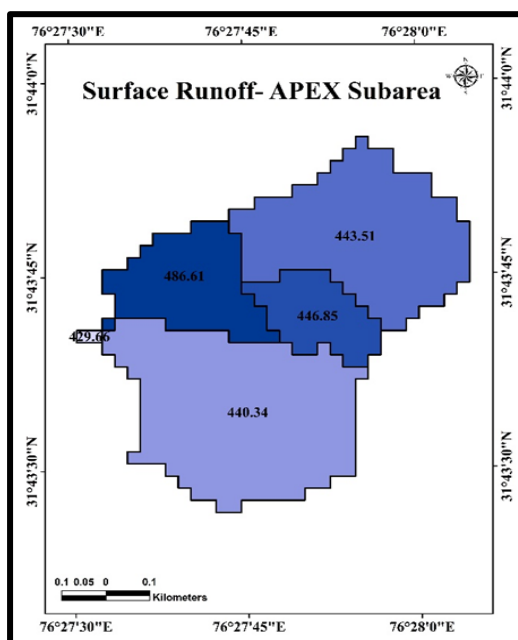


**Figure 105. Surface runoff from various subareas of Nano watershed**

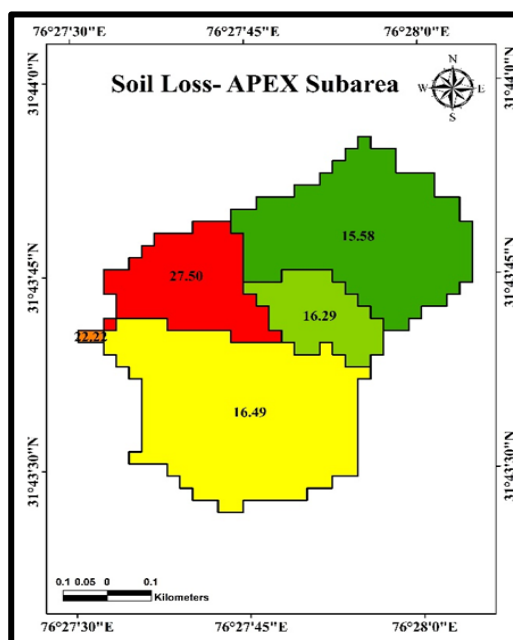


**Figure 106. Sediment yield from various subareas of Nano watershed**



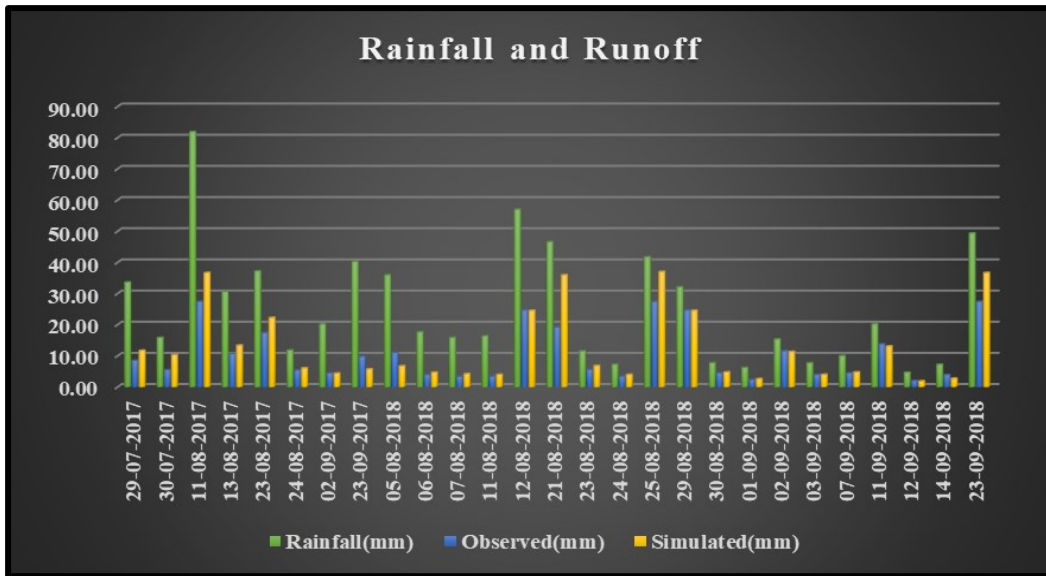


Figure 107. Rainfall and simulated surface runoff from calibrated APEX model

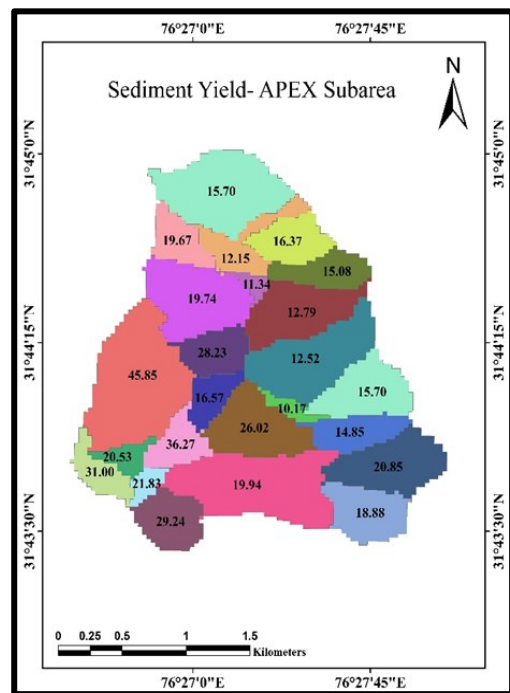
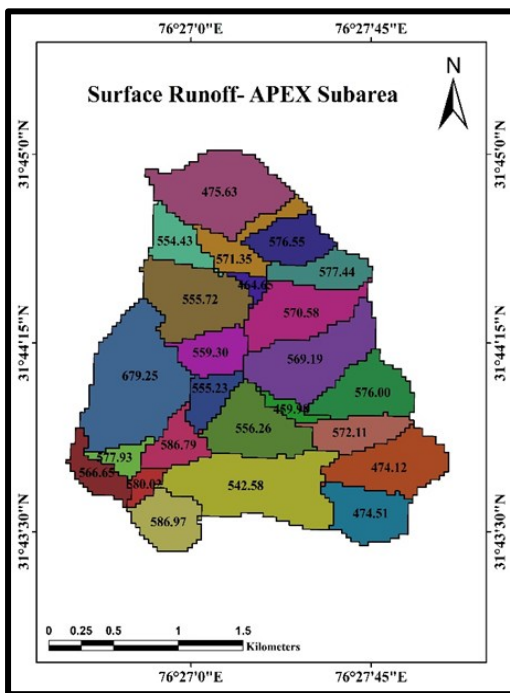


Figure 108. Surface runoff from various subareas of Micro-watershed      Figure 109. Sediment yield from various subareas of Micro-watershed

After calibration and validation, the APEX model was also run on a yearly scale to identify sediment yield from the whole micro watershed (Table 39). APEX divided the micro-watershed into 24 subareas based on dominant land use, slope



and soil properties. Very less surface runoff of 459.98 mm was observed in the subarea-12 with a slope of 20-35 and land use of the dense forest. Scrubland subarea-16 with a slope of 10 -20 per cent gives more surface runoff of 679.25 mm. Similarly, the forest subarea gives low soil loss of 10.17 ton ha<sup>-1</sup> yr<sup>-1</sup> and high loss of 45.85 ton ha<sup>-1</sup> yr<sup>-1</sup> is seen for scrub land.

The APEX model computes average soil loss for each subarea (Table 39). Highest average annual soil loss in the subarea is the area most critical for soil loss. Subarea describing land use of scrub land was showed highest soil loss of 45.85 tons/ha annually followed by subarea composed of maize cropped areas. Subarea covered by middle hill slope having dense forest simulated least soil loss of 10.17 tons/ha annually.

According to land use (Table 41), dense forest observed very less average surface runoff and soil loss of 530.17 mm and 14.70 ton ha<sup>-1</sup> yr<sup>-1</sup>. Runoff contributes 40.93% of total rainfall. It is because of cover factor, and dense forest has a good land cover. It reduces the direct contact of rainfall with the soil surface. Thus slope factor is diminished by the cover factor, then followed by less runoff (553.92 mm) and soil loss (21.69 ton ha<sup>-1</sup> yr<sup>-1</sup>) were observed in the open forest followed by surface runoff (582.92 mm) and soil loss (26.97 ton ha<sup>-1</sup> yr<sup>-1</sup>) were observed in the maize field (Agriculture). Higher surface runoff (622.95 mm) and soil loss (38.42 ton ha<sup>-1</sup> yr<sup>-1</sup>) were observed in the scrubland.

Runoff from scrubland is about 48.10 per cent of total rainfall. Very less land cover and absence of conservation practices contribute to higher surface runoff and soil loss from the scrubland. Fig. 108 and 109 represents the spatial extent of runoff and soil loss from different subareas.

The average annual soil degradation rate in India is 16 t/ha/yr (Babu and Narayan, 1983). In the current examination, it is 25.45 t/ha/yr, which is far above the average annual soil degradation rate. Gardey and Kothiyari, 1987 has likewise evaluated the normal soil erosion from the northern Himalayan area as 20-25 t/ha/yr.

**Table 39. Average soil loss in various sub-areas of micro watershed**

<b>Subarea No.</b>	<b>Land use</b>	<b>Slope (%)</b>	<b>Area (%)</b>	<b>Surface runoff (mm/ year)</b>	<b>Soil Loss (ton ha<sup>-1</sup> yr<sup>-1</sup>)</b>
1	Dense Forest	>35	8.31	475.63	15.70
2	Dense Forest	>35	3.21	576.55	16.37
3	Open Forest	20-35	2.53	554.43	19.67
4	Dense Forest	>35	3.04	571.35	12.15
5	Dense Forest	20-35	0.61	464.65	11.34
6	Dense Forest	>35	2.90	577.44	15.08
7	Dense Forest	20-35	5.57	570.58	12.79
8	Open Forest	20-35	6.66	555.72	19.74
9	Open Forest	>35	2.90	559.30	28.23
10	Dense Forest	20-35	7.32	569.19	12.52
11	Dense Forest	>35	4.64	576.00	15.70
12	Dense Forest	20-35	0.82	459.98	10.17
13	Dense Forest	>35	3.01	572.11	14.85
14	Open Forest	20-35	2.04	555.23	16.57
15	Open Forest	20-35	5.44	556.26	26.02
16	Scrub Land	10-20	11.23	679.25	45.85
17	Scrub Land	10-20	2.15	566.65	31.00
18	Agriculture(Maize)	10-20	2.47	586.79	36.27
19	Agriculture(Maize)	5-10	1.27	577.93	20.53
20	Agriculture(Maize)	5-10	0.91	580.02	21.83
21	Dense Forest	>35	5.57	474.12	20.85
22	Open Forest	10-20	9.92	542.58	19.94
23	Agriculture(Maize)	5-10	3.44	586.97	29.24
24	Dense Forest	>35	4.03	474.51	18.88

**Table 40. Average soil loss in various slopes of micro watershed**

Sl. No.	Land use	Slope (%)	Area (%)	Average Soil Loss (ton ha <sup>-1</sup> yr <sup>-1</sup> )
1	Dense Forest	>35	34.71	16.20
		20-35	14.32	11.71
2	Open Forest	>35	2.9	28.23
		20-35	16.67	20.50
		10-20	9.92	19.94
3	Agriculture(Maize)	10-20	2.47	36.27
		5-10	5.62	23.87
4	Scrub Land	10-20	13.38	38.43

**Table 41. Average soil loss in various land uses of micro watershed**

Sl. No.	Land use	Subarea (%)	Average surface runoff (mm/year)	Average Soil Loss (ton ha <sup>-1</sup> yr <sup>-1</sup> )
1	Dense Forest	49.05	530.17	14.70
2	Open Forest	29.65	553.92	21.69
3	Agriculture (Maize)	6.82	582.92	26.97
4	Scrub Land	14.55	622.95	38.42
5	Average	100	572.49	25.45

Singh *et al.* (1992) additionally express that the north-western hills of Himachal Pradesh contribute 20Mg/ha/yr. A significant examination conducted at Pathri Rao sub-watershed in the Himalayan Shivalik region, Kumar and Kushwaha (2013) anticipated an average yearly soil erosion rate of 35.47 t/ha/yr utilizing RUSLE 3D and GIS methods. In the current investigation, it is 25.45 t/ha/yr, which is over the normal yearly soil disintegration rate. Also, India's normal soil disintegration rates were assessed to be 0.5-5 t/ha/yr for zones under natural vegetation, 0.3-40 t/ha/yr for cropland, and 10-185 t/ha/yr for exposed soil locales (Singh *et al.*, 1981; Morgan, 2005). As indicated by Mandal *et al.* (2010) in the

north-western Himalayas the default soil loss tolerance limit (SLTL) is running from 2.5 - 12.5 t/ha/yr is followed for placing soil preservation activities.

#### 4.14 SOIL LOSS RISK ASSESSMENT

The potential annual soil loss was simulated using Onstad- Foster modification of the USLE equation in the APEX model. It was found that the majority of the study area is under severe soil loss due to water. There is no area with (Table 42) very low soil loss <10 ton ha<sup>-1</sup> yr<sup>-1</sup> class. The almost whole area was affected by soil loss. 64.61 per cent of the area has moderate (10-20 ton ha<sup>-1</sup> yr<sup>-1</sup>) loss. 24.15 per cent of the total area comes under severe loss risk class. A total of 11.23 per cent area is in the very severe loss class of >40 ton ha<sup>-1</sup> yr<sup>-1</sup>. Analysing the soil loss risk classes, it is seen that the majority of the watershed is facing moderate to very severe soil loss risk.

**Table 42. Soil loss risk classes in the micro watershed**

Soil Loss Risk Classes	Rate of Soil Loss (ton ha <sup>-1</sup> yr <sup>-1</sup> )	Area (%)
Very Low	<5	0
Low	5-10	0
Moderate	10-20	64.61
Severe	20-40	24.15
Very Severe	>40	11.23

The APEX model has successfully assessed the attainable degree of soil loss risk over the area. It was identified from the study that moderate to very low risk of soil loss is in most cases related to dense forest land followed by open forest which is located basically on steep and undulating slopes. About 65 per cent of the region comes under dense forest and open forest cover located in hilly terrain is anticipated to be under a moderate risk of soil loss. It was recognized that severe to very severe risk of soil loss is linked with scrub land and followed by agricultural land which is located in most cases on gentle to moderately steep and undulating slopes.



(a)



(b)



(c)



(d)

**Plate 9. (a, b, c) exposed rocks visible in the study area (d) Coarse fragment percentage.**

There is a close agreement between the degree of soil loss risk and slope of the area; greater slopes are more prone to soil loss, also there is a close relationship between soil loss risk and cover factor; good canopy areas (dense forest) are more resistance to soil loss. The attainable high and very excessive hazard of soil loss area of the watershed needs appropriate land management practices for a sustainable degree of existing.

#### 4.15 FUTURE SOIL LOSS SCENARIO

Analysis reveals that future soil loss rates are increasing due to the increase in rainfall amount and intensity, also increase in temperature decreases the growing degree days and results in early maturity. It may cause a decrease in cover during late monsoon periods which will lead to an increase in soil loss. The different possible soil loss scenarios are classified according to each consecutive 30 year period till 2100.

##### 4.15.1 Soil loss under A2 scenario

**Table 43. Soil loss ( $t\ ha^{-1}\ yr^{-1}$ ) under A2 scenario**

Land Use	Current Period	2020	2050	2080	Base to Year(2020)	Base to Year(2050)	Base to Year(2080)
Dense Forest	14.70	17.81	17.01	19.91	21.16%	15.71%	35.46%
Open Forest	21.69	26.98	26.03	30.18	24.39%	20.01%	39.16%
Maize	26.97	35.26	33.35	39.91	30.74%	23.36%	47.97%
Scrub Land	38.42	51.69	49.29	63.46	34.54%	28.29%	65.17%
Average	25.45	32.94	31.42	38.37	27.71%	21.84%	46.94%

The model was run for future climate scenarios after the calibration and validation of the APEX model. The results (Table 43) exposed that the average annual soil loss may increase by 27.21 per cent, 21.84 per cent and 46.94 per cent in year 2020s, 2050s and 2080s, respectively from the baseline period of 1985-2014. H3A2 scenario predicts more amount of rainfall so that soil loss will be more in this scenario. Soil loss was analysed in various land use/land cover and the highest soil loss rate was identified in scrublands ( $38.42$  to  $63.46\ t\ ha^{-1}\ yr^{-1}$ ) because of less land cover and higher erodibility of soil. In many of the scrublands exposed

rocks are visible (Plate 9) which indicates the severity of erosion, and is followed by agricultural fields (Maize) (26.97 to 39.91 t ha<sup>-1</sup> yr<sup>-1</sup>), and open forest (21.69 to 30.18 t ha<sup>-1</sup> yr<sup>-1</sup>). However, dense forest (*Senegalia catechu*, *Pinus roxburghii*, and *Dalbergia sissoo*) was found to have less soil loss risk (14.70 to 19.91 t ha<sup>-1</sup> yr<sup>-1</sup>). Dense forest areas have a good canopy and the thick layer of leaf litter helps to reduce soil loss.

Various types of land use often play a major role in deciding the soil loss rate. Changes in the land use can lead to a decrease or higher soil loss levels. The forest areas have minimal rate of soil loss, which in terms of adaptation measure is very important (3.11 to 5.21 t / ha/year). The soil surface is held by the plants and trees which reduces the rate of soil loss in this region. The erosion rate, though steadily rising, is relatively low compared to other forms of land use (increase by 3.11 tonnes/ha/year in 2020, 2.31 tonnes/ha/year in 2050s and 5.21 tonnes/ha/year in 2080s). Apart from the dense forest, open forest has a soil loss rate of 5.29 t ha<sup>-1</sup> year<sup>-1</sup> to 8.49 t ha<sup>-1</sup> year<sup>-1</sup>. In agricultural land a low level of soil loss rate next to the open forests. Present soil loss of agricultural land is 26.97 t/ha/yr, it will rise in the years 2020 by 35.26 t/ha/yr, in 2050 and 2080 it will increase from 33.35 t/ ha/yr to 39.91 t/ha/yr. Over the years farming increase soil exposure, increases the rate of soil loss. The highest soil loss rate on scrub lands, however, it is very common, because grass, vegetation or plantations are not present here (currently 38.42 t/ha/year). Consequently, high-intensity rainfall on the exposed soil surface contributes to higher soil loss rates, causing potential soil loss of approximately 63.46 tons/ha/yr by 2080s. Akarsh (2013) conducted a study that shows the soil erosion increases 37.97 per cent to 221.99 per cent under A2a scenario from 2020 to 2080 period from the base period over the Doon valley. Gupta and Kumar (2017) performed a study at the mid-Himalayan landscape that showed that, during the 2020s, 2050s and 2080s, the average annual soil erosion rate will rise at 28.38 per cent, 25.64 per cent and 20.33 per cent in line with the H3A2 emissions scenario.

#### 4.15.2 Soil loss under B2 scenario

**Table 44. Soil loss (t ha<sup>-1</sup> yr<sup>-1</sup>) under B2 scenario**

Land Use	Current Period	2020	2050	2080	Base to Year (2020)	Base to Year (2050)	Base to Year (2080)
Dense Forest	14.70	16.92	18.07	19.31	15.10%	22.93%	31.36%
Open Forest	21.69	26.05	27.67	29.21	20.12%	27.59%	34.67%
Maize	26.97	34.23	36.15	38.36	26.92%	34.04%	42.23%
Scrub Land	38.42	50.25	53.12	56.46	30.80%	38.26%	46.95%
Average	25.45	31.86	33.75	35.84	23.24%	30.71%	38.80%

The results ( Table 44) showed that the average annual soil loss under the B2 scenario will increase by 23.24 per cent, 30.71 per cent and 38.80 per cent in the 2020, 2050 and 2080 years from the 1985-2014 baseline period. H3B2 scenario estimates a comparatively lower rainfall level compared to H3B2 so that in this case soil loss, it is lower than H3A2. Soil loss was assessed in various areas shows that agricultural fields (maize) have (26.97 to 38.36 t/ha/yr), and open forest (21.69 to 29.21 t/ha/yr). The highest soil loss rates were observed on scrublands (38.42 to 56.46 t/ha/yr). Lower soil loss risk (14.70 to 19.31 t/ha/yr) has also been identified for the dense forest.

Similarly in the scenario of H3B2, forest areas have a low rate of soil loss that is 2.22 to 4.61 t /ha/year, a very important indicator for adaptation measure. Though the soil loss rate in dense forest is gradually rising, it is relatively small compared with other land-use types. In comparison to dense forests, open forest land has higher soil loss rate that ranges from 4.36 t ha/yr to 7.52 t/ha/yr. Agricultural land is next to that with a higher level of soil loss compared to the open forests. Highest soil loss rate in scrub land (currently 38.42 tonnes/ha/year).



Consequently, high intensity rainfall on the exposed soil surface subsequently led to increased soil loss, it is an indicator that possible soil loss in the 2080s will approximately 56.46 t/ha/year.

The estimated annual soil loss could be 27.06 per cent, 25.31 per cent and 23.38 per cent, in the H3B2 emission scenario in the 2020s, 2050s and 2080s at Mid- Himalayan landscape similar to H3A2 scenario (Gupta and Kumar, 2017). Mondal *et al.* (2014), examined the sediment yield in the Narmada river basin in the 2020s, showing negative trend (−5.5 to −8.5 %). Following this prolonged degradation in the 2050s, higher sediment load is observed with the shift from the current period, under SDSM and SVM prediction, ranging between 15.5 per cent and 18 per cent. In 2080, increased rainfall contributes to prolonged erosion, with the rising change ranging from 59 to 106 per cent above the present rate of soil degradation.

Climate change is activating factor in precipitation pattern, Which additionally influences the diminution of soil. Numerous researchers anticipate more notable change in future precipitation over different parts of India. Prolonged precipitation is seen in the studies (Rupakumar *et al.*, 2006; Kannan and Ghosh, 2011; Meenu *et al.*, 2013; Mondal *et al.*, 2014) in different areas of India are similarly sighted increased precipitation. The research of Mondal *et al.* (2015; 2016), soil degradation in Central India is due to variability of slope, showed later an increase in soil degradation due to variations in precipitation. However, in the work of Simonneaux *et al.* (2015) in Morocco and Maeda *et al.* (2010), Kenya, an increased soil degradation and precipitation erosivity due to climate change is also observed in various parts of the world. Using future climatic data of precipitation, potential soil loss was estimated and can be used for adaptation and mitigation strategies.

## 5. SUMMARY AND CONCLUSION

The study was conducted in the outer Himalayan landscape named as Shivalik region for modelling climate change impact on surface runoff and soil loss for H3A2 and H3B2 scenarios. The study results are abridged as:

- ✍ The study area located in the Hamirpur district of Himachal Pradesh. It was characterised as moderately steep to very steep sloping (47.66%) and covered with mainly dense forest (45.24%), open forest (26.75%), agriculture (Maize and Paddy) (18.90%), scrub/barren land (5.87%), settlements (3.10%), and water bodies (0.14%).
- ✍ The Cartosat DEM analysis reveals that the study area has a minimum elevation of 475m and a maximum elevation of 821m.
- ✍ The study area is divided into four significant landforms named as upper hillslope, middle hillslope, upper piedmont and middle piedmont and area covered by each landform is 26.02 per cent, 27.95 per cent, 27.90 per cent and 18.13 per cent respectively.
- ✍ The majority of area based on aspect is west and south-west (36.96%) facing. 15.79 per cent, 14.30 per cent, 13.27 per cent, 7.60 per cent and 7.03 per cent facing north-west, south-east, south, north, and east respectively with 0.03 per cent flat area.
- ✍ The dominant textural class is identified as sandy loam. Soil colour varies from light yellowish brown (10 YR 6/4) to brown (10 YR 5/3). The bulk density of soils ranges from 1.10 g/cm<sup>3</sup> to 1.65 g/cm<sup>3</sup>.
- ✍ Aggregate stability of soils varies from 0.54- 0.78 for <0.25 mm soil particles and for <50 mm soil particles, it is from 0.54-0.74. It was observed that smaller soil particles are more stable than higher particles.

- ✍ The soils in the study area mainly acidic in nature range from pH 5.2 to 6.7, also identified that the soils are non-saline.
- ✍ More organic matter was found in agriculture and forest soil. It was estimated that, forest soil contain average of 1.67 per cent of organic matter in surface soil and 1.23 per cent in subsurface soil. In the Agriculture field, organic matter in surface soil contains 2.33 per cent and 1.86 per cent in subsurface soil. Scrubland contains a very less organic matter of 0.52 per cent in the surface layer, and the sub-surface layer has 0.39 per cent.
- ✍ High soil nutrients were observed in the agricultural field, due to the application of farmyard manure and followed by forest. Very low amount of nutrients were observed in scrubland soils.
- ✍ A higher infiltration rate of 7.8 cm/hr was observed in the agricultural field, and a lower infiltration rate of 3 cm/hr was observed in scrubland. Similarly, a higher unsaturated hydraulic conductivity of 1.9 cm/hr was observed in the agricultural field, and a lower of 0.6 cm/hr was observed in scrubland. Although a higher saturated hydraulic conductivity of 8.1 cm/hr was observed in the agricultural field and lower of 2.3 cm/hr in scrubland. The agricultural land has ploughed loose soil, which helps water to enter soil quickly, but the unploughed compact soil in scrub land restricts the movement of water.
- ✍ The major hydrologic soil groups of the watershed were identified as B, C, and D. Scrubland has D hydrologic group, forest and agriculture has both B and C. The permeability of soil ranges from moderate to moderately slow. Although drainage class from well to excessive.
- ✍ The forest soils have a lower erodibility (USLE K) of 0.08 and a higher erodibility of 0.11 for scrubland. The higher carbon content in forest soil is the primary reason for lower erodibility.

- ✍ During the year 2017 and 2018, the maximum temperature was observed in May month and the minimum average temperature in January. The majority of the rainfall occurred in July, August and September. During the year 2017 and 2018 maximum half-hour rainfall observed was 67.06 mm/hr and 73.66 mm/hr, respectively.
- ✍ The statistical downscaling model (SDSM) was adopted for downscaling the climate parameters such as maximum and minimum temperature, and rainfall from coarse resolution GCM data to high-resolution local scale. The most appropriate predictor variable for maximum temperature is near-surface temperature (ncep\_temp), geopotential height at 500hPa (ncep\_p500), relative humidity at 850hPa (ncep\_r850), and near-surface specific humidity (ncep\_shum).
- ✍ The most appropriate predictor variable identified for explaining the variation of minimum temperature is near surface temperature (ncep\_temp), geopotential height at 500hPa (ncep\_p500), and near surface specific humidity (ncep\_shum).
- ✍ For rainfall predictor variable selected is near surface specific humidity (ncep\_shum), relative humidity at 500hPa (ncep\_r500), divergence at 500hPa (ncep\_p5zh), wind direction near the surface (ncep\_pth) and divergence near surface (ncep\_pzh).
- ✍ During the calibration of SDSM, the explained variance and standard error of maximum and minimum temperature and rainfall are 68.1 per cent, 2.64 °C, 83.8 per cent, 2.01 °C and 23.9 per cent, 35.00 mm/month.
- ✍ During the validation of the model coefficient of determination ( $r^2$ ) and root mean square error (RMSE) for maximum and minimum temperature and rainfall is 0.86, 2.51 °C, 0.72, 2.48 °C and 0.94, 32.02 mm/month. The overall calibration and validation performance shows that model downscaled temperature better than rainfall.

- ✍ The study reveals that for both scenarios, the temperature may increase. It has been found that for the H3A2 emission scenarios in the 2020s, 2050s and the 2080s the average annual maximum temperature is likely to rise by 1.6 °C, 2.5 °C and 3.7 °C. The annual minimum temperature in the H3A2 scenario may arise, in the 2020s, 2050s and 2080s, increase by 1.2 °C, 2.3 °C, and 3.6 °C, respectively.
- ✍ It has been found that for the H3B2 emission scenarios in the 2020s, 2050s and the 2080s the average annual maximum temperature is likely to rise by 1.9 °C, 2.2 °C and 2.6 °C. The annual minimum temperature in the H3B2 scenario may arise, in the 2020s, 2050s and 2080s, increase by 1.3 °C, 2.0 °C, and 2.7 °C, respectively.
- ✍ The rainfall under the H3A2 scenario from the base period increases by 27.27 per cent, 20.14 per cent, and 41.35 per cent in the years the 2020s, 2050s and 2080s, respectively. Also under the H3B2 scenario from the base period, rainfall increases by 24.71 per cent, 29.13 per cent and 35.16 per cent in the years the 2020s, 2050s and 2080s, respectively.
- ✍ In monsoon months (June to September), the rainfall amount received contributed to 77.25 per cent of the total rainfall in the base period. In the 2020s, 2050s and 2080s however, it could be increased by 94.18 per cent, 92.56 per cent and 96.85 per cent under H3A2 scenario, 94.46 per cent, 95.40 per cent and 95.83 per cent under the H3B2 emission scenarios.
- ✍ In the study area, the watershed runoff is generated mostly by saturation excess due to rainfall. The dominant soil observed in the study area is sandy loam, which contains 60 per cent of sand and only 10.58 per cent of clay. This type of soils is permeable. In addition to this, the infiltration rate of the study area is higher at a range of 33- 78 mm/hr, which is higher than the average rainfall intensity of 18 mm/hr in most regions of the study area.

- ✍ The sensitivity analysis of surface runoff showed that curve number (CN) is the most sensitive parameter, followed by curve number retention parameter (CNRN), average upland slope (S), available water content (AWC), and curve number index coefficient (CNIC).
- ✍ The evaluation of sediment yield sensitivity showed that the erosion control factor (P), the cover factor (C), the average upland slip (S) and the erodibility factor (K), are most sensitive.
- ✍ APEX, a process-based model, was used for estimating surface runoff and sediment yield at the watershed scale. APEX model calibrated for the Nano watershed, and it predicts quite well for the surface runoff ( $r^2=0.928$ ), sediment yield ( $r^2=0.881$ ), and root mean square error (RMSE) of surface runoff and sediment yield is 4.982 mm/ day and 0.201 t/ha/day.
- ✍ APEX model validated for the Nano watershed, and it predicts quite well for the surface runoff ( $r^2=0.809$ ), sediment yield ( $r^2=0.809$ ), and root mean square error (RMSE) of surface runoff and sediment yield is 2.616 mm/day and 0.11 t/ha/day.
- ✍ Runoff was projected very well for low and medium precipitation, but over predicted for heavy rainfall. Over prediction may be attributed to the unaccountable conservation measures and practices which were not accounted by the model that may have resulted higher prediction.
- ✍ Similarly, sediment yield was estimated daily at the watershed scale and was well predicted for low and medium rainfalls but under-estimated for high rainfall events. The area is prone to landslips at high rainfalls, which was not accounted by the model.
- ✍ Model performance for surface runoff and sediment yield was evaluated by Nash Sutcliffe model Efficiency, which gives a satisfactory NSE value of

0.71 and 0.70 respectively. Runoff was quite well predicted than sediment yield.

- ✍ In this study, the average annual soil loss is 25.45 t/ha/yr, which is above the average annual soil loss rate in India (16 t/ha/yr).
- ✍ APEX model helped determine the critical source area of soil loss. Average annual soil loss was estimated by the model for each subarea for identifying critical source area. Average annual soil loss was predicted highest in subarea consisting of scrub land with a soil loss of 45.85 tons/ha/yr.
- ✍ The erosion was also estimated regarding various land use/land cover which revealed that the dense forest has very little surface runoff and soil loss of 530.17 mm and 14.70 ton ha<sup>-1</sup> yr<sup>-1</sup>. Then followed by in open forest of 553.92 mm and 21.69 ton ha<sup>-1</sup> yr<sup>-1</sup>, Then more surface runoff and soil loss were observed in the maize field (Agriculture) of 582.92 mm and 26.97 ton ha<sup>-1</sup> yr<sup>-1</sup>. The more surface runoff and soil loss were observed in the scrubland of 622.95 mm and 38.42 ton ha<sup>-1</sup> yr<sup>-1</sup>.
- ✍ The model predicted that 64.61 per cent of total land area under moderate (10-20 ton ha<sup>-1</sup> yr<sup>-1</sup>) soil loss, 24.15 per cent area with severe (20-40 ton ha<sup>-1</sup> yr<sup>-1</sup>) soil loss and 11.23 per cent area contribute very severe (>40 ton ha<sup>-1</sup> yr<sup>-1</sup>) soil loss. Almost all region of the watershed is affected by soil loss.
- ✍ Further soil loss was predicted for future periods, and the results showed that for dense forest soil loss increases up to 35.46 per cent under H3A2 scenario while 31.36 per cent for H3B2 scenario.
- ✍ The open forest has soil erosion increases up to 39.16 per cent and 34.67 per cent for H3A2 and H3B2 scenarios respectively, also for agricultural land, soil erosion increases up to 47.97 per cent and 42.23 per cent for H3A2 and H3B2 respectively.

- ✍ The average soil loss during the 2020s, 2050s, and 2080s increases 27.71 per cent, 21.84 per cent and 46.94 per cent for H3A2 scenario respectively. Similarly, 23.24 per cent, 30.71 per cent and 38.80 per cent under H3B2 during 2020s, 2050s, and 2080s.

Consideration of other adjustable components affecting soil loss is equally important as precipitation is the key variable taken for future investigation. Although all land use type, slope and soil type are alterable, the development rate is too slow to even consider. Nevertheless, the future rate of soil loss can decline or incline according to various components, given the possibility that increasing precipitation is exclusively considered to increase at this stage. Different land-use approaches to management can alter the rate of soil loss by either rising it or decreasing it. This study provides more flexibility to understand the prediction of soil loss alongside the increase in precipitation with the potential change in temperature. This analysis provided a few results which will help to understand the effect on soil loss and thereby soil productivity.

The current study quantifies the present state of soil loss in the watershed and also states the future climate of the study area, which will be helpful for the government and other bodies to make different policies according to climate change. The study also represents future possible soil loss scenarios for the watershed, representing Shivalik Himalayas, which also will be helpful for government bodies to take preventive conservation measures to avoid massive soil erosion.



## **Suggestions**

The following soil and water conservation measures need to be scientifically planned and adopted to reduce soil erosion, which will be hazardous in the predicted scenario of high rainfall, temperature, runoff and sediment yield.

- ✍ In agricultural land –agronomic measures- growing maize with an intercrop of legumes, mulching, practising minimum tillage, contour farming, agroforestry, agro- horticulture, etc.
- ✍ Mechanical measures- improving bunds, the embankment of channels, providing safe disposal of runoff water (grassed waterways- Vetiveria, Saccharum) etc.
- ✍ In scrub land and forest- trenching.
- ✍ Gully control structures- drop spillways, chute spillways and drop inlet spillways.
- ✍ Watershed based land-use system- Agri- Horticulture, Agri-Horti-Silvi-pastoral and Multi-tier horticultural system etc.
- ✍ Reforestation of the degraded lands.
- ✍ Using the geotextiles to prevent river bank erosion.

## **Future line of work**

- ✍ Future climate change scenario using RCP.
- ✍ Comparison of both SRES scenario with RCP scenario.
- ✍ Consideration of certain changeable factors that cause soil erosion.
- ✍ Studying the effect of soil loss with the potential change in land-use along with the increase in precipitation.

- ✍ Identify the most reliable scenario concerning present-day greenhouse gas emission.
- ✍ Validation of projected weather parameters.
- ✍ To find out best management practise for the area using the APEX calibrated model.
- ✍ Comparison of different management practices.

## REFERENCES

- Abbott, M.B., Bathurst, J.C., Cunge, J.A., O'Connell, P.E., and Rasmussen, J. 1986. An introduction to the European Hydrological System- Systeme Hydrologique European, "SHE," 1: History and philosophy of a physically-based, distributed modelling system. *Journal. of Hydrology*, 87 (1-2): 45-59.
- Ahmed, S.A., Chandrashekarappa, K.N., Raj, S.K., Nischitha, V., and Kavitha, G. 2010. Evaluation of morphometric parameters derived from ASTER and SRTM DEM-a study on Bandihole sub-watershed basin in Karnataka. *Journal of the Indian society of remote sensing*, 38 (2): 227-238.
- Akarsh, A., 2013. Surface runoff, Soil erosion and Water Quality estimation using APEX model integrated with GIS -A case study in Himalayan Watershed, M.Tech (RS& GIS) thesis, Andra University, Andra Pradesh, 80p.
- Angima, S.D., Stott, D.E., O'neill, M.K., Ong, C.K., and Weesies, G.A. 2003. Soil erosion prediction using RUSLE for central Kenyan highland conditions. *Agriculture, ecosystems & environment* 97 (1-3): 295-308.
- Bakker, M.M., Govers, G., Jones, R.A., and Rounsevell, M.D. 2007. The effect of soil erosion on Europe's crop yields. *Ecosystems* 10 (7): 1209-1219.
- Barnett, T.P., Adam, J.C., and Lettenmaier, D.P. 2005. Potential impacts of a warming climate on water availability in snow-dominated regions. *Nature* 438 (7066): 303.
- Beck, M.B. 1987. Water quality modelling: a review of the analysis of uncertainty. *Water Resources Research* 23 (8): 1393-1442.
- Becker, A., and Bugmann, H. (eds.), 1997. *Predicting Global Change Impacts on Mountain Hydrology and Ecology: Integrated Catchment Hydrology/Altitudinal Gradient Studies*. IGBP Report 43, Stockholm.

- Beniston, M. 2003. Climatic change in mountain regions: a review of possible impacts. *Climatic Change* 59: 5–31.
- Bennett, J.P. 1974. Concepts of mathematical modelling of sediment yield. *Water Resources Research* 10 (3): 485-492.
- Besler, H. 1987. Slope properties, slope processes, and soil erosion risk in the tropical rain forest of Kalimantan Timur (Indonesian Borneo). *Earth Surface Processes and Landforms* 12: 195-204.
- Beven, K. 1989. Changing ideas in hydrology- the case of physically-based models. *Journal of hydrology* 105 (1-2): 157-172.
- Beven, K. 1991. Spatially distributed modelling: conceptual approach to runoff prediction. *Recent Advances in the Modeling of Hydrologic Systems*. 373-387.
- Bharti, V.I.D.H.I., 2015. *Investigation of extreme rainfall events over the northwest Himalaya Region using satellite data*. University of Twente Faculty of Geo-Information and Earth Observation (ITC).
- Bhutiyani, M.R., Kale, V.S. and Pawar, N.J., 2009. Climate change and the precipitation variations in the northwestern Himalaya: 1866–2006. *International Journal of Climatology: A Journal of the Royal Meteorological Society* 30 (4): 535-548.
- Blake, G.R., and Hartge, K.H. 1986. Bulk density. In: Klute, A. (ed.), *Methods of Soil Analysis. Part 1, Physical and Mineralogical Methods*, (2<sup>nd</sup> ed.), *Agronomy* 9: 363–382.
- Blodget, H., Taylor, P., and Roark, J. 1991. Shoreline changes along the Rosetta-Nile Promontory: monitoring with satellite observations. *Marine Geology* 99: 67–77.
- Bouyoucos, G.J. 1962. Hydrometer method improved for making particle size analyses of soils. *Agronomy journal* 54 (5): 464-465.

Bray, R.H., and Kurtz, L.T. 1945. Determination of total, organic, and available forms of phosphorus in soils. *Soil science* 59 (1): 39-46.

Brown, C., Greene, A. M., Block, P., and Giannini, A. 2008. *Review of downscaling methodologies for Africa climate applications*. IRI Technical Report 08-05: IRI Downscaling Report, International Research Institute for Climate and Society, Columbia University.

Budyko, M.I. 1969. The effect of solar radiation variations on the climate of the Earth. *tellus* 21 (5): 611-619.

Burrough, P.A. 1987. Mapping and map analysis: new tools for land evaluation. *Soil use and Management* 3 (1): 20-25.

Buytaert, W., Vuille, M., Dewulf, A., Urrutia, R., Karmalkar, A., and Celleri, R. 2010. Uncertainties in climate change projections and regional downscaling in the tropical Andes: implications for water resources management. *Hydrology and Earth System Sciences* 14 (7): 1247-1258.

Byg, A., and Salick, J. 2009. Local perspectives on a global phenomenon - climate change in Eastern Tibetan villages. *Global Environmental Change* 19 (2): 156-166.

Carter, T.R., Parry, M.L., Harasawa, H., and Nishioka, S. 1994. IPCC technical guidelines for assessing climate change impacts and adaptations. Department of Geography, University College London and Center for Global Environmental Research. *National Institute for Environmental Studies, Japan*, 59p.

Cayan, D.R., and Riddle, L.G. 1993. The influence of temperature and precipitation on seasonal stream flow in California. *Water Resources Research* 29: 1127–1140.

Chang, K.T. 2006. Introduction to geographic information systems. Boston: McGraw-Hill Higher Education. 117-122.

Chiew, F.H.S., Whetton, P.H., McMahon, T.A., and Pittock, A.B. 1995. Simulation of the impacts of climate change on runoff and soil moisture in Australian catchments. *Journal of Hydrology* 167: 121–147.

Chu, J.T., Xia, J., Xu, C.Y., and Singh, V.P. 2010. Statistical downscaling of daily mean temperature, pan evaporation, and precipitation for climate change scenarios in Haihe River, China. *Theor. Appl. Climatol.* 99 (1–2): 149–161.

Chuvieco, E., and Congalton, R.G. 1989. Application of remote sensing and geographic information systems to forest fire hazard mapping. *Remote sensing of Environment* 29 (2): 147-159.

Cochrane, T.A., and Flanagan, D.C. 1999. Assessing water erosion in small watersheds using WEPP with GIS and digital elevation models. *Journal of soil and water conservation* 54 (4): 678-685.

Colwell, R. N. (ed.), 1983. *Manual of Remote Sensing*, (2<sup>nd</sup> Ed.) Falls Church, Virginia American Society of Photogrammetry.

Coppin, P., Jonckheere, I., Nackaerts, K., Muys, B., and Lambin, E. 2004. Digital change detection methods in ecosystem monitoring: a review. *International Journal of Remote Sensing* 25 (9): 1565–1596.

Cruz, R.V., Harasawa, H., Lal, M., Wu, S., Anokhin, Y., Punsalmaa, B., Honda, Y., Jafari, M., Li, C. and Huu Ninh, N. 2007. Asia. In: Parry, M. L., Canziani, O. F., Palutikof, J.P., van der Linden, P.J. and Hanson, C. E. (eds) *Climate Change 2007: Impacts, Adaptation, and Vulnerability*. Cambridge University Press, Cambridge: 469–506.

Dabral, P.P., Baithuri, N., and Pandey, A. 2008. Soil erosion assessment in a hilly catchment of North Eastern India using USLE, GIS, and remote sensing. *Water Resour Manag.* 22:1783–1798.

Dairaku, K., and Emori, S., 2006. Dynamic and thermodynamic influences on intensified daily rainfall during the Asian summer monsoon under doubled atmospheric CO<sub>2</sub> conditions. *Geophysical Research Letters*, 33 (1).

Das, D.C. 1985. Problem of soil erosion and land degradation in India. In: *Abstracts, National Seminar on Soil Conservation and Watershed Management*, 17-18 September 1985, New Delhi.

De Roo, A.P.J., Wesseling C.G., and Ritsema, C.J. 1996. LISEM: a single event physically-based hydrologic and soil erosion model for drainage basins. I: theory, input, and output. *Hydrological Processes* 15: 1107–1117.

Diaz, H.F., and Markgraf, V. (eds.), 2000. *El Niño and the southern oscillation, multiscale variability, and global and regional impacts*. Cambridge University Press, Cambridge, 497p.

Doran, J.W., and Parkin, T.B., 1997. Quantitative indicators of soil quality: a minimum data set. *Methods for assessing soil quality* 49: 25-37.

Duriancik, L.F., Bucks, D., Dobrowolski, J.P., Drewes, T., Eckles, S.D., Jolley, L., Kellogg, R.L., Lund, D., Makuch, J.R., O'Neill, M.P., and Rewa, C.A. 2008. The first five years of the Conservation Effects Assessment Project. *Journal of soil and water conservation* 63 (6): 185A-197A.

Easterling, D.R., Meehl, G.A., Parmesan, C., Changnon, S.A., Karl, T.R., and Mearns, L.O. 2000. Climate extremes: observations, modelling, and impacts. *Science* 289: 2068–2074.

FAO, I., IMF, O., and UNCTAD, W. 2011. the World Bank, the WTO, IFPRI, and the UN HLTF (2011). *Price Volatility in Food and Agricultural Markets: Policy Responses*. Rome.

Favis-Mortlock, D.T., and Savabi, M.R. 1996. Shifts in rates and spatial distributions of soil erosion and deposition under climate change. Available: agris.fao.org [21 March 2019].

Favis-Mortlock, D.T., Evans, R., Boardman, J., and Harris, T.M. 1991. Climate change, winter wheat yield, and soil erosion on the English South Downs. *Agricultural Systems* 37: 415 – 433.

Fistikoglu, O., and Harmancioglu, N.B. 2002. Integration of GIS with USLE in assessment of soil erosion. *Water Resources Management* 16 (6): 447-467.

Flanagan, D.C., and Nearing, M.A. 1995. *USDA-Water Erosion Prediction Project: Hillslope profile and watershed model documentation*. NSERL report. 10: 1603-1612.

Flato, G., Marotzke, J., Abiodun, B., Braconnot, P., Chou, S.C., Collins, W., Cox, P., Driouech, F., Emori, S., Eyring, V., and Forest, C. 2013. Climate change 2013: the physical science basis. Contribution of working group I to the fifth assessment report of the intergovernmental panel on climate change. K., Tignor, M., Allen, SK, Boschung, J., Nauels, A., Xia, Y., Bex, V., and Midgley, PM, Cambridge University Press, Cambridge, UK and New York, NY, USA.

Fournier, F. 1972. *Soil conservation*. Nature and Environment Series, Council of Europe.

Fowler, H.J., Blenkinsop, S., and Tebaldi, C. 2007. Linking climate change modelling to impacts studies: recent advances in downscaling techniques for hydrological modelling. *International journal of climatology* 27 (12): 1547-1578.

Franklin, S.E. 2001. *Remote Sensing for Sustainable Forest Management*, Lewis Publishers, Boca Raton, FL, 407p.



Fritz, L.W. 1996. The era of commercial earth observation satellites. *Modular optoelectronic multispectral stereo-scanner on the second German spacelab mission*. 259-267.

Garde, R.J., and Kothiyari, U.C. 1987. Estimation of sediment yield. *Journal Central Board of Irrigation and Power* 44 (3): 7.

Gassman, P.W., Williams, J.R., Wang, X., Saleh, A., Osei, E., Hauck, L.M., Izaurralde, R.C., and Flowers, J. 2009. The Agricultural Policy Environmental Extender model: An emerging tool for landscape and watershed environmental analyses. *Trans. ASABE* 53 (3): 711-740.

Goswami, B.N., Venugopal, V., Sengupta, D., Madhusoodanan, M.S., and Xavier, P.K. 2006. Increasing trend of extreme rain events over India in a warming environment. *Science* 314 (5804): 1442-1445.

Green, W.H., and Ampt, G.A. 1911. Studies on Soil Physics. *The Journal of Agricultural Science*, 4 (1): 1-24.

Gupta, S. 2015. Simulating Climate Change Impact on Soil Erosion and Soil Carbon Sequestration. M. Tech. (RS&GIS) thesis, Andhra University, Visakhapatnam, 80p.

Gupta, S., and Kumar, S. 2017. Simulating climate change impact on soil erosion using RUSLE model- A case study in a watershed of mid-Himalayan landscape. *Journal of Earth System Science* 126 (3): 43.

Guyennon, N., Romano, E., Portoghese, I., Salerno, F., Calmanti, S., Perangeli, A.B., Tartari, G., and Copetti, D. 2013. Benefits from using combined dynamical-statistical downscaling approaches- lessons from a case study in the Mediterranean region. *Hydrology and Earth System Sciences* 17 (2): 705-720.

Hanway, J.J., and Heidel, H. 1952. Soil analysis methods as used in Iowa state college soil testing laboratory. *Iowa Agriculture* 57: 1-31.

Hardin, P. J., Jackson, M. W., and Otterstrom, S. M. 2007. Mapping, measuring, and modelling urban growth. In: Jensen, R. R., Gatrell, J. D. and McLean, D. (eds.). *Geo-spatial technologies in urban environments: Policy, practice, and pixels* (2<sup>nd</sup> Ed.). 141–176.

Hashmi, M.Z., Shamseldin, A.Y. and Melville, B.W. 2009. Downscaling of future rainfall extreme events: a weather generator based approach. In *18th World IMACS/MODSIM Congress*, 13-17 July 2009, Cairns, Australia, 3928-3934.

Hashmi, M.Z., Shamseldin, A.Y., and Melville, B.W. 2011. Comparison of SDSM and LARS-WG for simulation and downscaling of extreme precipitation events in a watershed. *Stochastic Environmental Research and Risk Assessment* 25 (4): 475-484.

Hassan, Z., Shamsudin, S., and Harun, S. 2014. Application of SDSM and LARS-WG for simulating and downscaling of rainfall and temperature. *Theoretical and applied climatology* 116 (1-2): 243-257.

Hasselmann, K. 1988. PIPs and POPs: The reduction of complex dynamical systems using first interaction and oscillation patterns. *Journal of Geophysical Research: Atmospheres* 93 (D9): 11015-11021.

Hathout, S. 2002. The use of GIS for monitoring and predicting urban growth in East and West St Paul, Winnipeg, Manitoba, Canada. *Journal of Environmental Management* 66: 229–238.

Hawkins, E., and Sutton, R. 2009. The potential to narrow uncertainty in regional climate predictions. *Bulletin of the American Meteorological Society* 90 (8): 1095-1108.

Hellstrom, C., Chen, D., Achberger, C., and Raisanen, J. 2001. Comparison of climate change scenarios for Sweden based on statistical and dynamical downscaling of monthly precipitation. *Climate Research* 19 (1): 45-55.

Horton, R.E. 1945. Erosional development of streams and their drainage basins: a hydro physical approach to quantitative morphology. *Bulletin of the Geological Society of America* 56: 275–370.

Hoyos, N. 2005. Spatial modelling of soil erosion potential in a tropical watershed of the Colombian Andes. *CATENA* 63 (1): 85-108.

Huang, J., Zhang, J., Zhang, Z., Sun, S., and Yao, J. 2012. Simulation of extreme precipitation indices in the Yangtze River basin by using statistical downscaling method (SDSM). *Theoretical and applied climatology* 108 (3-4): 325-343.

ICAR [Indian Council of Agricultural Research] and NAAS [National Institute of Agricultural Sciences] 2010. Degraded and Wastelands of India, Status and Spatial Distribution'. *Indian Council of Agricultural Research and National Academy of Agricultural Science*, New Delhi, 158p.

IFPRI [International Food Policy Research Institute] 2011. Global food policy report. International Food Policy Research Institute, Washington, DC.

Immerzeel, W.W., Van Beek, L.P., and Bierkens, M.F. 2010. Climate change will affect the Asian water towers. *Science* 328 (5984): 1382-1385.

IPCC [Intergovernmental Panel on Climate Change] 1990. Houghton, J.T., Jenkins, G.J., and Ephraums, J.J (eds.). *Climate Change: The IPCC Scientific Assessment*. Cambridge University Press, Cambridge, UK, 310p.

IPCC [Intergovernmental Panel on Climate Change] 1992. *Climate Change 1992: The Supplementary Report to the IPCC Scientific Assessment*. Houghton, J. T., B. A. Callander, and S. K. Varney (eds). Cambridge University Press, Cambridge, United Kingdom, and New York, NY, USA, 116 p.

IPCC [Intergovernmental Panel on Climate Change] 1999. Task Group on Scenarios for Climate Impact Assessment, Guidelines on the use of scenario data for climate impact, and adaptation assessment. Version 1, 69 p.

IPCC [Intergovernmental Panel on Climate Change] 2000 *Special report on emission scenarios*. Intergovernmental panel on climate change. Accessed at <http://www.grida.no/climate/ipcc/emission/index.html>. [29 Apr. 2019].

IPCC [Intergovernmental Panel on Climate Change] 2001. Working Group I, 2001. *Climate Change 2001: the scientific basis*. Contribution of Working Group I to the Third Assessment Report of the IPCC. Cambridge University Press, Cambridge, UK.

IPCC [Intergovernmental Panel on Climate Change] 2007. *Climate change 2007: impacts, adaptation, and vulnerability*. Parry, M., Parry, M.L., Canziani, O., Palutikof, J., Van der Linden, P. and Hanson, C. (eds.). *Contribution of Working Group II to the Fourth assessment report of the Intergovernmental Panel on Climate Change*. Cambridge University Press, Cambridge, United Kingdom, pp.470–506.

IPCC [Intergovernmental Panel on Climate Change] 2014. Synthesis Report. Contribution of working groups I, II and III to the Fifth Assessment Report of the Intergovernmental Panel on Climate Change 151: (10.1017).

Ives, J.D., Bruno, M., and Rhoades, R.E. 1997. Agenda for sustainable mountain development. In: Messerti B, Ives JD (eds.), *Mountains of the world*. The Parthenon Publishing Company, New York, pp. 409–445.

Jain, S.K., and Dolezal, F. 2000. Modelling soil erosion using EPIC supported by GIS, Bohemia, Czech Republic. *Journal of Environmental Hydrology* 8.

Jakeman, A.J., and Hornberger, G.M. 1993. How much complexity is warranted in a rainfall-runoff model?. *Water resources research* 29 (8), pp.2637-2649.

Jenness, J. 2006. Topographic Position Index extension for ArcView 3. x, v. 1.3 a. Jenness Enterprises.

Jensen, J.R. 2000. An earth resource perspective. *Remote Sensing of the Environment* 72: 361-365.

Jensen, J.R., 1996. *Introductory digital image processing: a remote sensing perspective* ( 2<sup>nd</sup> Ed.), Prentice-Hall Inc.

Jetten, V., and De Roo, A.P.J. 2001. Spatial analysis of erosion conservation measures with LISEM. In: Harmon R.S. and Doe, W.W. (eds.), *Landscape Erosion and Evolution Modelling*, Kluwer Academic, New York, 429–445.

Johnston, C.A., and Naiman, R.J. 1990. Aquatic patch creation in relation to beaver population trends. *Ecology* 71 (4): 1617-1621.

Kandel, D.D., Western, A.W., Grayson, R.B., and Turrall, H.N. 2004. Process parameterization and temporal scaling in surface runoff and erosion modelling. *Hydrological Processes* 18 (8): 1423-1446.

Kannan, S., and Ghosh, S., 2011. Prediction of daily rainfall state in a river basin using statistical downscaling from GCM output. *Stochastic Environmental Research and Risk Assessment*, 25 (4), pp.457-474.

Karamouz, M., Nazif, S., and Fallahi, M. 2010. *Rainfall downscaling using Statistical Downscaling Model and Canonical Correlation Analysis: a case study*. Proceedings of the World Environmental and Water Resources Congress 2010, Providence, Rhode Island, USA, 4579-4587.

Karl, T.R., and Knight, R.W. 1998. Secular trends of precipitation amount, frequency, and intensity in the United States. *Bulletin of the American Meteorological society* 79 (2): 231-242.

Kerr, J.M., and Sanghi, N.K. 1992. *Indigenous soil and water conservation in India's semi-arid tropics*. IIED International Institute for Environment and Development, Sustainable Agriculture Programme.

- Khan, M.S., Coulibaly, P., and Dibike, Y. 2006. Uncertainty analysis of statistical downscaling methods. *Journal of Hydrology* 319 (1-4): 357-382.
- Knutti, R., Joos, F., Müller, S.A., Plattner, G.K., and Stocker, T.F. 2005. Probabilistic climate change projections for CO<sub>2</sub> stabilization profiles. *Geophysical Research Letters* 32 (20).
- Knutti, R., Stocker, T.F., Joos, F., and Plattner, G.K., 2002. Constraints on radiative forcing and future climate change from observations and climate model ensembles. *Nature* 416 (6882): 719-723.
- Kothyari, U.C. 1996. Erosion and sedimentation problems in India. *IAHS Publications-Series of Proceedings and Reports-Intern Assoc Hydrological Sciences* 236: 531-540.
- Kothyari, U.C., and Jain, S.K. 1997. Sediment yield estimation using GIS. *Hydrological sciences journal* 42 (6): 833-843.
- Kumar, K.K., Kamala, K., Rajagopalan, B., Hoerling, M.P., Eischeid, J.K., Patwardhan, S.K., Srinivasan, G., Goswami, B.N., and Nemani, R. 2011. The once and future pulse of Indian monsoonal climate. *Climate Dynamics* 36 (11-12): 2159-2170.
- Kumar, K.R., Sahai, A.K., Kumar, K.K., Patwardhan, S.K., Mishra, P.K., Revadekar, J.V., Kamala, K., and Pant, G.B. 2006. High-resolution climate change scenarios for India for the 21st century. *Current science* 90 (3): 334-345.
- Kumar, S., Kushwaha, S.P.S. 2013. Modelling soil erosion risk based on RUSLE-3D using GIS in a Shivalik sub-watershed. *Journal of Earth System Science* 122 (2): 389-398.
- Kumar, S., Udawatta, R.P., Anderson, S.H., and Mudgal, A. 2011. APEX model simulation of runoff and sediment losses for grazed pasture watersheds with agroforestry buffers. *Agroforestry systems* 83 (1): 51-62.

- Kurihara, Y. 1970. A statistical-dynamical model of the general circulation of the atmosphere. *Journal of the Atmospheric Sciences* 27 (6): 847-870.
- Lal, D. 1991. Cosmic ray labelling of erosion surfaces: in situ nuclide production rates and erosion models. *Earth and Planetary Science Letters* 104 (2-4): 424-439.
- Lal, R. 1994. Soil Erosion Research Methods; CRC Press: Boca Raton, FL, USA, 352p.
- Lal, R., and Stewart, B.A., 1990. Soil degradation: A global threat. *Advances in Soil*.
- Leggett, J., Pepper, W.J., Swart, R.J., Edmonds, J., Meira Filho, L.G., Mintzer, I., and Wang, M.X. 1992. Emissions scenarios for the IPCC: an update. *Climate change*. 69-95.
- Leung, L.R., Mearns, L.O., Giorgi, F., and Wilby, R.L. 2003. Regional climate research: needs and opportunities. *Bulletin of the American Meteorological Society* 84 (1): 89-95.
- Lilhare, R., Garg, V., and Nikam, B.R. 2014. Application of GIS-coupled modified MMF model to estimate sediment yield on a watershed scale. *Journal of Hydrologic Engineering* 20 (6): C5014002.
- Liu, X., Coulibaly, P., and Evora, N. 2007. Comparison of data-driven methods for downscaling ensemble weather forecasts. *Hydrol Earth Syst. Sci. Discuss.* 4 (1):189–210.
- Loukas, A., Vasiliades, L., and Dalezios, N.R. 2002. Potential climate change impacts on flood producing mechanisms in southern British Columbia, Canada using the CGCMA1 simulation results. *Journal of Hydrology* 259 (1-4), pp.163-188.

- Ma, X., Xu, J., Luo, Y., Aggarwal, S.P., and Li, J. 2009. Response of hydrological processes to land-cover and climate changes in Kejie watershed, south-west China. *Hydrological Processes: An International Journal* 23 (8), pp.1179-1191.
- Maeda, E.E., Pellikka, P.K., Siljander, M., and Clark, B.J. 2010. Potential impacts of agricultural expansion and climate change on soil erosion in the Eastern Arc Mountains of Kenya. *Geomorphology* 123 (3-4): 279-289.
- Magrath, W., and Arens, P. 1989. *The costs of soil erosion on Java: a natural resource accounting approach*. World Bank Policy Planning and Research Staff, Environment Department, Washington, DC.
- Mahmood, R., and Babel, M.S. 2013. Evaluation of SDSM developed by annual and monthly sub-models for downscaling temperature and precipitation in the Jhelum basin, Pakistan and India. *Theoretical and Applied Climatology* 113 (1-2): 27-44.
- Manabe, S., and Bryan, K. 1969. Climate calculations with a combined ocean-atmosphere model. *Journal of the Atmospheric Sciences* 26 (4): 786-789.
- Manabe, S., and Strickler, R.F. 1964. Thermal equilibrium of the atmosphere with a convective adjustment. *Journal of the Atmospheric Sciences* 21 (4): 361-385.
- Mandal, D., Singh, R., Dhyani, S.K., and Dhyani, B.L., 2010. Landscape and land use effects on soil resources in a Himalayan watershed. *Catena* 81 (3): 203-208.
- McDonnell, R.A. 1996. Including the spatial dimension: using geographical information systems in hydrology. *Progress in Physical Geography* 20 (2): 159-177.
- McGuffie, K., and Henderson-Sellers, A. 2005. A climate modelling primer . Online ISBN: 9780470857618. *John Wiley & Sons, Ltd. DOI, 10(047085761), 7.*
- Meehl G.A., and Arblaster J.M. 2003. Mechanisms for projected future changes in south Asian monsoon precipitation. *Clim. Dyn.* 21:659–675.



- Meenu, R., Rehana, S., and Mujumdar, P.P. 2013. Assessment of hydrologic impacts of climate change in Tunga–Bhadra river basin, India with HEC-HMS and SDSM. *Hydrological Processes* 27 (11): 1572-1589.
- Meltan, M.A. 1957. An analysis of the relations among the elements of climatic, surface properties, and geomorphology, Dept of Geology, Columbia University, New York.
- Millward, A.A., and Mersey, J.E. 1999. Adapting the RUSLE to model soil erosion potential in a mountainous tropical watershed. *Catena* 38 (2): 109-129.
- Misra, P. R., Kaushal, R. C., Dayal, S.K.N., and Shanker, P. 1975. *Studies on the rates of annual water and sediment yields in reservoirs and ponds*. Central Soil and Water Cons. Res. Training Inst., Dehradun, India.17-18.
- Mondal, A., Khare, D., and Kundu, S. 2016. Impact of climate change on future soil erosion and SOC loss in different slope, soil and land use condition. *Nat Hazards*. doi:10.1007/s11069-016-2255-7.
- Mondal, A., Khare, D., Kundu, S., Meena, P.K., Mishra, P.K., and Shukla, R. 2015. Impact of climate change on future soil erosion in different slope, land use, and soil-type conditions in a part of the Narmada River Basin, India. *Journal of Hydrologic Engineering* 20 (6): p.C5014003.
- Moore, I.D., Grayson, R.B., and Ladson, A.R. 1991. Digital terrain modelling: a review of hydrological, geomorphological, and biological applications. *Hydrological processes* 5 (1): 3-30.
- Mora, D., Campozano, L., Cisneros, F., Wyseure, G., and Willems, P. 2014. Climate changes of hydrometeorological and hydrological extremes in the Paute basin, Ecuadorean Andes, *Hydrology and Earth System Sciences* 18 (2) pp. 631–648.

Morgan, R. P. C., 2005. *Soil Erosion and Conservation*, Blackwell Publishing, USA ,304p.

Morgan, R.P.C, Morgan, D.D.V., and Finney, H.J. 1984. A predictive model for the assessment of erosion risk. *Journal of Agricultural Engineering Research* 30: 245–253.

Morgan, R.P.C. 2001. A simple approach to soil loss prediction: a revised Morgan–Morgan–Finney model. *Catena* 44: 305–322.

Morgan, R.P.C. 2009. *Soil erosion and conservation*. Blackwell Publishing, Victoria, 304p.

Morgan, R.P.C., and Finney, H.J. 1982. Stability of Agricultural Ecosystems: Validation of a Simple Model for Soil Erosion Assessment, Institute of Applied Systems Analysis Collaborative Paper CP-82-76.

Morgan, R.P.C., Martin, L., and Noble, C.A. 1986. Soil erosion in the United Kingdom: a case study from mid-Bedfordshire. Silsoe College Occasional Paper no. 14. Silsoe College, Cranfield Univ., Silsoe, UK.

Murphy, P.N., Ogilvie, J., Meng, F.R., and Arp, P. 2008. Stream network modelling using lidar and photogrammetric digital elevation models: a comparison and field verification. *Hydrological Processes: An International Journal* 22 (12): 1747-1754.

Mythili, G., and Goedecke, J. 2016. Economics of land degradation in India. In: Mirzabaev, M. and von Braun, J. (eds.). *Economics of land degradation and improvement—a global assessment for sustainable development*. Springer, Cham.431-469.

Nakicenovic, N., Alcamo, J., Grubler, A., Riahi, K., Roehrl, R.A., Rogner, H.H., and Victor, N. 2000. *Special report on emissions scenarios (SRES), a special report*

of Working Group III of the intergovernmental panel on climate change. Cambridge University Press.

Narayan, V.V.D., and Babu, R. 1983. Estimation of soil erosion in India. *Journal of Irrigation and Drainage Engineering* 109 (4): 419-434.

Nash, J.E., and Sutcliffe, J.V. 1970. River forecasting using conceptual models, 1. A discussion of principles. *J. Hydrol* 10: 280-290.

NBSS&LUP [National Bureau of Soil Survey & Land Use Planning.] 2004. *Soil Map (1:1 Million Scale)*; NBSS&LUP: Nagpur, India.

NBSS&LUP [National Bureau of Soil Survey and Land Use Planning] 2005. *Annual Report 2005*, Nagpur; NBSS&LUP: Nagpur, India.

Nie, N.H., Bent, D.H., and Hull, C.H. 1975. *SPSS: Statistical package for the social sciences* 227: 226-227.

Noori, M., Sharifi, M.B. and Heydari, M. 2014. Comparison of the SDSM and LARS-WG weather generators in Modeling of Climate Change in Golestan Province of Iran. In *8th National Congress on Civil Engineering, Babol Noshirvani University of Technology*. 7-8.

O'Neal, M.R., Nearing, M.A., Vining, R.C., Southworth, J., and Pfeifer, R.A. 2005. Climate change impacts on soil erosion in Midwest United States with changes in crop management. *Catena* 61: 165–184.

Onstad, C.A., and Foster, G.R. 1975. Erosion modelling on a watershed. *Transactions of the ASAE* 18 (2): 288-0292.

Ozdemir, H., and Bird, D. 2009. Evaluation of morphometric parameters of drainage networks derived from topographic maps and DEM in point of floods. *Environmental Geology* 56 (7): 1405-1415.

- Pandey, A., Mathur, A., Mishra, S.K., and Mal, B.C. 2009. Soil erosion modelling of a Himalayan watershed using RS and GIS. *Environmental Earth Sciences* 59 (2): 399-410.
- Parmesan, C. 2006. Ecological and evolutionary responses to recent climate change. *Annual Review of Ecology, Evolution, and Systematics* 37:637–669.
- Patnaik, N. 1981. Role of soil conservation and afforestation for flood moderation. *Proceedings of the International Conference on Flood Disasters, INSA, New Delhi, circulated mimeo.*
- Pepper, W., Leggett, J., Swart, R., Wasson, J., Edmonds, J., and Mintzer, I. 1992. Emission Scenarios for the IPCC, An Update, Assumptions, Methodology, and Results, prepared for the Intergovernmental Panel on Climate Change, Working Group 1, Geneva, Switzerland.
- Pervez, M.S., and Henebry, G.M. 2014. Projections of the Ganges- Brahmaputra precipitation-Downscaled from GCM predictors. *Journal of Hydrology* 517: 120-134.
- Pike, R.J. 2000. Geomorphometry–diversity in quantitative surface analysis. *Progress in Physical Geography* 24: 1–20.
- Pimentel, D., Allen, J., Beers, A., Guinand, L., Linder, R., McLaughlin, P., Meer, B., Musonda, D., Perdue, D., Poisson, S., and Siebert, S. 1987. World agriculture and soil erosion. *BioScience* 37 (4), 277-283.
- Pimentel, D., Harvey, C., Resosudarmo, P., Sinclair, K., Kurz, D., McNair, M., Crist, S., Shpritz, L., Fitton, L., Saffouri, R., and Blair, R. 1995. Environmental and economic costs of soil erosion and conservation benefits. *Science* 267 (5201): 1117-1123.
- Prasannakumar, V., Vijith, H., Abinod, S., and Geetha, N. 2012. Estimation of soil erosion risk within a small mountainous sub-watershed in Kerala, India, using

Revised Universal Soil Loss Equation (RUSLE) and geo-information technology. *Geoscience Frontiers*, 3 (2): 209-215.

Prosser, I.P., Young, B., Rustomji, P., Hughes, A., and Moran, C. A. 2001. Model of river sediment budgets as an element of river health assessment. *Proceedings of the International Congress on Modelling and Simulation (MODSIM'2001)*, Canberra, Australia, 10–13.

Prudhomme, C., Reynard, N., and Crooks, S. 2002. Downscaling of global climate models for flood frequency analysis: where are we now? *Hydrol. Processes* 16: 1137–1150.

Pruski, F.F. and Nearing, M.A. 2002. Climate-induced changes in erosion during the 21st century for eight US locations. *Water Resources Research*, 38 (12): 34-1.

Rawls, W.J., Gimenez, D., and Grossman, R. 1998. Use of soil texture, bulk density, and slope of the water retention curve to predict saturated hydraulic conductivity. *Transactions of the ASAE*, 41 (4): 983.

Raymo, M.E., and Ruddiman, W.F. 1992. Tectonic forcing of late Cenozoic climate. *nature*, 359 (6391): 117.

Reichler, T. and Kim, J. 2008. How well do coupled models simulate today's climate?. *Bulletin of the American Meteorological Society* 89 (3): 303-312.

Renard, K.G., and Freimund, J.R. 1994. Using monthly precipitation data to estimate the R-factor in the revised USLE. *Journal of hydrology* 157 (1-4): 287-306.

Renard, K.G., Foster, G.R., Weesies, G.A., McCool, D.K., and Yoder, D.C. 1997. *Predicting soil erosion by water: a guide to conservation planning with the Revised Universal Soil Loss Equation (RUSLE)* 703. United States Department of Agriculture, Washington, DC.

- Renard, K.G., Foster, G.R., Yoder, D.C., and McCool, D.K., 1994. RUSLE revisited: status, questions, answers, and the future. *Journal of soil and water conservation*, 49 (3), pp.213-220.
- Ridd, M. K., and Liu, J. J. 1998. A comparison of four algorithms for change detection in an urban environment. *Remote Sensing of Environment* 63: 95–100.
- Roose, E.J 1967. Ten years of measuring erosion and runoff in Senegal. *Agron. Too.* 22 (2): 123-152.
- Roy, L., Leconte, R., Brissette, F.P. and Marche, C. 2001. The impact of climate change on seasonal floods of a southern Quebec River Basin. *Hydrological processes* 15 (16): 3167-3179.
- Rupakumar K, Sahai A.K., Kumar, K.K., Patwardhan, S.K., Mishra, P.K, Revadekar, J.V., Kamala, K., Pant, G.B. 2006. High-resolution climate change scenarios for India for the 21st century. *Curr. Sci.* 90 (3): 334–345.
- Sabins, F. F. 1987. Remote Sensing: principles and interpretation. (2<sup>nd</sup> Ed.). Freeman and company, New York.
- Saha, S.K. 2003. Water and Wind Induced Soil Erosion Assessment and Monitoring Using Remote Sensing and GIS. In: Satellite Remote Sensing and GIS Applications in Agricultural Meteorology, 315-330.
- Saltzman, B. 1968. Surface boundary effects on the general circulation and macroclimate: A review of the theory of the quasi-stationary perturbations in the atmosphere. In *Causes of Climatic Change*. American Meteorological Society, Boston, MA. 4-19.
- Sano, E.E., Rosa, R., Brito, J.L., and Ferreira, L.G. 2010. Land cover mapping of the tropical savanna region in Brazil. *Environmental monitoring and assessment* 166 (1-4): 113-124.

- Saraf, V.R., and Regulwar, D.G. 2016. Assessment of climate change for precipitation and temperature using statistical downscaling methods in Upper Godavari River basin, India. *Journal of Water Resource and Protection* 8 (01): 31.
- Savabi, M.R., Arnold, J.G., and Nicks, A.D. 1993. Impact of global climate change on hydrology and soil erosion: a modelling approach. In: Eckstein, Y. and Zaporozec, A. (eds.), *Proceedings of Industrial and Agricultural Impact of Environmental and Climatic Change on Global and Regional Hydrology*. Water Environment Federation, Alexandria, Virginia, 3 -18.
- Saxton, K.E., and Willey, P.H. 2005. The SPAW model for agricultural field and pond hydrologic simulation. *Watershed models* 400-435.
- Saxton, K.E., Rawls, W., Romberger, J.S., and Papendick, R.I. 1986. Estimating generalized soil-water characteristics from texture. *Soil Science Society of America Journal*, 50 (4): 1031-1036.
- Serra, P., Pons, X., and Sauri, D. 2008. Land-cover and land-use change in a Mediterranean landscape: a spatial analysis of driving forces integrating biophysical and human factors. *Applied Geography* 28: 189–209.
- Sharda, V.N., Dogra, P., and Prakash, C. 2010. Assessment of production losses due to water erosion in rainfed areas of India. *Indian J. Soil Water Conserv.* 65: 79–91.
- Shrestha, A.B., and Aryal, R. 2011. Climate change in Nepal and its impact on Himalayan glaciers. *Regional Environmental Change* 11 (1): 65-77.
- Shrestha, D.P. 1997. Assessment of soil erosion in the Nepalese Himalaya: a case study in Likhu Khola Valley, Middle Mountain Region. *Land Husbandry* 2 (1): 59–80.
- Shreve, R.L. 1966. Statistical law of stream numbers. *The Journal of Geology* 74 (1): 17-37.

- Simanton, J.R., Rawitz, E., and Shirley, E.D. 1984. Effects of rock fragments on erosion of semiarid rangeland soils. *Erosion and productivity of soils containing rock fragments*, 7: 65-72.
- Simonneaux, V., Cheggour, A., Deschamps, C., Mouillot, F., Cerdan, O., Bissonnais, Y.L. 2015. Land use and climate change effects on soil erosion in a semi-arid mountainous watershed (High Atlas, Morocco). *J. Arid Environ.* 122: 64–75.
- Singh, A. 1989. Digital change detection techniques using remotely sensed data. *International Journal of Remote Sensing*, 10 (6): 989–1003.
- Singh, D., Jain, S.K., and Gupta, R.D. 2015. Statistical downscaling and projection of future temperature and precipitation change in middle catchment of Sutlej River Basin, India. *Journal of Earth System Science* 124 (4): 843-860.
- Singh, G., Babu, R., and Chandra, S. 1981. *Soil loss prediction research in India*. Central Soil and Water Conservation Research and Training Institute Bulletin No. T12/D9, Dehra Dun.
- Singh, G., Babu, R., Narain, P., Bhushan, L.S., and Abrol, I.P. 1992. Soil erosion rates in India. *Journal of Soil and water Conservation* 47 (1): pp.97-99.
- Singh, P., and Kumar, N. 1997. Effect of Orography on Precipitation in the Western Himalayan Region. *Journal of Hydrology* 199 (1997): 183-206.
- Singh, R.P. 2012. Surface runoff, Soil erosion and Water Quality estimation using APEX model integrated with GIS -A case study in Himalayan Watershed. M. Tech. (RS & GIS) thesis, Andhra University, Visakhapatnam, 98p.
- Smith, R.E., and Parlange, J.Y. 1978. A parameter-efficient hydrologic infiltration model. *Water Resources Research* 14 (3): 533-538.



Smith, R.E., Goodrich, D.C., and Quinton, J.N. 1995. Dynamic, distributed simulation of watershed erosion: the KINEROS2 and EUROSEM models. *Journal of Soil and Water Conservation* 50 (5): 517-520.

Soil Survey Staff. 1996. Soil Survey Laboratory methods manual. Soil Survey Investigations Rep. 42, Version 2.0, National Soil Survey Center, Soil Conservation Service, U.S. Department of Agriculture, Lincoln, NE, 693–1036.

Stocking, M. 1986. *The Cost of Soil Erosion in Zimbabwe in Terms of the Loss of Three Major Nutrients*. Soil Conservation Programme, Land and Water Development Division, Consultants Working Paper No. 3. Rome: AGLS, FAO.

Stokes, G.G. 1851. *On the effect of the internal friction of fluids on the motion of pendulums* 9: 8. Cambridge: Pitt Press.

Stoms, D.M. and Estes, J.E. 1993. A remote sensing research agenda for mapping and monitoring biodiversity. *International journal of remote sensing* 14 (10): 1839-1860.

Stone, J.R., Gilliam, J.W., Cassel, D.K., Daniels, R.B., Nelson, L.A., and Kleiss, H.J. 1985. Effect of Erosion and Landscape Position on the Productivity of Piedmont Soils. *Soil Science Society of America Journal* 49 (4): 987-991.

Stone, J.R., Gilliam, J.W., Cassel, D.K., Daniels, R.B., Nelson, L.A., and Kleiss, H.J. 1985. Effect of erosion and landscape position on the productivity of Piedmont soils. *Soil Sci. Soc. Am. J.* 49: 987–991.

Stott, P.A. and Kettleborough, J.A. 2002. Origins and estimates of uncertainty in predictions of twenty-first century temperature rise. *Nature* 416 (6882): 723.

Strahler, A.N. 1953. Revisions of Horton's quantitative factors in erosional terrain. *Trans. Am. Geophys. Union* 34: 345.

Sugi, M. and Yoshimura, J. 2004. A mechanism of tropical precipitation change due to CO<sub>2</sub> increase. *J. Clim.* 17:238–243.

- Suhara, S. K. K., 2018. Soil erosion risk assessment in Kunthippuzha sub-watershed using remote sensing and gis. M. Tech. (S & WE) thesis, Kerala Agricultural University, Thrissur, 151p.
- Tang, J., Niu, X., Wang, S., Gao, H., Wang, X. and Wu, J. 2016. Statistical downscaling and dynamical downscaling of regional climate in China: Present climate evaluations and future climate projections. *Journal of Geophysical Research: Atmospheres* 121 (5): 2110-2129.
- Tebaldi, C., Hayhoe, K., Arblaster, J.M., and Meehl, G.A. 2006. Going to the extremes: an intercomparison of model-simulated historical and future changes in extreme events. *Clim. Change* 79:185-211.
- Thenkabail, P.S., Schull, M. and Turrall, H. 2005. Ganges and Indus river basin land use/land cover (LULC) and irrigated area mapping using continuous streams of MODIS data. *Remote Sensing of Environment* 95 (3): 317-341.
- Trenberth, K.E., and Caron, J.M. 2000. The Southern Oscillation revisited: sea level pressures, surface temperatures and precipitation. *J Clim.*13:4358–4365.
- Tripathi, C.N. and Gosain, A.K. 2013. Micro watershed modelling in India using GIS technologies and agricultural policy environmental extender (APEX) model. A case study. *International Journal of Engineering Research and Applications*, 3 (2): 1640-1648.
- Tuppad, P., Winchell, M.F., Wang, X., Srinivasan, R., and Williams, J.R. 2009. ArcAPEX: ArcGIS interface for Agricultural Policy Environmental eXtender (APEX) hydrology/water quality model. *International Agricultural Engineering Journal* 18 (1): 59.
- Turcotte, R., Fortin, J.P., Rousseau, A.N., Massicotte, S., and Villeneuve, J.P. 2001. Determination of the drainage structure of a watershed using a digital elevation model and a digital river and lake network. *Journal of Hydrology* 240 (3-4): 225-242.

U.S. NAST [United States National Assessment Synthesis Team] 2001. Climate change impacts on the United States: the potential consequences of climate variability and change. Foundation Report. U.S. Global Change Research Program. Cambridge University Press, Cambridge, UK.

UN [United Nations] 1992. Earth Summit: Agenda 21. The United Nations Programme of Action from Rio The final text of agreements negotiated by governments at the United Nations Conference on Environment and Development (UNCED), 3- 14 June 1992, Rio de Janeiro, Brazil. 294p.

UNCCD [United Nations Convention to Combat Desertification], 1994. Elaboration of an international convention to combat desertification in countries experiencing serious drought and/or desertification, particularly in Africa. *UN Doc. A/AC. 241/27, 33 ILM 1328*.

Uri, N.D., and Lewis, J.A., 1998. The dynamics of soil erosion in US agriculture. *Science of the total environment* 218 (1), pp.45-58.

Ursic, S.J., and Dendy, F.E. 1965. Proceedings of the Federal Inter-Agency Sedimentation Conference, US Department of Agriculture, Washington, DC, 47–52.

USDA-SCS [U.S. Department of Agriculture-Soil Conservation Service], 1972. SCS National Engineering Handbook, Section 4, Hydrology. Chapter 10, Estimation of Direct Runoff from Storm Rainfall. U.S. Department of Agriculture, Soil Conservation Service, Washington, D.C., pp10.1-10.24.

Valdiya, K.S. 1985. Accelerated erosion and landslide-prone zones in the central Himalayan region. In: Singh, J. S. (ed.), *Environmental regeneration in Himalaya: concepts and strategies*. Central Himalayan Environment Association and Gyanodaya Prakashan, Nainital. 12-39.

Valentin, C. 1998. Towards an improved predictive capability for soil erosion under global change. *Modelling soil erosion by water* 7-16.

Van Vuuren, D.P., Edmonds, J., Kainuma, M., Riahi, K., Thomson, A., Hibbard, K., Hurtt, G.C., Kram, T., Krey, V., Lamarque, J.F. and Masui, T. 2011. The representative concentration pathways: an overview. *Climatic change* 109 (1-2): p.5.

Varughese, A. 2016. Impact of climate change and watershed development on river basin hydrology using SWAT—a case study. Doctoral thesis, Kerala Agricultural University, Thrissur, 167p.

Verma, B., Tejwani, K. G., Kale, M. V., and Patel, A. P. 1968. Evaluation of different cropping patterns for runoff and soil loss in ravine lands. *Jnl. Ind. Soc. Agron.* 13: 262-270.

Vitek, J.D., Giardino, J.R., and Fitzgerald, J.W. 1996. Mapping geomorphology: A journey from paper maps, through computer mapping to GIS and Virtual Reality. *Geomorphology* 16 (3): 233-249.

Viviroli, D., Durr, H.H., Messerli, B., Meybeck, M. and Weingartner, R. 2007. Mountains of the world, water towers for humanity: Typology, mapping, and global significance. *Water resources research*, 43 (7).

von Storch, H. 1999. The global and regional climate system. In: von Storch, H., and Floscr, G. (eds.) *Anthropogenic climate change*. Springer, Berlin 3–36.

von Storch, H., 1992. Inconsistencies at the interface of climate impact studies and global climate research. *Meteorologische Zeitschrift* 72-80.

Vrac, M., Vaittinada Ayar, P. 2017. Influence of bias correcting predictors on statistical downscaling models. *Jnl. Appl Meteorol Climatol* 56 (1):5–26.

Walkely, A. and Black, I.A. 1934. An examination of the defy are method for determination of chronic acid method. *Soil Sci*, 37, pp.29-38.

- Wang, G. X., Qian, J., Cheng, G. D., and Lai, Y.M. 2002. Soil organic carbon pool of grassland soils on the Qinghai-Tibetan Plateau and its global implication. *Science of the Total Environment*. 291:207–217.
- Wang, X., Gassman, P.W., Williams, J.R., Potter, S., and Kemanian, A.R. 2008. Modelling the impacts of soil management practices on runoff, sediment yield, maize productivity, and soil organic carbon using APEX. *Soil and Tillage Research* 101 (1-2): 78-88.
- Wang, X. Kannan, N., Santhi, C., Potter, S., Williams, J. R., and Arnold J. G. 2011a. Integrating APEX output for cultivated cropland with SWAT simulation for regional modelling. *Trans. ASABE* 54 (4): 1281-1298.
- Wang, X., Tuppad, P. and Williams J. R. 2011b. Modeling agricultural management systems with APEX. In: Shukla, M. K. (ed.) *Soil Hydrology, Land Use, and Agriculture: Measurement and Modelling*, CABI Press, Wallingford, U.K. 117-136.
- Wang, X., Yen, H., Jeong, J., and Williams, J.R., 2015. Accounting for conceptual soil erosion and sediment yield modeling uncertainty in the APEX model using Bayesian model averaging. *Journal of Hydrologic Engineering* 20 (6): p.C4014010.
- Wetterhall, F., Bardossy, A., Chen, D., Halldin, S. and Xu, C.Y. 2006. Daily precipitation-downscaling techniques in three Chinese regions. *Water Resources Research* 42 (11).
- Wheater, H.S., Jakeman, A.J., Beven, K.J. 1993. *Progress and Directions in Rainfall-Runoff Modelling*; FAO, Rome, Italy.
- Wigley, T.M.L., Jones, P.D., Briffa, K.R. and Smith, G. 1990. Obtaining sub-grid scale information from coarse-resolution general circulation model output. *Journal of Geophysical Research* 95: 1943–53.

Wilby, R.L. and Dawson, C.W. 2007. SDSM 4.2-A decision support tool for the assessment of regional climate change impacts. *User manual*, 94p.

Wilby, R.L. and Dawson, C.W. 2013. The statistical downscaling model: insights from one decade of application. *International Journal of Climatology* 33 (7): 1707-1719.

Wilby, R.L., Charles, S.P., Zorita, E., Timbal, B., Whetton, P. and Mearns, L.O. 2004. Guidelines for use of climate scenarios developed from statistical downscaling methods. Supporting material of the Intergovernmental Panel on Climate Change, Available at DDC of IPCC TGCIA, 27.

Wilby, R.L., Dawson, C.W. and Barrow, E.M. 2002. SDSM- a decision support tool for the assessment of regional climate change impacts. *Environmental Modelling & Software* 17 (2): 145-157.

Wilby, R.L., Dawson, C.W., Murphy, C., Connor, P.O., and Hawkins, E. 2014. The statistical downscaling model-decision centric (SDSM-DC): conceptual basis and applications. *Climate Research* 61 (3): 259-276.

Wilby, R.L., Hay, L.E., Gutowski, W.J., Arritt, R.W., Takle, E.S., Pan, Z., Leavesley, G.H., and Clark, M.P. 2000. Hydrological responses to dynamically and statistically downscaled climate model output. *Geophysical Research Letters* 27 (8): 1199-1202.

Wilby, R.L., Troni, J., Biot, Y., Tedd, L., Hewitson, B.C., Smith, D.M., and Sutton, R.T. 2009. A review of climate risk information for adaptation and development planning. *International Journal of Climatology: A Journal of the Royal Meteorological Society* 29 (9): 1193-1215.

Williams, J. R. 1975. Sediment-yield prediction with universal equation using runoff energy factor. In '*Present and Prospective Technology for Predicting Sediment Yields and Sources*'.

Williams, J. R., and R. C. Izaurralde. 2006. Chapter 18: The APEX model. In *Watershed Models*, 437-482. V. P. Singh and D. K. Frevert, (eds.), Boca Raton, Fla.: CRC Press, Taylor and Francis Group.

Williams, J.R. 2008. Agricultural Policy/Environmental eXtender Model: Theoretical Documentation Version 0604 (Draft). BREC Report # 2008-17. Texas AgriLIFE Research, Texas A&M University, Blackland Research and Extension Center, Temple, TX.

Williams, J.R., and Berndt, H.D. 1977. Sediment yield prediction based on watershed hydrology. *Transactions of the ASAE* 20 (6), pp.1100-1104.

Williams, J.R., and Izaurralde, R.C. 2005. The APEX model. BRC Rep (2005)-02, Blackland Res Center, Texas, A&M University, Temple, TX.

Williams, J.R., Arnold, J.G., Kiniry, J.R., Gassman, P.W. and Green, C.H. 2008a. History of model development at Temple, Texas. *Hydrological sciences journal* 53 (5): 948-960.

Williams, J.R., Harman, W.L., Magre, M., Kizil, U., Lindley, J.A., Padmanabhan, G., Wang, E. 2006. APEX feedlot water quality simulation. *Trans ASABE* 49: 61–73.

Williams, J.R., Izaurralde, R.C., Steglich, E.M. 2008b. Agricultural policy/environmental eXtender model: theoretical documentation version 0604 (draft). BREC report # 2008-17. Texas AgriLIFE Research, Texas A&M University, Temple, TX.

Williams, J.R., Jones, C.A. and Dyke, P.T. 1984. A modelling approach to determining the relationship between erosion and soil productivity. *Transactions of the ASAE* 27: 129-0144.

Williams, J.R., Wang, E., Meinardus, A., Harman, W.L., Siemers, M., Atwood, J.D. 2006, *APEX users guide v2110*. Texas A&M University, Texas Agricultural

Extension Service, Texas Agricultural Experiment Station, Blacklands Research Center, Temple, TX.

Wilson, J.P., Gallant, J.C. 2000. Terrain Analysis- Principles and Applications. *Wiley*, New York 479p.

Wischmeier, W.H., and Smith, D.D. 1965. Predicting rainfall erosion losses from cropland east of the Rocky Mountains: guide for selection of practices for soil and water conservation. *Agriculture handbook*, 282. USDA, Washington, 47p.

Wischmeier, W.H., and Smith, D.D. 1978. Predicting rainfall erosion losses. *Agricultural Handbook* 537. Agricultural Research Service, United States Department of Agriculture, Washington.

Woolard, J.W., and Colby, J.D. 2002. Spatial characterization, resolution, and volumetric change of coastal dunes using airborne LIDAR: CapeHatteras, North Carolina. *Geomorphology* 48 (1-3): 269-287.

Xu, C.Y. 1999. From GCMs to river flow: a review of downscaling methods and hydrologic modelling approaches. *Progress in physical Geography* 23 (2): 229-249.

Xu, J. C., and G. M. Rana. 2005. Living in the mountains. In: Jeggle, T. (ed.), Know risk. *U. N. Inter-agency Secretariat of the International Strategy for Disaster Reduction*, Geneva. 196–199.

Yang, D., Kanae, S., Oki, T., Koike, T. and Musiaka, K., 2003. Global potential soil erosion with reference to land use and climate changes. *Hydrological processes*, 17 (14), pp.2913-2928.

Yildiz, O., 2002. An investigation of the effect of drainage density on hydrologic response. *Turkish Jnl. Engg. Environ. Sci*, 28: 85-94.



Yin, L., Wang, X., Pan, J. and Gassman, P.W. 2009. Evaluation of APEX for daily runoff and sediment yield from three plots in the Middle Huaihe River Watershed, China. *Transactions of the ASABE* 52 (6): 1833-1845.

Young, A. 1969. Present rate of land erosion. *Nature* 224: 851-2.

Yuan, F., Sawaya, K. E., Loeffelholz, B. C., and Bauer, M. E. 2005. Land cover classification and change analysis of the Twin Cities (Minnesota) Metropolitan Area by multi-temporal Landsat remote sensing. *Remote Sensing of Environment* 98 (2-3): 317-328.

Zhang, B. P., Yao, Y. H., Cheng, W. M., Zhou, C. H., Lu, Z., and Chen, X. D. 2002. Human-induced changes to biodiversity and alpine pastureland in the Bayanbulak Region of the East Tianshan Mountains. *Mountain Research and Development* 22: 1-7.

Zhang, W. and Montgomery, D. 1994. Digital elevation model grid size, landscape representation, and hydrologic simulations, *Water Resour. Res.* 30 (4): 1019-1028.

Zhang, X., Drake, N.A., Wainwright, J. and Mulligan, M. 1999. Comparison of slope estimates from low resolution DEMs: Scaling issues and a fractal method for their solution. *Earth Surface Processes and Landforms: The Journal of the British Geomorphological Research Group* 24 (9): 763-779.

Zhang, X.C. and Liu, W.Z. 2005. Simulating potential response of hydrology, soil erosion, and crop productivity to climate change in Changwu tableland region on the Loess Plateau of China. *Agricultural and Forest Meteorology* 131 (3-4): 127-142.

Zorita, E. and Von Storch, H. 1999. The analog method as a simple statistical downscaling technique: comparison with more complicated methods. *Journal of climate* 12 (8): 2474-2489.

**MODELLING CLIMATE CHANGE IMPACT ON SURFACE RUNOFF  
AND SEDIMENT YIELD IN A WATERSHED OF SHIVALIK REGION**

**By**

**ANU D RAJ**

**(2014-20-112)**

**ABSTRACT**

**Submitted in partial fulfilment of the  
requirements for the degree of**

**B. Sc. - M. Sc. (Integrated Climate Change Adaptation)**

**Faculty of Agriculture**

**Kerala Agricultural University**



**ACADEMY OF CLIMATE CHANGE EDUCATION AND RESEARCH**

**VELLANIKKARA, THRISSUR - 680 656**

**KERALA, INDIA**

**2020**

## ABSTRACT

The climate change refers to the seasonal changes over a long duration in relation to the increasing amount of greenhouse gasses in the atmosphere. Global warming leads to a more vigorous hydrological cycle, including higher amount rainfall and more frequent high-intensity rainfall events. The Himalayan region is suffering from a serious problem of soil erosion and rivers flowing through this region transport a massive load of sediment. Climate change has a significant contribution to soil erosion. It leads to loss of nutrient-rich top soil which in turn can affect the nation's food security.

The present study depicts modelling climate change impact on surface runoff and sediment yield in a watershed of Shivalik region of Himachal Pradesh using a process-based Agricultural Policy/ Environmental eXtender(APEX) model. Terrain characteristics were analysed with the aid of Cartosat DEM. Land use/land cover characteristics were extracted from Resourcesat-2 LISS-IV and ground observations. Soil samples were collected from the field were analysed to identify soil physical and chemical properties. Surface runoff and sediment yield data required for model calibration and validation were collected from the gauging station constructed in the field. The future climate scenarios (temperature and rainfall) namely A2 and B2 of the study area were downscaled using statistical downscaling model (SDSM).

APEX model parameterization was done as per local conditions. The APEX model was calibrated on a daily basis for 2017 and 2018. For calibration and validation of the model used low to medium rainfall days. The model calibrated quite well for surface runoff ( $r^2 - 0.92$ ) and sediment yield ( $r^2 - 0.88$ ) with RMSE of 4.98 mm and 0.20 t/ ha for surface runoff and sediment yield, respectively. The model was validated well for surface runoff ( $r^2 - 0.81$ ) and sediment yield ( $r^2 - 0.81$ ) with RMSE of 2.6 mm and 0.11 t/ha for surface runoff and sediment yield respectively. The model performance was identified based on Nash- Sutcliffe efficiency (NSE). The model performed quite well for surface runoff and sediment

yield of NSE 0.71 and 0.70 respectively. The change in soil loss under A2 and B2 scenarios with respect to baseline period were predicted for the study area to recognize the effect of climate change on soil loss.

The general trend in future climate shows there is an increase in rainfall under both A2 and B2 scenario. Under the A2 scenario, rainfall increases marginally higher than B2 scenario. A total of 41.35 per cent increase in rainfall during 2080, 20.14 per cent during 2050, and 27.27 per cent during 2020 were observed. But in B2 scenario due to lower emission, change in rainfall is relatively lower than A2 scenario. It was observed that 24.71 per cent, 29.13 per cent and 35.16 per cent increase during 2020, 2050 and 2080 respectively. Maximum temperature increases 3.7 °C during 2080 under A2, while under B2 scenario the increase is 2.6 °C. Similarly, minimum temperature also rising at 3.6 °C during 2080 under A2 scenario and 2.7 °C under B2 scenario. The increase in temperature under both scenarios is almost similar and a marginal difference was observed.

Highest soil loss was estimated from scrub land (38.42 t/ha/yr) followed by agriculture (26.97 t/ha/yr) then open forest (21.69 t/ha/yr) and lowest in the dense forest cover (14.70 t/ha/yr) under baseline period. The average annual soil loss from the watershed is 25.45 t/ha/yr. It was observed that 64.61 per cent of the study area was under moderate (10-20 t/ha/yr) erosion risk class. 24.15 per cent area with severe (20-40 ton ha<sup>-1</sup> yr<sup>-1</sup>) erosion and 11.23 per cent area contribute very severe (>40 ton ha<sup>-1</sup> yr<sup>-1</sup>) erosion. Under A2 scenario the average soil loss during 2020s, 2050s and 2080s may increase 27.71, 21.84 and 46.94 per cent respectively. Similarly under B2 scenario average soil loss may increase 23.24, 30.71 and 38.80 per cent, respectively. The climate change impact on soil erosion under both scenarios suggests that there is an increasing soil erosion due to the increase in rainfall in Shivalik region of Himachal Pradesh. Due to the high intensity of rainfall and steep slopes of the study area the mechanical conservation measures are preferred. The agronomic, mechanical and biological measures can be also used to conserve the soil and water.